

**ELECTRONIC PACKAGING AND ENVIRONMENTAL TEST AND ANALYSIS OF  
AN EMI SHIELDED ELECTRONIC UNIT FOR NAVAL PLATFORM**

**A THESIS SUBMITTED TO THE GRADUATE SCHOOL  
OF  
NATURAL AND APPLIED SCIENCES  
OF  
MIDDLE EAST TECHNICAL UNIVERSITY**

**BY**

**YÜCEL DEVELLİOĞLU**

**IN PARTIAL FULFILLMENT OF THE REQUIREMENTS  
FOR  
THE DEGREE OF MASTER OF SCIENCE  
IN  
AEROSPACE ENGINEERING**

**APRIL 2008**

Approval of the thesis:

**ELECTRONIC PACKAGING AND ENVIRONMENTAL TEST AND  
ANALYSIS OF AN EMI SHIELDED ELECTRONIC UNIT FOR NAVAL  
PLATFORM**

submitted by **YÜCEL DEVELLİOĞLU** in partial fulfillment of the requirements for  
the degree of **Master of Science in Aerospace Engineering Department, Middle  
East Technical University** by,

Prof. Dr. Canan Özgen \_\_\_\_\_  
Dean, Graduate School of **Natural and Applied Sciences**

Prof. Dr. İsmail Hakkı Tuncer \_\_\_\_\_  
Head of Department, **Aerospace Engineering**

Assoc. Prof. Dr. Altan Kayran \_\_\_\_\_  
Supervisor, **Aerospace Engineering Dept., METU**

**Examining Committee Members:**

Assist. Prof. Dr. Melin Şahin \_\_\_\_\_  
Aerospace Engineering Dept., METU

Assoc. Prof. Dr. Altan Kayran \_\_\_\_\_  
Aerospace Engineering Dept., METU

Dr. Volkan Nalbantoğlu \_\_\_\_\_  
Aerospace Engineering Dept., METU

Dr. Güçlü Seber \_\_\_\_\_  
Aerospace Engineering Dept., METU

Nadir Çetinkaya \_\_\_\_\_  
MİKES A.Ş

**Date:** 21.04.2008

**I hereby declare that all information in this document has been obtained and presented in accordance with academic rules and ethical conduct. I also declare that, as required by these rules and conduct, I have fully cited and referenced all material and results that are not original to this work.**

Name, Last name: Yücel DEVELLİOĞLU

Signature:

## **ABSTRACT**

### **ELECTRONIC PACKAGING AND ENVIRONMENTAL TEST AND ANALYSIS OF AN EMI SHIELDED ELECTRONIC UNIT FOR NAVAL PLATFORM**

Devellioğlu, Yücel

M.Sc., Department of Aerospace Engineering

Supervisor: Assoc. Prof. Dr. Altan Kayran

April 2008, 232 pages

The scope of this thesis is the design and verification of an electronic packaging of a device which is a subunit of a network system that is designed for combat communication in sheltering ship. According to the project requirements this device is subjected to some environmental and electromagnetic interference tests. This thesis includes design and manufacturing steps as well as vibration, shock and thermal analyses. Electromagnetic interference is examined through the design procedure and total shielding effectiveness of the device is calculated after the applications of some electromagnetic interference precautions which are given in details.

Keywords: Electromagnetic Packaging, EMI/EMC Shielding, Environmental Tests, Naval Platform, Random Vibration, Steady-State Thermal Analysis, Shock, MIL-STD-810 F, MIL-STD-461

## ÖZ

### DENİZ PLATFORMLARI İÇİN EMI UYUMLU ELECTRONİK BİR BİRİMİN ELEKTOMAGNETİK PAKETLEMESİ, ANALİZİ VE TESTİ

Devellioğlu, Yücel

Yüksek Lisans, Havacılık ve Uzay Mühendisliği Bölümü

Tez Yöneticisi: Doç. Dr. Altan Kayran

Nisan 2008, 232 sayfa

Bu tezin konusu deniz platformuna entegre edilen bir sistemin parçası olan bir cihazın elektronik paketlemesinin tasarım süreci ve bu tasarımın testler ve analizlerle doğrulanmasıdır. Tezin öznesi olan cihaz çalışır durumda çevresel şartlar testlerine ve elektromanyetik uyumluluk testlerine maruz bırakılmıştır. Tez, tasarım ve üretim adımlarının yanı sıra şok, titreşim ve sıcaklık analizlerini de içermektedir. Cihazın elektromanyetik uyumluluğu da tasarım süreci boyunca incelenmekte, elektromanyetik girişim için alınan önlemler ve uygulamaların detayları anlatılmakta ve bu uygulamalar sonrasında cihazın toplam ekranlama verimliliği hesaplanmaktadır.

Anahtar kelimeler: Elektromanyetik Paketleme, EMI/EMC, Ekranlama, Çevresel Testler, Deniz Platformu, Titreşim, Şok, Sıcaklık, MIL-STD-810F, MIL-STD-461

*To my mother, Elveda*

## ACKNOWLEDGEMENTS

This study took long way to run. I have many thanks.

Firstly, I would like to thank deeply my adviser Assoc. Dr. Altan KAYRAN for his patience and guidance.

I am grateful to my dear friend İlke AYDINCAK for his support from the very beginning of this thesis to the last day. I thank Evrim DİZEMEN as a cheerful working friend through courses. I thank Ahmer PEKDEMİR and Çağla ÖZTÜRK for their hospitality during final exams. I thank Seçil GÜLCAT; she is my thesis muse. I thank Müzeyyen ALPARSLAN for her endless encouragement and I thank my dear friends Bahar HASER and Yasemin TEKELİ for their support.

I thank Sabire HACIOMEROĞLU, once my manager but always a good friend of mine, for her kindness and cooperation.

I thank Koray NARBAY, Cem ÇANDAR, Dursun ÖNER, Ayhun ÜNAL and Mehmet YENER for their patience and suggestions.

I thank Nadir ÇETİNKAYA and Levent ÖZKAN for their percipient attitudes as managers.

And finally, my special thanks goes to my mother Elveda GÜRSES for her delicious pastries, her endless love and belief in me, my husband Umur DEVELLİOĞLU for his technical support and his patience, I thank my father Erdal GÜRSES for all his done for me, and my brother Onur GÜRSES for his being.

# TABLE OF CONTENTS

ABSTRACT .....	iv
ÖZ .....	v
ACKNOWLEDGEMENTS .....	vii
TABLE OF CONTENTS .....	viii
LIST OF FIGURES .....	xii
LIST OF TABLES .....	xvii
SYMBOLS AND ABBREVIATIONS .....	xix
CHAPTERS	
1.INTRODUCTION .....	1
1.1 DESIGN OF ELECTRONIC PACKAGING.....	2
1.1.1 COMPONENT (DEVICE) PACKAGING .....	4
1.1.2 MODULE (BOARD) PACKAGING .....	5
1.1.3 CHASSIS (SYSTEM) PACKAGING .....	6
1.2 RELIABILITY OF ELECTRONIC PACKAGING .....	8
2.DESIGN AND MANUFACTURING OF THE PACKAGING UNIT .....	14
2.1 REFERENCE DOCUMENTS .....	16
2.2 ELECTRONIC SPECIFICATIONS .....	17
2.3 MECHANICAL SPECIFICATIONS .....	17
2.4 DETAILS OF DESIGN .....	19
2.5 MANUFACTURING OF THE ELECTRONIC PACKAGING .....	26
2.6 ANALYSES PERFORMED ON THE PACKAGING UNIT .....	27
3.SHOCK TEST AND ANALYSIS FOR ENVIRONMENTAL QUALIFICATION... 28	
3.1 INTRODUCTION.....	28
3.2 THEORY.....	29
3.3 PRE-ANALYSIS .....	31
3.3.1 CASE 1: SOLID MODEL .....	35
3.3.2 CASE 2: HYBRID MODEL.....	41

3.3.3 CASE 3: FULL SHELL MODEL.....	46
3.4 SHOCK ANALYSIS .....	53
3.4.1 GEOMETRY .....	53
3.4.2 MESHING .....	55
3.4.3 LOADING AND BOUNDARY CONDITIONS.....	56
3.4.4 EVALUATION OF ANALYSIS RESULTS .....	60
3.5 SHOCK TEST.....	74
3.5.1 TEST LEVELS .....	74
3.5.2 TEST STEPS.....	78
3.6 RESULTS .....	78
4.VIBRATION TEST AND ANALYSIS FOR ENVIRONMENTAL QUALIFICATION.....	79
4.1 INTRODUCTION.....	79
4.2 THEORY.....	80
4.3 ANALYSIS .....	87
4.3.1 GEOMETRY .....	87
4.3.2 MESHING .....	88
4.3.3 LOADING AND BOUNDARY CONDITIONS.....	89
4.3.4 EVALUATION OF ANALYSIS RESULTS .....	95
4.4 VIBRATION TEST .....	99
4.4.1 TEST LEVELS .....	100
4.4.2 TEST STEPS.....	101
4.5 RESULTS .....	102
5.TEMPERATURE TEST AND ANALYSIS FOR ENVIRONMENTAL QUALIFICATION.....	103
5.1 INTRODUCTION.....	103
5.2 THEORY.....	104
5.3 ANALYSIS .....	112
5.3.1 GEOMETRY .....	112

5.3.2 MESHING .....	117
5.3.3 LOADING AND BOUNDARY CONDITIONS.....	118
5.3.4 EVALUATION OF ANALYSIS RESULTS .....	131
5.4 THERMAL TEST .....	133
5.4.1 TEST LEVELS .....	134
5.4.2 TEST STEPS.....	135
5.5 RESULTS .....	136
6.ELECTROMAGNETIC INTERFERENCE SHIELDING AND TEST FOR EMI/EMC QUALIFICATION .....	137
6.1 INTRODUCTION.....	137
6.2 DEFINITIONS.....	140
6.2.1 ELECTROMAGNETIC WAVES .....	140
6.2.2 EMISSIONS SUSCEPTIBILITY .....	144
6.2.3 DIFFERENTIAL AND COMMON MODE INTERFERENCES.....	145
6.2.4 ATTENUATION .....	146
6.3 STANDARDS.....	146
6.3.1 US MILITARY .....	147
6.3.2 EUROPEAN UNION (EU) .....	148
6.4 SHIELDING .....	149
6.4.1 SHIELDING THEORY AND SHIELDING EFFECTIVENESS .....	150
6.4.2 REFLECTION AND ABSORPTION LOSSES .....	153
6.4.3 SHIELDING AT APERTURES .....	158
6.4.4 CONDUCTIVE COATINGS .....	173
6.4.5 GALVANIC CORROSION.....	173
6.5 ELECTROSTATIC DISCHARGE.....	174
6.6 GROUNDING.....	175
6.6.1 SAFETY GROUND .....	176
6.6.2 SIGNAL GROUND.....	176
6.7 DESIGN .....	179

6.7.1 MATERIAL SELECTION .....	180
6.7.2 FIXED SEAMS AND FASTENERS .....	192
6.7.3 APERTURES AND AIR GAPS .....	195
6.7.4 GASKETS.....	195
6.7.5 FINISHINGS .....	197
6.7.6 GROUNDING AND ESD .....	197
6.8 TEST .....	198
6.8.1 CONDUCTED EMISSION TEST (CE102).....	201
6.8.2 RADIATED EMISSION TEST (RE101) .....	202
6.8.3 RADIATED EMISSION TEST (RE102).....	203
6.8.4 CONDUCTED SUSCEPTIBILITY TEST (CS101) .....	208
6.8.5 CONDUCTED SUSCEPTIBILITY TEST (CS114) .....	209
6.8.6 CONDUCTED SUSCEPTIBILITY TEST (CS116) .....	211
6.8.7 RADIATED SUSCEPTIBILITY TEST (RS101).....	212
6.8.8 RADIATED SUSCEPTIBILITY TEST (RS103).....	213
6.8.9 ESD TEST.....	213
6.9 RESULTS .....	214
7.CONCLUDING REMARKS AND FUTURE WORK .....	215
REFERENCES.....	220
APPENDICIES	
A. ELECTROMAGNETIC SHIELDING: SOME USEFUL DATA AND BASIC EQUATIONS .....	227
B. SHIELDING EFFECTIVINESS OF ALUMINUM, STEEL AND COPPER	230
C. GALVANIC CORROSION .....	231

## LIST OF FIGURES

Figure 1.1 Design process [3] .....	2
Figure 1.2 An electronic package of a device [5] .....	3
Figure 1.3 Hermetic vs. non-hermetic components [1].....	5
Figure 1.4 Typical chassis level packaging [1].....	7
Figure 1.5 Three levels of design [4] .....	8
Figure 2.1 3-D Model of the rack cabinet .....	15
Figure 2.2 19" Cabinet dimensions .....	17
Figure 2.3 "U" Dimensions .....	18
Figure 2.4 Properties of DIN 7985 M3x12 .....	
Phillips cross recessed pan head screw [15] .....	23
Figure 2.5 Internal environment of the device .....	24
Figure 2.6 Cabinet of the device .....	25
Figure 2.7 Tray with drawers used under the device .....	26
Figure 3.1 Various types of shock pulses [6].....	30
Figure 3.2 Analyzed model.....	32
Figure 3.3 State of stress for 3-D structue [20].....	33
Figure 3.4 Element types of ANSYS [19] .....	34
Figure 3.5 Loads for pre-analysis models .....	35
Figure 3.6 Boundary conditions for solid model .....	36
Figure 3.7 Contact regions for solid model.....	37
Figure 3.8 Deformation of solid model.....	38
Figure 3.9 Equivalent Von-Misses stresses of solid model after loading .....	39
Figure 3.10 Maximum shear stresses of solid model after loading.....	40
Figure 3.11 Loading and meshing of the hybrid model .....	41
Figure 3.12 Contact Regions of the Hybrid Model.....	42
Figure 3.13 Deformation of hybrid model .....	43
Figure 3.14 Equivalent Von-Misses stresses of hybrid model after loading .....	44
Figure 3.15 Maximum shear stresses of hybrid model after loading .....	45
Figure 3.16 Meshing of shell model .....	46
Figure 3.17 Loads and boundary conditions for shell model.....	47
Figure 3.18 Deformation of shell model .....	48
Figure 3.19 Equivalent Von-Misses stresses of shell model after loading .....	48
Figure 3.20 Maximum shear stresses of shell model after loading .....	49
Figure 3.21 Deformation and stress probes for mesh size study.....	52
Figure 3.22 Features of analyzed model .....	53
Figure 3.23 Point mass of the model excluding the chassis, cover and handles.....	54
Figure 3.24 Meshing through contact region .....	55
Figure 3.25 Acceleration shock load profile used in shock analysis .....	56

Figure 3.26 Modal frequencies .....	58
Figure 3.27 Boundary condition for shock analysis .....	59
Figure 3.28 Loading and boundary conditions in +x-direction .....	60
Figure 3.29 Deformation through +x-direction.....	61
Figure 3.30 Equivalent Von-Mises stresses through +x-direction.....	61
Figure 3.31 Maximum shear stresses through +x-direction.....	62
Figure 3.32 Deformation through -x-direction.....	62
Figure 3.33 Equivalent Von-Mises stresses through -x-direction.....	63
Figure 3.34 Maximum shear stresses through -x-direction.....	63
Figure 3.35 Deformation through +y-direction.....	64
Figure 3.36 Equivalent Von-Mises stresses through +y-direction.....	64
Figure 3.37 Maximum shear stresses through +y-Direction.....	65
Figure 3.38 Deformation through -y-Direction.....	65
Figure 3.39 Equivalent Von-Mises stresses through -y-direction.....	66
Figure 3.40 Maximum shear stresses through -y-direction.....	66
Figure 3.41 Deformation through +z-direction.....	67
Figure 3.42 Equivalent Von-Mises stresses through +z-direction .....	67
Figure 3.43 Maximum shear stresses through +z-direction .....	68
Figure 3.44 Deformation through -z-direction.....	68
Figure 3.45 Equivalent Von-Mises stresses through -z-direction.....	69
Figure 3.46 Maximum shear stresses through -z-direction.....	69
Figure 3.47 Deformation vs. time graph in -y-direction .....	71
Figure 3.48 Von-Mises stress vs. time graph in -y-direction .....	72
Figure 3.49 Maximum Von-Mises stress through -y-direction with different scale ..	73
Figure 3.50 Derritron VP 85 .....	75
Figure 3.51 Shaker profile in +z-direction shock loading .....	77
Figure 4.1 Relationship between time domain and frequency domain [25] .....	82
Figure 4.2 Gaussian distribution curve [6].....	83
Figure 4.3 A time history of a typical random vibration acceleration trace [6].....	84
Figure 4.4 Typical PSD curve.....	85
Figure 4.5 Positive and Negative Curve Slopes [6] .....	86
Figure 4.6 Geometry used for vibration analysis .....	88
Figure 4.7 Shipboard vibration exposure [7] .....	89
Figure 4.8 First harmonic mode .....	91
Figure 4.9 Second harmonic mode.....	91
Figure 4.10 Third harmonic mode .....	92
Figure 4.11 Eight harmonic mode.....	92
Figure 4.12 Boundary condition for modal analysis.....	93
Figure 4.13 PSD excitation used by ANSYS.....	94
Figure 4.14 Directional deformation through x-axis (Random vibration).....	96
Figure 4.15 Equivalent Von-Mises stress through x-axis (Random vibration) .....	96
Figure 4.16 Directional deformation through y-axis (Random vibration).....	97
Figure 4.17 Equivalent Von-Mises stress through y-axis (Random vibration) .....	97

Figure 4.18 Directional deformation through z-axis (Random vibration) .....	98
Figure 4.19 Equivalent Von-Mises stress through z-axis (Random vibration).....	98
Figure 4.20 Shaker profile in x axis random vibration loading .....	101
Figure 5.1 Component and PCB oriented approaches [31].....	104
Figure 5.2 Heat flow patterns on a test PCB [32] .....	105
Figure 5.3 Cross-sectional area of PCB [34] .....	106
Figure 5.4 Cross section through a vertical heated plate [37].....	110
Figure 5.5 Heated horizontal surface facing upward [37].....	110
Figure 5.6 Heated horizontal surface facing downward [37].....	111
Figure 5.7 The geometry of the thermal model.....	113
Figure 5.8 Representation of audio card .....	114
Figure 5.9 Meshing of thermal model.....	117
Figure 5.10 Heat sources on audio cards .....	119
Figure 5.11 Heat sources on control cards .....	119
Figure 5.12 Heat sources on main board.....	120
Figure 5.13 Surfaces where vertical convection coefficient is applied.....	125
Figure 5.14 Surfaces where upper and lower convection coefficients are applied...	125
Figure 5.15 Overall thermal loading .....	126
Figure 5.16 Temperature distributions after the second iteration .....	
(a)Bottom surface of Chassis, (b) Cover, (c) Vertical Plates, (d) PCBs .....	127
Figure 5.17 Temperature Distribution in Different Parts of the Chassis .....	
(a)Chassis-Bottom, (b) Cover, (c) Chassis-Sides, (d) PCBs.....	131
Figure 5.18 Temperature distributions on audio card .....	132
Figure 5.19 Temperature distributions on control card.....	133
Figure 5.20 Test chamber [38] .....	133
Figure 5.21 Thermal chamber obtained data during operational high temperature test .....	135
Figure 6.1 Electromagnetic spectrum [40].....	139
Figure 6.2 Propagation of an electromagnetic wave [58] .....	140
Figure 6.3 Electric field vs. magnetic field [41] .....	141
Figure 6.4 Electromagnetic wave behavior [41] .....	142
Figure 6.5 Emission susceptibility mechanism [40] .....	144
Figure 6.6 An electromagnetic shield [48].....	150
Figure 6.7 Reflection and absorption in a metal barrier [40].....	151
Figure 6.8 Electromagnetic attenuation through a conducting barrier.....	
of infinite extent [41] .....	153
Figure 6.9 Absorption loss as a function of skin depth [43] .....	156
Figure 6.10 Losses due to a conductive barrier [41].....	157
Figure 6.11 Electromagnetic wave propagation.....	
through a shield with an aperture [40] .....	159
Figure 6.12 Slot vs. holes [48] .....	160
Figure 6.13 Slots on a barrier [40] .....	161
Figure 6.14 Mesh panels and waveguide below cut-off [41].....	163

Figure 6.15 Shielding effectiveness and spacing between screws [39] .....	164
Figure 6.16 Lid designs [39] .....	165
Figure 6.17 Shielded glasses [43] .....	166
Figure 6.18 Joint cross sections [41].....	167
Figure 6.19 Seam overlap and spacing [43].....	168
Figure 6.20 Gasket and finger stock mounting [41] .....	170
Figure 6.21 Knitted wire mesh [58] .....	171
Figure 6.22 Oriented wire mesh [58] .....	171
Figure 6.23 Conductive elastomers [58] .....	172
Figure 6.24 Spiral metal strips [58].....	172
Figure 6.25 Signal point ground [48].....	177
Figure 6.26 Multi-point ground [48].....	178
Figure 6.27 Floating ground [48].....	179
Figure 6.28 The electronic design of the device .....	179
Figure 6.29 Reflection loss nomogram [39] .....	181
Figure 6.30 The inner source of the device.....	182
Figure 6.31 Shielding effectiveness of chassis for different frequencies.....	190
Figure 6.32 Shielding effectiveness of chassis between 10 Hz-30 MHz.....	191
Figure 6.33 Reflection and absorption losses for different frequencies.....	192
Figure 6.34 Back view of electronic equipment .....	193
Figure 6.35 Duosil wire mesh and silicone gasket [43].....	196
Figure 6.36 Shielding effectiveness for different finishings [39].....	197
Figure 6.37 Grounds for the Device.....	198
Figure 6.38 General test setup used through the tests of the device [46].....	200
Figure 6.39 Test set up for free standing EUT [46] .....	201
Figure 6.40 Limit curve used through RE101 test .....	202
Figure 6.41. RE102 Experiment graph of back plane noise 10 kHz - 30 MHz .....	204
Figure 6.42 RE102 Experiment graph of back plane noise .....	
vertical polarization 30-200 MHz .....	204
Figure 6.43 RE102 Experiment graph of back plane noise .....	
horizontal polarization 30-200 MHz.....	205
Figure 6.44 RE102 Experiment Graph of Back Plane Noise.....	
Horizontal Polarization 200-1000 MHz.....	206
Figure 6.45 RE102 Experiment Graph of Back Plane Noise.....	
Vertical Polarization 200-1000 MHz .....	206
Figure 6.46 RE102 Experiment Graph of Back Plane Noise.....	
Vertical Polarization 1-18 GHz.....	207
Figure 6.47 RE102 Experiment graph of back plane noise .....	
horizontal polarization 1-18 GHz.....	208
Figure 6.48 CS101 Voltage limit curve [46].....	209
Figure 6.49 CS114 Limiting levels .....	210
Figure 6.50 Packaging device under CS114 .....	211
Figure 6.51 Limit curve for RS101 test .....	212

Figure 6.52 Application of ESD test..... 213  
Figure A-1 Conductive Barrier ..... 227  
Figure A-2 A shield in a Media..... 229

## LIST OF TABLES

Table 1.1 Environmental failures outlined in MIL-A-87244.....	10
Table 1.2 Tests applied to the electronic packaging .....	12
Table 2.1 Shock absorber parameters .....	15
Table 2.2 Properties of aluminum alloy Al 5083 [12] .....	20
Table 2.3 Properties of castamide [13] .....	21
Table 2.4 Mechanical properties of structural steel R St 37-2 fo 2 mm [14].....	22
Table 3.1 Elements used in static analysis of solid model.....	37
Table 3.2 Statistics of solid model .....	40
Table 3.3 Elements used in static analysis of hybrid model .....	42
Table 3.4 Statistics of Hybrid Model .....	45
Table 3.5 Elements used in static analysis of shell model .....	46
Table 3.6 Statistics of shell model .....	49
Table 3.7 Overview of the models .....	50
Table 3.8 Mesh size study.....	52
Table 3.9 Moment of inertia of the model excluding the chassis, cover and handles	55
Table 3.10 Time increments for shock analysis.....	58
Table 3.11: Maximum Von-Mises stresses.....	70
Table 3.12: Maximum shear stresses .....	70
Table 3.13: Maximum deformation .....	70
Table 3.14 Specifications of Derritron VP 85.....	75
Table 4.1 Spectral densities.....	87
Table 4.2 10 Modes of the equipment.....	90
Table 4.3 Results of the analyses performed for different number of modes .....	95
Table 4.4 Maximum deformation occurred in random vibration.....	99
Table 4.5 Maximum Von-Mises stresses occurred in random vibration .....	99
Table 5.1 Characteristic length for various surfaces [37] .....	108
Table 5.2 Values for constants based upon the surface geometry [37].....	109
Table 5.3 Thermal conductivities of PCBs used in the analysis .....	116
Table 5.4 Elements used in thermal model .....	118
Table 5.5 Convection coefficients for first iteration .....	123
Table 5.6 Results of first iteration.....	123
Table 5.7 Convection coefficients @ $t_1=131$ degrees Fahrenheit.....	124
Table 5.8 Results of second iteration .....	128
Table 5.9 Convection coefficients for second iteration .....	128
Table 5.10 Results of third iteration.....	129
Table 5.11 Convection coefficients for fourth iteration.....	129
Table 5.12 Results of fourth iteration .....	130
Table 6.1 Test examples of MIL-STD-461 E [47].....	147

Table 6.2 Immunity test examples of EU [47]..... 148  
Table 6.3 Frequency, wavelength and skin depth values for inner source ..... 184  
Table 6.4 Losses due to inner source ..... 185  
Table 6.5 Frequency, wavelength and skin depth values for inner source ..... 186  
Table 6.6 Losses due to outer source ..... 188  
Table 6.7 Shielding effectiveness of Duosil .....  
for an aperture of 127 mm x 127 mm [43]..... 196

## SYMBOLS AND ABBREVIATIONS

$x, y, z$	Rectangular Coordinates
$\sigma_x, \sigma_y, \sigma_z$	Normal Stresses
$\tau_{xy}, \tau_{yz}, \tau_{zx}$	Shear Stresses
FEA	Finite Element Analysis
EMI	Electromagnetic Interference
RFI	Radio Frequency Interface
SE	Shielding Effectiveness
$a$	Acceleration
$t$	time
$g$	Earth gravity
$K$	Stiffness matrix
$M$	Mass matrix
$D_j$	Nodal displacement matrix
$R_j$	Time-dependent forcing matrix
ITS	Integration time step
$\sigma_{uts}$	Ultimate tensile strength
$\sigma_y$	Yield strength
$G$	Gravity units
$Y$	Probability density function
$X$	Instantaneous acceleration
$P$	Power spectral density
$g_d$	Acceleration density
$k_{p,e}$	In-plane thermal conductivity
$k_{n,e}$	Normal thermal conductivity
$N_c$	Number of copper layers

$N_g$	Number of glass epoxy layers
$t_t$	Total thickness
$t_{g,i}$	Thickness of the $i$ th glass-epoxy layer
$t_{c,i}$	Thickness of the $i$ th copper layer
$L$	Characteristic length
$h$	Natural convection coefficient
$\Delta t$	Time increment
$\Delta T$	Temperature difference
$k_c$	Thermal conductivity of copper
$k_g$	Thermal conductivity of glass-epoxy
$t_l$	Panel temperature
$\mu_o$	Permeability of free space
$\epsilon_o$	Permittivity of free space
$\eta_w$	Wave impedance
$\lambda$	Wave length
$f$	Frequency
$n$	Frequency counter
$E$	Electric field
$H$	Magnetic field
$d$	Distance from source
$Z_w$	Impedance of free space
$R$	Reflection loss
$R_e$	Electric field reflection loss
$R_p$	Plane wave reflection loss
$R_m$	Magnetic field reflection loss
$A$	Absorption loss
$B$	Re-reflection loss
$\sigma_r$	Relative conductivity with respect to copper

$\mu_r$	Relative permeability with respect to copper
C	Propagation velocity of electromagnetic waves
$f_c$	Cut-off frequency
k	Foundation modulus of seal
$t_b$	Barrier thickness
$E_f$	Modulus of elasticity of the flange
$I_f$	Moment of inertia of the flange
$d_f$	Spacing between fasteners
$t_d$	Depth of honeycomb
w	Width of honeycomb
r	Distance of shielded barrier from the source
D	Diameter of the hole

# CHAPTER 1

## INTRODUCTION

Electronic packaging is [1] “the technology of packaging electronic equipment” which includes the interconnection of electronic components into printed wiring boards (PWBs) and the interconnection of printed wiring boards to electronic assemblies.

Especially during the years following World War II, after the innovations in electronics, materials and production methods, electronic packaging became an important issue for the design process of a device. Today, electronic packaging has a wide range of use like in automotives, computers, telephones, entertainment equipment consumer products, aerospace, military equipment, marine equipment, medical equipment etc. Due to new manufacturing processes and new materials, there exists compact packing systems and the cost is reduced and the maintainability, ergonomics and favorable appearance is increased. This leads to mass production of products, especially for consumer goods.

When looking at the whole picture, it can be easily observed that electronic packaging is a “multi disciplinary design process” [2]. This process consists of conceptual design, relevant analyses, manufacturing, tests and field support required. At the end of these steps, an electronic circuit is turned into an electronic device. This design process is illustrated in Figure 1.1

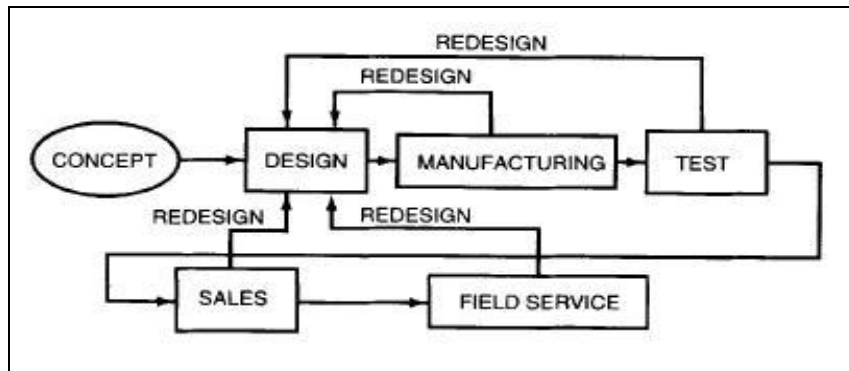


Figure 1.1 Design process [3]

Through the packaging design process some critical issues must be identified like,

- Performance requirements
- Working environment
- Manufacturability
- Reliability
- Cost

A product must meet the performance requirements while it is working in a specified environment with failure-free condition for a specified period of time. Besides these, its cost should not be so high to avoid its sale. The chosen reliable manufacturing methods and materials used in the production, usually results in an increase of the cost of the product, and a compromise has to be made to make the product affordable.

## 1.1 DESIGN OF ELECTRONIC PACKAGING

Any electronic packaging, such as the one in Figure 1.2, serves a fourfold function for the electronic circuit by providing it with power and signal interconnection, a path to dissipate heat, mechanical support, and a protected environment [4].



Figure 1.2 An electronic package of a device [5]

Environmental issues with regard to enclosure and product design include the following [3]:

- Emission of any fluids, whether liquid or gas, during operation
- Safety operators and personnel in the immediate area (cannot be compromised by any discharge from the unit)
- Provision for safe storage or disposal of any waste materials generated by the product
- Protection of any moving equipment from incidental contact
- Reduction of any emitted EMI/RFI to an allowable level, generally described as a “not harmful” level
- For most devices, acceptance of any EMI/RFI received
- Ability to withstand anticipated shipping and storage conditions while in an unpowered state, without any damage
- Ability to withstand expected operating environments while powered, and not allow damage to the operating parts of the unit
- Ability to withstand “reasonable” abuse and continue to operate (while a personal computer would not be expected to operate properly after being dropped off a desk, a calculator would be expected to operate properly.)

- The need for all materials used in the construction of the enclosure to be resistant to, or be protected from, all corrosive elements in the environment in which the device is expected to be used.
- Ability of protecting the environment from contamination by the electronics, like biomedical applications.

Through the years, the design of electronic packaging is divided into some levels due to the issues involved in the materials, configuration and space allocation. These levels are respectively [1];

- 1.Component (Device [4]) Packing Level
- 2.Module (Board [4]) Packing Level
3. Chassis (System [4]) Packing Level.

### **1.1.1 COMPONENT (DEVICE) PACKAGING**

Component-level packaging provides a method for attaching and interconnecting a silicon microcircuit to the next packaging level, and protecting the microcircuit from the environment [1] of corrosion,contamination and handling.

There are two kinds of technology is used for this level of packaging. If the silicone die is bonded to a ceramic package which has a lid for sealing the configuration, this is called “hermetic packaging”. If silicone die is bonded to a heat spreader in a plastic encapsulant, then this configuration is called “non-hermetic packaging”. These methods are illustrated in Figure 1.4.

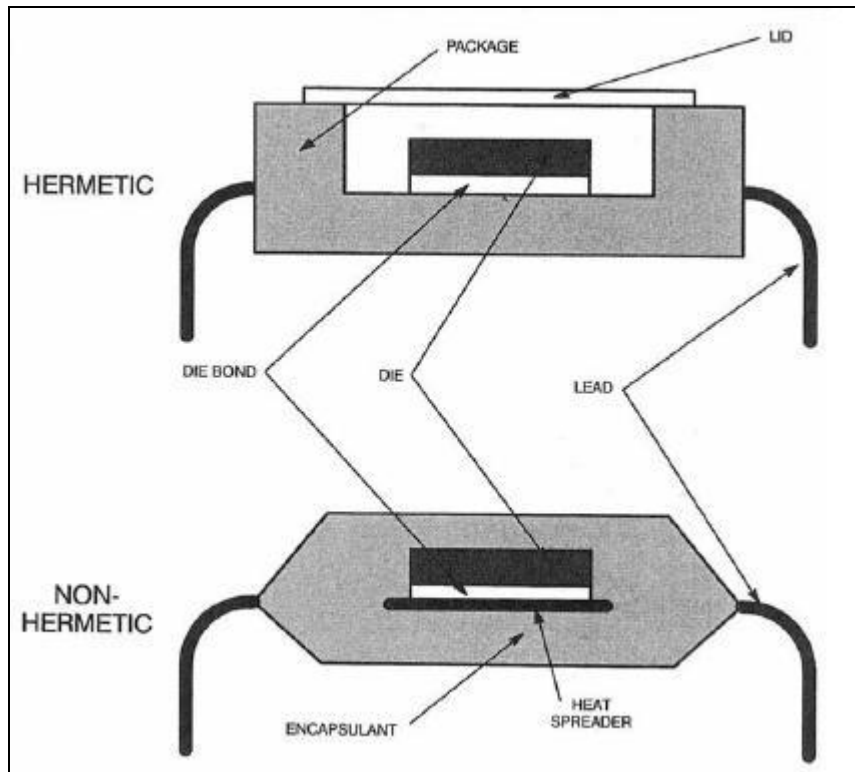


Figure 1.3 Hermetic vs. non-hermetic components [1]

All leaded and unlead components are [4]encapsulated in epoxy or silicone, or coated with inorganic materials such as silicone nitride in order to protect the package from handling and environmental effects like corrosion, humidity, contamination.

### 1.1.2 MODULE (BOARD) PACKAGING

Module packaging provides a method for interconnecting and attaching the components for the chassis packaging level.

The attaching methods, whose details of these methods are out of the scope of this thesis, have been developed in a way of generating miniaturized systems, optimum

performance and testable substeps. Mainly, the attaching method is divided into two groups according to the components used with leads and without leads. Leaded components are mounted by inserting component leads through holes in the printed circuit board and soldering the leads into place[2] like dual in-line package (DIP). On the other hand, methods like multichip module (MCM) or Chip-on-Board (COB) are types of Surface-Mount Technology (SMT) consisting of attaching non-leaded packages to the printed circuit board by placing the components on patterns of conductors that have been coated with solder paste [2]. (See Figure 1.3)

Conformal coating is applied on the components which are assembled onto boards in order to protect them from moisture and ionic contamination between components.

### **1.1.3 CHASSIS (SYSTEM) PACKAGING**

The third level of packaging is the chassis packaging which connects the components and mounts them into a chassis, forming a system. Sometimes this is the level of packaging seen by the user like computers - or subsystem [4].

Printed boards are mounted to the chassis by card slides, card cages, clamps, spacers and fasteners. The method differs from design to design. Although card slides increases heat dissipation, sometimes extra cooling methods are required in chassis packaging like the use of fins or cold plates.

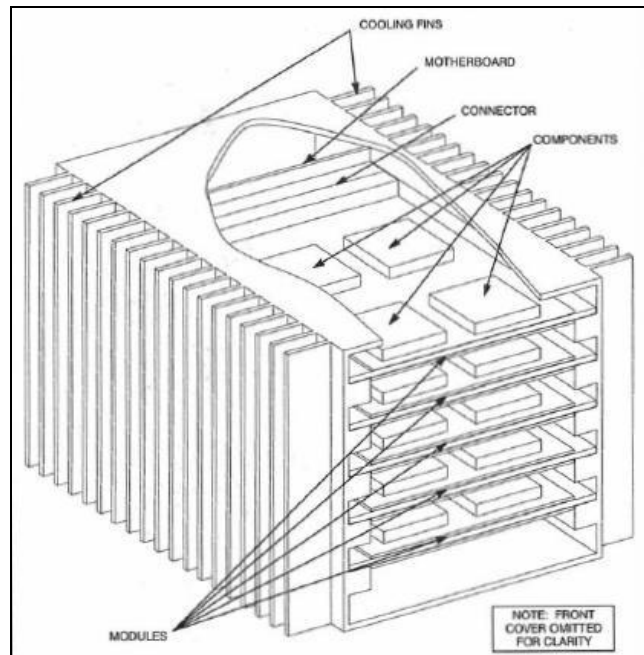


Figure 1.4 Typical chassis level packaging [1]

To conserve space, reduce costs, and improve reliability, many new systems are being packaged into a common chassis. A typical common chassis packaging, shown in Figure 1.4, includes support rails (card guides) by which the circuit boards are inserted into chassis or removed from it, and a motherboard with connectors that provides [1] electrical interconnection to other modules and the main chassis connectors.

Briefly, in the design of an electronic packaging; components are mounted, then the components are assembled on the board, and finally the board is installed into chassis of the subsystem as shown in Figure 1.5.

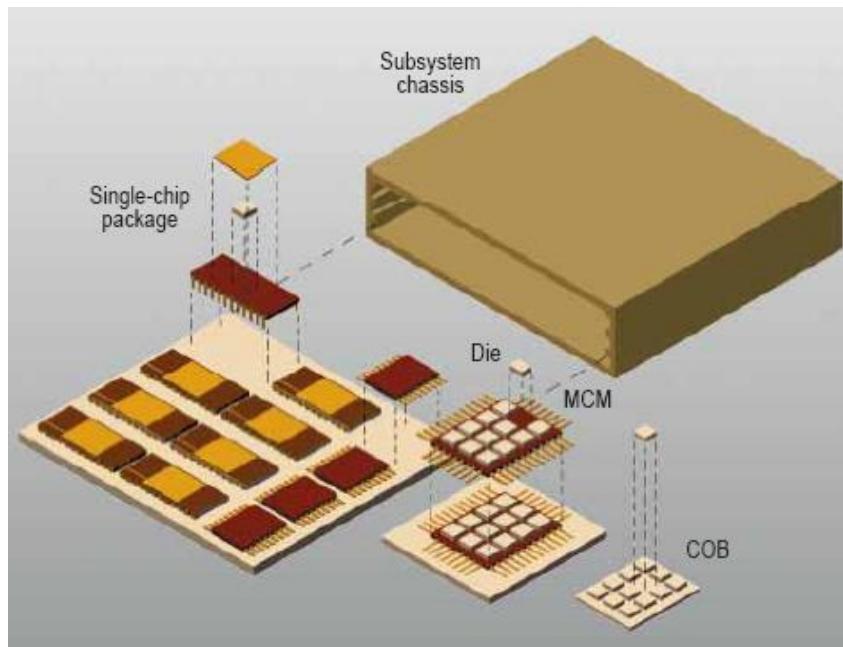


Figure 1.5 Three levels of design [4]

## 1.2 RELIABILITY OF ELECTRONIC PACKAGING

An important issue in electronic packaging concept is to get a reliable product at the end of whole processes. Reliability can be defined as [6] the probability of a product or device performing adequately for the period of time intended under the operating conditions encountered.

In another words, reliability is the fatigue/failure-free working condition of the design for the specific time period. The reliability of an electronic packaging has mechanical and electrical reliability aspects.. Electrical reliability is affected by temperature, current and voltage levels, corrosion , moisture, aging, solderability etc. Mechanical reliability is mainly influenced by vibration and shock as well as temperature.

Extensive military testing experience over a period of many years has shown that about 80% of the electromechanical failures are due to some type of thermal condition and about 20% of the failures are due to some form of vibration and shock [6]. Typical mechanical failures can be counted as broken wire leads, cracked solder joints, cracked ceramic packages, cracked silicone dies, broken connector pins such as module level and warped chassis, broken handles, broken card guides/cages, broken fasteners like spacers or screws in system level. Electromagnetic interference (EMI), Electrostatic Discharge (ESD) and noise induced failures are other important electromechanical failures.

There are two main sources of these failures which are poor design and manufacturing. Electronic packaging technology uses a variety of fabrication techniques such as welding, electroplating, and injection molding to accomplish its purposes [4]. The method of the manufacturing process is determined by the optimization of cost and manufacturing tolerances. Tight manufacturing tolerances can improve the quality and reliability of a product, but it also increases the costs [6]. To ensure the reliability of the electronic packaging, higher safety factors must be used, manufacturing processes must be checked carefully and analysis must be performed along with prototype testing.

For a computer or a television a temporary or a permanent system failure is not a critical case when it is compared to the failure of military or transportation equipments such as the ones used in aerospace, naval or land platforms . For this reason, some standards were developed to verify the electronic packaging by testing it at every level since failures were observed in component level as well as chassis level. For example field failures in electronic equipment hardware compiled by the U.S. Air Force over a period of about 20 years show that about 40% of these failures are related to connectors, 30% to interconnects, and 20% to component parts [6]. Failures in these areas can be due to handling, vibration, shock, and thermal cycling.

Field failures related to operating environments show that about 55% of the failures are due to high temperatures and temperature cycling, 20% of the failures are related to vibration and shock, and 20% are due to humidity [6].

After many years of tracing the sources of common failures, some standards and programmes are introduced in both component and system level. One example of this is MIL-A-87244. It is the document of U.S Air Force Avionic Integrity Program (AVIP) specifications. This document describes three environments that are known to produce many electronic failures, as shown in Table 1.1 [6].

Table 1.1 Environmental failures outlined in MIL-A-87244

A. Fatigue Failures Due to Vibration, Shock, and Thermal Cycling	
Electrical Lead Wires	Solder Joints
Plated Through Holes	Component case
B. High Operating Temperatures	
C. Aging Effects	
Corrosion	Water vapor
Embrittlement	Electrical drift

From the Table 1.1, it can be easily seen that AVIP examines the critical structures like leads, solder joints, and component packages under critical conditions like vibration, shock and thermal cycling environment.

The AVIP philosophy is to examine the geometric factors that have the greatest influence on the fatigue life of the electronic equipment [6]. These geometric factors are called ten “integral drivers” which are briefly; 1) Component Lead Wire Length, 2) Component Lead Wire Diameter, 3) PCB Thickness, 4) Large Component, 5)

Heavy Components , 6) Plug-in PCB Edge Supports, 7) Component Mounting on PCB, 8) Sharp-Bend Radius in the Lead Wire, 9) Conformal Coating Filling Under Small Square Mounted Chip Resistors and 10) Capacitors Solder Wicking Up into the Bend Radius on Small Axial Leaded Through-Hole Parts.

There are other military and non-military standard systems which define critical test environments and test methods especially for vibration, shock and thermal cycling like MIL-STD 810 F (Department of Defense (DOD) Test Method Standard for Environmental Engineering Considerations and Laboratory Tests) [7], MIL-STD 167-1A (Mechanical Vibrations of Shipboard Equipment) [8], MIL-S 901D (Shock Tests H.I. (High-Impact) Shipboard Machinery, Equipment, and Systems, Requirement For) [9], MIL-T-18303B (Test Procedures; Preproduction, Acceptance, and Life for Aircraft Electronic Equipment, Format For ) [10], STANAG 4370 (NATO Environmental Testing) [11], etc.

The primary purpose of all the testing related to shock and vibration [2] is to verify and characterize the dynamic response of the equipment and components thereof to a dynamic environment and to demonstrate that the final equipment design will withstand the test environment specified for the equipment under evaluation. Primary purpose of thermal tests is to verify that the equipment will operate properly under critical high and low temperatures.

The scope of this thesis is to present the design and analysis/test verification procedure of an electronic packaging of a device which is a subunit of a network system that is designed for combat communication in sheltering ship. In Chapter 2 the design procedure of the electronic packaging is briefly explained. The design is verified mostly by the operational tests and relevant analyses. The tests are planned to be applied to the electronic equipment after the related analysis has been completed. In Chapter 3, verification of the electronic packaging due to the mechanical shock

analysis and tests are given with its theory and application story. Shock test is applied in accordance with the specification set forth in MIL-STD 810 F. In Chapter 4, random vibration response of the electronic packaging has been obtained. The input power spectrum density function is again referenced to MIL-STD 810 F. Random vibration test has also been performed and the operational control of the device is performed. In Chapter 5, the thermal analysis of the packaging unit has been performed to determine the temperature distribution in the device base on the thermal loading supplied by the electronic units inside the device. Thermal analyses have been performed by finite element method and the device is also subjected to thermal test to verify the operability of the device under the thermal loads induced. It should be noted that the tests were merely operational tests to verify that the device works properly under the specified loading. In Chapter 6, fundamental information has been given about the EMI/EMC issues in electronic devices, and the shielding design of the device, which is designed and analyzed within the scope of this thesis, against electromagnetic interference has been described. In addition, Chapter 6 also contains the results of the electromagnetic interference tests which are performed in accordance with the standard MIL-STD 461 and Electrostatic Discharge test performed in accordance with the standard EN61000-4-2.

The list of the tests, which are performed, are indicated in Table 1.2. These tests are decided based on the project requirements imposed. The tests mainly cover certain environmental and electromagnetic interference tests.

Table 1.2 Tests applied to the electronic packaging

<b>TEST NAME</b>	<b>STANDARD NAME</b>
Vibration Test	MIL-STD-810F
Shock Test	MIL-STD-810F

Table 1.2 Tests applied to the electronic packaging (Cont'd)

Drip Test	MIL-STD-108E
Humidity Test	MIL-STD-810F
High Temperature Test	MIL-STD-810F
Low Temperature Test	MIL-STD-810F
Acoustic Noise Level Test	MIL-STD-1474D
Conducted Emission Test (CE 102)	MIL-STD-461E
Radiated Emission Test-Magnetic (RE 101)	MIL-STD-461E
Radiated Emission Test Electric (RE 102)	MIL-STD-461E
Conducted Susceptibility Test (CS 101)	MIL-STD-461E
Conducted Susceptibility Test (CS 114)	MIL-STD-461E
Conducted Susceptibility Test (CS 116)	MIL-STD-461E
Radiated Susceptibility Test (RS 101)	MIL-STD-461E
Radiated Susceptibility Test (RS 103)	MIL-STD-461E
Inclination	
Electrostatic Discharge	EN61000-4-2

## **CHAPTER 2**

### **DESIGN AND MANUFACTURING OF THE PACKAGING UNIT**

The device whose electronic packaging is the subject of this thesis, is a part of combat communication network system of a frigate. The device functions as an interface for master and slave units with the audio/control lines of radio equipment.

Ships and submarines will generally make use of console cabinets to support their electronic equipment, since there is usually more room available and weight is not very critical [6]. The particular “device” is mounted in a 19” cabinet by front panels. The cabinet is placed in the deck below the cabin.

The working environment of the device is a shipboard. The vibration range for ship is taken as between 1 Hz and 50 Hz [6]. The most common range specified in the documents is 12 Hz to 33 Hz. This is low frequency compared to the air platforms but this range is critical because of their larger wavelengths of the waves. For shipboards, the maximum acceleration in the 1-50 Hz range is 1g, and this level of acceleration is mainly due to the working engines and propellers. For military ships, shock is an important loading due to explosions and therefore shock tests are critical for reliability of electronic equipments.

There can be serious damages caused by shocks experienced in electronic equipments so it is not desirable to have a very rigid structure supporting the electronics, because a very rigid structure may not deform enough to absorb much of the strain energy [6]. Because of this there are two wire rope shock isolators that are mounted under the

rack cabinets and two of them is placed in the back part of the cabinet to protect the equipments from shock and vibrations. The three dimensional model of the rack cabinet and the layout of the shock isolators is shown Figure 2.1.

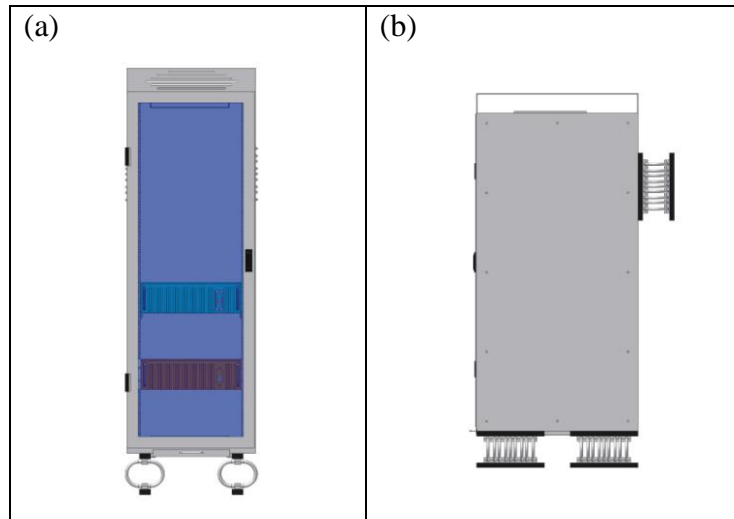


Figure 2.1 3-D Model of the rack cabinet

The parameters of the absorbers used are given in Table 2.1. The device is mounted near the center of cabinet since there are some sensitive components in the device that cannot withstand high g forces. These components should be mounted at the maximum elastic distance from the application points of the shock load [6].

Table 2.1 Shock absorber parameters

Parameter	Value	Origin
Nominal Weight	300 kg	Specified
Dimensions	X: 599.4 mm Y: 1783.1 mm Z: 816.4 mm	Specified

Table 2.1 Shock absorber parameters (Cont'd)

Shock Input	30 g, 18 ms sawtooth 20 g, 11 ms sawtooth	Specified
Vibration Input	MIL-STD-810 F	Specified
Center of Gravity	Centered	Assumed
Fragility	20 G	Assumed

Sea environment is also a harsh corrosive environment. Therefore, serious precautions must be taken for corrosion in the electronic packaging of devices even if they work in a cabinet in a cabin below the deck.

## 2.1 REFERENCE DOCUMENTS

There are certain reference documents which are used throughout the design, analysis and testing of the electronic packaging of the device. Since the device is mounted in a military frigate, the documents were all military standards. The military standards referenced within the context of the present work are listed below.

- MIL-STD-461E Requirements for the Control of the Electromagnetic Interference Characteristics of Subsystems.
- MIL-STD-462D EMI Characteristics.
- MIL-STD-810F Environmental Engineering Considerations and Laboratory Tests
- MIL-STD-2036A General Requirements for Electronic Equipment Specifications.
- MIL-STD-167/1 Vibration Tests
- MIL-STD-454 Safety Characteristics

## 2.2 ELECTRONIC SPECIFICATIONS

The main electronic specifications for this device are given below in items.

- The device is fed by 28 VDC, and this voltage will be provided by the power supply units which will work through 115 VAC of frigate's main current.
- The unit must have a safety ground.
- All the PCB's should have an internal ground plate which must be tied to a single point ground.
- The unit must be compatible with MIL-STD-462 for EMI/RFI. All wires must be shielded, and military connectors should be used.

## 2.3 MECHANICAL SPECIFICATIONS

The main mechanical specifications for this device are given below in items.

- The unit must weight less than 25 kg.
- The unit will be panel mounted in a 19" Rack Cabinet, as shown in Figure 2.2

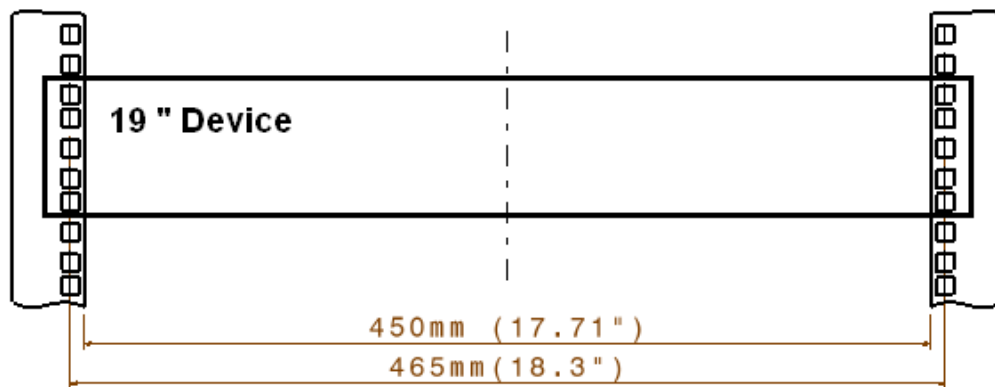


Figure 2.2 19" Cabinet dimensions

The height of the unit shall not exceed 3 U (1 U = 44.45 mm, 3 U is 133.35 mm), the length of the unit must not exceed 420 mm and the depth of the unit must not exceed 500 mm. The standard U dimension which are used in the rack cabinets are given in Figure 2.3.

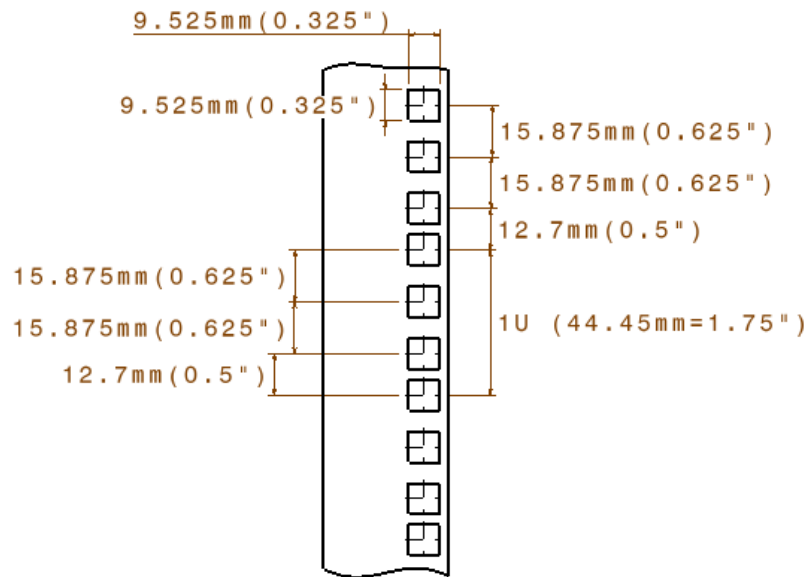


Figure 2.3 "U" Dimensions

Thus, the dimensions of the unit will be less than or equal to :

500 mm (width) x 420 mm (length) x 133.35 mm (height) (W x L x H).

The limitations about length and width of the unit is due to the specifications about 600 mm, 19" Rack Cabinet. Here, 600 mm is the depth of the cabinet and other dimensions for a 19" system is given in Figure 2.3. In addition, other main design specifications were decided as:

- All screws, washers, and nuts must compatible with military standards. Fasteners and inserts must have self locking property.

- The temperature range is from -15°C to 55°C for storage, and -15°C to 55°C for operating conditions.
- For the Aluminum usage, Aluminum 5000 or 6000 series must be preferred.

## **2.4 DETAILS OF DESIGN**

The radio trunk interface unit is modeled by commercial 3-D modeling program Autodesk Inventor Professional 11.

There is a limit for the dimensions of the chassis. Within these limitations, the dimensions are determined by the PCB's used in the device. The dimensions of the mainboard mainly fixed the length and width of the chassis and the dimensions of the slave cards set the height of the chassis. So, the borders of the chassis is defined by the rack cabinet, and the details are fixed by the modules mounted in the device.

Aluminum is preferred as the built-up material of the main chassis and cover of the electronic packaging. This decision was made by considering the the following properties of Aluminium.

- Formability
- Mechanical Properties of its alloys
- Thermal and Electrical Conductivity
- Corrosion Resistance
- Strength-to-Weight-Ratio
- Reflectivity
- Cryogenic Property
- Finishability

In general, metals that are mechanically formed are more desirable than cast metals, which have a relatively low percentage elongation. The materials that are best suited for shock are ductile materials with a high yield point, a high ultimate strength, and a high percentage elongation [6]. Therefore, wrought aluminum alloy is preferred.

Wrought Aluminum alloys are grouped as the percentage of the elements other than aluminum. Aluminum 5000 series have magnesium as major alloying element whereas for 6000 series silicon and magnesium are the major alloying elements. For marine applications, mainly, Aluminum 6061, 6063, 5083, 5086, 5182, 5454, 5456 are used. For the chassis at first, Al 6061-T6 was selected as the build-up material. Here T6 indicates artificial aging after heat treatment. But then it was realized that 5000 series offer better corrosion resistance property than 6000 series. So, Al 5083 H321 was used throughout the manufacturing process. This aluminum series could not be subjected to heat treatment, they are subjected to work hardening process indicated by H321. This material has a good combination of strength and corrosion resistance, and the mechanical and physical properties are summarized in Table 2.2.

Table 2.2 Properties of aluminum alloy Al 5083 [12]

Typical Mechanical Properties of Al 5083 H321	
Ultimate Tensile Strength (MPa)	317
Tensile Yield Strength (MPa)	228
Shear Strength (MPa)	190
Elongation at Break (%)	16
Hardness Vickers (HV)	96
Machinability (%)	30
Physical Properties of Al 5083	
Density	2.66 g/cm <sup>3</sup>
Modulus of Elasticity	71 GPa

Table 2.2 Properties of aluminum alloy Al 5083 [12] (Cont'd)

Melting Point	591-638 °C
Electrical Resistivity	5.9e-006 Ω.cm
Thermal Conductivity	117 W/m.K

Besides aluminum, also steel and cast polyamide (castamide) were used as a manufacturing material of some parts. Castamide is an engineering plastic which has good material properties like impact resistance, manufacturability, low friction constant. The detailed list of the mechanical and physical properties is given in Table 2.3.

Table 2.3 Properties of castamide [13]

Typical Mechanical Properties of Castamide	
Tensile Strength (MPa)	85
Compressive Strength (MPa)	95
Impact Resistance (Charpy, without notch, ISO 179)	Not Broken
Impact Resistance (Izod, with notch, ISO 179) (Kj/m <sup>2</sup> )	5.6
Friction Coefficient	0.39
Elongation (%)	>20
Physical Properties of Castamide	
Density	1.15 g/cm <sup>3</sup>
Melting Point	220 °
Modulus of Elasticity	4000 MPa
Electrical Resistivity	>10 <sup>14</sup> Ω.m
Max. Working Temperature	110 °C

Steel is used as a built-up material of the 19” Rack Handles which are the main assembly interface of the equipment to the rack cabinet . Since steel has a larger tensile strength than aluminum, a thin steel sheet will work as a handle. Therefore 2 mm thickness is used. The type of steel used in the handles is a structural steel, DIN 17100 R St 37-2 ."R" indicates the deoxidation level of "killed" meaning anti-corrosive and "2" is the grade. The mechanical properties of R St 37-2 is given in Table 2.4.

Table 2.4 Mechanical properties of structural steel R St 37-2 fo 2 mm [14]

Typical Mechanical Properties of R St 37-2	
Proof Stress 0.2% (MPa)	235
Tensile Strength (MPa)	360-510
Shear Strength (MPa)	175
Elongation (%)	18-20

Screw head selection is also an important criteria in electronic equipment applications. Phillips-head screws are preferred over slotted head screws due to their ability of increased tightening torque, and pan head screws are preferred over round-head screws due to absence of sharp edges in them [2]. Therefore, especially for the cover, stainless steel DIN 7985 A Phillips Cross Recessed Pan Head M3x12 Machine Screws are used (Figure 2.4). The spacing between cover screws is calculated based on the electromagnetic interference (EMI) criteria since there is a gap between cover and chassis which causes reduction in shielding effectiveness. The details of these calculations are given in Chapter 6.

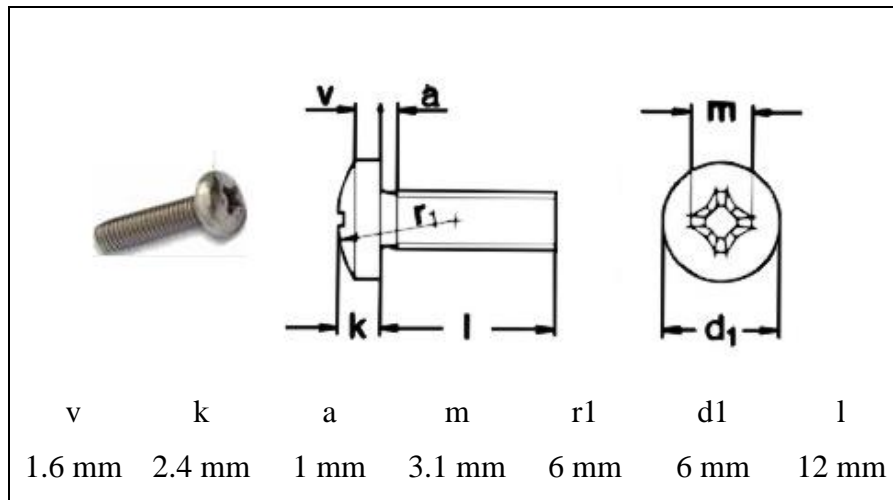


Figure 2.4 Properties of DIN 7985 M3x12 Phillips cross recessed pan head screw [15]

Another important design criteria for the electronic packaging of this device was the thermal design. Thermal design includes [2]:

1. Equipment total heat generation and how that heat will be dissipated to the local external environment
2. Equipment internal environment, which is the environment experienced by modules, subassemblies, and components
3. Control of critical temperatures of the components

The initial analysis results showed that no fans were needed for heat dissipation, implying that all cooling for this device could be based on conduction cooling, and on convection cooling both free and forced since there are some fans placed on the upper and bottom parts of the cabinet..

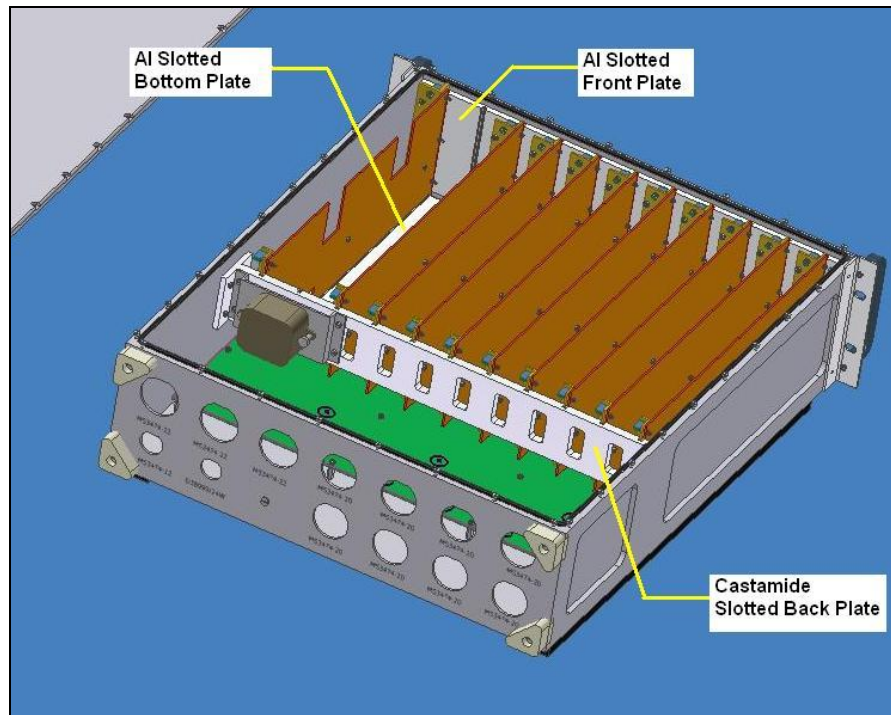


Figure 2.5 Internal environment of the device

As the internal environment, there are 9 audio cards, one control card and a main board inside the device. Audio cards and control card is placed on the main board. There was no card cage for this placement, instead there were slotted plates. The front and bottom plates were made up of aluminum and the back plate is made up of castamide (cast polyamide). Actually, all the slotted plates had been made up of polyamide at first, but it was recognized that some critical modules on the boards must be cooled by conduction, so aluminum was preferred because of its better thermal conductivity. These plates were assembled to the chassis directly by screws. The inner configuration of the device is illustrated in Figure 2.5.



Figure 2.6 Cabinet of the device

Although the device is panel mounted in a cabinet as shown in Figure 2.5, because of its weight, it is supported by a tray under it which is assembled to the side profiles of the cabinet by telescopic slides which has a lock which can be opened and closed. These drawers have an advantage of easy access to the device without taking it out of the cabinet. Figure 2.6 shows both tray and the telescopic slides.

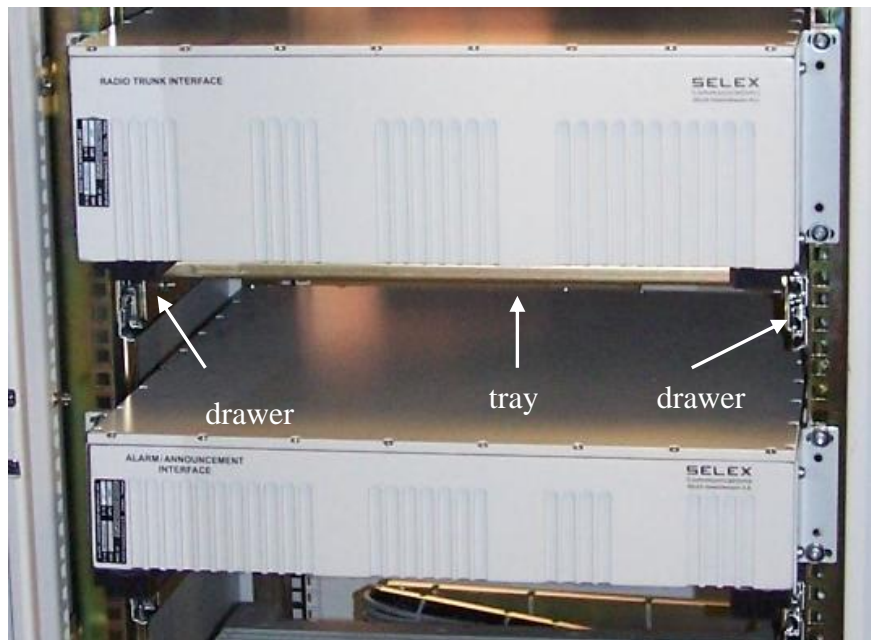


Figure 2.7 Tray with drawers used under the device

## **2.5 MANUFACTURING OF THE ELECTRONIC PACKAGING**

The manufacturing of the electronic packaging of the device is based on aluminum welding. The chassis is divided into sub-panels. The panels were manufactured separately, then they came together by a welding process which was applied from outside. Since the thickness of the panels are 9 mm at welding points, there no warping occurred.

## **2.6 ANALYSES PERFORMED ON THE PACKAGING UNIT**

Within the scope of this thesis, three major analyses have been performed to aid the qualification of the unit together with the operational environmental tests that have been performed. The results of the analyses will be used to aid the improvement of the design of the packaging unit.

The analyses focuses on the following three areas:

- Shock analysis will be performed to investigate the effect of a 20 g for 11ms load applied in three axes based on the procedures given in MIL-STD-810 F. This analysis will ensure that the ultimate stresses are not exceeded and the electronic packaging is designed to ensure that the unit will remain in tack [16].
- Random vibration simulation according to the MIL-STD-810F. In this analysis procedure, a pre-modal analysis is performed since random vibration method is based on modal superposition. The results of the analysis helps the determination of the probabilistic stress levels which occur due to random vibration environment of the ship
- Thermal analysis to ensure that average surface temperatures do not exceed 60°C for high temperature and -10 °C for low temperature per MIL-STD-810 F procedures.

## **CHAPTER 3**

### **SHOCK TEST AND ANALYSIS FOR ENVIRONMENTAL QUALIFICATION**

#### **3.1 INTRODUCTION**

The mechanical shock is defined as a transmission of energy to a system which takes place in a short time compared with the natural period of oscillation of the system [17]. The excitation of shock is non-periodic. It is usually in the form of a pulse or a step. If the excitation continues for a longer period of time lasting for several periods then shock loading is treated as transient loading.

The important characteristic of shock is that the motion of the system upon which the shock acts is affected both by the frequency of the shock excitation and the natural frequency of the system [18]. The excitation of the natural frequencies in a complex structure can produce four basic types of failures in electronic systems [6]; (1) high stresses, which can cause fractures or permanent deformations in the structure; (2) high acceleration levels, which can cause relays to chatter, potentiometers to slip, and bolts to loosen; (3) high displacements, which can cause impact between adjacent circuit boards-cracking components and solder joints, breaking cables and harnesses, and fracturing castings; and (4) electrical malfunctions that occur during the shock but disappear when the shock energy dissipates.

For naval equipments, underwater explosions are the main and the most severe design criteria for shock environment. Other sources of shock loads include objects striking

an equipment, structural borne stress waves such as caused by gunfire recoil, the equipment falling and striking other objects, and forces induced by handling and shipment [2].

In this chapter, the effect of the shock load on the equipment is examined, the analysis procedure of the model is explained and discussed, finally test result and analysis data are compared.

## **3.2 THEORY**

Due to the different sources of shock load, different methods are developed for specifying shock motion and its effects. The three most popular methods are [6] ;

- (1) pulse shock,
- (2) velocity shock, and
- (3) shock response spectrum.

Pulse shock is concerned with accelerations or displacements. There are many pulse shock forms like half sine wave, square wave, and different types of triangular waves. Some of them are illustrated in Figure 3.1.

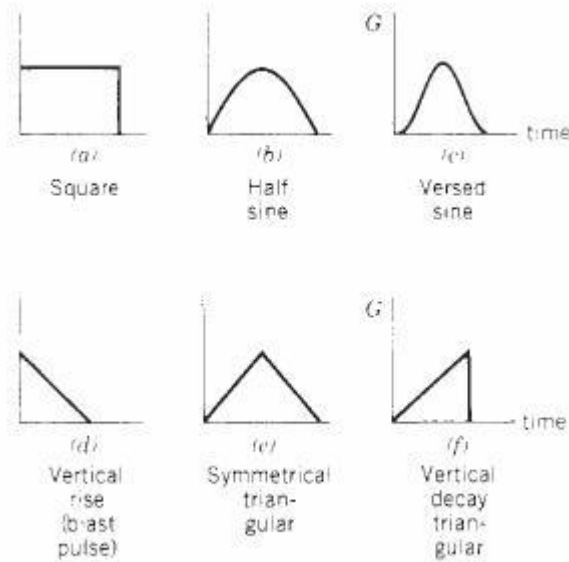


Figure 3.1 Various types of shock pulses [6]

Velocity shock deals with systems which go through a sudden velocity change. The most well-known example of the velocity shock is a falling equipment. The simulating test of a velocity shock of this type is drop test.

Pulse shocks are often specified for testing electronic equipment, and many military specifications such as MIL-E-5400, MIL-STD-810, and MIL-T-5422 define different types of shock pulses and detailed methods for testing with these pulses [6].

The most common pulse shock used for testing equipment of commercial, industrial, or military service is half-sine pulse shock. This pulse is easy to generate, analyze and evaluate. Pulse shocks are measured with an accelerometer and defined by acceleration and time. The area under the shock pulse represents the change in velocity and the area under the velocity curve represents the displacement. But

besides all the benefits of this method, it does not reflect the actual shock environment.

In this thesis, the shock environment is defined by MIL-STD-810 F MIL-STD-810F, method 516.5, Procedure I (Functional Shock). In this specification, shock is described in terms of acceleration as saw-tooth type with 20 g peak acceleration for 11 ms. Saw tooth shock profile is applied to the mechanical unit designed during the shock tests. However, during the shock analysis performed by the finite element method half sine wave shock is used for 11 ms. The peak acceleration level is kept same as the test case, and it is intended to check the shock response of the mechanical unit with a shock pulse different from the one used in the test.

### **3.3 PRE-ANALYSIS**

The 3-Dimensional solid model design of the packaging is created with the commercial program Inventor 11.0 and all the analysis in this thesis is performed by the commercial finite element program ANSYS Workbench 11.0.

Before simulating shock analysis with ANSYS, there are some pre-steps done for deciding the most effective and useful analysis model. Firstly, the 3-D solid model is simplified for the analysis. The analyzed model is a combination of four basic parts which are the cover, chassis and two 19" Rack handles as shown in Figure 3.2. The PCB cards, modules, card interface structures for mounting PCB Cards into the chassis are not modeled, instead they are represented by point masses. The connectors in the back part of the chassis are not placed, but their cut outs are left at the back part.

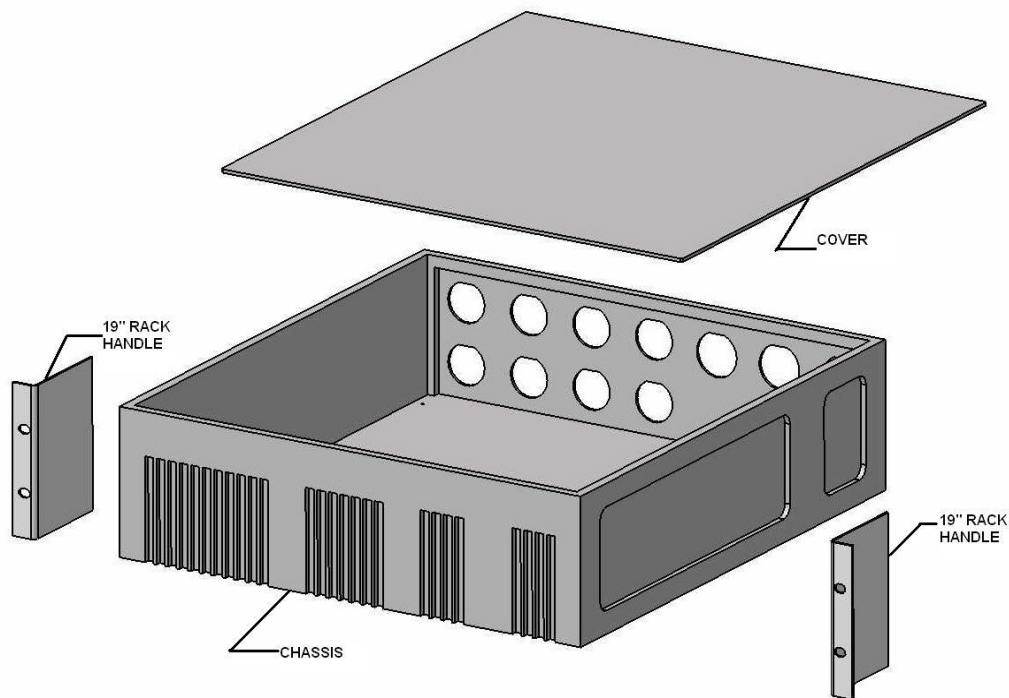


Figure 3.2 Analyzed model

Three different kinds of finite element models for analyzing such a geometry could be created since the structure is relatively a thin walled structure. These models are:

- Solid model
- Hybrid model
- Shell model

Solid Model is 3-D structure. The solid elements used for this analysis of the model are solid 186 and solid 187. These are structural solid elements which consist of six stresses (all normal and shear stresses) shown in Figure 3.3. Solid 186 is a 20 noded quadratic hexahedron element. Solid 187 is a 10 noded quadratic tetrahedral element.

Solid 186 elements can also be tetrahedral and can automatically create transition between hexahedral and tetrahedral using pyramids [19].

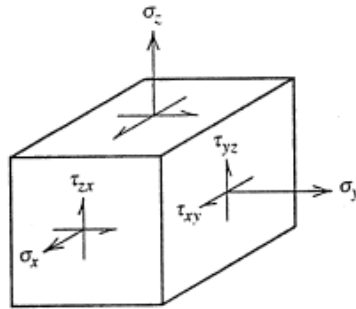


Figure 3.3 State of stress for 3-D structure [20]

Shell model is used for mathematically simulating 3-D structure with a 2-D structure. The analysis of 3-D structure is simplified through the plane stress or plain strain assumptions.

A structure can be assumed as in a plane stress state when [21]:

- The structure has a "thin" dimension relative to other two dimensions.
- All loads lie in a plane.
- Surface shears  $\tau_{zy}$  and  $\tau_{zx}$  vanish and  $\sigma_z = 0$
- $\sigma_x, \sigma_y, \tau_{xy}$  do not depend on the thickness coordinate.

The elements used for shell analysis are Shell 181 elements. These are four noded linear quadrilateral elements. Shell elements offer computationally efficient solutions for modelling shell structures when compared to solid elements [22].

Hybrid model is a mixture of solid and shell model. In this study, hybrid model is created as a combination of solid chassis with shell cover and shell handles.

All structural element types of ANSYS are shown in Figure 3.4.

Element Order	2D Solid	3D Solid	3D Shell	Line Elements
Linear	 PLANE42 PLANE182	 SOLID45 SOLID185	 SHELL63 SHELL181	 BEAM3/44 BEAM188
Quadratic	 PLANE82/183 PLANE2	 SOLID95/186 SOLID92/187	 SHELL93	 BEAM189

Figure 3.4 Element types of ANSYS [19]

In order to decide the appropriate model for the analysis, 3 models are prepared for doing pre-analysis on the model. Pre-analysis a simple analysis performed by static analysis module of ANSYS to compare the three different finite element models and decide on an appropriate mesh size. A 2g load is applied both in x and y directions as a ramped function. x and y directions with respect to the mechanical unit are shown in Figure 3.5.

$$\vec{a} = 19620 \ i + 19620 \ j \ (\text{mm/s}^2)$$

The slots on the handles are chosen as fixed support condition. Same loads are applied under same boundary conditions for all models.

### 3.3.1 CASE 1: SOLID MODEL

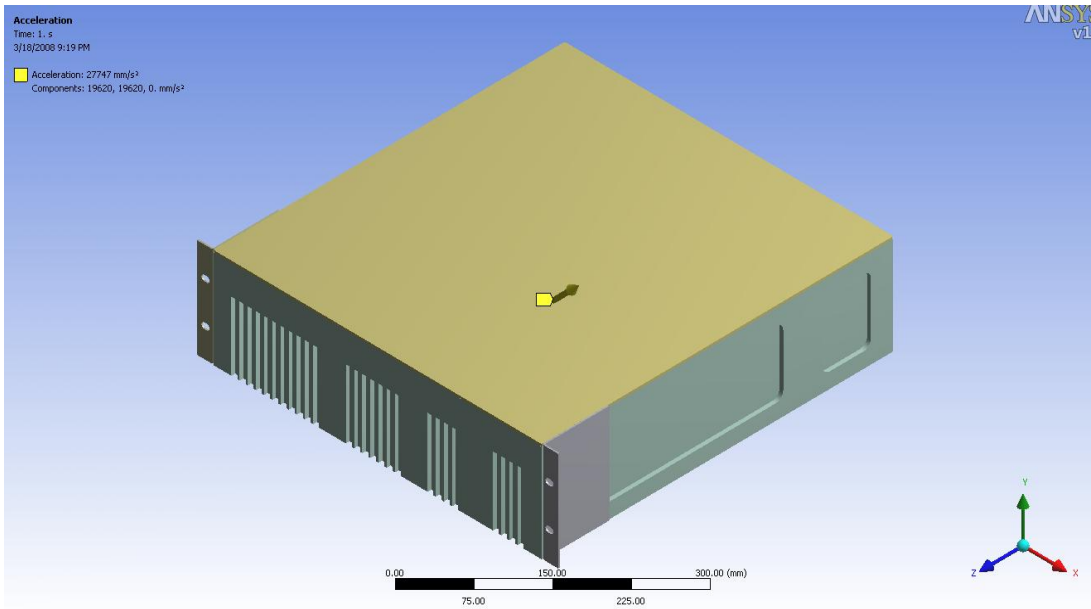


Figure 3.5 Loads for pre-analysis models

The inner faces of the front slots shown in Figure 3.6 are chosen as fixed supports since the equipment is assembled to the 19" rack cabinet from front handle screws.

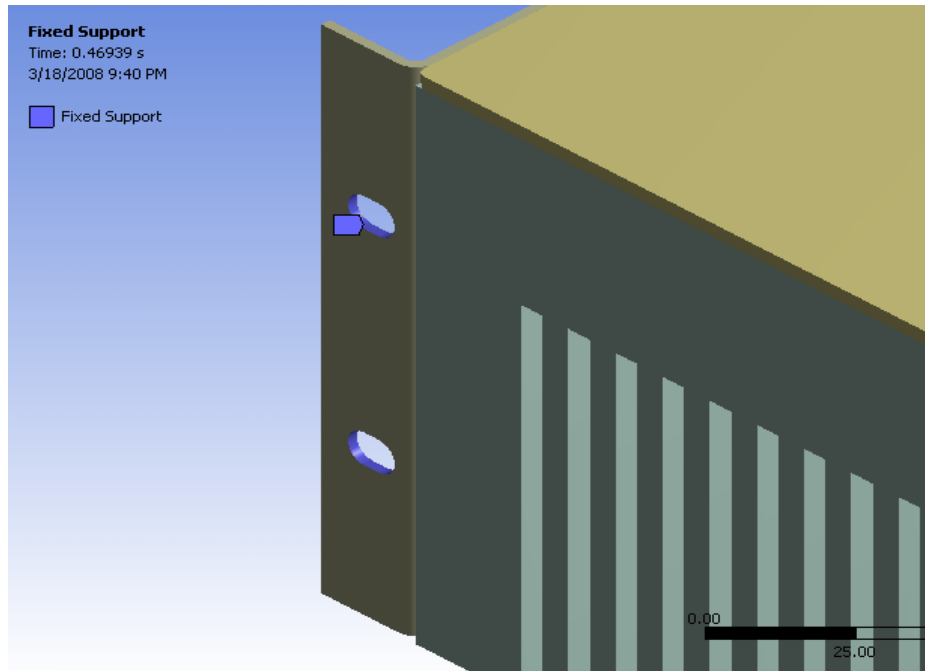


Figure 3.6 Boundary conditions for solid model

The elements used in the solid model analysis are listed in Table 3.1. These elements are solid elements and contact elements. ANSYS Workbench 11.0 has a property of contacting specified surface-to-surface, edge-to-edge, edge-to-surface. There are some methods developed for these contact situations like normal lagrange, multi point contact or pure penalty.

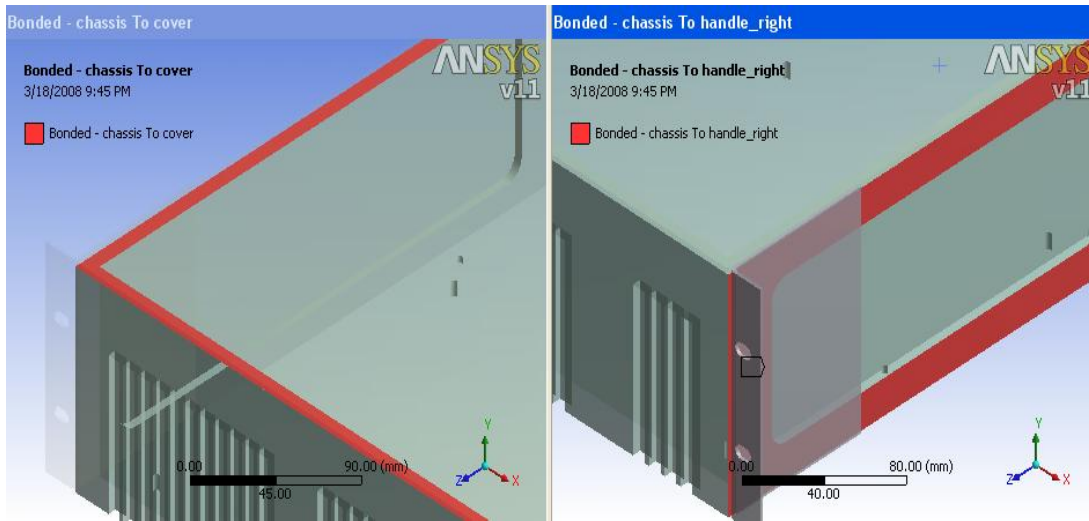


Figure 3.7 Contact regions for solid model

Through the pre-analysis steps and other structural analysis in this thesis pure penalty method is used for joining cover to chassis and joining handles to the sides of the chassis. When defining a contact region between two features, ANSYS defines one contacting feature as “contact” and the other as “target”. The order of selecting or the feature definition as target or contact does not make any difference. These contact regions are illustrated in Figure 3.7 and contact element type is given in Table 3.1. In the pure penalty method, permanent contact is generated between the contact and target elements.

Table 3.1 Elements used in static analysis of solid model

ANSYS Element Name	Description	Location
Solid 187	10 Node Tetrahedral Structural Solid	Chassis, Cover and Handles
Solid 186	20 Node Hexahedron Structural Solid	Chassis, Cover and Handles

Table 3.1 Elements used in static analysis of solid model (Cont'd)

Targe 170	3D Quadrilateral Target Segment	Mating Surfaces of Handles with Chassis
Conta 174	3D 8 Node Surface to Surface Triangular Contact	Mating Surfaces of Chassis with HANDLES

Figure 3.8 shows the deformation contour plot of the unit. It is seen that the maximum deformation after the loading occurs on the top cover and it is approximately 0.082 mm.

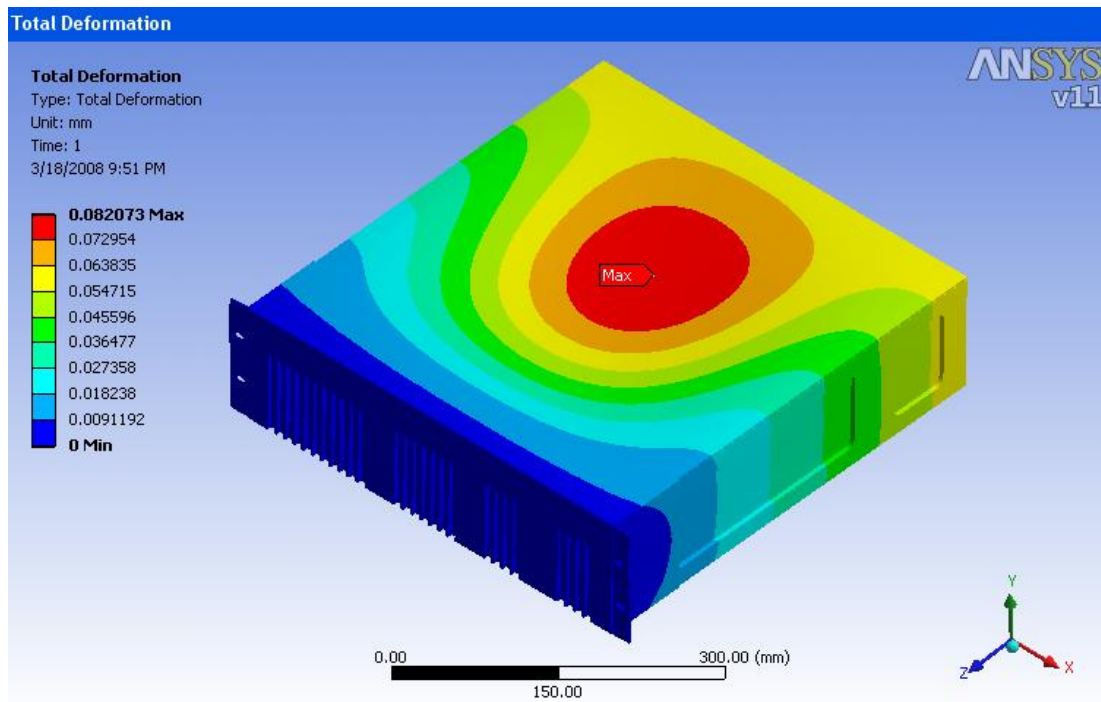


Figure 3.8 Deformation of solid model

Figures 3.9 and 3.10 show the equivalent Von-Misses stresses and maximum shear stresses respectively. Maximum stresses occur near the slot edges as expected. Figures also shows the stresses of some points. Similar points will be hold for other two model for reference points to compare the results.

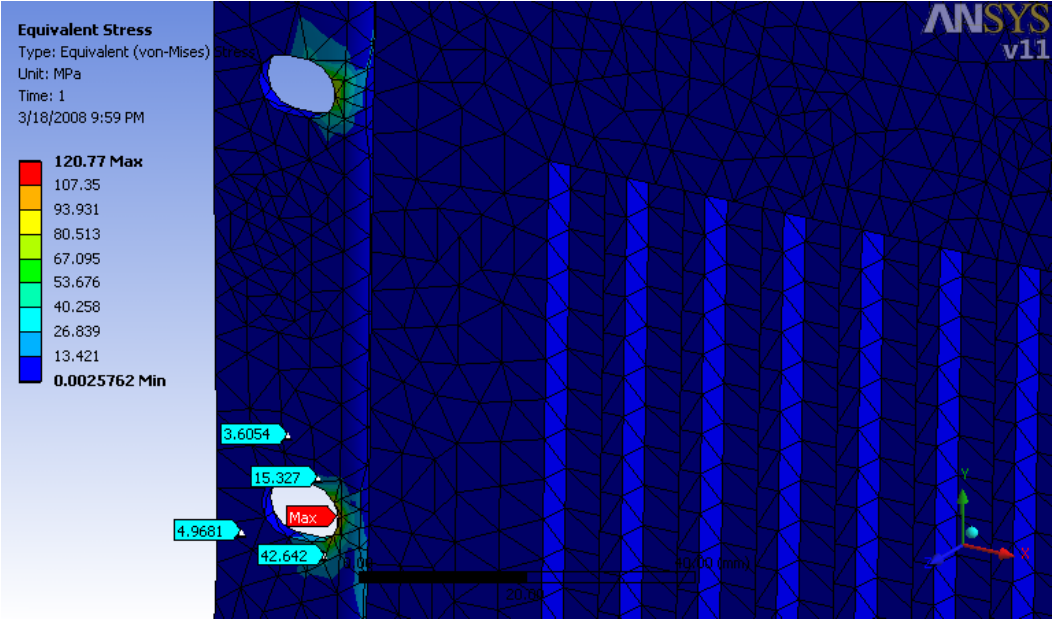


Figure 3.9 Equivalent Von-Misses stresses of solid model after loading

Von Mises Sress is a

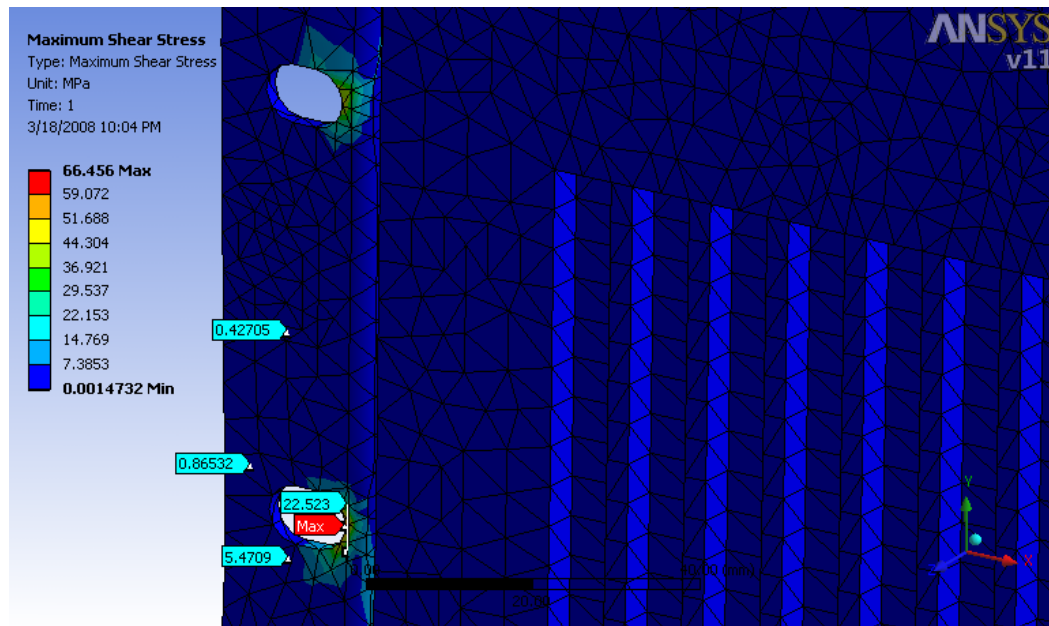


Figure 3.10 Maximum shear stresses of solid model after loading

Another important criteria in deciding on a model type is the solution time and memory requirement. In the initial analyses element size is chosen as 5 mm for solid model and for the initial analyses by the other finite element models, 5 mm element size will be kept for comparison purposes. Table 3.2 gives information about the number of elements and nodes used in the finite element model. Table 3.2 also shows the used memory end time in order to solve the solid model under given loading and boundary conditions

Table 3.2 Statistics of solid model

General Element Size	5 mm
Number of Nodes	453032
Number of Elements	247377
Maximum Scratch Memory Used	1540.011 MB
Elapsed Time	1097.00 sec

### 3.3.2 CASE 2: HYBRID MODEL

Same loading is applied to the hybrid model which is composed of solid and shell elements. The hybrid model is given in Figure 3.11. In the hybrid model chassis is meshed with solid elements whereas cover and handles are approximated as shell since the thickness of cover is 3 mm and the thickness of handle is 2 mm, and they can be assumed to be thin enough to be meshed with shell elements. Front slots are taken as fixed supports similar to the full solid model.

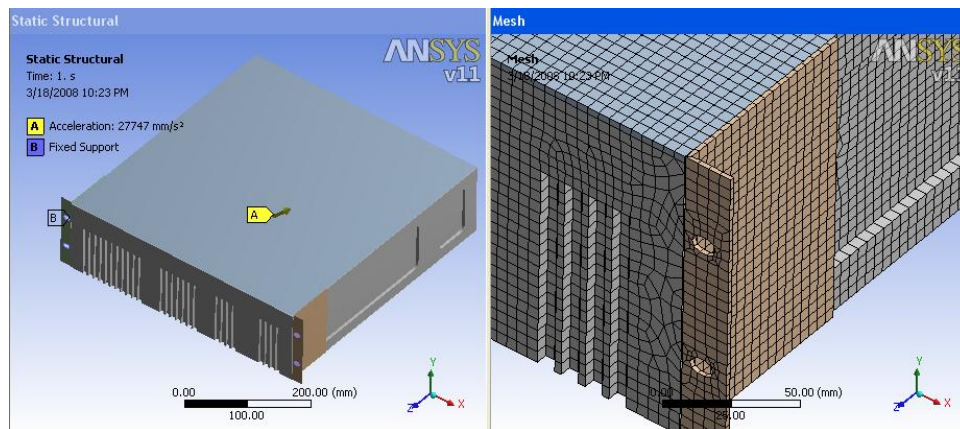


Figure 3.11 Loading and meshing of the hybrid model

In this finite element model, since the cover and handles are joined to the chassis through screws, the interface between the chassis and the handle and the top cover is approximated as the contact region. Figure 3.12 shows the contact regions of the model. Cover is the chassis through the contact region shown in Figure 3.12, and the contact region between handles and the chassis is the touching surfaces of the handles and the chassis.

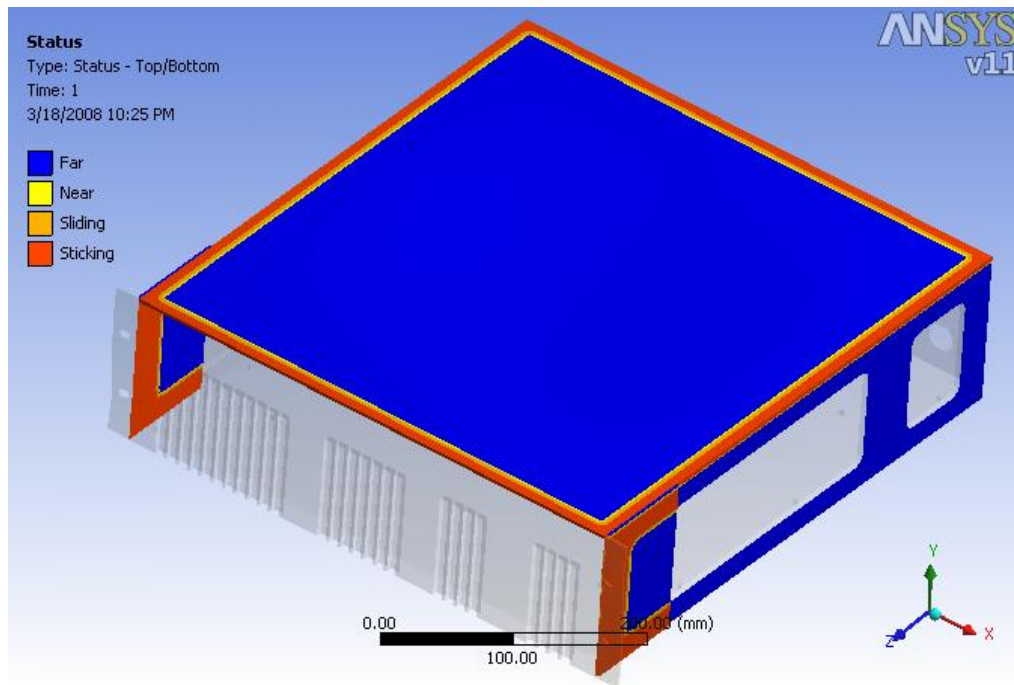


Figure 3.12 Contact Regions of the Hybrid Model

In addition to the solid elements and contact elements, shell elements are added to the hybrid model. Table 3.3 summarizes the element types used in the hybrid model. Target elements are formed in the chassis and contact elements are formed in the handle and cover parts.

Table 3.3 Elements used in static analysis of hybrid model

ANSYS Element Name	Description	Location
Solid 187	10 Node Tetrahedral Structural Solid	Chassis
Solid 186	20 Node Hexahedron Structural Solid	Chassis
Shell 181	4 Node Linear Quadrilateral Finite Strain Shell	Cover and Handles

Table 3.3 Elements used in static analysis of hybrid model (Cont'd)

Targe 170	3D Quadrilateral Target Segment	Mating Surfaces of Handles with Chassis
Conta 174	3D 8 Node Surface to Surface Triangular Contact	Mating Surfaces of Chassis with Handles

Figure 3.13 illustrates the deformation of the hybrid model. In this case, maximum stress area is larger than solid model. The maximum deformation is about 0.13 mm which is also larger than the deformation of the solid model.

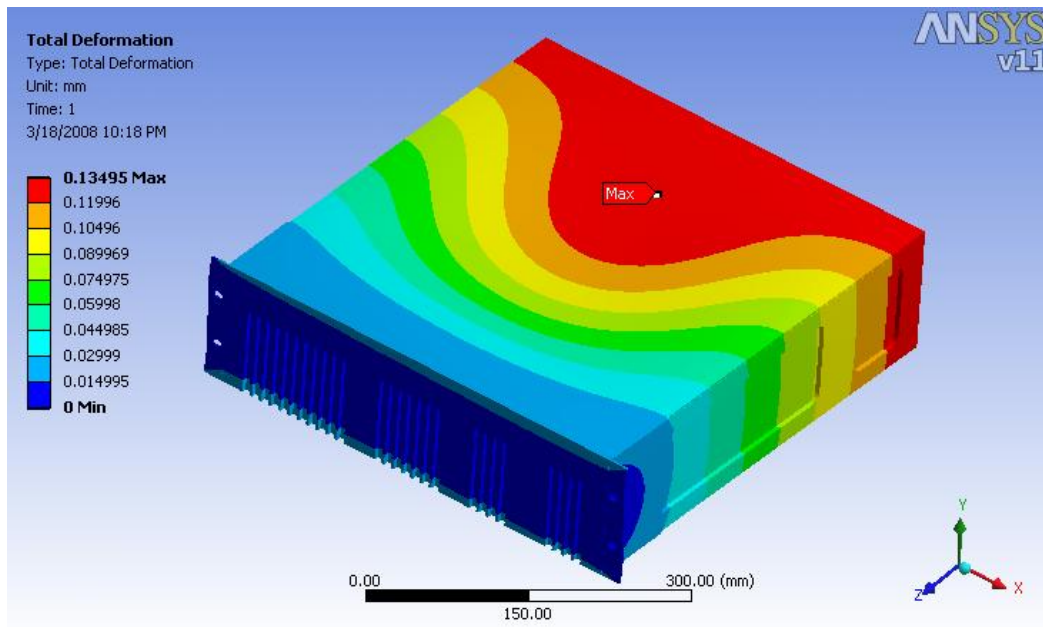


Figure 3.13 Deformation of hybrid model

Figures 3.14 and 3.15 show the equivalent Von-Mises and maximum shear stresses, respectively. Although the maximum stresses are formed in the expected regions,

these stresses and other probe stresses are larger than the ones obtained by the solid model .

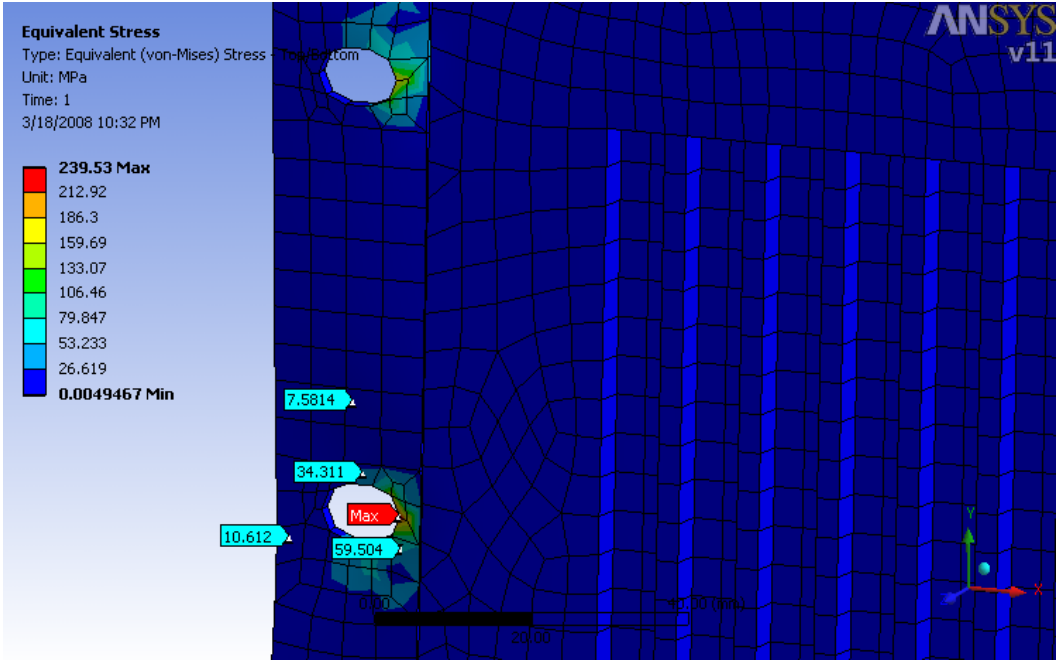


Figure 3.14 Equivalent Von-Mises stresses of hybrid model after loading

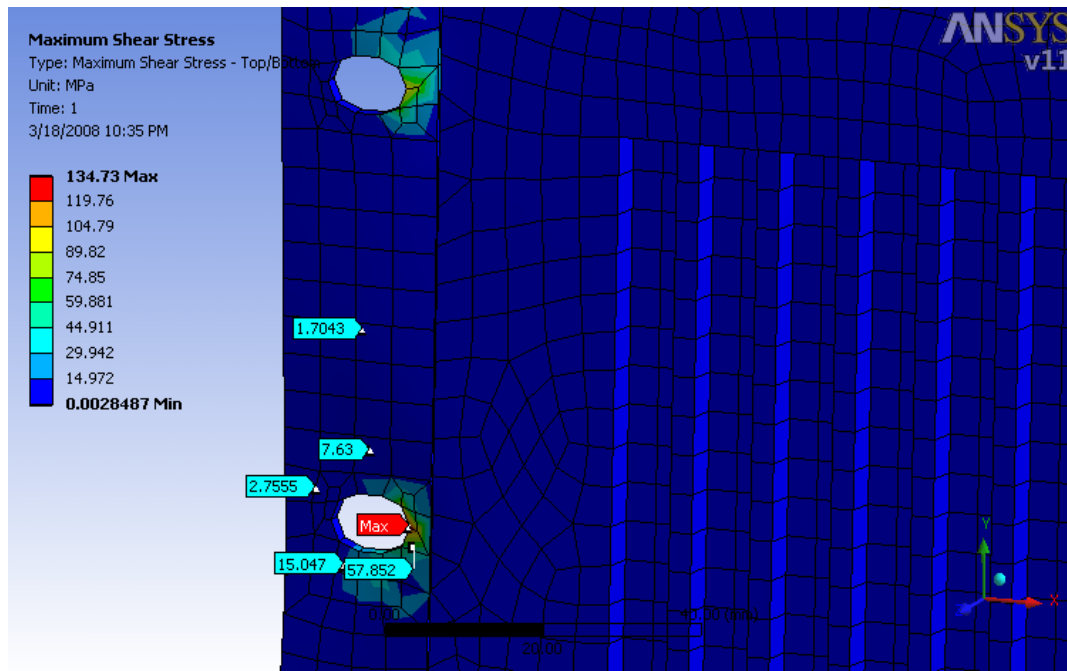


Figure 3.15 Maximum shear stresses of hybrid model after loading

From Table 3.4, it can be easily observed that although element size is not changed, because of the use of shell elements, number of elements and nodes are decreased. As a result, used memory and evaluating time are reduced.

Table 3.4 Statistics of Hybrid Model

General Element Size	5 mm
Number of Nodes	223245
Number of Elements	60556
Maximum Scratch Memory Used	1100.214 MB
Elapsed Time	651.00 sec

### 3.3.3 CASE 3: FULL SHELL MODEL

Shell model of the 3-D model is generated by forming the mid-planes of the features. The meshed model with 5 mm element size is illustrated in Figure 3.16 and Table 3.5 shows the components of this meshing.

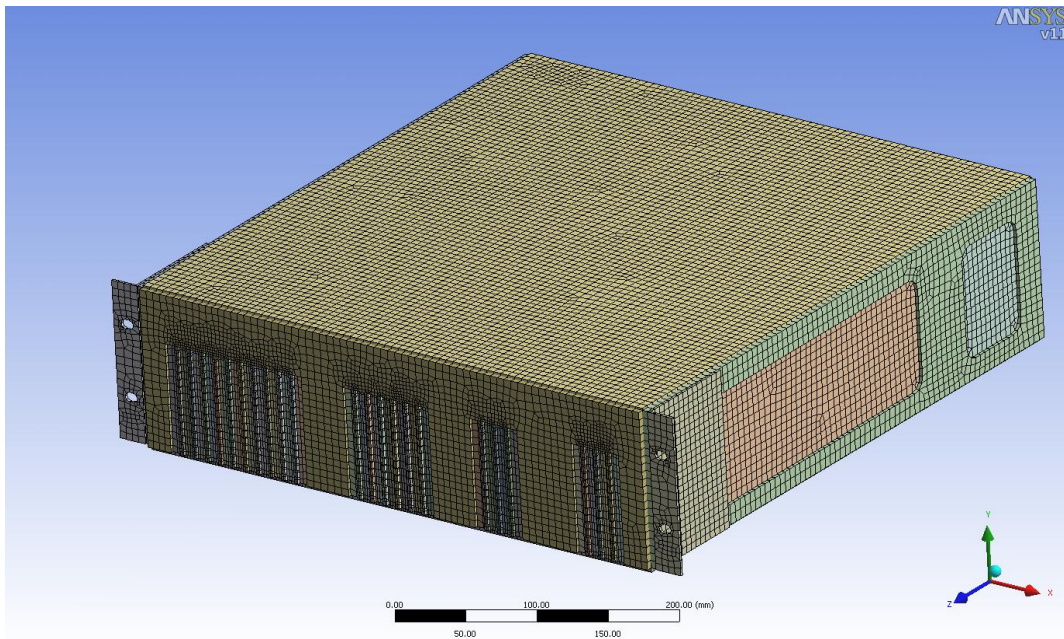


Figure 3.16 Meshing of shell model

Table 3.5 Elements used in static analysis of shell model

ANSYS Element Name	Description	Location
Shell 181	4 Node Linear Quadrilateral Finite Strain Shell	Chassis, Cover and Handles
Targe 170	3D Linear Target Segment	Mating Surfaces of Handles with Chassis
Conta 173	3D 4 Node Surface to Surface Linear Contact	Mating Surfaces of Chassis with Handles

2g load is applied to the model both in +x and +y directions. Applied loads and boundary conditions are shown in Figure 3.17.

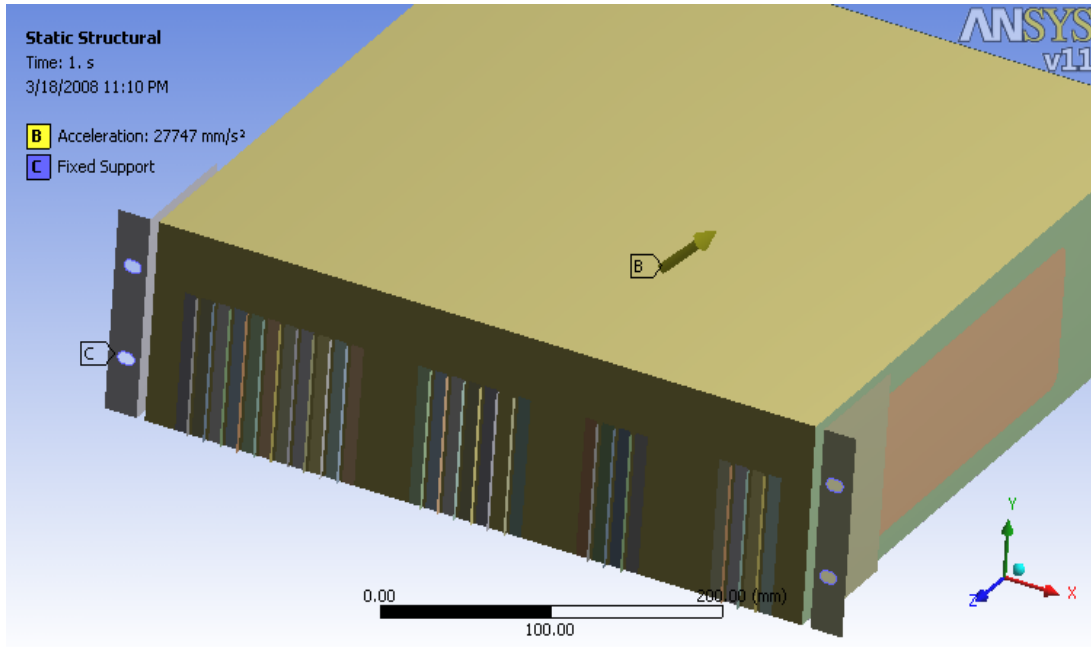


Figure 3.17 Loads and boundary conditions for shell model

In the full shell modeling, total deformation of shape of the shell model is similar to the solid model as shown in Figure 3.18. The maximum deformation is determined as 0.084 mm which is very close to the maximum deformation of the full-solid model. Like deformation, regardless of the maximum values, equivalent Von-Misses and Shear stresses of the probes are close to the results of solid model. The stress results are given in Figures 3.19 and 3.20.

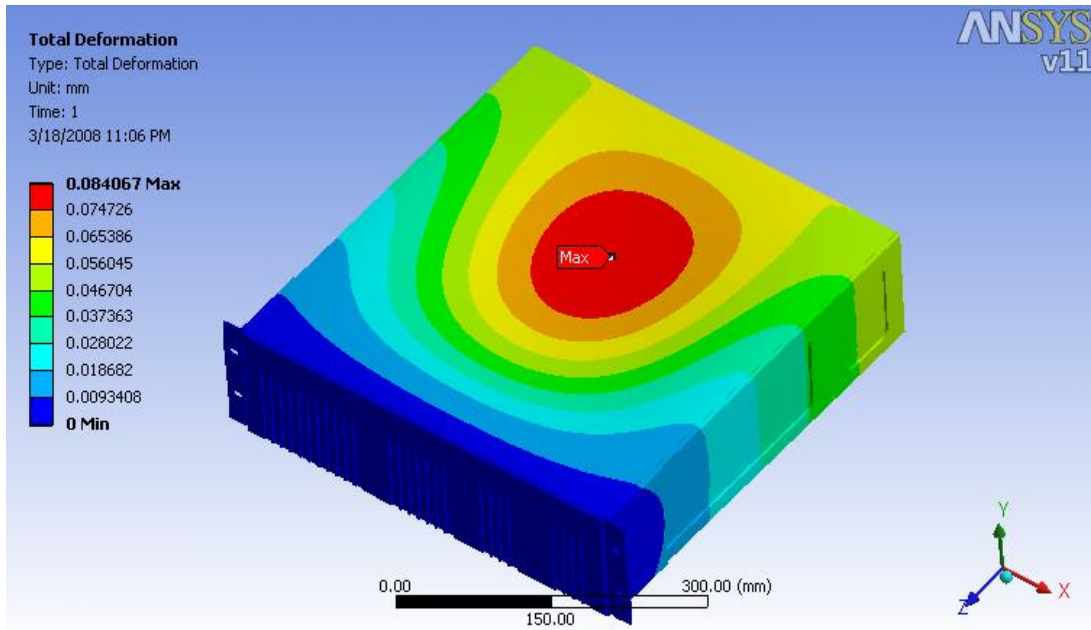


Figure 3.18 Deformation of shell model

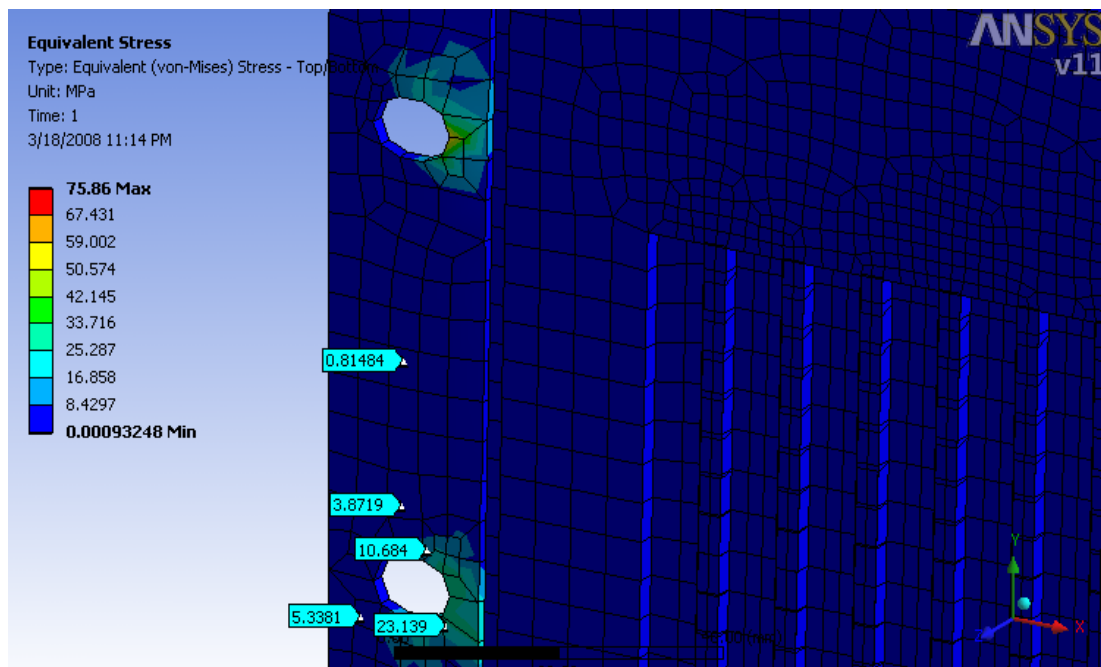


Figure 3.19 Equivalent Von-Misses stresses of shell model after loading

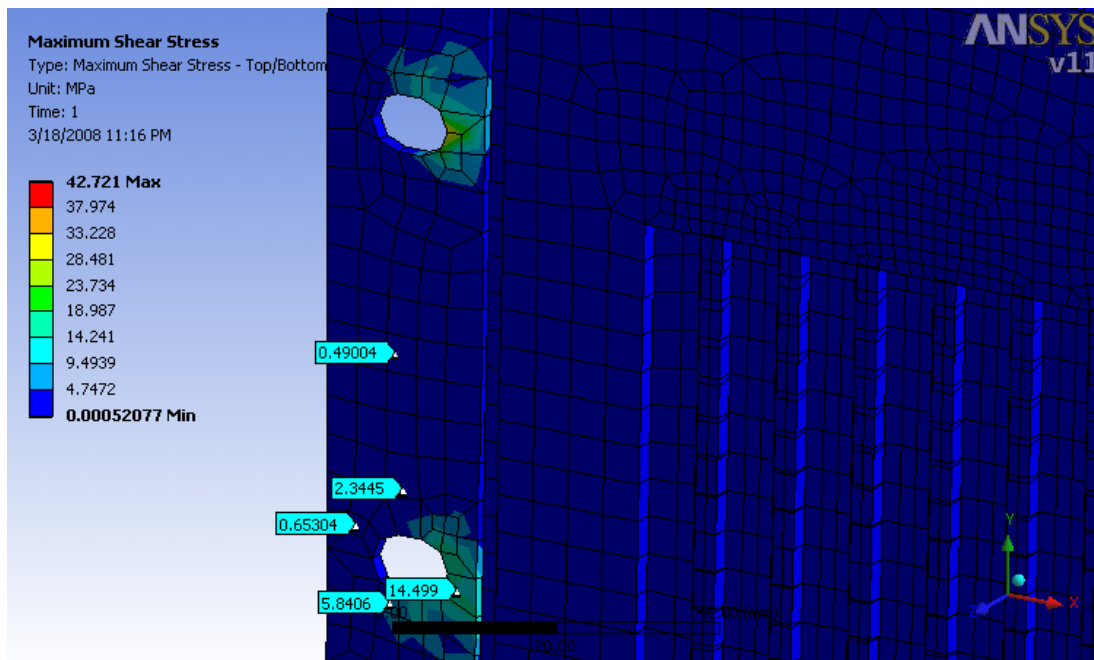


Figure 3.20 Maximum shear stresses of shell model after loading

The statistics of shell model is given by Table 3.6. This model is the easiest model to work considering its memory and time usage due to the more reduced node and element number compared to other two models.

Table 3.6 Statistics of shell model

General Element Size	5 mm
Number of Nodes	46184
Number of Elements	45867
Maximum Scratch Memory Used	1068.423 MB
Elapsed Time	44.00 sec

The results of the models are gathered in Table 3.7 for comparison purposes. Examining these results, the similarity between solid and shell model is undeniable.

Table 3.7 Overview of the models

Model Type	Solid	Hybrid	Shell
Element Size	5 mm	5 mm	5 mm
Max. Deformation	0.0820 mm	0.1349 mm	0.0840 mm
Max. Von-Mises Stress	120.77 Mpa	239.53 Mpa	75.86 Mpa
Max. Shear Stress	66.456 Mpa	134.73 Mpa	42.721 Mpa
Number of Nodes	453032	223245	46184
Number of Elements	247377	60556	45867
Memory Used	1540.011 MB	1100.214 MB	1068.423 MB
Time Elapsed	1097.00 sec	651.00 sec	44.00 sec

In theory, when solid models are meshed, there must be at least three elements through the thickness in order to achieve better modeling of the bending effects. The minimum thickness of the designed package is 2.5 mm which is the back part of the chassis where connectors are assembled. This means that some parts of this model must be meshed by an element smaller than 1 mm. Such a meshing creates a huge number of elements, requiring huge memory for the solution.

In order to eliminate the drawback in solid modeling, the model is meshed by 5 mm element size with patch conforming method through solid case. By Patch Conforming Method, ANSYS arranges the element size through the thickness and tries to invoke the bending effect as much as it can to get reasonable the solutions. So the results of the solid model could be taken as the reference model to compare against in the pre-analysis step. When compared with the results of the full solid model, the static inertia load case results of the hybrid model is not as good as the results of the shell model. Some simple shock analysis was also performed in one direction for

comparing hybrid and shell models. Again, stress results of the hybrid and shell model were found to be not very close to each other. The discrepancy between the results of the hybrid model and the shell model is deemed due to the connections between solid and shell elements. There is a difficulty creating an interface between shell and solid elements. Although mating two different surfaces of shell and solid structures is possible with commercial FEA programs, the connection of these surfaces are not totally appropriate because of their nature. Therefore, the results of hybrid model is much more different than the other results.

Besides the closer results with the full solid model, since the shell model has significant advantages related to the computer resource requirement. Time required to complete the analysis and the memory requirement of the shell model is lower and therefore, shell model selected for structural analysis of the packaging subject to shock loading.

The final step of the pre-analysis is the mesh size study. In order to achieve this, the pre-analysis step is done for every element size. Two probes are taken as reference for deformation and stress comparison. The location of the stress probe is near the application of fixed supports, (Stress Probe = (10,95,360)) where the stress is larger and the location of the deformation probe is far away from the fixed support (Deformation Probe = (-210,-18,80)). The loads applied for the mesh size study is 5g in +x and +y direction. The washer surfaces of the front slots are chosen as fixed support locations. The results are listed in Table 3.8. From this table, it can be observed that stress and deformation results become larger as element size gets smaller, since the difference among the different mesh size results are very small and the results are start to converge around the mesh size of 5 mm, this element size is chosen as the effective element size for shell model.

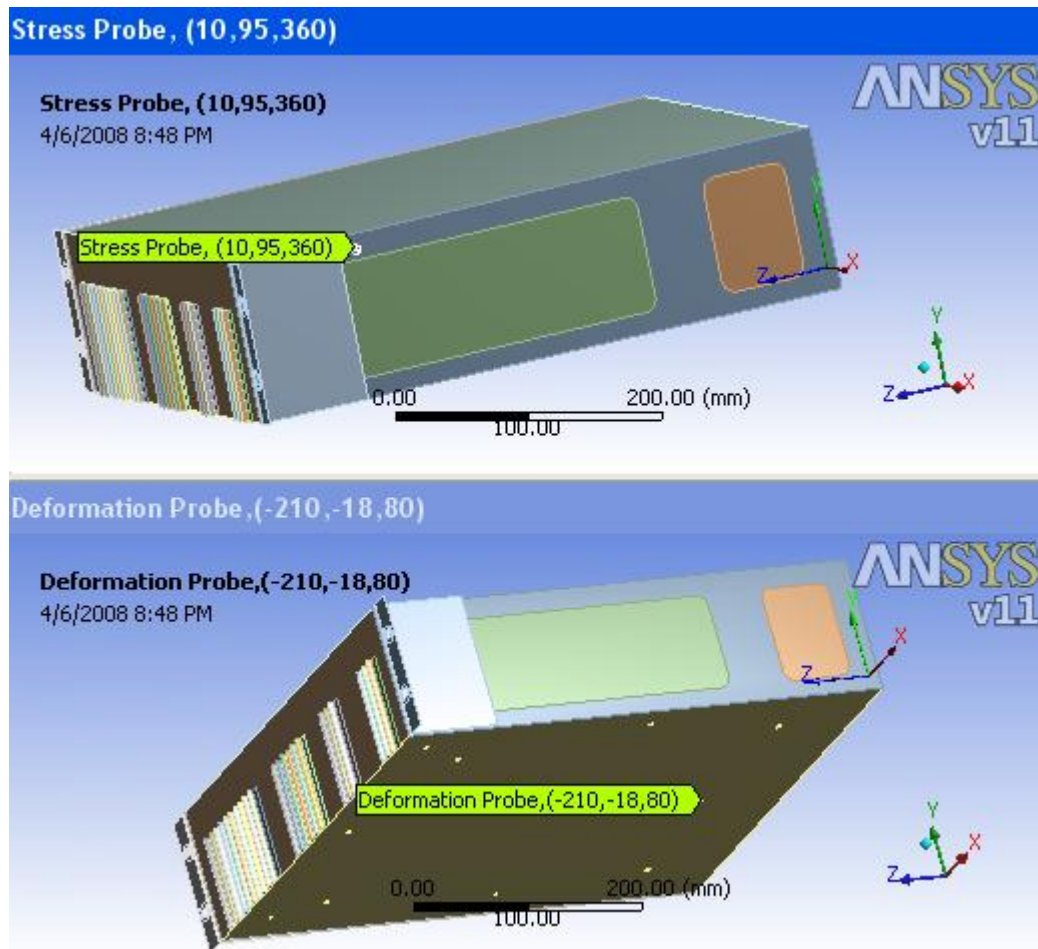


Figure 3.21 Deformation and stress probes for mesh size study

Table 3.8 Mesh size study

Element Size (mm)	Deformation Probe (mm)	Stress Probe (Mpa)	Number of Nodes	Number of Elements
2	0.10833	1.1761	170718	169967
3	0.10832	1.1759	87229	86717
4	0.10630	1.1758	53944	53533
5	0.10628	1,1755	43234	42927
6	0.10621	1.1732	32203	31937
7	0.1056	1.1679	27808	27566
8	0.10491	1.1672	23899	23690

### 3.4 SHOCK ANALYSIS

#### 3.4.1 GEOMETRY

The geometry of the model is similar with the geometry of the shell model used in pre-analysis part. By using the mid-surfaces of the features, the 3-D solid model is converted to shell model. The thicknesses and the materials of features are defined in ANSYS. The model is basically formed by 19" Rack Handles, Cover and Chassis. Figure 3.22 shows the features of the analyzed model. The handles are joined to the chassis by defining their mating surfaces as contact region. The meshed illustration of contact surfaces is given in further section.

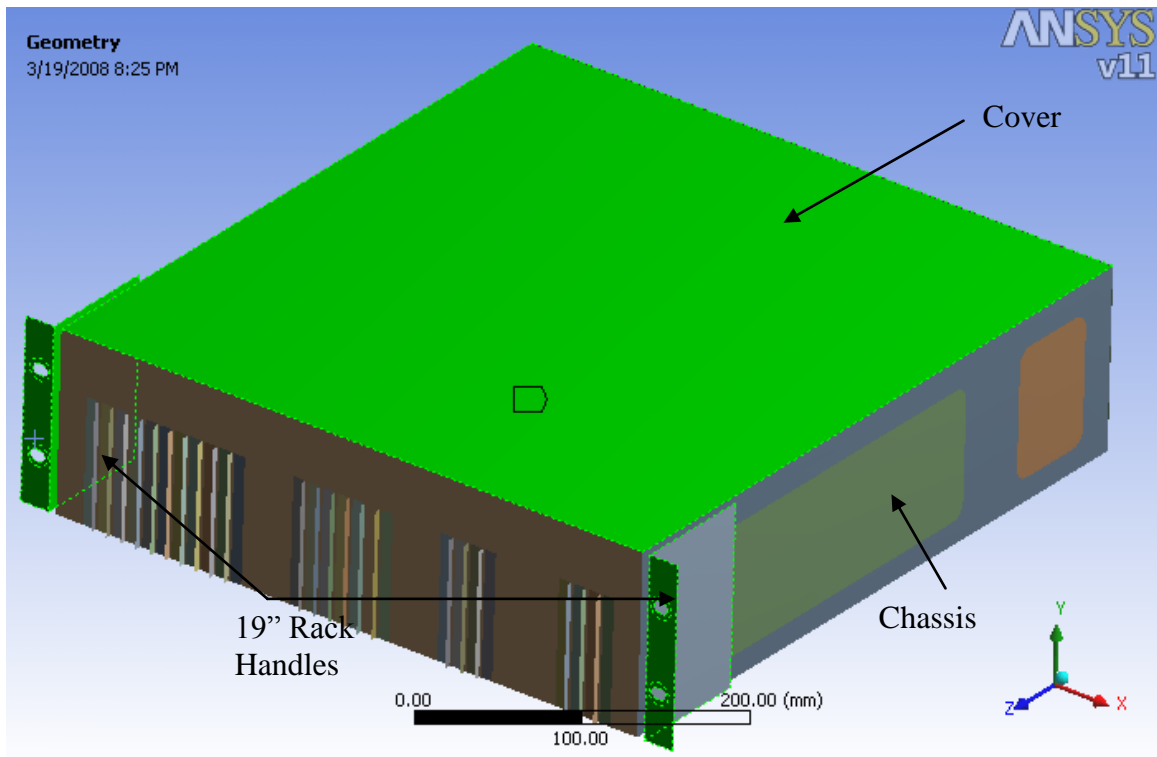


Figure 3.22 Features of analyzed model

Cards placed inside the chassis, their interfaces and filters are modeled as a point mass and their inertia tensors are defined in ANSYS. The moment of inertia of the point mass is given in Table 3.9. The mass is attached to 6 holes placed on the bottom plate of the chassis. The outer environment interfaces like connectors, ground screws are not modeled in this analysis since their inertia effects are small. The total mass of the model including the point mass is 11.9 kg.

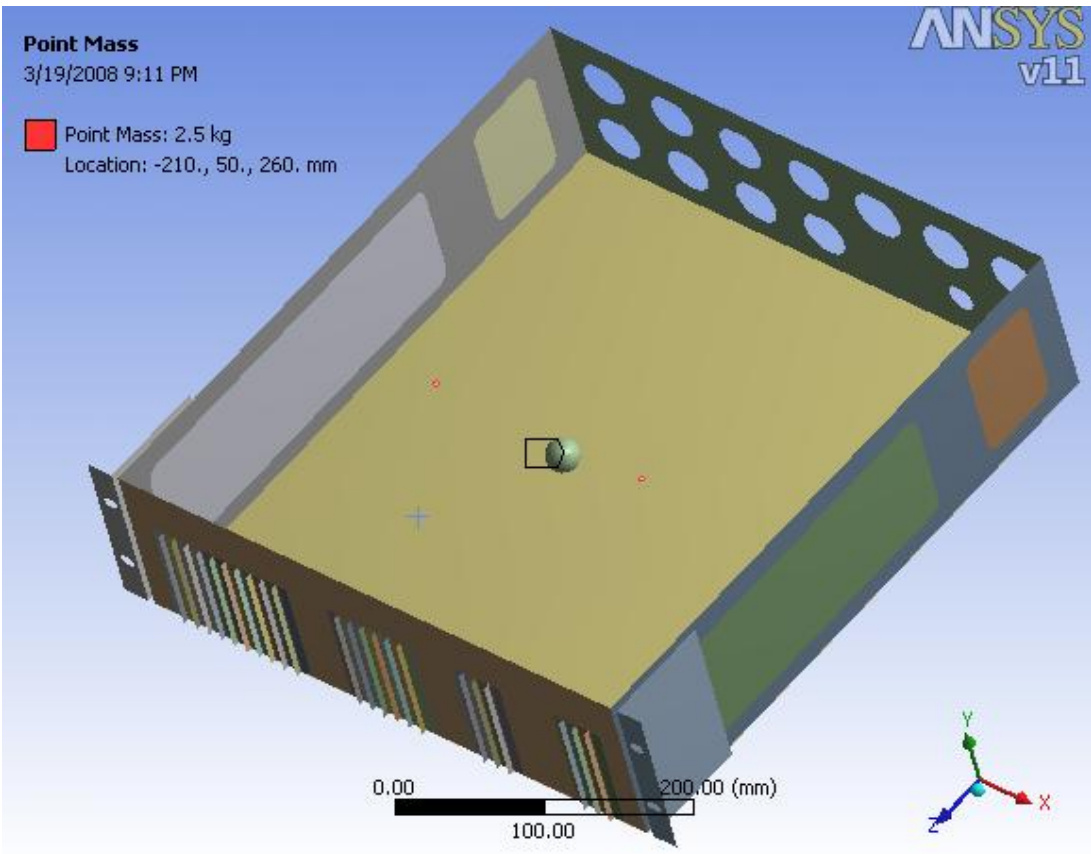


Figure 3.23 Point mass of the model excluding the chassis, cover and handles

Table 3.9 Moment of inertia of the model excluding the chassis, cover and handles

Mass Moment of Inertia x	28999.2 kg.mm <sup>2</sup>
Mass Moment of Inertia y	26928.1 kg.mm <sup>2</sup>
Mass Moment of Inertia z	2141.4 kg.mm <sup>2</sup>

### 3.4.2 MESHING

For the finite element model, 5 mm uniform quadrilateral elements are used. There are 33422 nodes and 33167 elements created for meshing the model. Elements used are Shell 181, four-node linear quadrilateral and triangular shell elements except in contact regions. For contact regions, conta 173 linear quadrilateral elements are used in chassis surface and Targe170 linear quadrilateral target elements are used in handle surfaces. The meshing through the contact region is given in Figure 3.24.

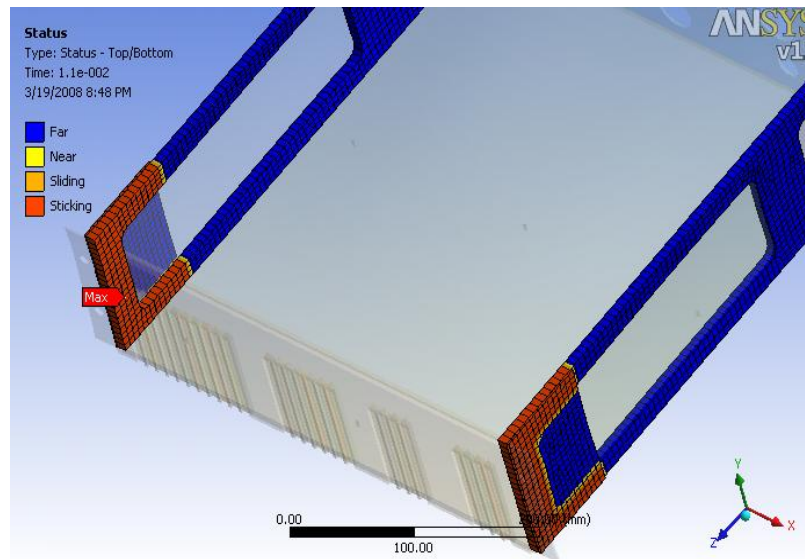


Figure 3.24 Meshing through contact region

### 3.4.3 LOADING AND BOUNDARY CONDITIONS

The shock analysis is performed for 3 axes, and in 6 directions; +x/-x, +y/-y, +z/-z. Shock load is simulated by a half sine function, with 20 g peak acceleration for duration of 11 ms. The mathematical representation of the shock acceleration is given by Equation 3.1:

$$a = 20 \cdot g \cdot \sin\left(\frac{\pi \cdot t}{0.011}\right) \quad (3.1)$$

where,

“g” is standard earth gravitational acceleration in mm/s<sup>2</sup> and “t” is time in second.

The graph of this loading is given by Figure 3.25.

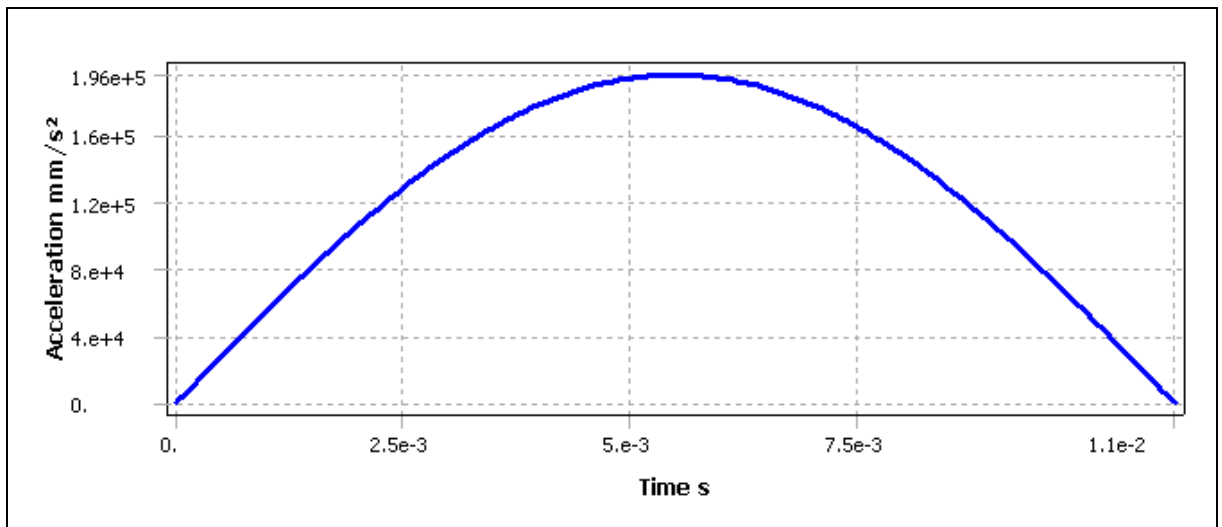


Figure 3.25 Acceleration shock load profile used in shock analysis

The shock load is defined by a suddenly applied sine function. Due to this condition a dynamic analysis is required. The shock analysis performed by ANSYS is done by Flexible Dynamic Analysis module. Flexible Dynamic Analysis (also called time-history analysis or transient response analysis) is a technique used to determine the dynamic response of a structure under the action of any general time-dependent loads [23]. Like static analysis, dynamic analysis uses a stiffness matrix, but it also uses a mass matrix and a damping matrix [20].

The equation of a dynamic response, which is also named as general forced vibration equation, is written as [20] :

$$K D_j + C \dot{D}_j + M \ddot{D}_j = R_j \quad (3.2)$$

where **K** is the stiffness matrix, **C** is the damping matrix, **M** is the mass matrix, **D<sub>j</sub>** is the nodal displacement matrix and **R<sub>j</sub>** is the known time-dependent forcing function at the nth instant. Here, the acceleration given by equation 3.1 is used to calculate the time dependent forcing function R<sub>j</sub>. In Equation 3.2, j values (j=0,1,2, ...) correspond to incremental times t=0,Δt,2Δt,..., etc. where Δt is the time increment. Before performing dynamic analysis, a model analysis is done for determining the first lowest modal frequency. This frequency is used to obtain the proper time increment for dynamic part of the analysis. The solver of ANSYS calculates an aggregate response frequency at every time point and uses approximately twenty points per cycle at the response frequency [23]. That is, if f is the frequency (in cycles/time), the integration time step (ITS) is given by equation (3.3) [23]:

$$ITS = 1/(20f) \quad (3.3)$$

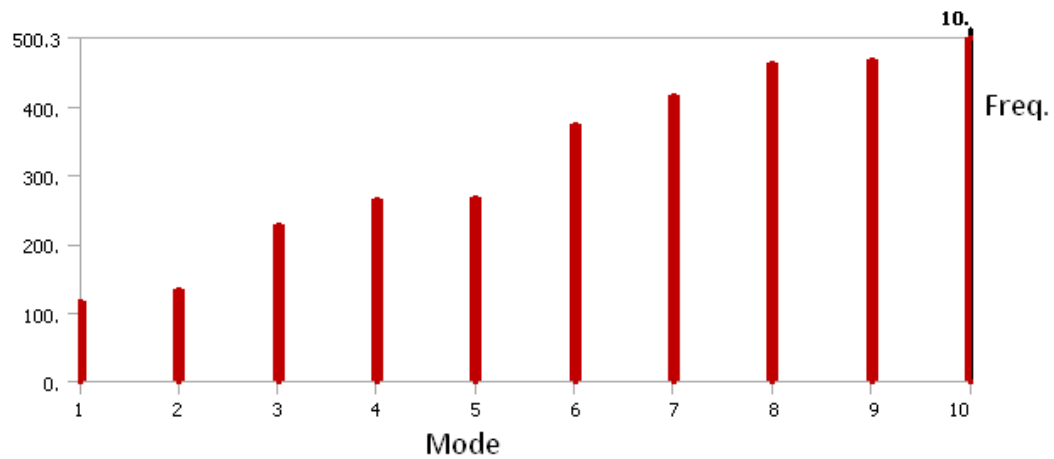


Figure 3.26 Modal frequencies

The lowest frequency of the related modes is 115.78 Hz (Figure 3.26). By using this frequency, the calculated initial time step is calculated as:

$$ITS = 1/(20 \times 115.78) = 4.3 \times 10^{-4} \text{ s}$$

The approximated initial time step and maximum/minimum values for this analysis are given by Table 3.10. The minimum and maximum time step values are given as a proper time tolerances of the order of four.

Table 3.10 Time increments for shock analysis

Initial Time Step	0.0004 s
Minimum Time Step	0.0001 s
Maximum Time Step	0.0005 s

The package is assembled to the 19" Rack Cabinet through the handles. Although there is a plate with drawers under the equipment, the chassis is not fastened this plate. So, 4 screws are taken as fixture points for the analysis, meaning the chassis is analyzed for the worst case.

There are M5 washers used under the screws of handles. The washer mating regions on the slots are defined in analyzed model and these regions are kept as fixed supports throughout the analysis. Figure 3.27 shows the boundary conditions used in the shock analysis. Similar boundary conditions are also defined in vibration analysis.

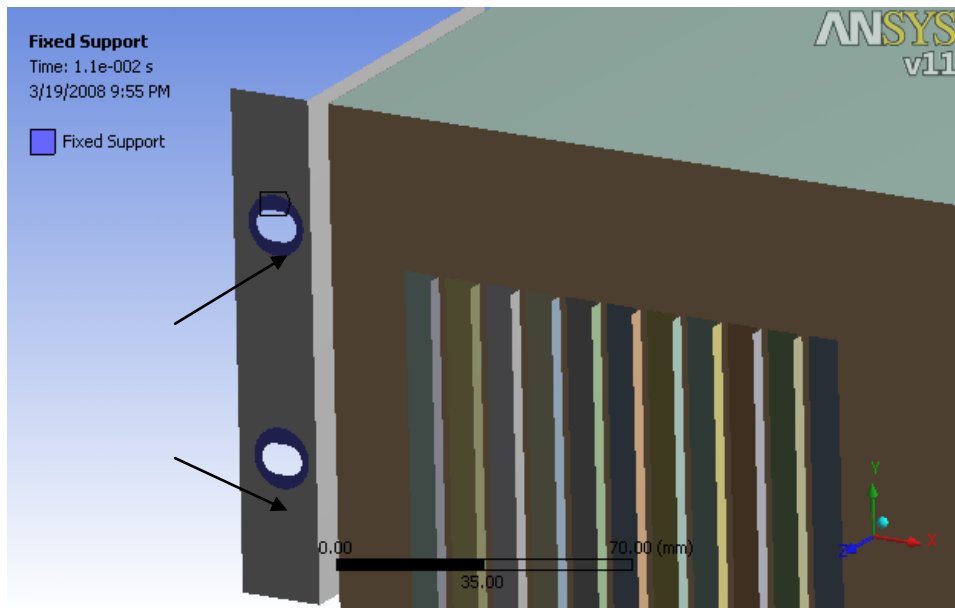


Figure 3.27 Boundary condition for shock analysis

Besides the defined shock loading, standard earth gravity is applied in  $-y$  direction. The point mass, loading and boundary conditions of the model for  $+x$ - direction is illustrated in Figure 3.28 as a sample shock analysis.

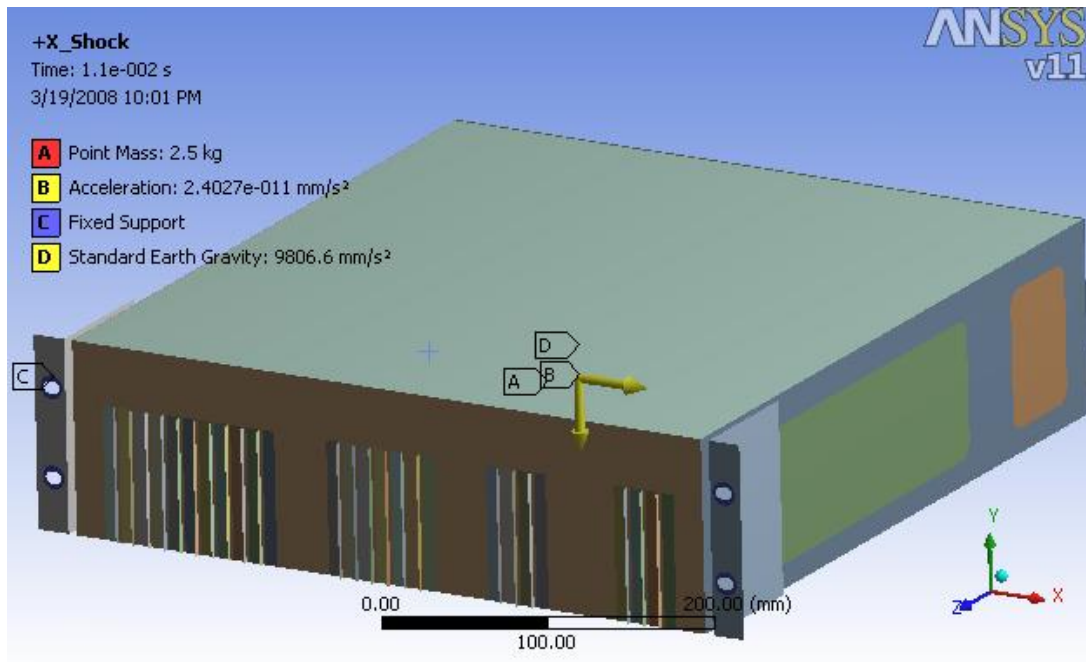


Figure 3.28 Loading and boundary conditions in +x-direction

### 3.4.4 EVALUATION OF ANALYSIS RESULTS

Based on the half sine shock loading, transient analysis is performed by ANSYS and the results in each direction are summarized in Figures 3.29 to 3.47. In these results, total deformation, maximum shear and maximum Von-Mises stresses are illustrated for each axes and direction.

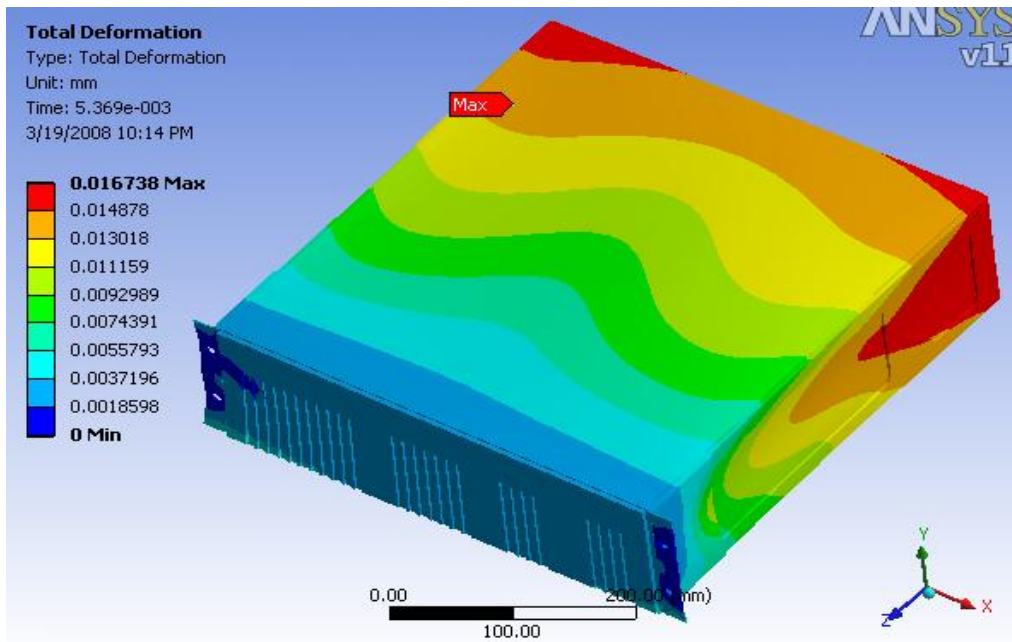


Figure 3.29 Deformation through +x-direction

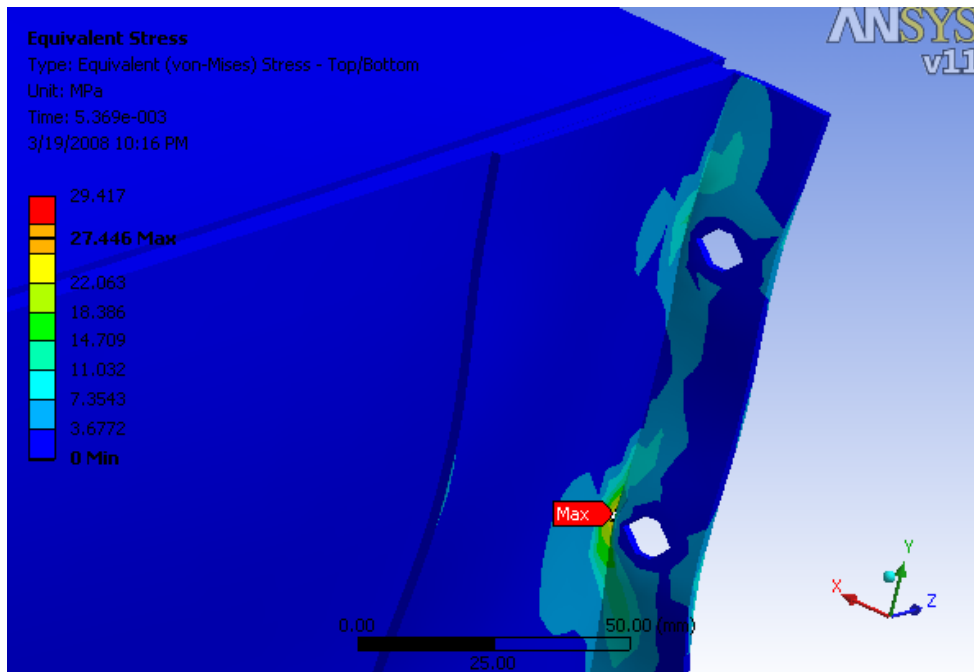


Figure 3.30 Equivalent Von-Mises stresses through +x-direction

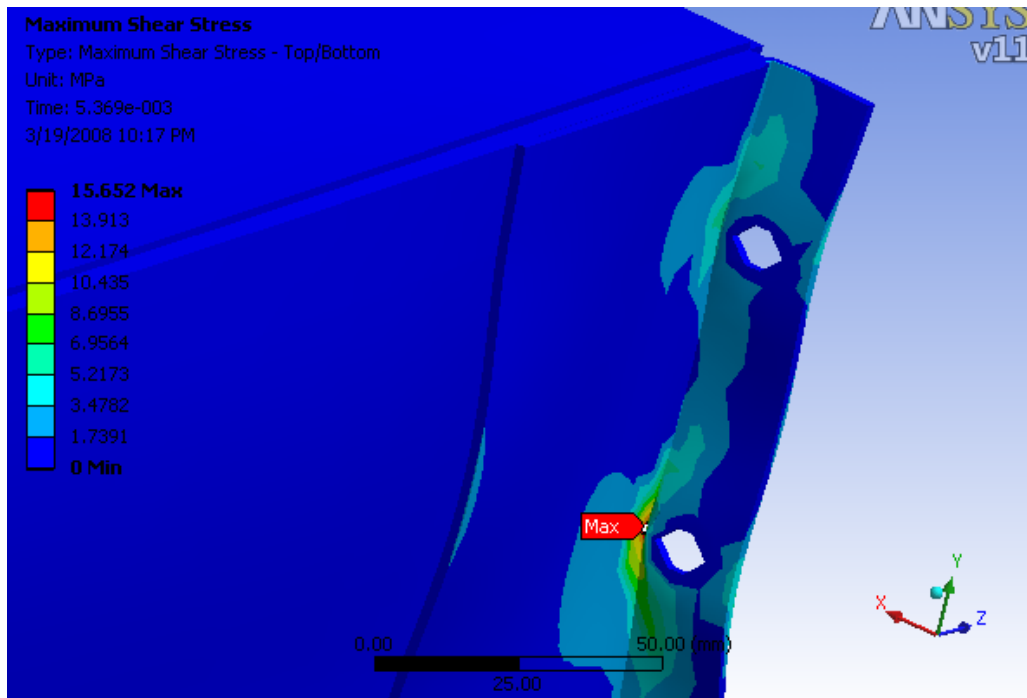


Figure 3.31 Maximum shear stresses through +x-direction

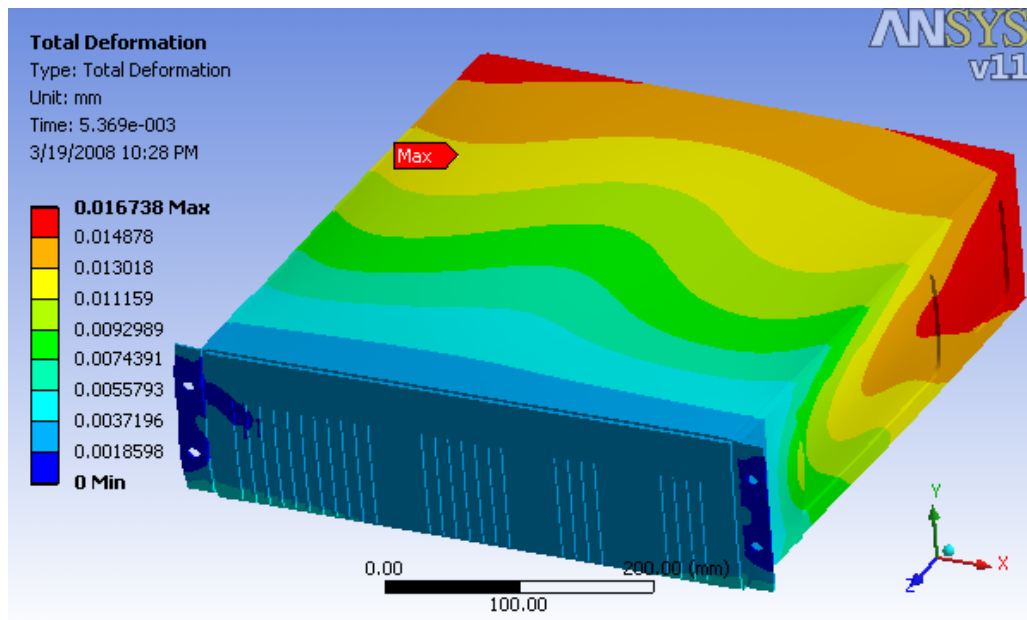


Figure 3.32 Deformation through -x-direction

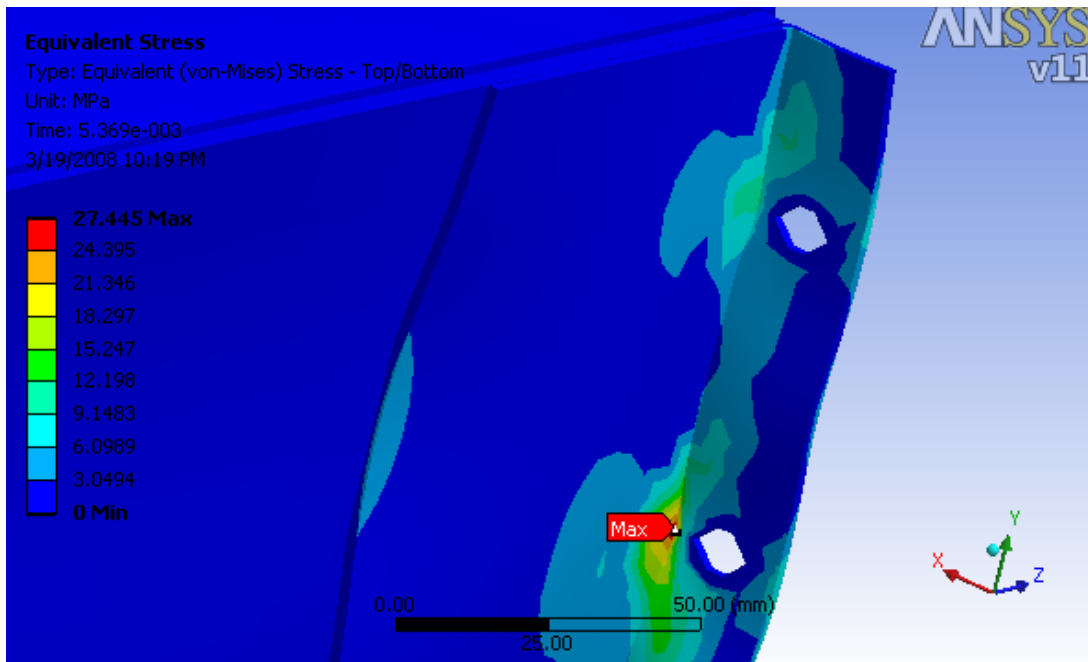


Figure 3.33 Equivalent Von-Mises stresses through -x-direction

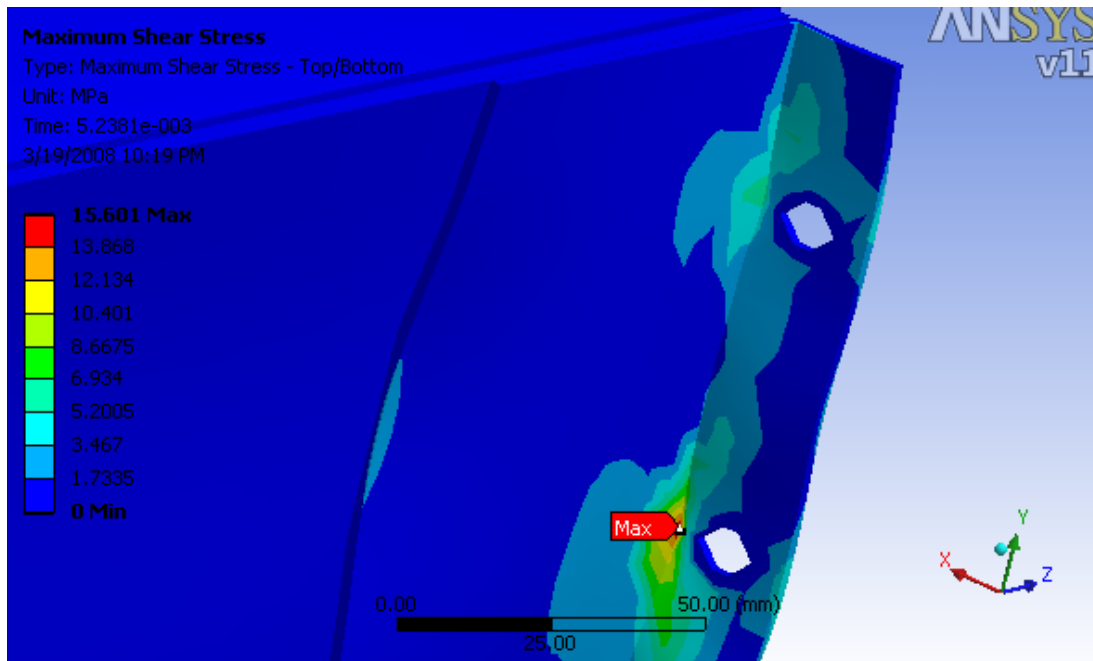


Figure 3.34 Maximum shear stresses through -x-direction

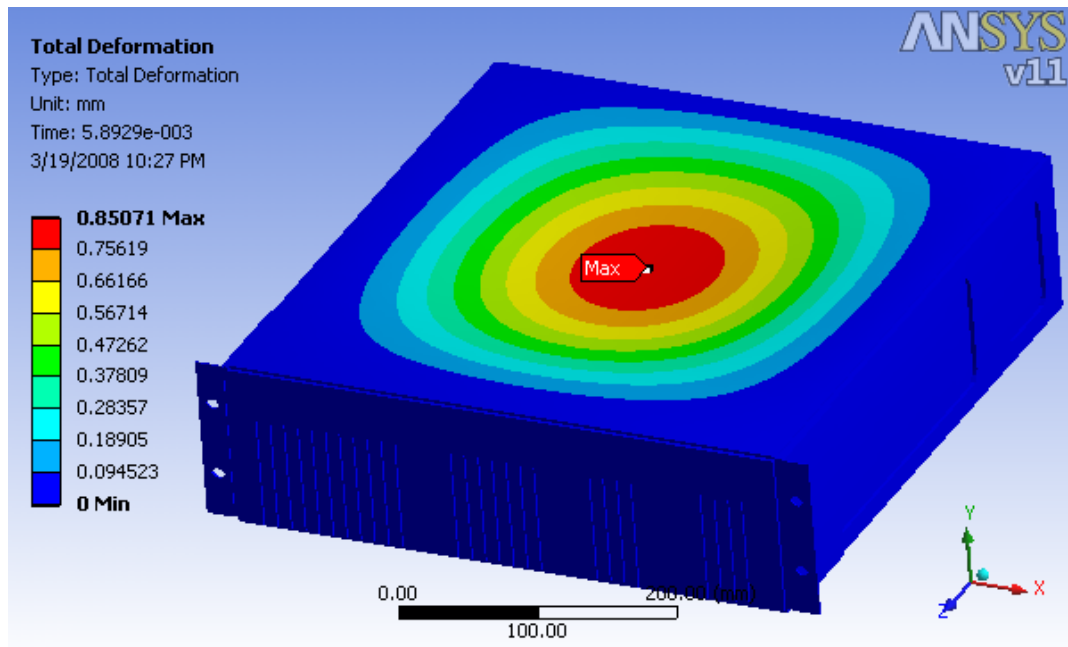


Figure 3.35 Deformation through +y-direction

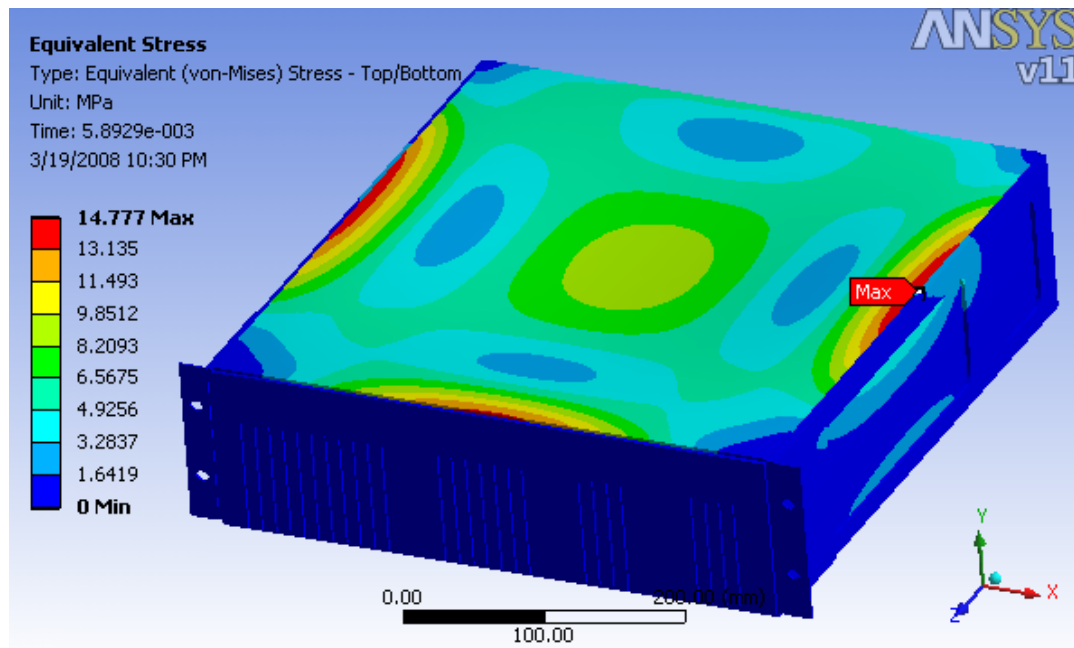


Figure 3.36 Equivalent Von-Mises stresses through +y-direction

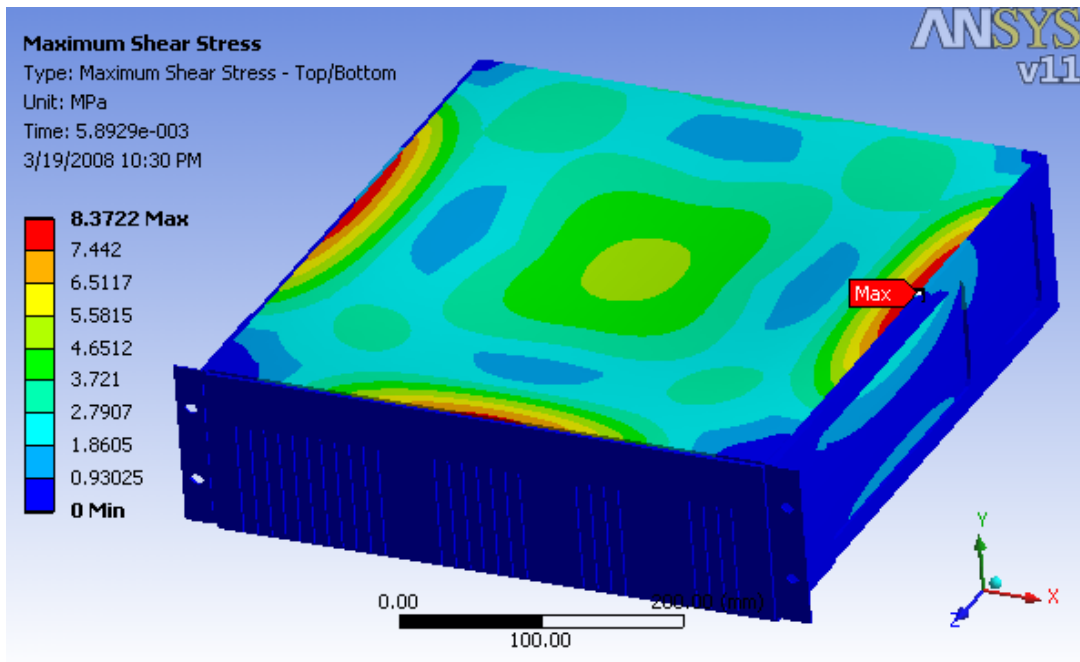


Figure 3.37 Maximum shear stresses through +y-Direction

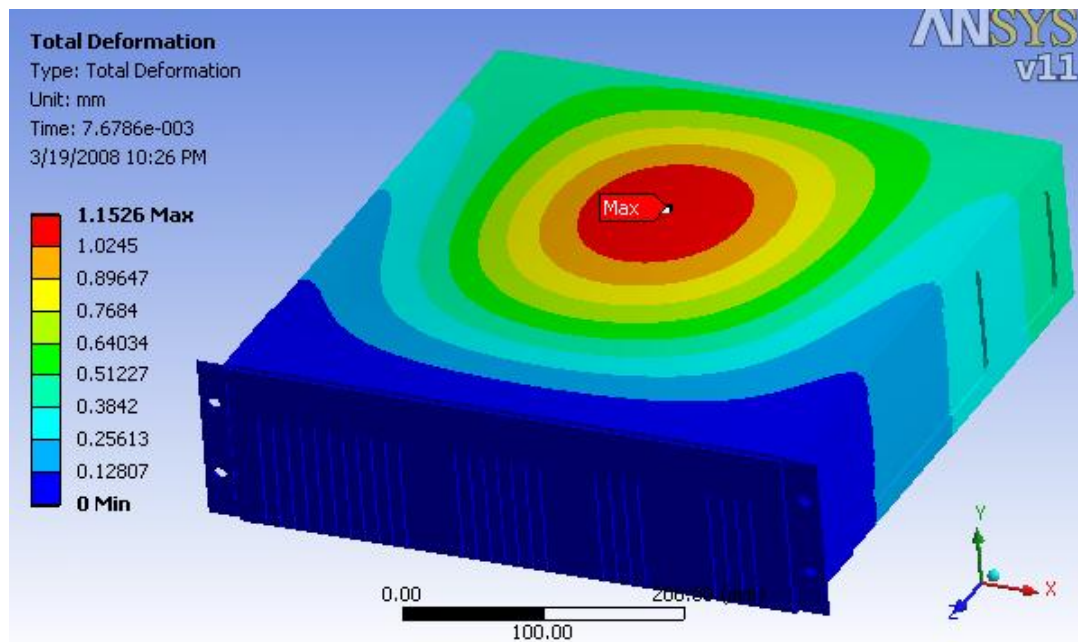


Figure 3.38 Deformation through -y-Direction

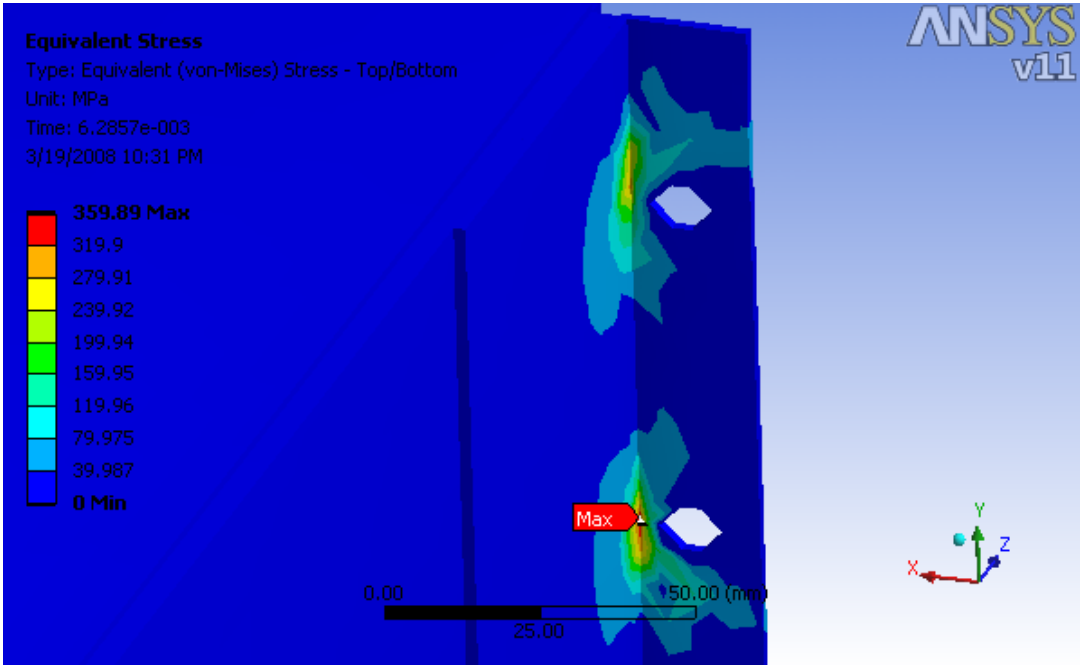


Figure 3.39 Equivalent Von-Mises stresses through -y-direction

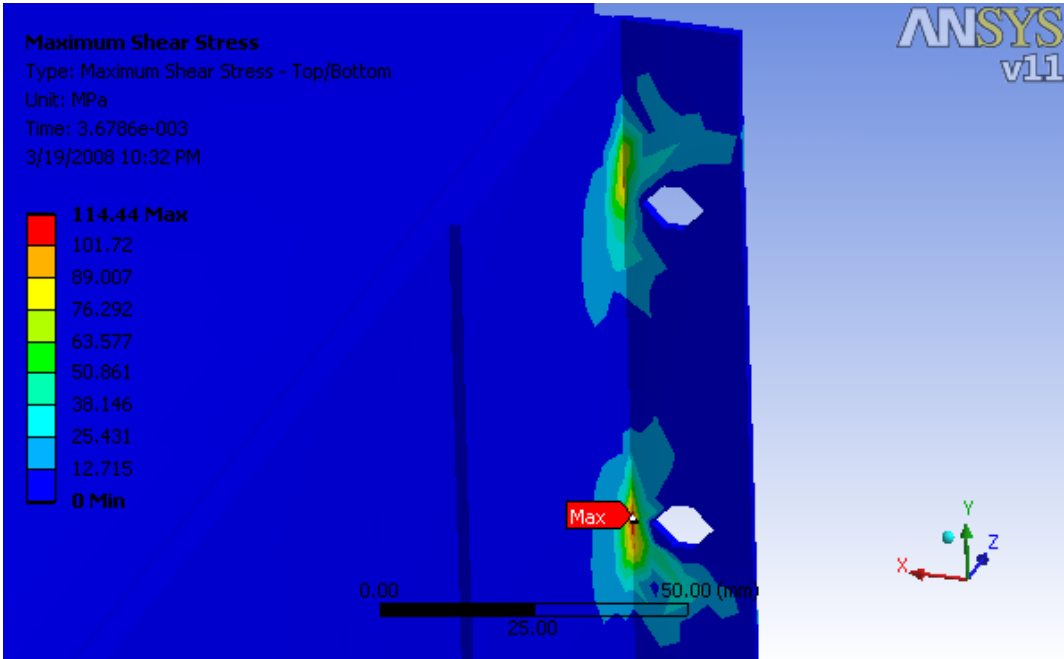


Figure 3.40 Maximum shear stresses through -y-direction

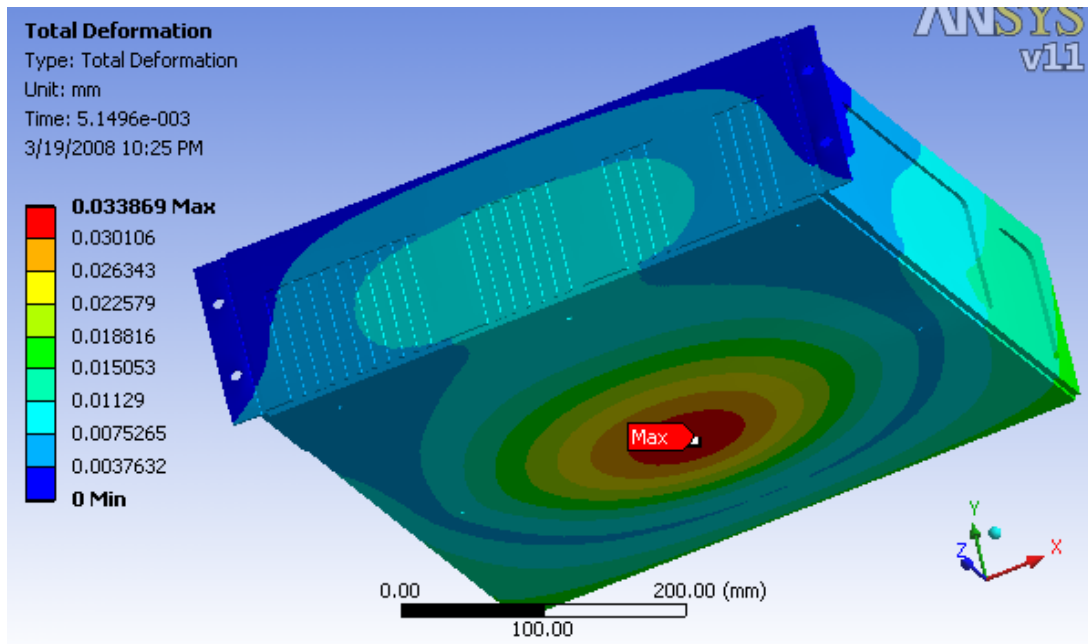


Figure 3.41 Deformation through +z-direction

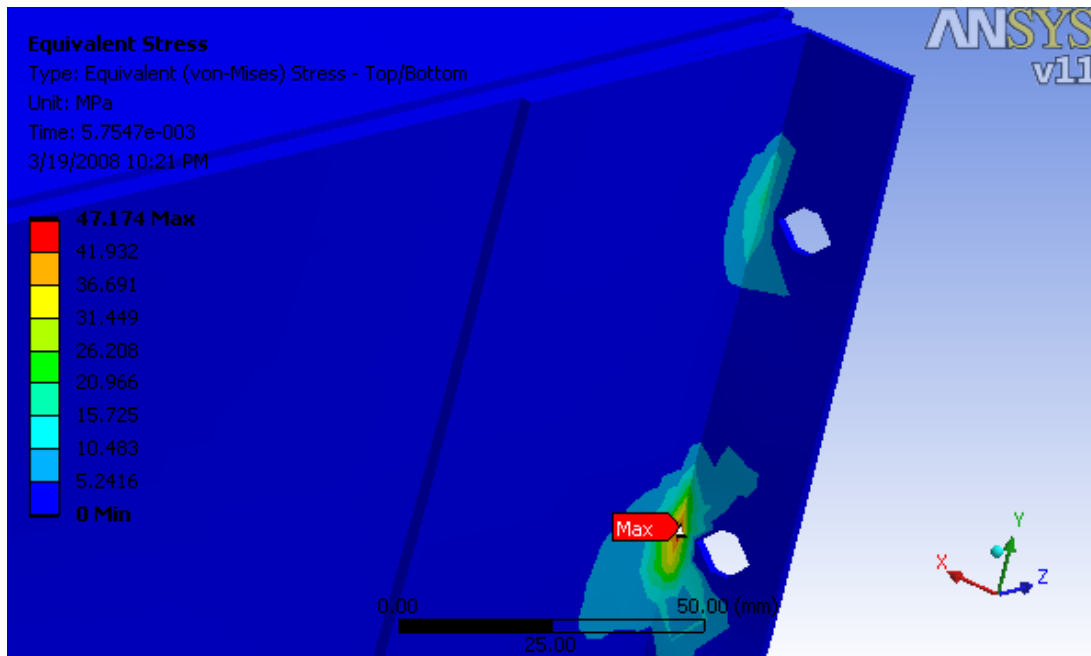


Figure 3.42 Equivalent Von-Mises stresses through +z-direction

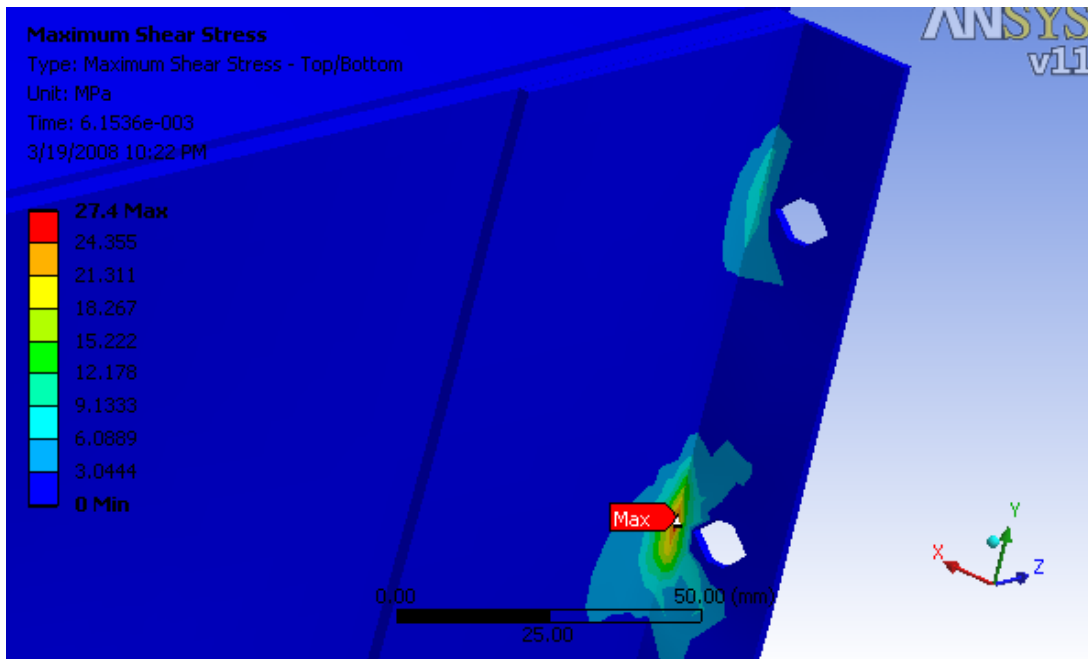


Figure 3.43 Maximum shear stresses through +z-direction

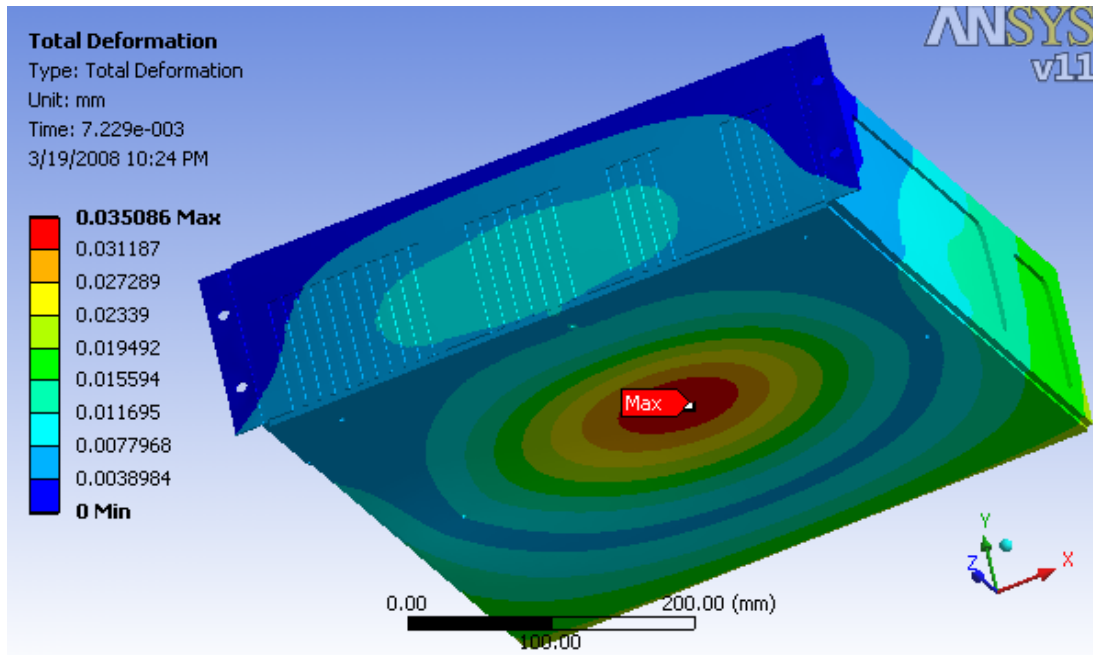


Figure 3.44 Deformation through -z-direction

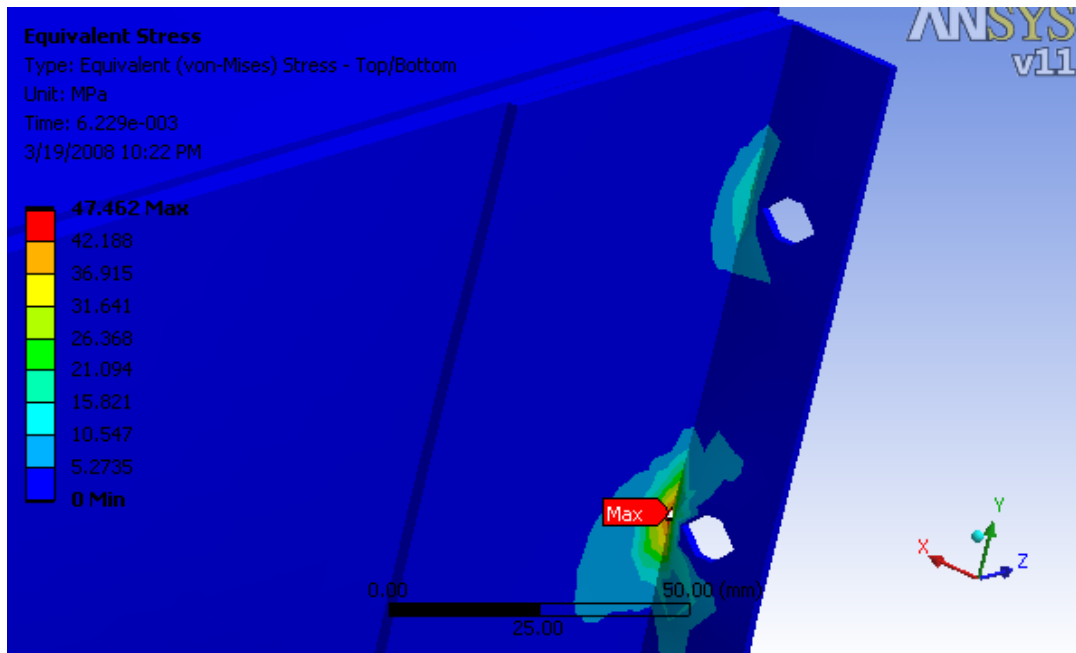


Figure 3.45 Equivalent Von-Mises stresses through -z-direction

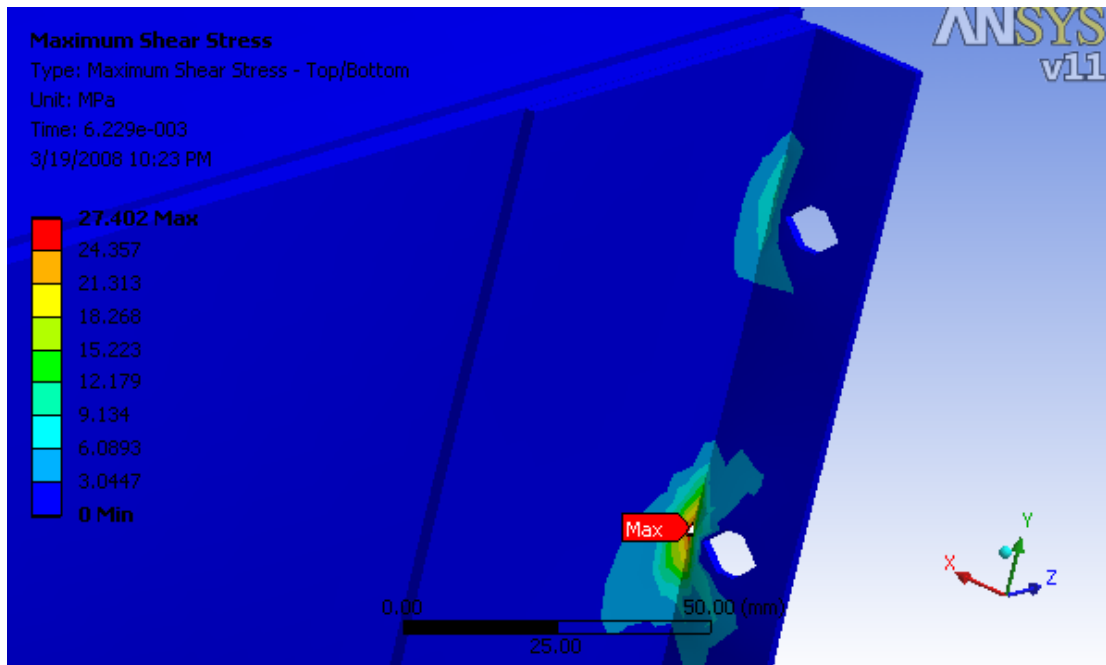


Figure 3.46 Maximum shear stresses through -z-direction

The results of analyses are summarized in Tables 3.11, 3.12 and 3.13.

Table 3.11: Maximum Von-Mises stresses

	+X	-X	+Y	-Y	+Z	-Z
Max Von Mises	29.417 MPa	27.445 MPa	14.777 MPa	359.89 MPa	47.174 MPa	47.462 MPa
Location	Handle Slots	Handle Slots	Cover Sides	Handle Slots	Handle Slots	Handle Slots

Table 3.12: Maximum shear stresses

	+X	-X	+Y	-Y	+Z	-Z
Max Shear	15.652 MPa	15.601 MPa	8.372 MPa	114.44 MPa	27.4 MPa	27.402 MPa
Location	Handle Slots	Handle Slots	Cover Sides	Handle Slots	Handle Slots	Handle Slots

Table 3.13: Maximum deformation

Direction	+X	-X	+Y	-Y	+Z	-Z
Max Def.	0.01673 mm	0.01673 mm	0.85071 mm	1.1526 mm	0.03386 mm	0.03508 mm
Location	Left Back of Chassis	Right Back of Chassis	Mid of Cover (-)	Mid of Cover (+)	Bottom of Chassis (+)	Bottom of Chassis (-)

Considering the overall Von-Mises and shear stresses, the maximum stresses occur on the handles when the loading is in  $-y$  direction. The corners in the back part of the handles cause a serious stress concentration, so 2 mm radius is given to these corners during the manufacturing process.

An example of deformation vs time and equivalent stress vs. time graphs are given in Figures 3.47 and 3.48 for  $-y$ -direction. It can be easily observed that the curves are similar to the curve which defines the shock profile. The curve which occurs after the releasing of shock excitation at 11 ms shows the transient response and damping of the excitation.

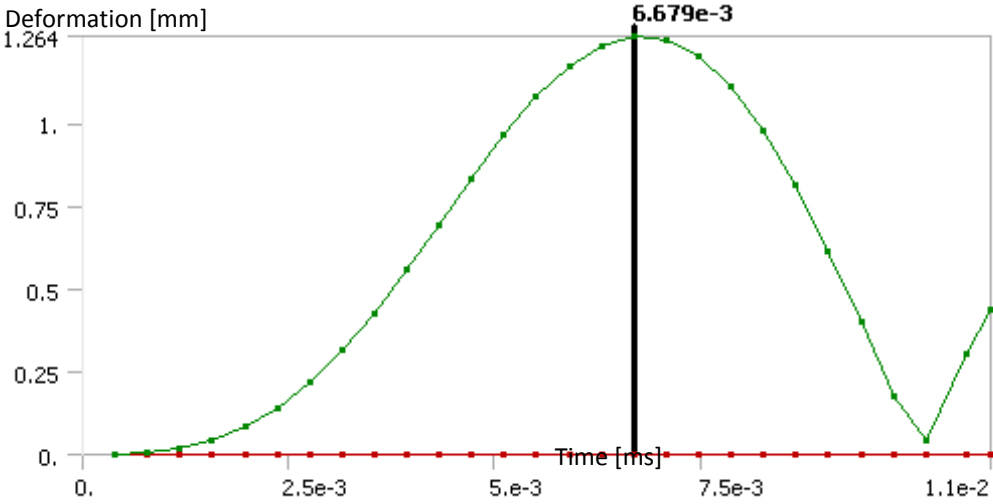


Figure 3.47 Deformation vs. time graph in  $-y$ -direction

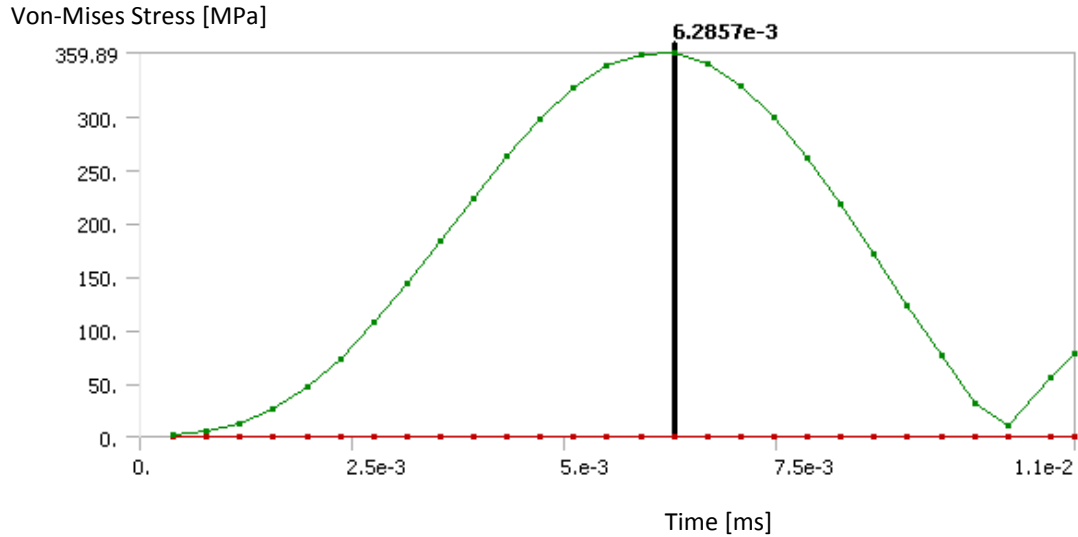


Figure 3.48 Von-Mises stress vs. time graph in  $-y$ -direction

There are two materials used in the design of the packaging. Al 5083 H321 is used for chassis and cover, and structural steel St 37 is used for handles. Ultimate and yield strengths of the materials used are given as.

For Aluminum Al 5083 H321;

$$\sigma_{UTS} = 317 \text{ MPa} \quad \text{and} \quad \sigma_Y = 228 \text{ MPa}$$

For R St 37-2

$$\sigma_{UTS} = 460 \text{ MPa} \quad \text{and} \quad \sigma_Y = 235 \text{ MPa}$$

The maximum stress on aluminum features occur again when the loading is in  $-y$  direction. The location of the stress is given in Figure 3.49. The factor of safety of this loading according to the aluminum features is calculated as:

$$r_{1,Al} = 317/17.036 = 18.60$$

For steel structures the maximum Von-Mises and shear stresses are 359.89 and 114.44 MPa respectively which corresponds to the safety factor calculated below.

$$\Gamma_{1,Al} = 460/359.89 = 1.27$$

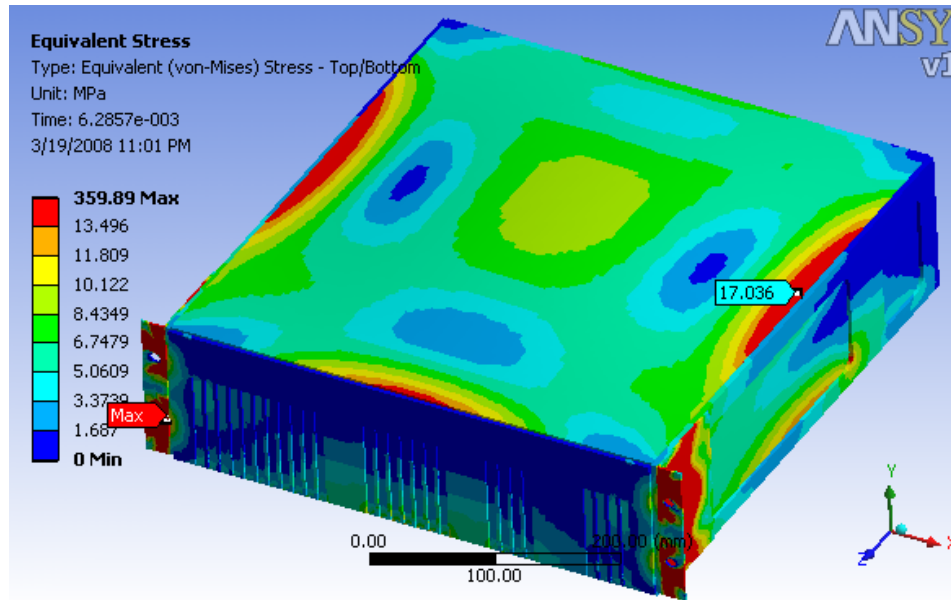


Figure 3.49 Maximum Von-Mises stress through –y-direction with different scale

The safety factors are calculated based on the Von-Mises Stresses since both aluminum and steel are ductile materials. Ultimate tensile stresses are used in safety factor calculations because in the finite element model the actual manufacturing details are not modeled resulting in peak stresses exceeding the yield limit near the corner regions. For instance, the maximum stress of handles is below the maximum ultimate strength level, it exceeds the yield strength level. The location of the maximum stress due to shock loading is in the inner corners of the handles. In the analysis model there are no radiuses, fillets and chamfers since such details cause

unnecessary memory and time usage. But, in actuality, the handles are manufactured by providing a 2 mm bending radius of the inner edge. Therefore, the actual maximum stress will be much lower than the maximum stress found in the sharp corner.

### **3.5 SHOCK TEST**

The equipment was tested according to MIL-STD-810F, method 516.5, Procedure I (Functional shock). The purpose of the test is to [7]:

- a. Provide a degree of confidence that material can physically and functionally withstand the relatively infrequent, non-repetitive shocks encountered in handling, transportation, and service environments.
- b. Determine the material's fragility level, in order that packaging may be designed to protect the material's physical and functional integrity; and
- c. Test the strength of devices that attach material to platforms that can crash.

#### **3.5.1 TEST LEVELS**

The EUT was operational, secured to the shock table with the fixture.

Shock test was performed in both directions along each of three orthogonal axes for three times (3x3x3). The EUT was expected not to be damaged nor not be degraded in its performance during and after having been subjected to shocks.

Shock pulse, which was like saw-tooth type pulse, its equivalent SRS (Shock Response Spectrum) datum of 20 g peak acceleration with an effective transient duration of 11 ms was used. The test is done by a vibration shaker Derritron VP 85

Electromagnetic Vibrator (Figure 3.50). The specifications of the shaker are given in Table 3.14.



Figure 3.50 Derritron VP 85

Table 3.14 Specifications of Derritron VP 85

Maximum thrust, sinusoidal	7500 N
Maximum thrust, random	4560 N
Maximum acceleration	94 g
Maximum stroke	$\pm 12,7$ mm
Frequency range	5 – 3000 Hz
Table size	$\varnothing 178$ mm
Slip Table	715 x 572 mm, 70 x 70 mm, M10
Temperature range	-50°C +80°C

The shaker is controlled by LDS Dactron Laser USB Control System. The accelerometer used through the tests is PCB Piezotronics 353B34 Shaker Accelerometer.

The data taken from the test machine for +z-direction shock loading is given in Figure 3.51. In this Figure, the shock profile is given as acceleration versus time curve. The acceleration used is in gravity units (in fact it is dimensionless) which is equal to the acceleration divided by gravity. It can be easily observed from the graph that the maximum acceleration level of the shock profile is 20 g at about 0.055 ms. Although the profile is in terms of saw-tooth type pulse, it is simulated by a half sine shock pulse through the ANSYS analysis. The important thing for the analysis is the peak value of the profile. Half sine pulse is applicable to the saw tooth pulse, as the maximum acceleration calculation gives the same result with the graph. (Equation 3.4 [6] )

$$G = \frac{a}{g} \quad (3.4)$$

Substituting half sine shock pulse into acceleration yields,

$$G = \frac{a}{g} = \frac{20 \text{ g} \sin\left(\frac{\pi \cdot 0.055}{0.011}\right)}{g} = 20$$

There are four curves illustrated in Figure 3.49. These are profile curve, high-abort curve, low-abort curve and control curve. Profile curve is the actual shock curve defined for the test. Control curve is data gathered from the equipment by a piezoelectric accelerometer. The difference between the profile and control curves is due to transmissibility. There is a loss of shock frequency through the fixtures and the parts of the device. The low and high abort curves are used in order to control the test

procedure. If the control curve transcends the high-abort curve or falls under the low-abort curve, the shaker automatically stops the test.

The shock loading in other directions are applied alternately with similar shock profiles as Figure 3.51.

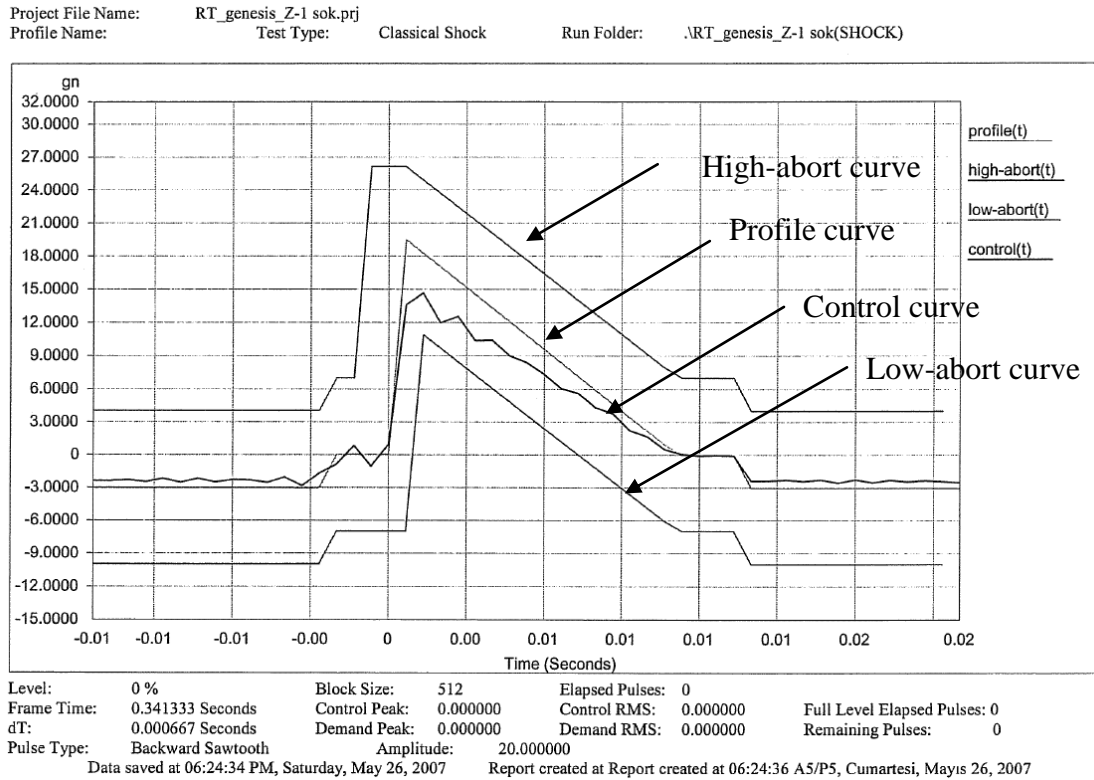


Figure 3.51 Shaker profile in +z-direction shock loading

Before performing the specified shock test, a few lower level shock pulses (10g, 15g) were applied to observe the effect on the equipment inside the EUT. Then the actual test was conducted according to the specified sequence in each of the principal axis.

### **3.5.2 TEST STEPS**

The steps of the test defined by MIL-STD-810 F are:

1. Mount EUT (Equipment Under Test) to the vibration shaker or slip table with mounting test fixture, check the EUT physically.
2. Prepare the functional test setup for EUT and perform visual and functional tests.
3. Place monitoring accelerometers to the hotspots determined during vibration tests.

The shock test for X-axis of the EUT shall be conducted in both directions along each of three orthogonal axes for three times.

4. Perform Visual & Functional Test one more time to EUT.
5. Repeat the steps for Y-axis.
6. Repeat the steps for Z-axis.

### **3.6 RESULTS**

MIL-STD-810F, method 516.5, Procedure I defines the functional test, meaning the equipment was working during the test. The electronic equipment successfully accomplished the shock test. Neither minor nor major functional and structural failures were observed during the test. The equipment worked properly during the test and continued its functions after the test. The visual test for the structural integrity of the equipment during test revealed that no failure of any form occurred during the shock test. This was expected based on the results of the shock analysis performed after the design process.

## **CHAPTER 4**

### **VIBRATION TEST AND ANALYSIS FOR ENVIRONMENTAL QUALIFICATION**

#### **4.1 INTRODUCTION**

Another important design criterion for electronic packaging is the vibration level of the working environment. The chassis and module installation of the device which is a concern of this thesis is analyzed and tested due to random vibration. Today, random vibration tests have common usage for qualification and acceptance of many types of equipment in different areas like military, industrial or commercial. Random vibration could represent real environments in which the electronic equipment should operate. This vibration environment includes automobiles, airplanes, ships, power plants, trains etc. Different environments have different vibration sources. Sources of vibration could be categorized as follows [16]:

- > In Stationary Systems: Unbalanced Loads
- > In Road Vehicles: Rough Surfaces of The Roads
- > In Sea Vehicles: Fluid/Structure Interaction
- > In Air Vehicles: Aerodynamic Loads

The response of the equipment to the random vibration is important since it also determines the reliability of the equipment. The vibration can cause fatigue and catastrophic failures.

The basic failure modes in random vibration are [6]:

- High acceleration levels
- High stress levels
- Large displacement amplitudes
- Electrical signal out of tolerance

The environmental vibration which is the concern of this thesis is caused by the hydrodynamic forces on the propeller blades interacting with the hull and reciprocating machinery of the engines [8]. The vibration frequency spectrum for ships defined by MIL-STD-810 F is between about 1 to 100 Hz. This is a low frequency spectrum but its amplitude is high. So this spectrum can cause high stress concentration on critical parts of the equipment. The design of the electronic packaging is done due to this severe vibratory condition, then the device is firstly analyzed by ANSYS and then verified by the vibration tests. This chapter explains the steps of analysis and the qualification test.

## **4.2 THEORY**

The study of vibration is concerned with the oscillatory motions of bodies and the forces associated with them [16]. All bodies possessing mass and elasticity are affected by vibration. Vibration is grouped according to its excitation as free or forced and according to its behavior as periodic (mostly sinusoidal) or random.

In this thesis random vibration response of the designed device is analyzed. Unlike sinusoidal vibration, random vibration is non-periodic. Random vibration analysis is based on statistical method of analysis and the time-history of the excitation is assumed to change random, as it is the case in real operational environments. The

random vibration data gathered from an environment or on a machine is the never same when it is measured twice.

Random vibration is based on probability. Knowledge of the past history of random motion is adequate to predict the probability of occurrence of various acceleration and displacement magnitudes [6]. It can be thought of as containing excitation at all frequencies within the specified frequency band but no excitation at any specific single frequency [24].

The process of vibration analysis requires the gathering of complex data, which must then be deciphered [25]. There are some transducers used for this purpose. The most common transducers are piezoelectric accelerometers. In these piezoelectric accelerometers, there is a weight between two piezoelectric (i.e., pressure-sensitive) films which moves in response to vibration and squeezes these piezoelectric films [25]. An electrical signal is sent each time the weight squeezes the films. By this way mechanical energy is converted into electrical signals. Other devices used as vibration sensors are electromagnetic transducers, electrical resistance strain-gage, and seismic spring-mass systems [26].

The basic measured data by the transducers are velocity, displacement, acceleration, and frequency. Velocity is the measurement of how fast an object is moving from zero-to-peak. The effective frequency range of most velocity transducers is from about 10 to 2,000 Hz. Displacement is the measurement of how far an object is moving from peak-to-peak. The effective frequency range of noncontacting displacement transducers is from about 0 to 600 Hz. For contacting displacement transducers, the effective frequency range is about 0 to 200 Hz. Acceleration measures the rate of change of velocity from zero-to-peak and is normally measured in units of gravitational force (g's). This means that high frequencies generate high g levels. The effective frequency range for low frequency accelerometers is from about

2 to 500 Hz. The effective range of high frequency accelerometers is from about 5 to 20,000 Hz [27].

The data collected from a source is used for a curve generation in order to define the profile of the vibration. These profiles can be formed in time domain and frequency domain.

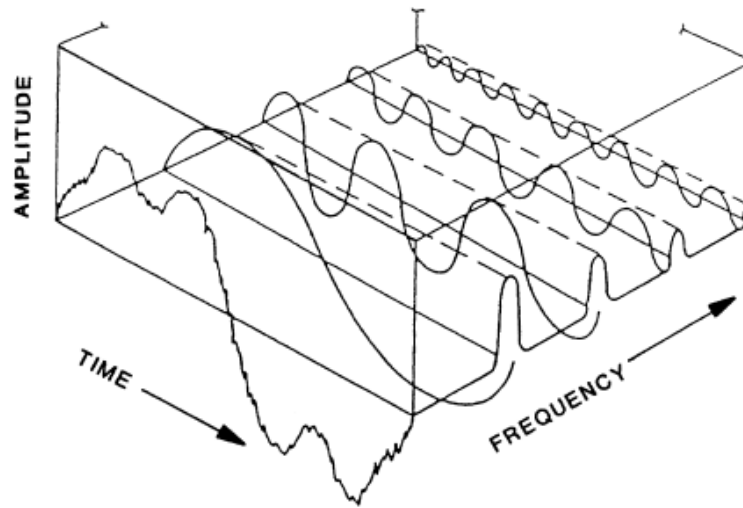


Figure 4.1 Relationship between time domain and frequency domain [25]

Vibration data plotted as amplitude versus time is referred to as a time-domain data profile [25]. With a mathematical method called Fast Fourier Transform (FFT), time-domain data is converted into Frequency-domain. FFT allows all complex wave forms could be broken down into their individual frequency components mathematically [27]. The frequency-domain amplitude can be the displacement per unit time related to a particular frequency, which is plotted as the y-axis against frequency as the x-axis; on the other hand the time-domain spectrum sums the velocities of all frequencies and plots the sum as the y-axis against time as the x-axis

[25]. The relationship between time and frequency domains is illustrated in Figure 4.1.

The instantaneous magnitudes of random vibration are specified only by probability distribution functions giving the probable fraction of the total time that the magnitude (or some sequence of the magnitudes) lies within a specified range [18]. The probability distribution is usually defined by *Gaussian Distribution* (or normal distribution) which is defined by equation 4.1 [6]:

$$Y = \frac{e^{-X^2/2\sigma^2}}{\sigma\sqrt{2\pi}} \quad (4.1)$$

where X is the instantaneous acceleration,  $\sigma$  is the RMS acceleration and Y is the probability density function which is defined per unit of X, for the ratio of X to  $\sigma$ .

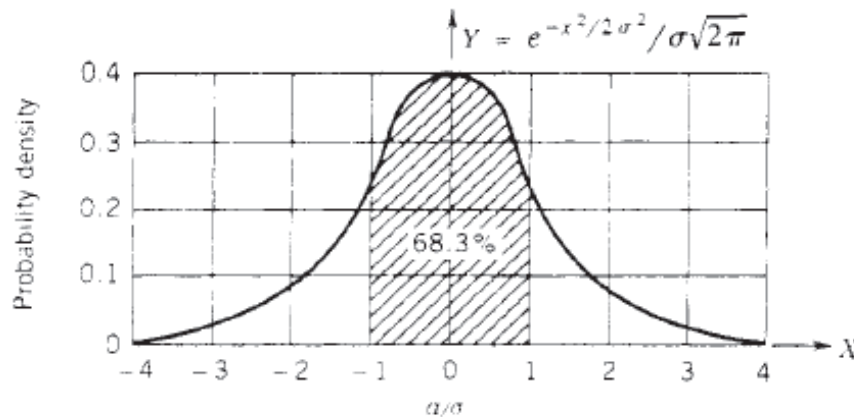


Figure 4.2 Gaussian distribution curve [6]

In true Gaussian random vibration, the amplitude value at any given time is a statistical relationship with time [24]. This relation is illustrated by Figure 4.2. This Figure shows the Gaussian distribution curve which represents the probability for the value of the instantaneous acceleration levels at any time [6]. From the curve it is easily observed that most of the time, the instantaneous acceleration values will be in the areas adjacent to zero. Generally speaking, Figure 4.2 shows how the Gaussian distribution relates to the magnitude of the acceleration levels expected for random vibration [6]. The instantaneous acceleration will be between the  $+1\sigma$  and the  $-1\sigma$  values 68.3% of the time. 95.4% of the time, the acceleration levels will be between the  $+2\sigma$  and the  $-2\sigma$  values, and the acceleration level will be between the  $+3\sigma$  and the  $-3\sigma$  values 99.73% of the time. Since  $+3\sigma$  and the  $-3\sigma$  levels are close to 100% of the time, these levels are considered as the maximum acceleration levels for random vibrations. Higher acceleration levels of  $4\sigma$  and  $5\sigma$  can occur in the real world, but they are usually ignored because virtually all of the test equipments for random vibration have  $3\sigma$  clippers built into the electronic control systems [6]. A real plot of the random vibration acceleration or displacement with respect to time is illustrated in Figure 4.3.

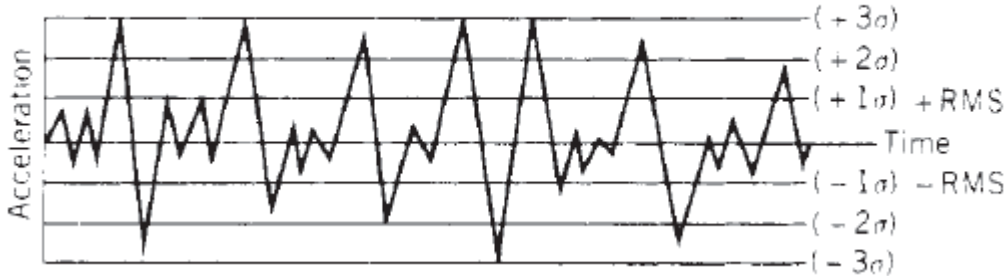


Figure 4.3 A time history of a typical random vibration acceleration trace [6]

Since random vibration is a sum of harmonic vibrations, most random vibration testing uses Gaussian random suppositions for both measurement and specification purposes [24]. With Gaussian assumptions, there is no definable maximum amplitude, and the amplitude levels are measured in root-mean-squared (RMS) values [24]. Random vibration is generally defined by power spectral density (PSD) curves and these curves are plotted on log-log papers. Power spectral density is defined as the power per unit frequency interval. Mathematically it is expressed as equation 4.2 [6]:

$$P = \lim_{\Delta f \rightarrow 0} \frac{G_{RMS}^2}{\Delta f} \quad (4.2)$$

where  $G$  is the root mean square (RMS) of the acceleration and  $\Delta f$  is the bandwidth of the frequency range expressed in Hertz.

A typical PSD curve is given in Figure 4.4. The area under the curve gives the overall RMS acceleration level. This summation over density is given by equation 4.3 [24] :

$$G_{RMS} = \left[ \int_{f_1}^{f_2} g_d^2 df \right]^{1/2} \quad (4.3)$$

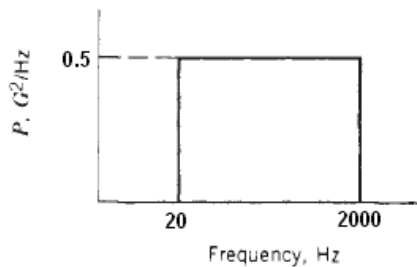


Figure 4.4 Typical PSD curve

If vibration spectrum has a flat PSD like in Figure 4.4, then the RMS acceleration is calculated by Equation 4.4 [24]:

$$G_{RMS} = \left[ \int_{f_1}^{f_2} g_d df \right]^{1/2} \quad (4.4)$$

where  $g_d$  is the acceleration density.

$G_{RMS}$  is expressed in gravity units, (Equation 4.5 [6] ),

$$G = \frac{a}{g} \quad (\text{dimensionless}) \quad (4.5)$$

where,

“a” is the acceleration and “g” is the standard earth gravity.

The PSD curves of random vibration mostly possess straight sloping lines. For these lines, sloping up to the right is considered to have a positive (+) and sloping down to the right is considered to have a negative (-) slope, which are shown in Figure 4.5.

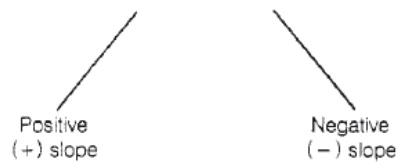


Figure 4.5 Positive and Negative Curve Slopes [6]

Besides acceleration spectral density, random vibration can be also specified by velocity spectral density and displacement spectral density defined in Table 4.

Table 4.1 Spectral densities

Definition	Dimension
Acceleration Spectral Density	$\frac{\text{Acceleration}^2}{\text{frequency}}$
Velocity Spectral Density	$\frac{\text{Velocity}^2}{\text{frequency}}$
Displacement Spectral Density	$\frac{\text{Displacement}^2}{\text{frequency}}$

### 4.3 ANALYSIS

Manufacturing high reliable electronic equipment safely operating in its working environment requires a proper design process substantiated with relevant analysis. This part of the Chapter 4 briefly explains the procedure of the vibration analysis performed by the random vibration module of ANSYS Workbench 11.0.

#### 4.3.1 GEOMETRY

The geometry of the vibration model is the same geometry of the shock model. Finite element model is the shell model of having three main parts; cover chassis and 19” rack handles. The contact regions are defined over the same regions used in the shock analysis model and they cover the region where two handles are bonded to the chassis and the mating surface of cover with the chassis illustrated as Figure 3.7. Cards which are placed inside the chassis, their interfaces and filters are modeled as point masses and their inertia tensors are defined in ANSYS. The moments of inertia of the point mass are given in Table 3.9 is also valid here for the random vibration analysis. The mass is attached to 6 holes placed on the bottom plate of the chassis. The outer

environment interfaces like connectors, ground screws are not modeled similar to the shock analysis since their inertia effects are negligible. The total mass of the model including the point mass is 11.9 kg. The geometry used for vibration analysis is shown by Figure 4.6.

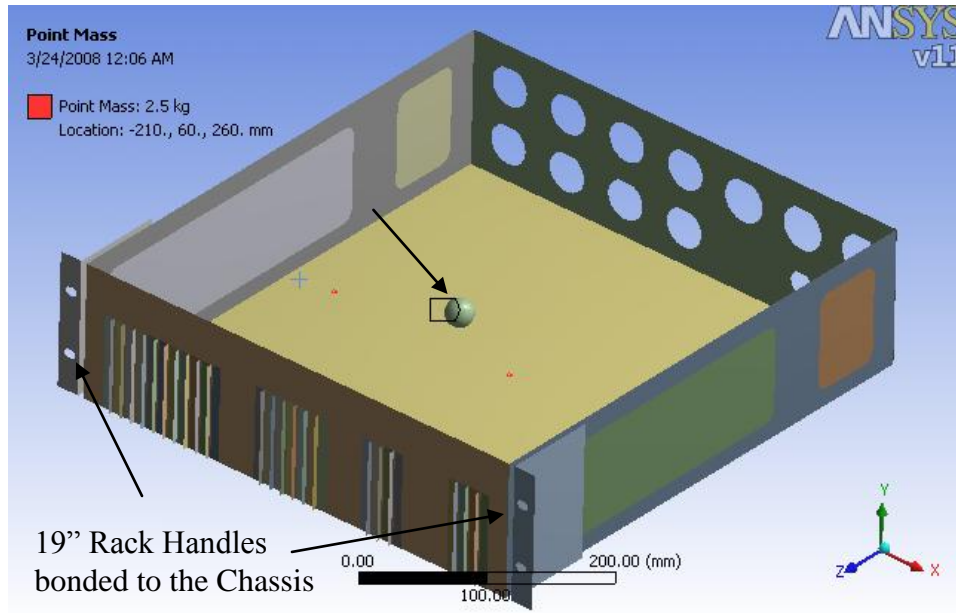


Figure 4.6 Geometry used for vibration analysis

### 4.3.2 MESHING

For finite element model, 5 mm uniform quadrilateral elements are used. There are 39152 nodes and 38860 elements created for meshing the model. Elements are Shell 181 for main parts of the geometry, Conta 173 and Targe170 linear for contact regions. The meshing used for random vibration analysis is similar to the one used for shock analysis.

### 4.3.3 LOADING AND BOUNDARY CONDITIONS

The vibration test is performed in 3 directions, x, y and z axes separately. The random vibration data is given by MIL-STD-810 F Method 514.5 Category 10 (Ship-Surface Ship) [7]. The PSD curve of this category is defined by Figure 4.7. This is an acceleration spectral density curve. The specified frequency range according to this PSD curve is between 1 Hz to 100 Hz.

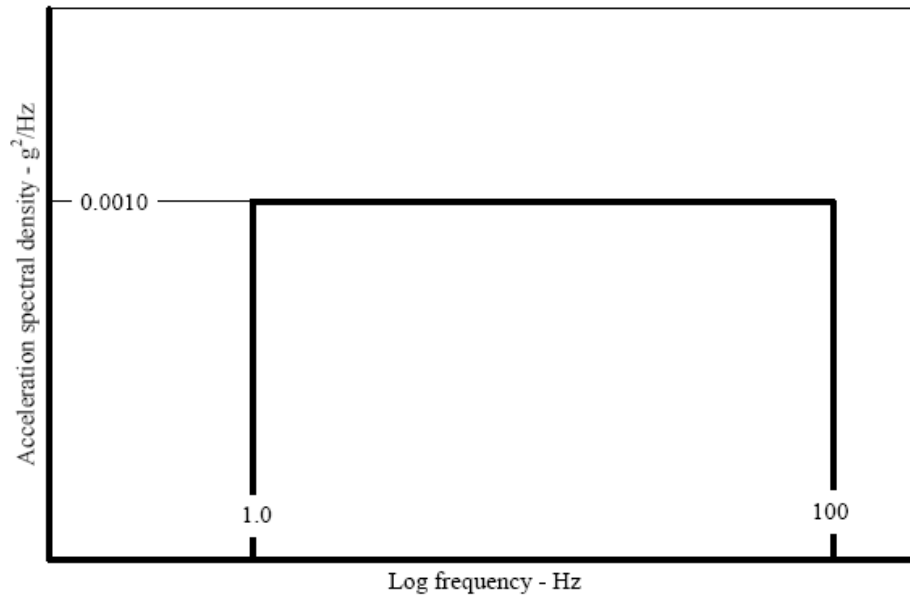


Figure 4.7 Shipboard vibration exposure [7]

The Random Analysis in ANSYS is based on the modal superposition method. In this method a modal analysis is done for extracting the natural frequencies and mode shapes. The analysis is done for 4 modes, 8 modes, 10 modes, and 12 modes. The 12 modes of the electronic equipment can be seen in Table 4.2.

Table 4.2 10 Modes of the equipment

Mode	Frequency (Hz)
1	115.78
2	133.88
3	227.57
4	265.65
5	266.78
6	374.98
7	415.66
8	464.27
9	468.68
10	500.32
11	549.01
12	601.1

In vibration analysis lower modes are important. The first mode, the lowest natural frequency, is the fundamental resonant mode of the vibrating system. For the equipment, the first harmonic mode occurred at 115.78 Hz on cover. The behavior of the equipment in this frequency is illustrated in Figure 4.8. The deformation shown in Figure 4.8 is only the relative deformation of the points, they do not mean anything in structural analysis. The second and the third mode shapes are also given in Figures 4.9 and 4.10. The wireframes illustrate the non-deformed forms of the structures.

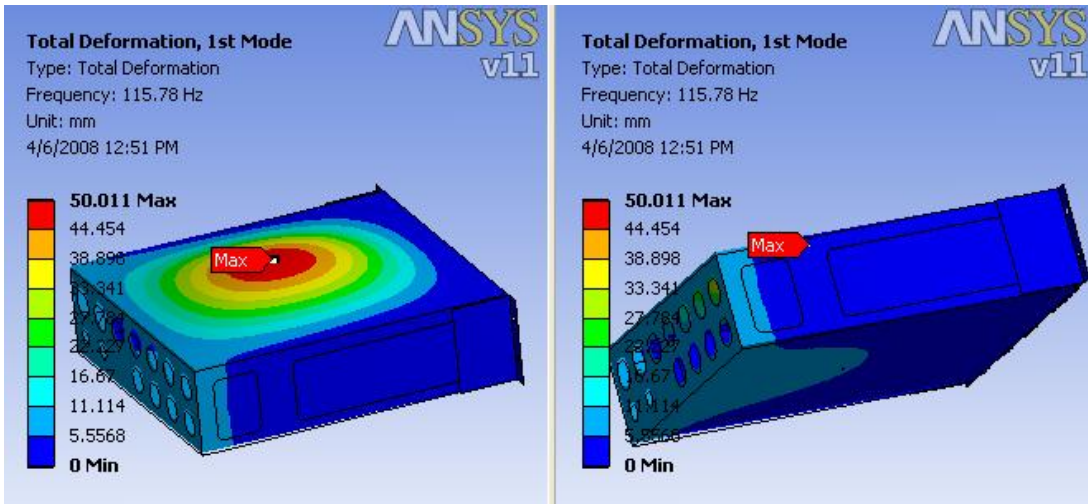


Figure 4.8 Oblique views of first harmonic mode

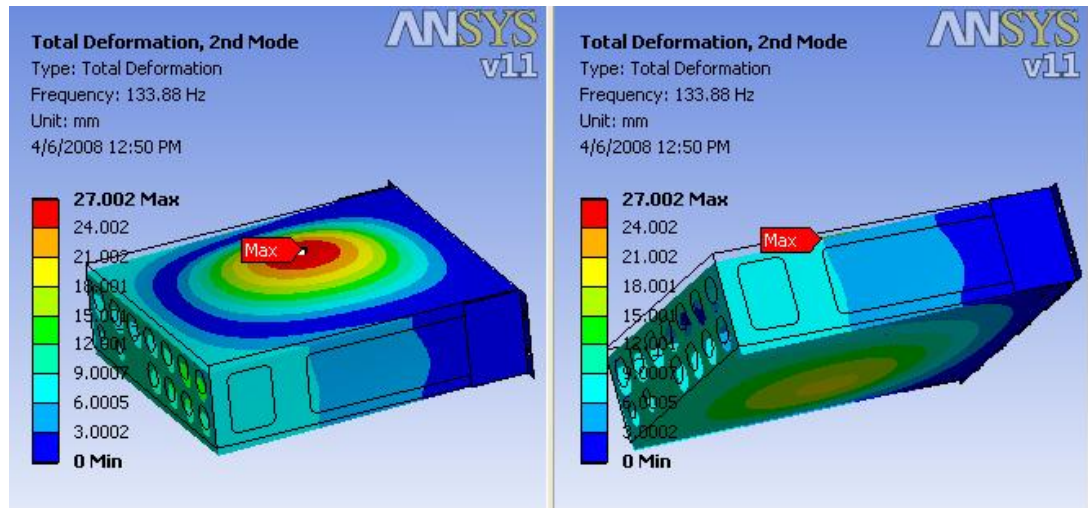


Figure 4.9 Oblique views of second harmonic mode

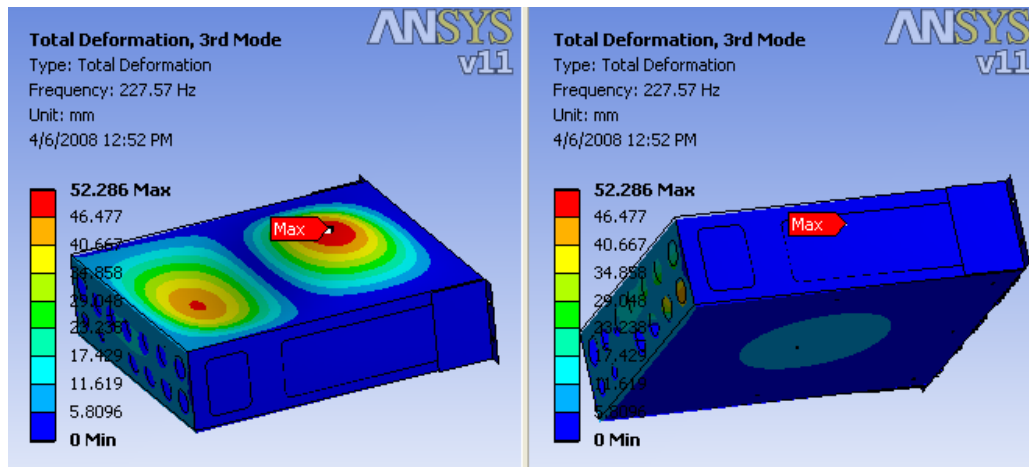


Figure 4.10 Oblique views of third harmonic mode

The first mode occurred on the chassis is the eight harmonic mode. Figure 4.11 shows the mode shape for this mode. It is occurred at frequency of 464.27 Hz. This is a very high frequency that the device probably will not be subjected to it for its whole working life.

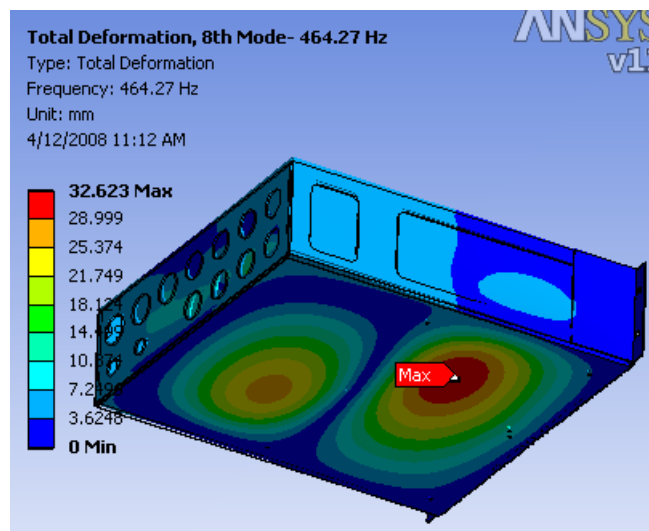


Figure 4.11 Oblique view of eight harmonic mode

The boundary condition of random vibration analysis uses the boundary condition of modal analysis. The boundary condition of the modal analysis is the fixed support condition of washer regions on the slots of the handles shown in Figure 4.12.

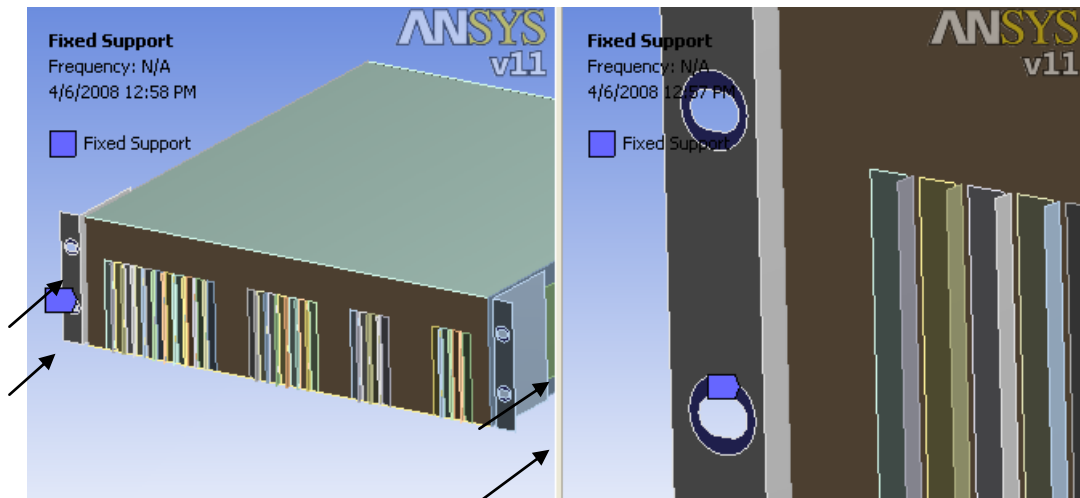


Figure 4.12 Boundary condition for modal analysis

The initial condition of the random vibration analysis is taken as the modal analysis. The PSD curve, given by Figure 4.7 and specified by the standard, is defined in ANSYS as a PSD excitation by a tabular data with a graph shown in Figure 4.10. The damping ratio for metal structures with joints is experimentally found between 0.03-0.07 [28]. This parameter is taken as 0.05 for this vibration analysis and it is defined in ANSYS. Finally, the PSD excitation shown in Figure 4.13 is applied in each direction.

The response of more complicated (multi-degree-of-freedom) linear systems is typically found by superimposing modal responses, each of which represents the response of single-degree-of-freedom system [29]. The modal matrix whose columns

are the normalized mode shapes corresponding to the chosen generalized coordinates. This matrix is used to uncouple and solve the differential equations for forced vibrations of a linear n-degree-of-freedom system [30]. In random vibration solution, the random acceleration profile given to the nodes as an inertia load and .The basic equation of the forced vibration is given in Equation 3.2 as:

$$KD_n + C \dot{D}_n + M \ddot{D}_n = R_n \tag{3.2}$$

The only difference between a transient solution and a random vibration solution is the right hand side of the equation which is the time-dependent forcing function, R. The value of this function is random magnitude within the range of specified profile.

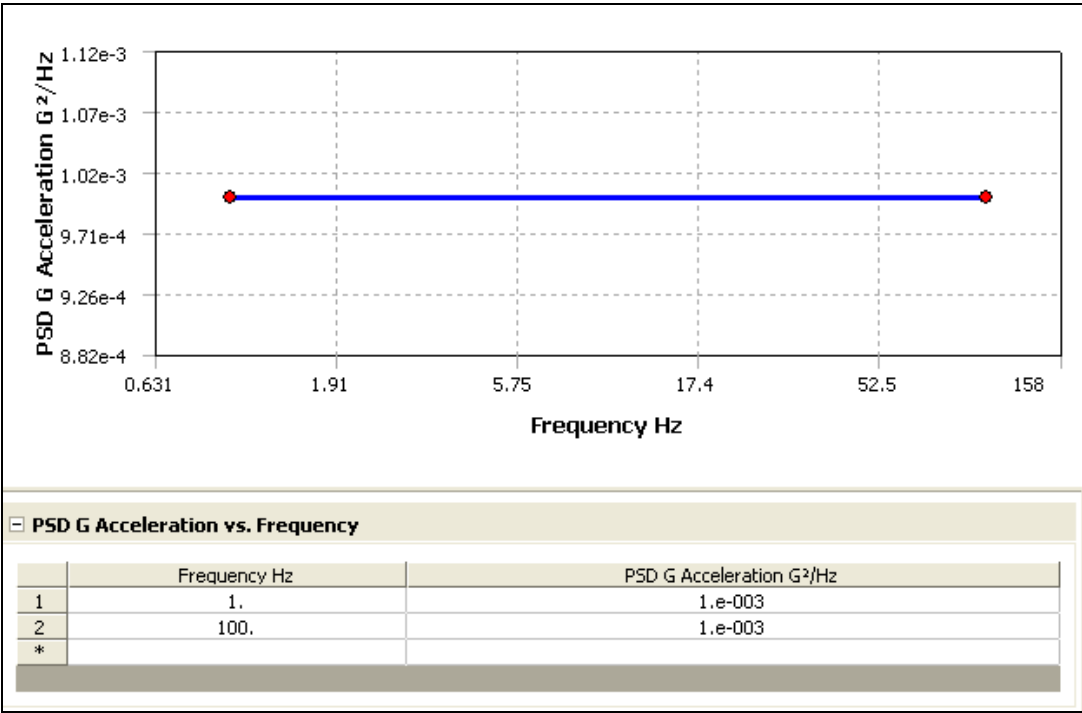


Figure 4.13 PSD excitation used by ANSYS

#### 4.3.4 EVALUATION OF ANALYSIS RESULTS

As the result option used in random vibration analysis,  $3\sigma$  probability method is used in order to obtain higher peak values throughout the analysis. This means the results of the all analysis given and discussed in this section are the results having %99.737 probability of occurrence in the given range of results.

The vibration analysis done for the equipment is actually based on the 10 modes. But it is performed again by including 3, 8 and 12 modes in the analysis. The results of these analyses are gathered in Table 4.3.

Table 4.3 Results of the analyses performed for different number of modes

	X	Y	Z
Max. Equivalent Stress (Analyzed for 3 Modes)	0.0543 MPa	14.417 MPa	0.3563 MPa
Max. Equivalent Stress (Analyzed for 8 Modes)	0.0651 MPa	14.467 Mpa	0.4329 MPa
Max. Equivalent Stress (Analyzed for 10 Modes)	0.1527 MPa	14.485 MPa	0.4550 MPa
Max. Equivalent Stress (Analyzed for 12 Modes)	0.1538 MPa	14.486 MPa	0.4600 MPa

It is seen from Table 4.3 that, the results of the  $3\sigma$  random stresses converge when the mode number gets closer to 12. So, 10 number of modes included for this analysis is enough to get satisfactory results. Figures 4.14 - 4.19 show the results of the random vibration analysis due to  $3\sigma$  method with 12 number of modes.

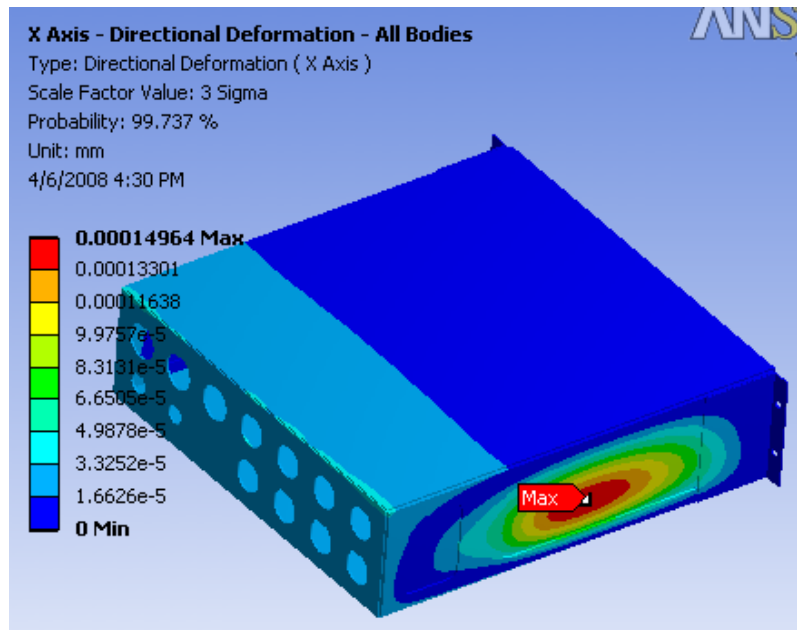


Figure 4.14 Directional deformations through x-axis (Random vibration)

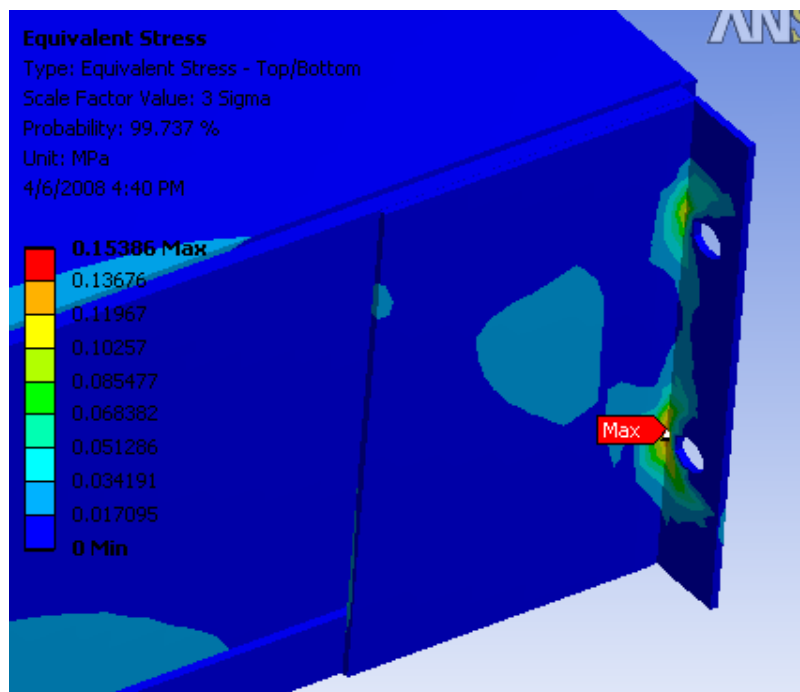


Figure 4.15 Equivalent Von-Mises stress through x-axis (Random vibration)

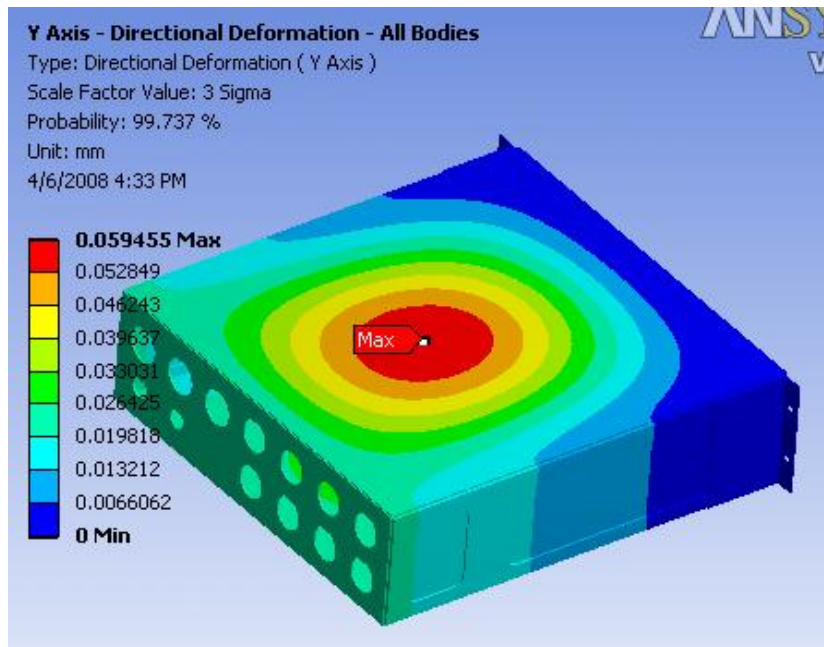


Figure 4.16 Directional deformations through y-axis (Random vibration)

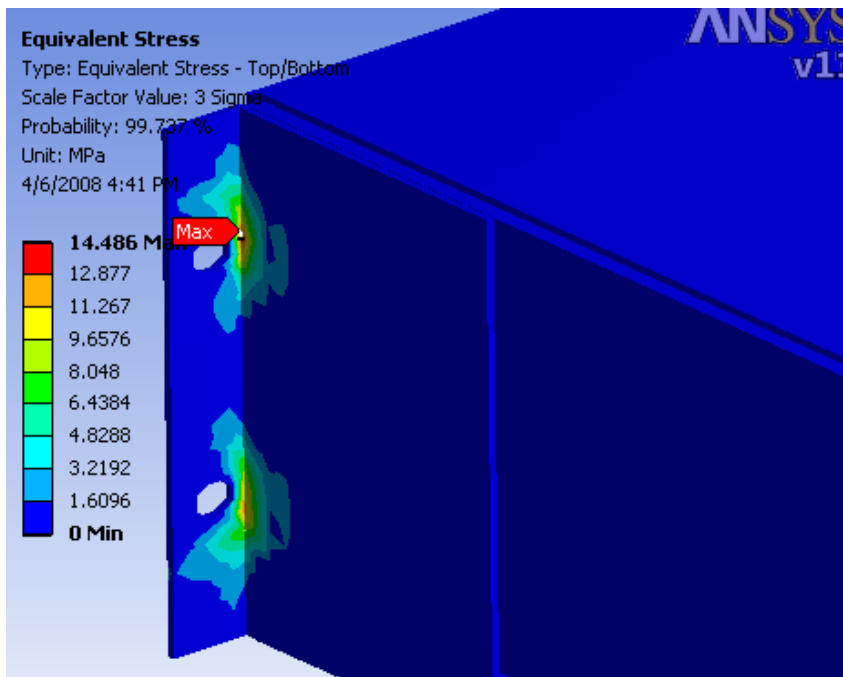


Figure 4.17 Equivalent Von-Mises stress through y-axis (Random vibration)

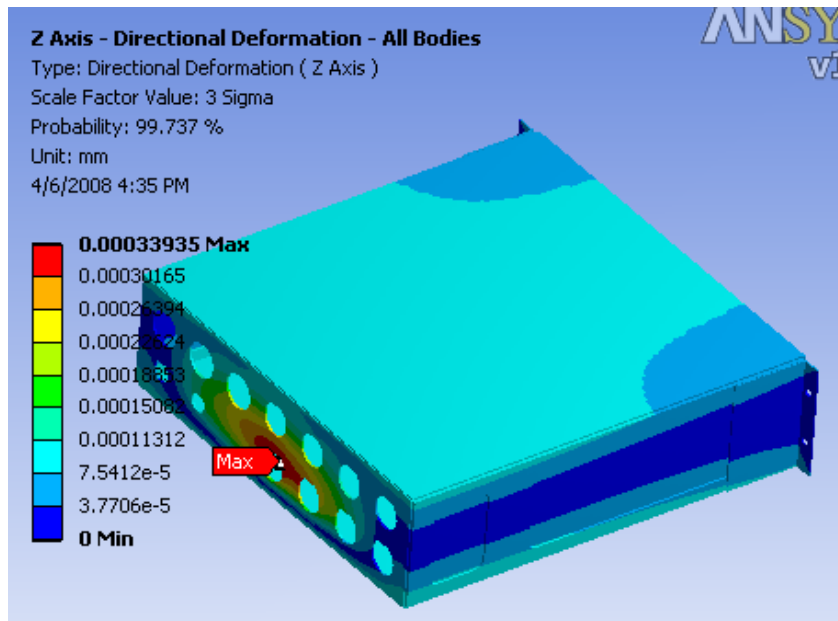


Figure 4.18 Directional deformations through z-axis (Random vibration)

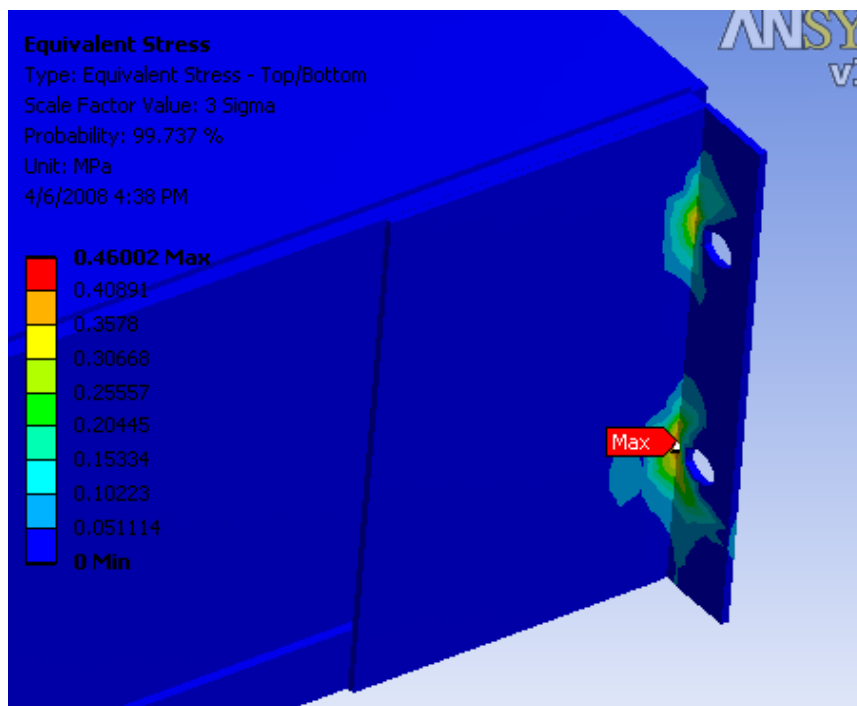


Figure 4.19 Equivalent Von-Mises stress through z-axis (Random vibration)

The results of the analysis are summarized in the Tables 4.4 and 4.5.

Table 4.4 Maximum deformation occurred in random vibration

	X	Y	Z
Max. Deformation (mm)	$0.1496 \times 10^{-3}$	$59.455 \times 10^{-3}$	$0.339 \times 10^{-3}$
Location	Left Side of Chassis	Middle of Upper Cover	Back Plate of Chassis

Table 4.5 Maximum Von-Mises stresses occurred in random vibration

	X	Y	Z
Max. Equivalent Stress (Mpa)	0.1538	14.486	0.4600
Location	Handle Slots	Handle Slots	Handle Slots

Similar to the shock analysis, the maximum stresses are occurred in the back corners of handle slots. Since the slots are taken as fixed support, the maximum stress is expected near these parts. From the tables, it can be observed that both stress and deformation levels are small. According to these results, the equipment will work properly under this vibration load.

#### **4.4 VIBRATION TEST**

The vibration test of the EUT (Equipment under Test) was performed according to MIL-STD-810F Method 514.5 Category 10. Method 514.5 defines the vibration tests and category 10 points ship and ship surface.

Random vibration test is performed to [7]:

- a. Develop material to function in and withstand the vibration exposures of a life cycle including synergistic effects of other environmental factors, material duty cycle, and maintenance.
- b. Verify that material will function and withstand the vibration excitations.

#### **4.4.1 TEST LEVELS**

The EUT was operational, secured to the vibration table and the fixture. Vibration test was performed along each of three orthogonal axes. All tests in one axis shall be completed before proceeding to tests in another axis. The EUT was expected not to be damaged nor not be degraded in its performance during and after having been subjected to random vibration excitation.

The test was done by a vibration shaker Derritron VP 85 Electromagnetic Vibrator. The shaker was controlled by LDS Dactron Laser USB Control System. The accelerometer used through the tests was PCB Piezotronics 353B34 Shaker Accelerometer. The shaker used for the test of random vibration was the same shaker used for shock analysis and it was in given in Figure 3.50.

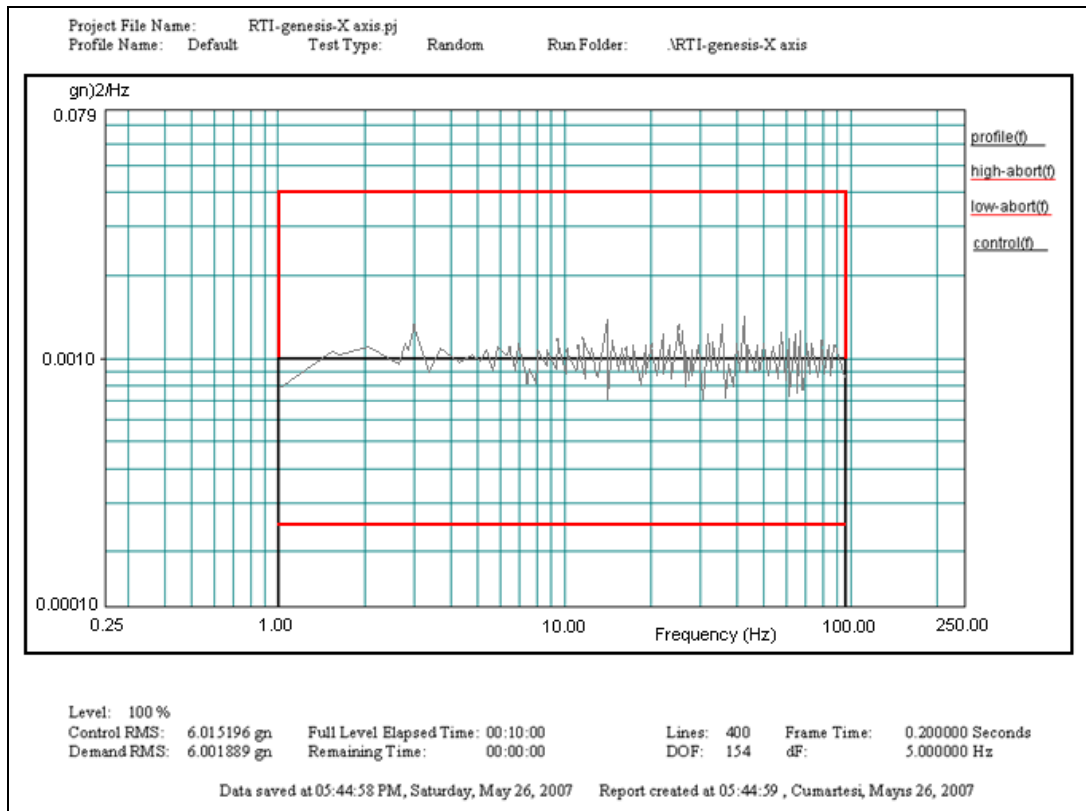


Figure 4.20 Shaker profile in x axis random vibration loading

The gathered data forming the control curve is not exceeding the high-abort curve. This graph shows the rigidity of the electronic equipment. The random vibration loading in other axes are applied alternately with similar vibration profiles as given in Figure 4.20.

#### 4.4.2 TEST STEPS

The steps of the test defined by MIL-STD-810F are:

1. Perform a visual inspection of the equipment and an operational test.

2. Mount EUT to the vibration shaker or slip table with mounting test fixture, check the EUT as physically.
3. Prepare the functional test setup for EUT and perform visual and functional tests.
4. Place monitoring accelerometers according to the possible resonating sections of EUT monitored in test step and record the response of accelerometers during the rest of the test.
5. Perform Visual and Functional Test one more time to EUT.
6. Repeat these steps for the Y-axes.
7. Repeat these steps for the Z-axes.

## **4.5 RESULTS**

The electronic equipment successfully completed the random vibration test. There were neither minor nor major functional failures observed through the test. The visual test for the structural integrity of the equipment during test revealed that failure of any form did not occur during the random vibration test. This was expected based on the results of the random vibration analysis performed after the design process.

In addition, the results of the ANSYS analysis also gives idea about the suitable locations of critical electrical modules since the solder of the modules are sensitive to vibration. The first three modes are illustrated by Figures 4.8-4.10. According to the mode shapes, the critical region is mainly cover of the device. The first chassis mode appears at eight mode which has a very high frequency. (Figure 4.11) So, it could be concluded that the placement of the cards seem not to be inappropriate based on the results of these analyses.

## **CHAPTER 5**

### **TEMPERATURE TEST AND ANALYSIS FOR ENVIRONMENTAL QUALIFICATION**

#### **5.1 INTRODUCTION**

There are three main points in the overall design of an electronic packaging: electromagnetic design, mechanical design and thermal design. The thermal design of an equipment plays an important role in the functioning of a device since it can cause thermal fatigue failures.

For naval applications, the electronic devices are mainly installed in a console or large cabinets. These cabinets are cooled by forced convection by fan systems or in case of air-conditioned rooms, they are cooled by natural convection with an opening on the top and bottom of cabinets or consoles.

The lids and covers supported by EMI or environmental gaskets make an equipment more sensitive about heating since it cuts the path of natural convection. So, if the cooling mechanism in the cabinets is not enough for the equipment and extra precaution for excessive heating is needed, the equipment could be cooled down by fin structures, internal fans or water/air cooled heat exchangers.

The electronic device which is the scope of this thesis is placed in a 19" rack cabinet which is assumed as cooled by natural convection. The thermal design criteria for this electronic equipment are that it should work between  $-15^{\circ}\text{C}$  and  $55^{\circ}\text{C}$ . In this

chapter, the equipment's packaging is examined and analyzed if its temperature exceeds the highest working temperature with its current cooling mechanisms under the specified thermal loading generated during the operation of the device.

## 5.2 THEORY

The electronic device designed in this thesis includes 10 audio and a control cards. The main heat sources and the main heat victims inside the device is the components placed on these printed circuits.

There are two approaches for thermal design and thermal analyses of an electronic device: 1) component oriented approach and 2) PCB oriented approach. The main difference between these approaches is shown in Figure 5.1. For component oriented approach the components are treated as an array of heated blocks from which all heat is dissipated. On the other hand, PCB oriented approach looks at the PCB as a thermally conductive plate with heat sources [31]

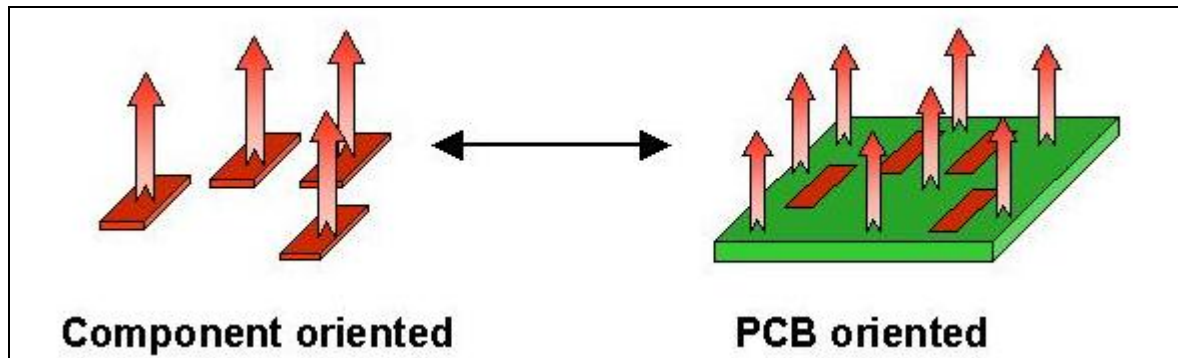


Figure 5.1 Component and PCB oriented approaches [31]

Through the years, PCB oriented approach gained an importance with the development of PCB plates having copper layers in it since these layers make PCB a high thermal conductive plate.

Basically, PCB oriented approaches calculates the thermal conductivity. But there is also a heat loss from the surface of a PCB to the ambient air. This situation is more challenging to describe mathematically since it involves the simultaneous processes of heat spreading by conduction and heat extraction over the surface of the board by convection and radiation where the efficiency of heat transfer from the PCB to air has a significant effect on the temperature difference between the chip and the air [32]. Figure 5.2 shows the related heat flow patterns of a test PCB with a lead frame on it. The heat convection and radiation is calculated for both regions separately, and schematically the heat flow pattern is shown in Figure 5.2. In this thesis convection and radiation over PCB and its modules are ignored, and PCB is examined as a conductive plate with heat sources on it.

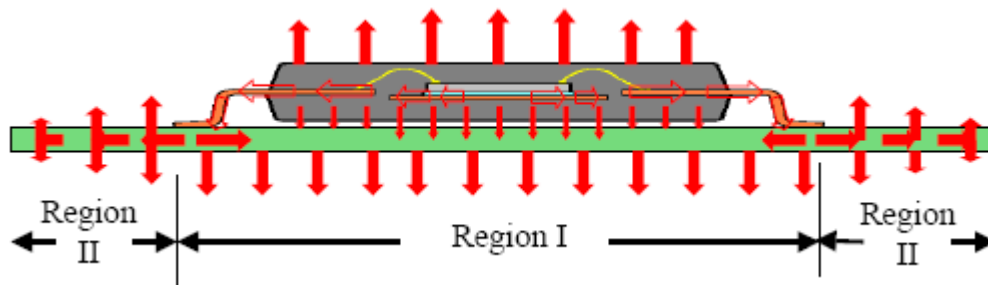


Figure 5.2 Heat flow patterns on a test PCB [32]

Today, most of the PCB's are laminated composites formed by copper foils and glass-epoxy as a base material which is also called FR-4. The "FR" means Flame

Retardant” and Type "4" indicates woven glass reinforced epoxy resin [33]. The general illustration of a laminated composite is given in Figure 5.3. In Figure 5.3, the numbering system for indicating different layers will be used as a reference.

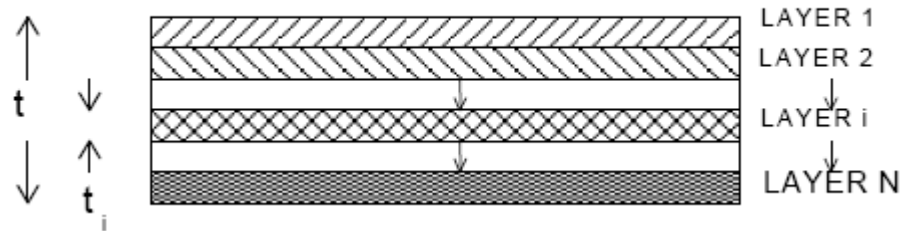


Figure 5.3 Cross-sectional area of PCB [34]

As mentioned before, the copper layers have high thermal conductivity whereas glass-epoxy has low thermal conductivity. A typical conductivity of copper layer ( $k_c = 385 \pm 15 \text{ Wm}^{-1}\text{K}^{-1}$ ) is very similar to that of bulk Cu, while the conductivity of glass-epoxy ( $k_g = 0.59 \text{ Wm}^{-1}\text{K}^{-1}$ ) is approximately 700 times smaller than the thermal conductivity of copper layers  $k_c$  [35]. The large difference of thermal conductivity between copper and glass-epoxy makes the PCB to behave in anisotropic fashion thermally. Therefore PCBs are modeled as a single object, without having a detailed representation of individual layers, with effective thermal conductivities in the in-plane direction (in the plane of the board) and normal direction (perpendicular to the board) [36]. The effective in-plane and normal thermal conductivities,  $k_{p,e}$  and  $k_{n,e}$  are typically calculated by assuming one-dimensional heat conduction through a composite layer, and neglecting the thermal contact resistance between the copper and glass-epoxy layers. The effective in-plane and normal thermal conductivities,  $k_{p,e}$  and  $k_{n,e}$  are given in Equations 5.1 and 5.2 [36].

$$k_{p,e} = \frac{\sum_{i=1}^{N_c} k_c t_{c,i} + \sum_{i=1}^{N_g} k_g t_{g,i}}{t_t} \quad (5.1)$$

$$k_{n,e} = \frac{t_t}{\sum_{i=1}^{N_c} \frac{t_{c,i}}{k_c} + \sum_{i=1}^{N_g} \frac{t_{g,i}}{k_g}} \quad (5.2)$$

where  $N_c$  is number of copper layers,  $N_g$  is number of epoxy layers,  $t_t$  is the total thickness of PCB,  $t_{c,i}$  and  $t_{g,i}$  are the thicknesses of the  $i$ th copper and glass-epoxy layers, and  $k_c$  and  $k_g$  are the thermal conductivities of copper and glass-epoxy.

Equations 5.1 and 5.2 are the effective thermal conductivities of the PCB. Other heat transfer mechanism of this equipment is the heat loss from the surface of the packaging to the ambient air. This is due to free convection and radiation. In this thesis, radiation is not taken into account during the thermal analysis.

Natural convection is the mechanism of heat transport by the fluid movement which results due to the decrease in the density of the surrounding air due to warming up. Natural convection is developed under the influence of buoyancy forces [16]. Depending on the orientation of heat source with respect to gravity, the flow field may be laminar or turbulent. The fluid flow considered in this thesis is a laminar flow and the simplified natural convection equation for laminar flow range is given by Equation 5.3 [37]:

$$h = 0.52 C \left( \frac{\Delta t}{L} \right)^{0.25} \quad (5.3)$$

where C is the constant based on geometry of the surface,  $\Delta t$  is temperature in degrees Fahrenheit and L is the characteristic length in feet.

The characteristic length, L, is determined by the flow path that the cooling air travels as it passes over the heated surface [37]. Some typical values of characteristic length is given in Table 5.1.

Table 5.1 Characteristic length for various surfaces [37]

Surface	Position	Characteristic Length (ft)
Flat plane	Vertical	Height, limited up to 2 ft (if maximum value exceeds 2 ft, use L=2 ft)
Flat plane (nonrectangular)	Vertical	$\frac{Area}{Horizontal \text{ width}}$
Flat plane (circular)	Vertical	$\frac{\pi}{4} \times diameter$
Cylinder	Vertical	Height, limited up to 2 ft (if maximum value exceeds 2 ft, use L=2 ft)
Flat plane	Horizontal	$\frac{2 \times length \times width}{length + width}$
Cylinder	Horizontal	Diameter
Sphere	Any	Radius

The distance of 2 feet is important since it is a distance where generally the transition from laminar to turbulent flow starts.

Some values of C constant based on surface geometry is given in Table 5.2.

Table 5.2 Values for constants based upon the surface geometry [37]

Shape of Position	Value of C
Vertical plates	0.56
Long vertical cylinders and pipes	0.55
Horizontal cylinder and pipes	0.52
Horizontal plates facing upward	0.52
Horizontal plates facing downward	0.26
Spheres (where L=radius)	0.63
Wires and small parts (L=diameter)	1.45
Components on circuit boards	0.96
Small components in free air	1.39
Components in cordwood modules	0.48

The chassis of the device which is the subject of this thesis is formed by rectangular flat plates. Therefore, the natural convection of flat plates is considered when the convective heat transfer coefficients are calculated. The simplified laminar flow natural convection equation for a heated flat vertical plate at ordinary temperatures and sea level conditions is obtained with Equation 5.3 and Table 5.2, as shown in Equation 5.4 [37].

$$h_c = 0.29 \left( \frac{\Delta T}{L} \right)^{0.25} \quad (5.4)$$

where  $\Delta T$  is temperature degrees Fahrenheit and L is the characteristic length in feet.

$h_c$  is the average natural convection coefficient which defines the characteristics of the air layer surrounding the plate shown in Figure 5.4.

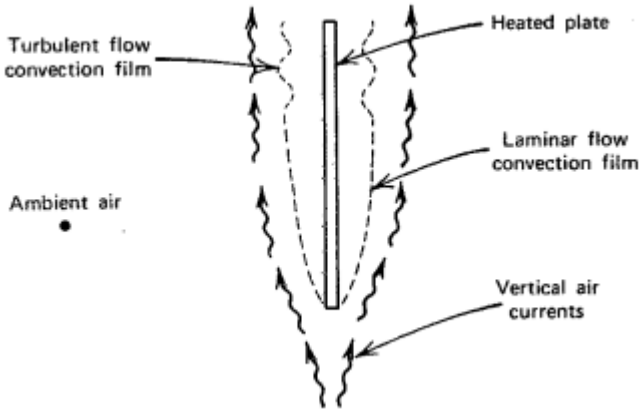


Figure 5.4 Cross section through a vertical heated plate [37]

Turbulent flow occurs at distances greater than approximately 2 ft from the bottom edge of the plate, depending upon the temperature difference between the plate and the ambient [37].

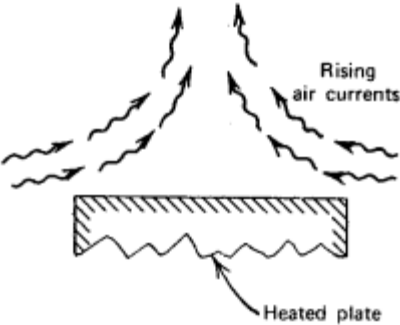


Figure 5.5 Heated horizontal surface facing upward [37]

The simplified laminar flow natural convection equation for heated horizontal flat plate facing upward, shown in Figure 5.5, or a cooled plate facing downward is obtained from Equation 5.3 and Table 5.2 as shown in Equation (5.5) [37]:

$$h_c = 0.27 \left( \frac{\Delta T}{L} \right)^{0.25} \quad (5.5)$$

where  $\Delta T$  is temperature in degrees Fahrenheit and  $L$  is the characteristic length in feet.

The natural convection coefficient for a heated plate facing downward, shown in Figure 5.6, or a cooled plate facing upward which has a value of about the half of a heated plate facing upward is calculated by the Equation 5.6 [37]:

$$h_c = 0.13 \left( \frac{\Delta T}{L} \right)^{0.25} \quad (5.6)$$

where  $\Delta T$  is temperature in degrees Fahrenheit and  $L$  is the characteristic length in feet.

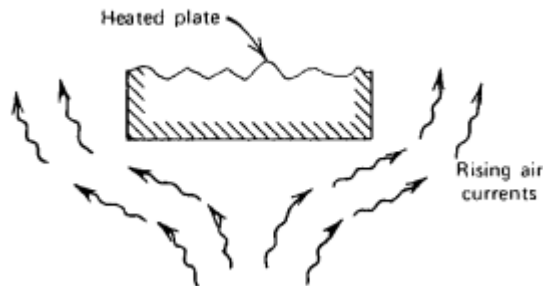


Figure 5.6 Heated horizontal surface facing downward [37]

## **5.3 ANALYSIS**

The thermal test of the equipment is composed of two parts. Operational high temperature and operational low temperature tests performed within the scope of MIL-STD-810F Method 501.4 Procedure II and 502.4 Procedure II, respectively. In this thesis, since it is more critical than low temperature test, instead of performing both high and low temperature thermal analysis, only high temperature test is examined and the high temperature test condition is simulated by the finite element method.

For the analysis of the electronic device, PCB oriented approach is used. The analysis of this approach is performed by Steady-State Module of ANSYS Workbench 11.0. A steady-state thermal analysis is used to determine temperatures, thermal gradients, heat flow rates, and heat fluxes in a an object that are caused by thermal loads that do not vary over time [23].

The details of PCB oriented method and the computer aided analysis steps which are given through this chapter.

### **5.3.1 GEOMETRY**

The geometry used for thermal analysis is the solid geometry since the heat transfer through 2-D model is not realistic for a 3-D geometry. As it is shown in Figure 5.6, the model contains 9 audio, one control, one main board with their assembly interfaces to the chassis. For thermal analysis, since the apertures of the connectors could strictly affect the results, the connectors are modeled by closing the end holes. In actual operating conditions, the chassis of the device is fully enclosed.

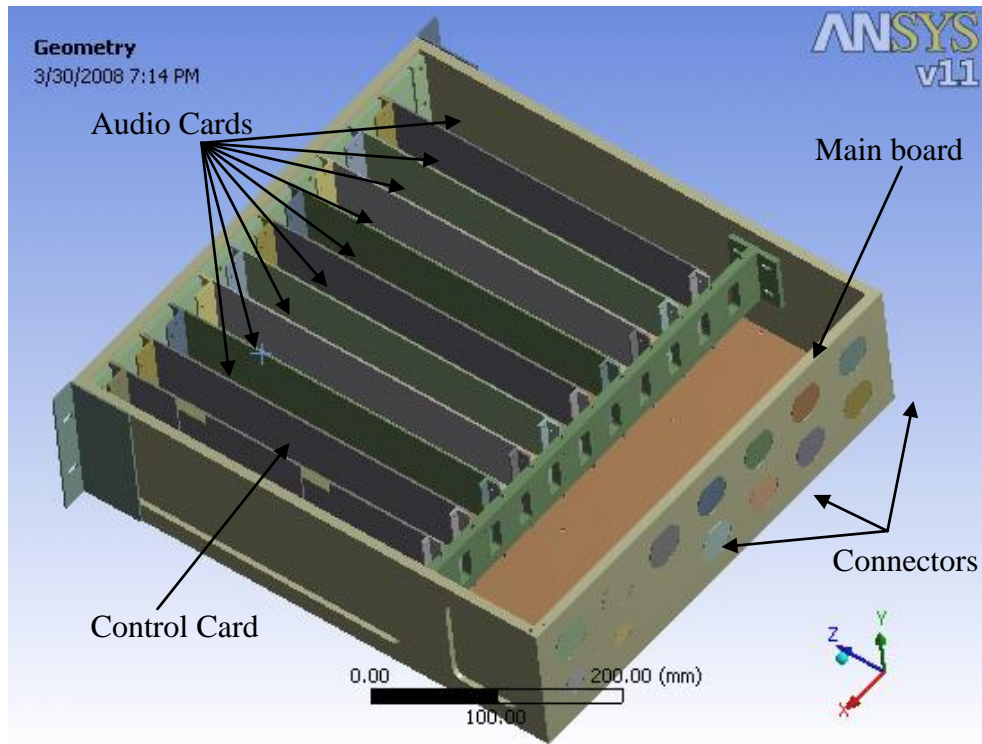


Figure 5.7 The geometry of the thermal model

In PCB oriented thermal analysis approach, as mentioned before, PCB is taken as a conductive plate and components are illustrated as heat sources on PCBs. Therefore, in this model, the critical components are represented with their areas imprinting on the surface of the related PCB. An example of this modeling is given in Figure 5.8.

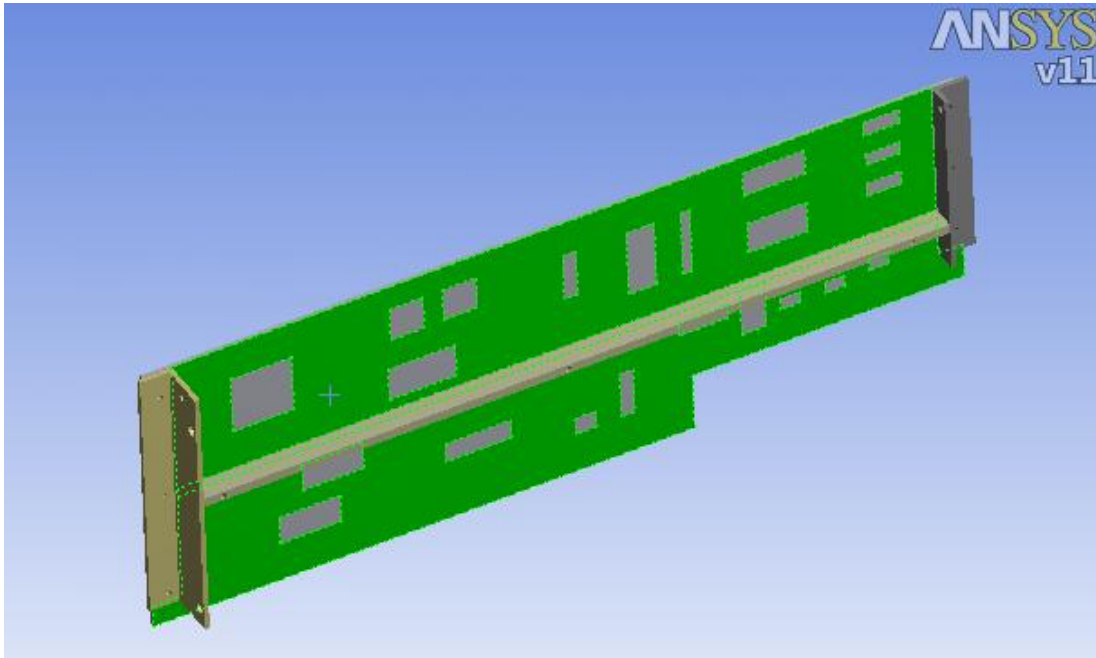


Figure 5.8 Representation of audio card

Another important part of the geometry is the definition of the materials. The handles of the packaging is made up of structural steel R St37-2. The other parts of the chassis except PCB are Aluminum. The Aluminum 5083 H321 is used for manufacturing. The properties of steel and aluminum are defined in ANSYS and attached to the related parts. Similarly, the properties of the PCBs are calculated in order to specify the material.

There are two types of PCB used in the electrical design of this device. These types differ in the according to the layout of the laminates. First type is used for Audio and Control cards with 6 copper layers and 1.6 mm total thickness (Type A), and the other kind is used for the main board with 8 copper layers with 2.2 mm total thickness (Type A). The thickness of a copper layer is typically 0.035 mm in PCBs.

Calculated values of the thermal conductivities of the PCBs by using Equations 5.1 and 5.2 are tabulated in Table 5.3. The details of the calculations are given below.

The total thickness of copper in Type-A PCB is:

$$t_c = 0.035 \times 6 = 0.21 \text{ mm}$$

The total thickness of the glass-epoxy in Type-A PCB is:

$$t_{ge} = t_t - t_c = 1.60 - 0.21 = 1.39 \text{ mm}$$

The in-plane conductivity for Type-A PCB is:

$$k_{p,e} = \frac{\sum_{i=1}^{N_c} k_c t_{c,i} + \sum_{i=1}^{N_g} k_g t_{g,i}}{t} = \frac{0.21 \text{ mm} \times 385 \text{ W / mK} + 1.39 \text{ mm} \times 0.59 \text{ W / mK}}{1.6 \text{ mm}}$$

$$k_{p,e} = 51.043 \text{ W / mK}$$

The normal conductivity for Type-A PCB is

$$k_{n,e} = \frac{t}{\sum_{i=1}^{N_c} \frac{t_{c,i}}{k_c} + \sum_{i=1}^{N_g} \frac{t_{g,i}}{k_g}} = \frac{1.6 \text{ mm}}{\frac{0.21 \text{ mm}}{385 \text{ W / mK}} + \frac{1.39 \text{ mm}}{0.59 \text{ W / mK}}} = 0.678 \text{ W / mK}$$

where  $k_c = 385 \text{ W / mK}$  and  $k_g = 0.59 \text{ W / mK}$

Similarly, the thicknesses of copper and glass-epoxy in Type-B PCB are:

$$t_c = 0.035 \times 8 = 0.28 \text{ mm}$$

$$t_{ge} = t_t - t_c = 2.2 - 0.28 = 1.92 \text{ mm}$$

The in-plane conductivity for Type-B PCB is:

$$k_{p,e} = \frac{\sum_{i=1}^{N_c} k_c t_{c,i} + \sum_{i=1}^{N_g} k_g t_{g,i}}{t} = \frac{0.28 \text{ mm} \times 385 \text{ W / mK} + 1.92 \text{ mm} \times 0.59 \text{ W / mK}}{2.2 \text{ mm}}$$

$$k_{p,e} = 49.514 \text{ W / mK}$$

The normal conductivity for Type-B PCB is:

$$k_{n,e} = \frac{t}{\sum_{i=1}^{N_c} \frac{t_{c,i}}{k_c} + \sum_{i=1}^{N_g} \frac{t_{g,i}}{k_g}} = \frac{2.2 \text{ mm}}{\frac{0.28 \text{ mm}}{385 \text{ W / mK}} + \frac{1.92 \text{ mm}}{0.59 \text{ W / mK}}} = 0.676 \text{ W / mK}$$

where  $k_c = 385 \text{ W / mK}$  and  $k_g = 0.59 \text{ W / mK}$

Table 5.3 Thermal conductivities of PCBs used in the analysis

	In-Plane Thermal Conductivity (W/mK)	Normal Thermal Conductivity (W/mK)
PCB, Type-A	51.043	0.678
PCB, Type-B	49.514	0.676

### 5.3.2 MESHING

The mesh used in the thermal model has an element size of 8 mm since a mesh with element size 5 mm will result in large number of elements. The resulting mesh is shown in Figure 5.9.

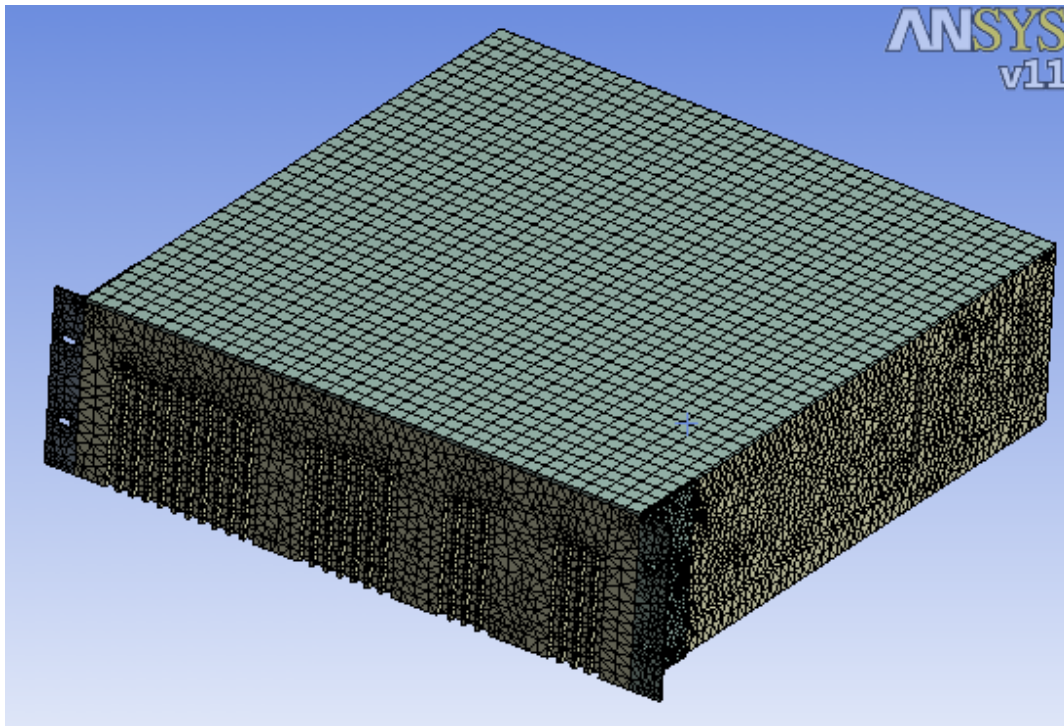


Figure 5.9 Meshing of thermal model

The mesh size of the cover is larger than the other parts and it is meshed by 12 mm hexahedral elements since there is no need for smaller element size or tetrahedral elements due to the simplicity of the geometry. The total number of elements and nodes are 357928 and 729876, respectively. The mating surfaces like PCB interfaces

with chassis, main board with chassis, cover with chassis and handles with chassis are defined as contact regions in ANSYS. The types of elements used in the model are given in Table 5.4.

Table 5.4 Elements used in thermal model

ANSYS Element Name	Description	Location
Solid 87	10 Node Tetrahedral Thermal Solid	All parts except cover and connectors
Solid 90	20 Node Hexahedron Thermal Solid	Cover and Connectors
Target 170	3D Quadrilateral and Triangular Target Segment	Mating Surfaces of Bonded Parts like Handles, Chassis, Cover, PCB Interfaces, etc.
Conta 174	3D 8 Node Surface to Surface Triangular Contact	Mating Surfaces of Bonded Parts like Handles, Chassis, Cover, PCB Interfaces, etc.

### 5.3.3 LOADING AND BOUNDARY CONDITIONS

‘On Work’ test of the unit is done according to “MIL-STD-810F, method 501.4, Procedure II“. This test is applied for 4 hours and during the test, the temperature will be fixed at max 35°C (for air conditioned systems). For simulating these conditions, steady-state thermal analysis module is used with an ambient air temperature at 35 °C. There are four main thermal loads for this analysis:

- 1) Heat Flow

- 2) Vertical Convection
- 3) Horizontal Upper Panel Convection
- 4) Horizontal Lower Panel Convection

The heat flows used in the analysis are given in Figures 5.10-5.12.

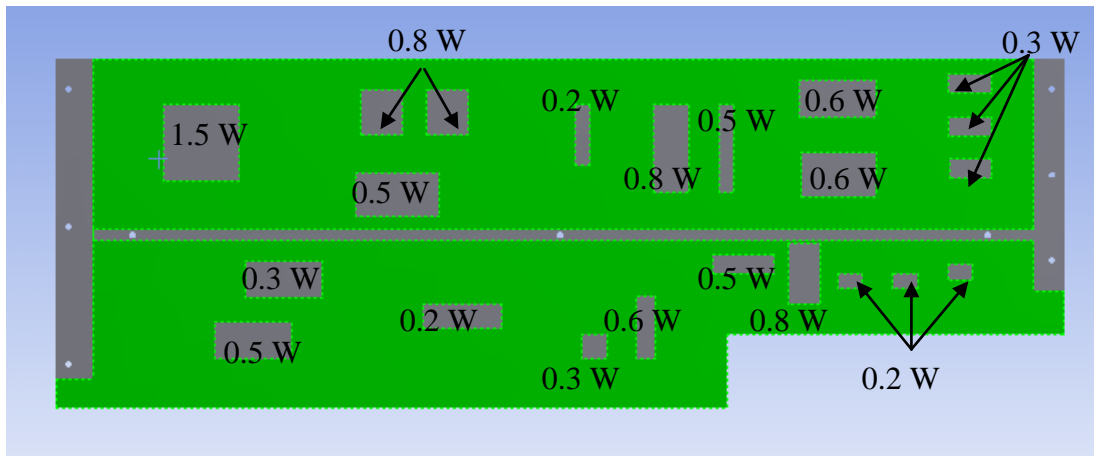


Figure 5.10 Heat sources on audio cards

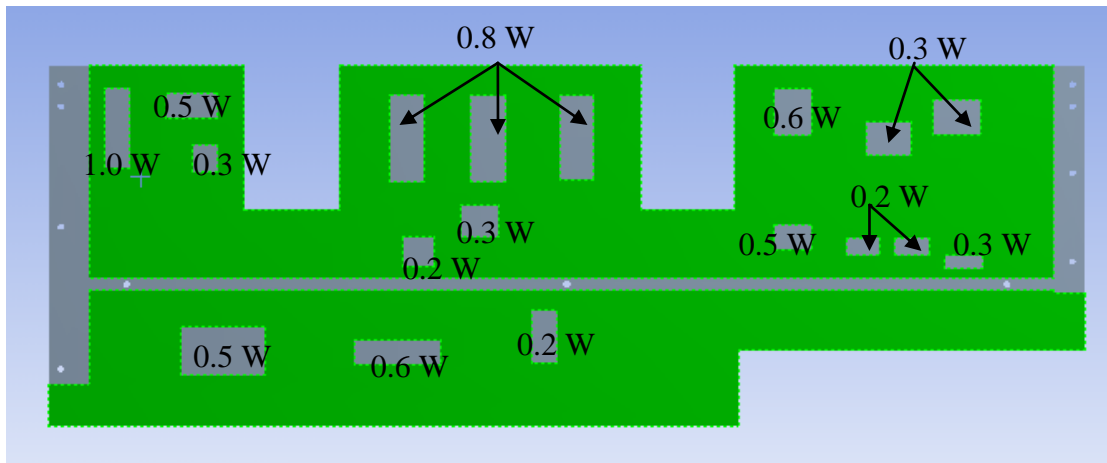


Figure 5.11 Heat sources on control cards

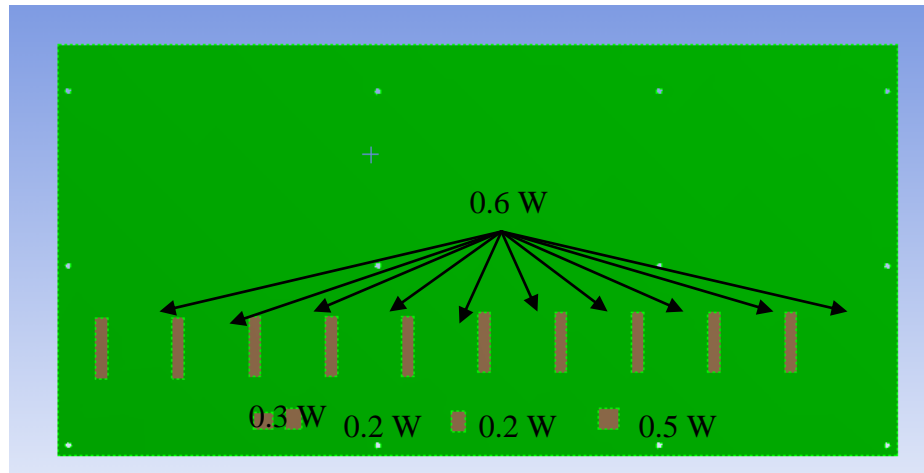


Figure 5.12 Heat sources on main board

These values are attached to the related surfaces in ANSYS as thermal loads.

The vertical convection coefficient is calculated from Equation (5.4).

$$h_c = 0.29 \left( \frac{\Delta T}{L} \right)^{0.25}$$

$\Delta T = t_1 - t_{amb}$  in degrees Fahrenheit, ambient temperature for the analysis is 35 degrees Celsius which is equal to 95 degrees Fahrenheit

For the calculation of all convection coefficients, the chassis is approximated as a simple rectangular box. Based on this assumption, the characteristic length L of vertical convection coefficient is equal to the height itself since the height is smaller than 2 ft. In the calculation of the convection coefficients, Table 5.1 is referenced.

$$L = 135 \text{ mm} = 0.442 \text{ ft.}$$

Substituting  $\Delta T$  and  $L$  into Equation 5.4 gives the convection coefficient as a function of the temperature as:

$$h_{c,ver} = 0.29 \left( \frac{t_1 - 95}{0.442} \right)^{0.25}$$

Similarly, the horizontal upper and lower panel convection coefficients are calculated from Equations 5.5 and 5.6, respectively. Upper panel convection coefficient is given by:

$$h_c = 0.27 \left( \frac{\Delta T}{L} \right)^{0.25}$$

Lower panel convection coefficient is given by:

$$h_c = 0.13 \left( \frac{\Delta T}{L} \right)^{0.25}$$

By referencing Table 5.1, the characteristic length  $L$  of horizontal panel convection coefficient is calculated as:

$$L = \frac{2(\text{length} \times \text{width})}{\text{length} + \text{width}} = \frac{2(1.551 \text{ ft} \times 1.450 \text{ ft})}{1.551 \text{ ft} + 1.450 \text{ ft}} = 1.498 \text{ ft}$$

where length of the chassis is 473 mm which is equal to 1.551 ft, and the width of the chassis is 442 mm which is equal to 1.45 ft.

Substituting  $\Delta t$  and  $L$  into Equations 5.5 and 5.6 yields:

$$h_{c,upper} = 0.27 \left( \frac{t_1 - 95}{1.498} \right)^{0.25}$$

$$h_{c,lower} = 0.13 \left( \frac{t_1 - 95}{1.498} \right)^{0.25}$$

where  $t_1$  is the panel temperature. At the beginning of the analysis, panel temperature  $t_1$  is assumed for vertical plates (for vertical convection), cover (for upper horizontal convection) and bottom of the chassis (for lower horizontal convection) separately. Then, after some iteration, the correct values will be found. The approach used in this analysis could be summarized as [16]:

- Assume a temperature difference ( $\Delta T$ )
- Calculate  $h$
- Calculate the temperature difference based on the generated heat,  $h$ , and the thermal resistance.
- Compare the assumed and calculated temperature difference  $\Delta T$
- Iterate if needed.

The assumed  $\Delta T$  is calculated for maximum temperature on the surface and the ambient temperature. The convection coefficient is considered as the average natural convection coefficient of the air film surrounding the related panel.

### 5.3.3.1 FIRST ITERATION

Since the ambient temperature is 35 °C, 45 °C (95 °F Fahrenheit) was tried as a first assumption for  $t_1$  for all convection calculations. These calculated convection coefficients are given in Table 5.5.

Table 5.5 Convection coefficients for first iteration

$h_{c,ver}$ ( @ $t_1=95$ °F )	$0.7322 \frac{Btu}{hrft^2 \cdot F}$
$h_{c,upper}$ ( @ $t_1=95$ °F )	$0.5025 \frac{Btu}{hrft^2 \cdot F}$
$h_{c,lower}$ ( @ $t_1=95$ °F )	$0.2419 \frac{Btu}{hrft^2 \cdot F}$

The results of the first analysis are given in Table 5.6.

Table 5.6 Results of first iteration

	Predicted Value , °C	Calculated Value, °C
Vertical Plates	45	58.52
Cover	45	58.30
Bottom of Chassis	45	58.55

### 5.3.3.2 SECOND ITERATION

The results of the first iteration show that,  $t_1$  is higher than  $45^\circ\text{C}$  for all surfaces. Therefore, The second temperature assumption done for all convections as  $t_1$  is  $55^\circ\text{C}$  which is equal to 131 degrees Fahrenheit. This temperature is substituted into the equations given above and the calculated values are given in Table 5.7.

Table 5.7 Convection coefficients @  $t_1=131$  degrees Fahrenheit

$h_{c,ver}$ ( @ $t_1=131$ degrees Fahrenheit )	$0.8707 \frac{Btu}{hrft^2 \cdot F}$
$h_{c,upper}$ ( @ $t_1=131$ degrees Fahrenheit )	$0.5976 \frac{Btu}{hrft^2 \cdot F}$
$h_{c,lower}$ ( @ $t_1=131$ degrees Fahrenheit )	$0.2877 \frac{Btu}{hrft^2 \cdot F}$

The calculated vertical convection coefficient is applied to the vertical plates of the chassis which are illustrated in Figure 5.13. In this figure, the specified vertical coefficient is shown with its application surfaces.  $35^\circ\text{C}$  stands for the ambient temperature. The “time” shown in the figure is meaningless since this analysis is steady-state. This module of ANSYS could also make transient analysis and as a analysis settings time must be entered.

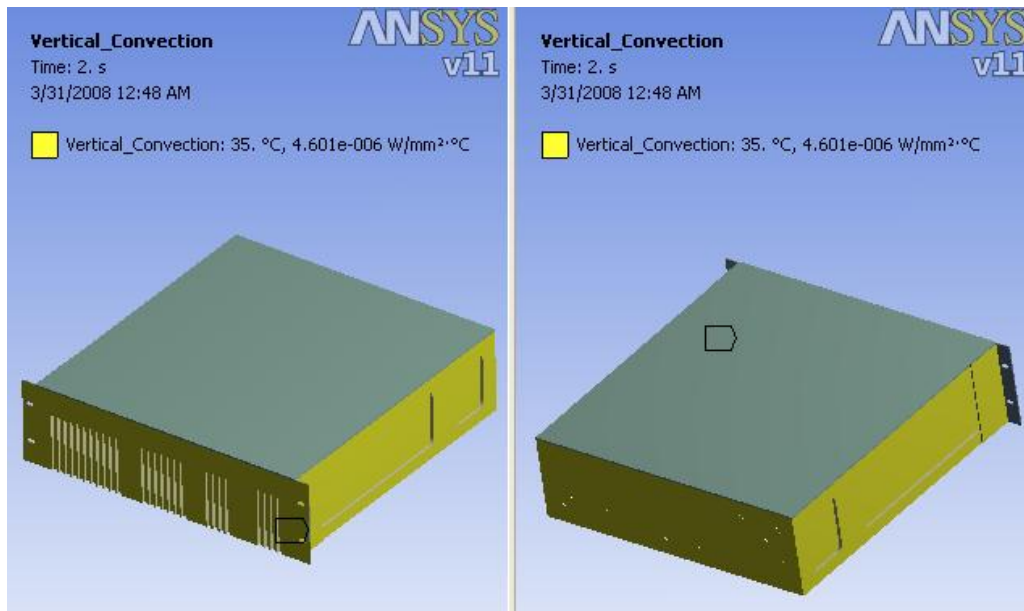


Figure 5.13 Surfaces where vertical convection coefficient is applied

The upper panel convection coefficient is applied to the upper surface of the cover and the lower panel convection coefficient is applied to the bottom surface of the chassis (Figure5.14).

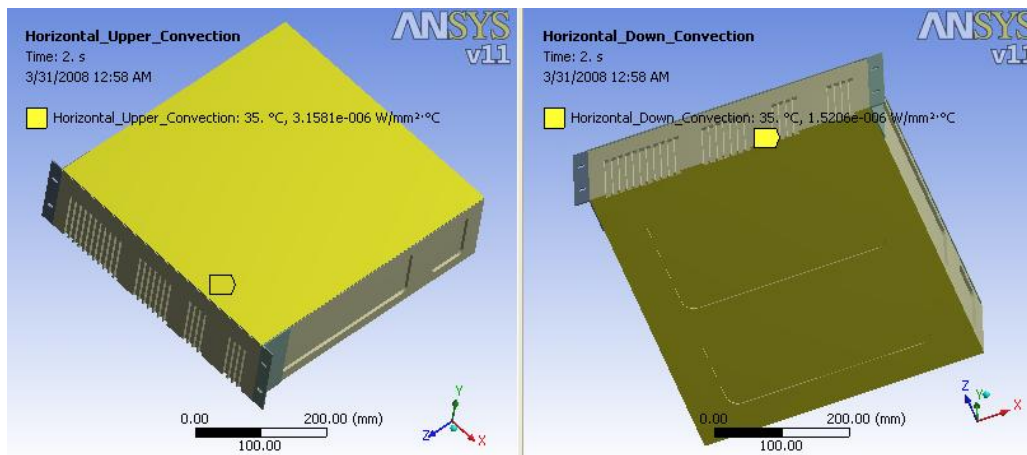


Figure 5.14 Surfaces where upper and lower convection coefficients are applied

The heat flows are applied to the related surfaces on PCBs. The overall loading is shown by Figure 5.15. Since there are many heat flows, only few of them could be listed in the figure.

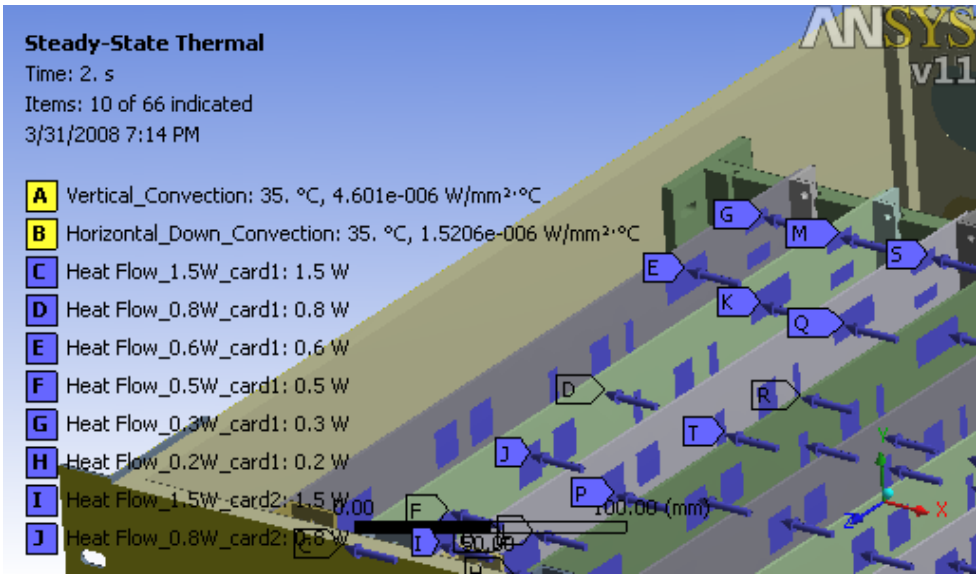


Figure 5.15 Overall thermal loading

The result of the second analysis exceeds the given ambient temperature for different locations of the chassis which is shown in Figure 5.16.

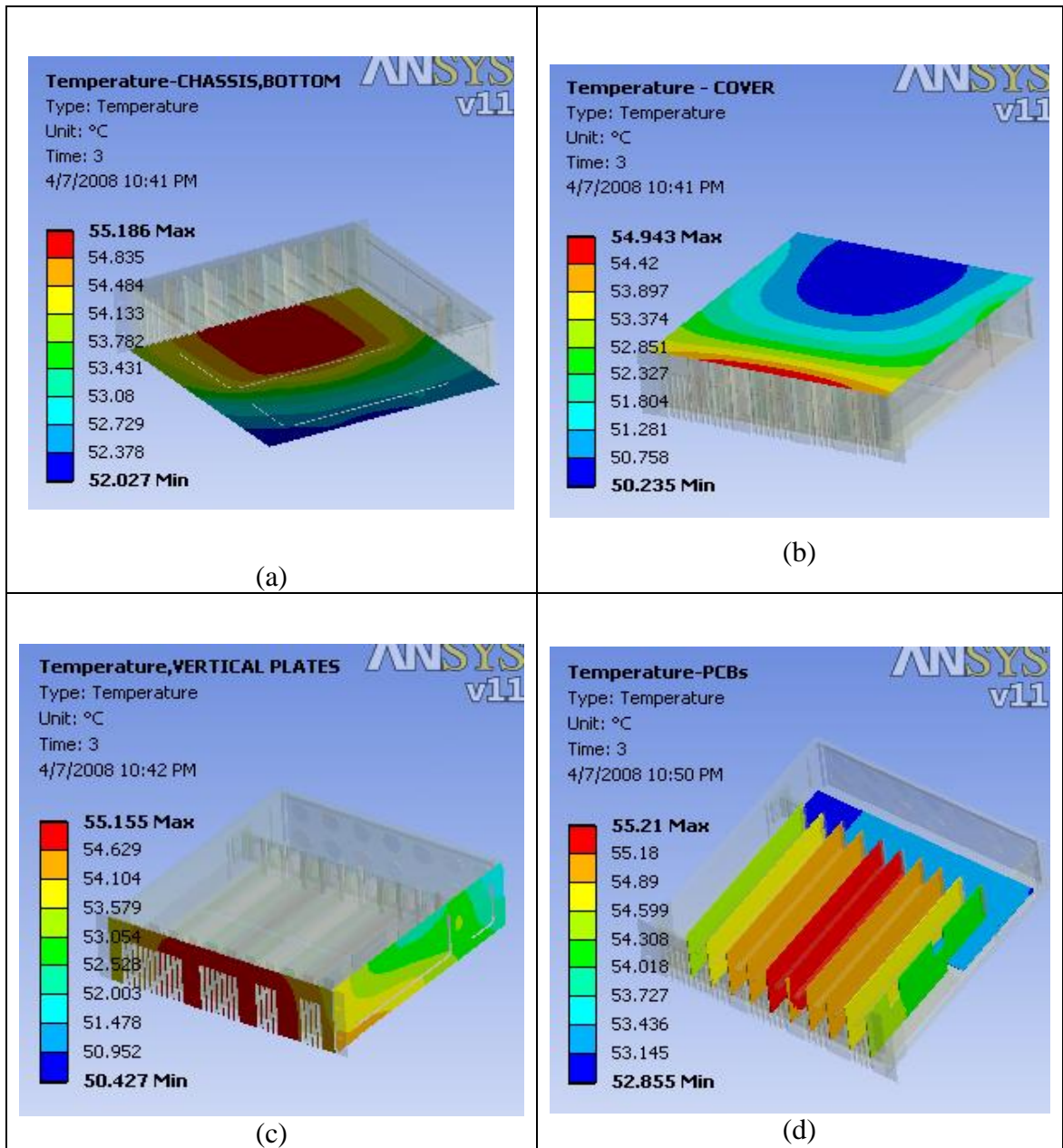


Figure 5.16 Temperature distributions after the second iteration  
 (a)Bottom surface of Chassis, (b) Cover, (c) Vertical Plates, (d) PCBs

These results are summarized in Table 5.8. There is a new iteration needed to approach the final temperatures of different surfaces.

Table 5.8 Results of second iteration

	Predicted Value °C	Calculated Value, °C
Vertical Plates	55	55.15
Cover	55	54.94
Bottom of Chassis	55	55.18

### 5.3.3.3 THIRD ITERATION

As a third iteration, the new temperature taken for vertical plates is 55.12 °C (131.216 °F) and bottom surface of chassis is 55.15 °C which is 131.27 °F. For cover temperature it is assumed as 54.9 °C (130.82 °F). The calculated values for these temperatures are given in Table 5.9.

Table 5.9 Convection coefficients for second iteration

$h_{c,ver}$ ( @ $t_1=131.216$ °F )	$0.8720 \frac{Btu}{hrft^2 \cdot F}$
$h_{c,upper}$ ( @ $t_1=130.82$ °F )	$0.5969 \frac{Btu}{hrft^2 \cdot F}$
$h_{c,lower}$ ( @ $t_1=131.27$ °F )	$0.2883 \frac{Btu}{hrft^2 \cdot F}$

The results of the third analysis are given in Table 5.10.

Table 5.10 Results of third iteration

	Predicted Value , ° C	Calculated Value, ° C
Vertical Plates	55.12	55.14
Cover	54.9	54.93
Bottom of Chassis	55.15	55.17

#### 5.3.3.4 FOURTH ITERATION

As a fourth iteration, the new temperature taken for vertical plates is 55.13 ° C (131.234 ° F) and bottom surface of chassis is 55.16 ° C which is equal to 131.288 ° F. For the cover temperature is assumed as 54.92 ° C (130.856 ° F). The calculated convection coefficient values for these temperatures are given in Table 5.11.

Table 5.11 Convection coefficients for fourth iteration

$h_{c,ver}$ ( @ $t_1=131.234$ ° F )	$0.8721 \frac{Btu}{hrft^2 \cdot F}$
$h_{c,upper}$ ( @ $t_1=130.92$ ° F )	$0.5970 \frac{Btu}{hrft^2 \cdot F}$
$h_{c,lower}$ ( @ $t_1=131.288$ ° F )	$0.2883 \frac{Btu}{hrft^2 \cdot F}$

The results of the fourth analysis are given in Table 5.12.

Table 5.12 Results of fourth iteration

	Predicted Value , °C	Calculated Value, °C
Vertical Plates	55.13	55.13
Cover	54.92	55.92
Bottom of Chassis	55.16	55.16

Finally, the result of the fourth iteration gives the same temperatures assumed in the beginning of the analysis. The total temperature obtained from the steady state analysis for ambient temperature of 35 °C is given in Figure 5.18. The iterations are done for two significant figures.

### 5.3.4 EVALUATION OF ANALYSIS RESULTS

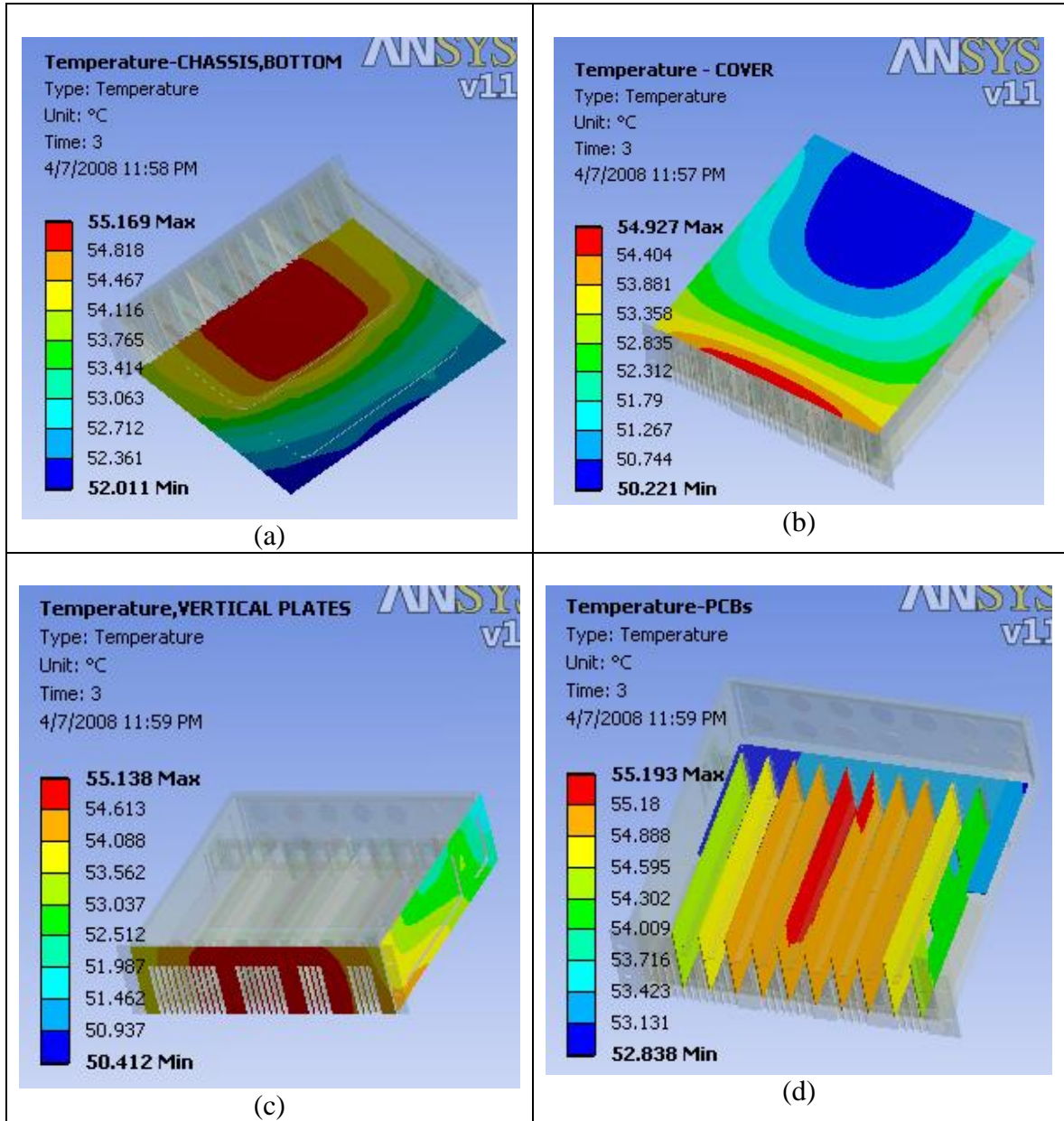


Figure 5.17 Temperature Distribution in Different Parts of the Chassis  
 (a)Chassis-Bottom, (b) Cover, (c) Chassis-Sides, (d) PCBs

The results of the analysis are given in Figures 5.17. This figure is showing the temperature distribution of PCBs (Figure 5.17 (d)), and it is also illustrating the temperature distributions in different parts of the chassis. From these figures, it is easily observed that the maximum temperature values are obtained in the front and bottom part of the chassis. These results are expected due to the locations of heat sources on the cards.

The value of maximum temperature is in the tolerable range for the critical components inside the equipment. The most critical component is the one with a heat source of 1 W which is the red region in Figure 5.18. This component has a working temperature between  $-25^{\circ}\text{C}$  and  $+60^{\circ}\text{C}$ . The result of the analysis is showing that the component will work properly under the thermal loading.

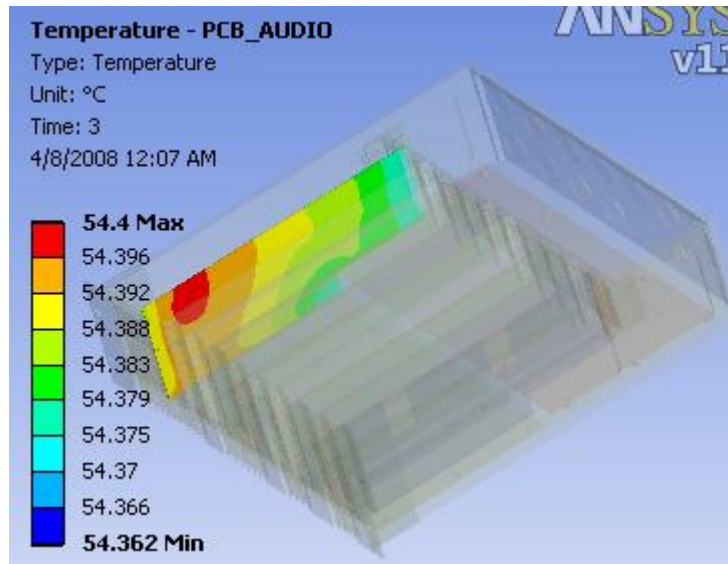


Figure 5.18 Temperature distributions on audio card

The temperature distributions of Control Card are given in Figure 5.19.

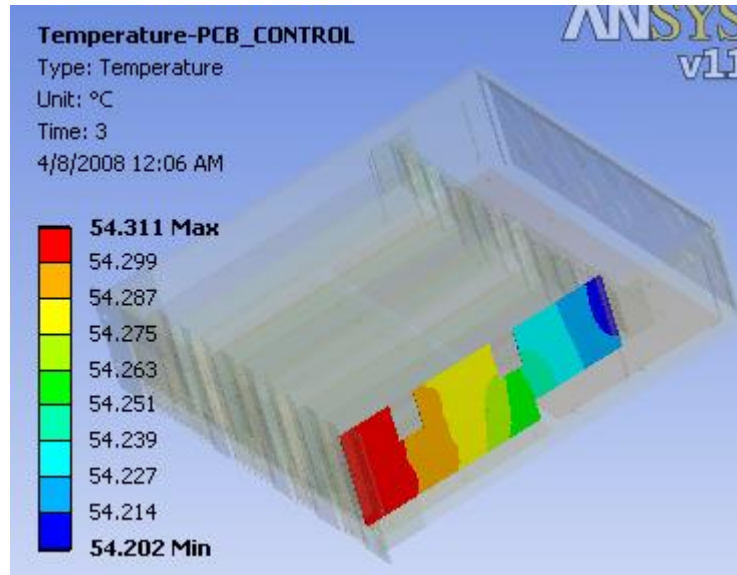


Figure 5.19 Temperature distributions on control card

## 5.4 THERMAL TEST

The thermal test of the EUT (Equipment under Test) was performed according to MIL-STD-810F Method 501.4 Procedure II. Method 501.4 defines the high temperature tests and procedure II indicates operational condition.

The purpose of this test is to obtain data to help evaluate the effects of high temperature conditions on material safety, integrity, and performance [7].

### 5.4.1 TEST LEVELS

The test is done in a thermal chamber of ANGELANTONI TC VT ESS shown in Figure 5.20. The related program used for setting the chamber is WINKRATOS Control Systems.



Figure 5.20 Test chamber [38]

'On Work Test' was applied for 4 hours and during the test, the temperature was fixed at a maximum value of 35°C. The chamber data is given in Figure 5.21. The profile of the chamber is set by the green curve number 02, and the temperature data obtained in the chamber is given by the red curve number 01.



Figure 5.21 Thermal chamber obtained data during operational high temperature test

## 5.4.2 TEST STEPS

The steps of the test defined by MIL-STD-810F are:

1. Setup the EUT into the test chamber; prepare the functional test setup for EUT
2. Check the EUT as physically and close the all unused connectors which are located at EUT.
3. Perform Visual and Functional tests to the EUT.
4. Start data picking for temperature of chamber with respect to the time.
5. Adjust the chamber environment to the appropriate test conditions (35°C) for the start of the test period.

6. Maintain the test chamber at 35°C for 4 hours.
7. Adjust the chamber temperature to room temperature and wait for stabilization at most 3 hour.
8. Perform Visual and Functional tests to the EUT and be sure all tests are successfully completed.

## **5.5 RESULTS**

The electronic equipment has passed the operational high temperature test without any minor or major failures. The mechanical part of the equipment and the electronic components continued their integrity during and after the test and this situation was decided on by the visual inspections. The equipment was operational during the test and it worked properly during and after the test. These results were predicted because the thermal analysis of the equipment showed that the temperature range, which the device would go through during the actual thermal test, was an acceptable range. The analysis showed that the maximum temperature was below the limit operating temperature of the thermally most critical component of the device.

## **CHAPTER 6**

### **ELECTROMAGNETIC INTERFERENCE SHIELDING AND TEST FOR EMI/EMC QUALIFICATION**

#### **6.1 INTRODUCTION**

Electromagnetic waves differ in wavelength as the frequency increases or decreases. Visible light, radio signals, television broadcasting, radars are all types of electromagnetic waves. Figure 6.1 illustrates the electromagnetic spectrum showing different types of electromagnetic waves due to their frequencies.

The subject of Electromagnetic Interference (EMI) is being more important through the causes and results in the history. There were many system failures due to the EMI in many fields such as transmission, telecommunication, transportation, and many applications like medical, industrial and military. The awareness of its practical importance, especially after the World War II, made technical people work on EMI seriously by developing some design procedures, civil and military regulations, standards, measurement techniques and test methodologies.

Electromagnetic interference (EMI) is the situation where one device produces unintentional signals that cause another device to malfunction [39]. Sometimes electromagnetic interference is called as radio frequency interference (RFI). But in fact,

RFI is the [40] degradation in the reception of a wanted signal caused by radio frequency disturbance which is an electromagnetic disturbance having components in the radio frequency range.

The threat of EMI is controlled by adopting the practices of *electromagnetic compatibility* (EMC) [41]. This is defined [42] as “the ability of a device, unit of equipment or system to function satisfactorily in its electromagnetic environment without introducing intolerable electromagnetic disturbances to anything in that environment”.

The term EMC has two complementary aspects [41]:

- It describes the ability of electrical and electronic systems to operate without interfering with other systems;
- It also describes the ability of such systems to operate as intended within a specified electromagnetic environment.

This relation between EMC and its operating environment results in two approaches for EMC specifications. In one case the nature of the installation determines the approach [43]. Especially for on board ship, satellite and aircraft applications, EMC is problematic since the installations of devices are very close to each other. On the other hand, in these cases if susceptible systems are located near to powerful emitters, then special precautions are also needed. To maintain compatibility, military, aerospace and vehicle EMC specifications involve a detailed knowledge of both the installation circumstances and the characteristics of the emitters and their potential victims. The second approach assumes that the system will operate in an environment which is electromagnetically benign within certain limits, and that its proximity to other sensitive equipment will also be controlled within limits [43]. These limits are directly related to the class of environment –domestic, commercial, industrial etc. – for which the device is marketed [43].

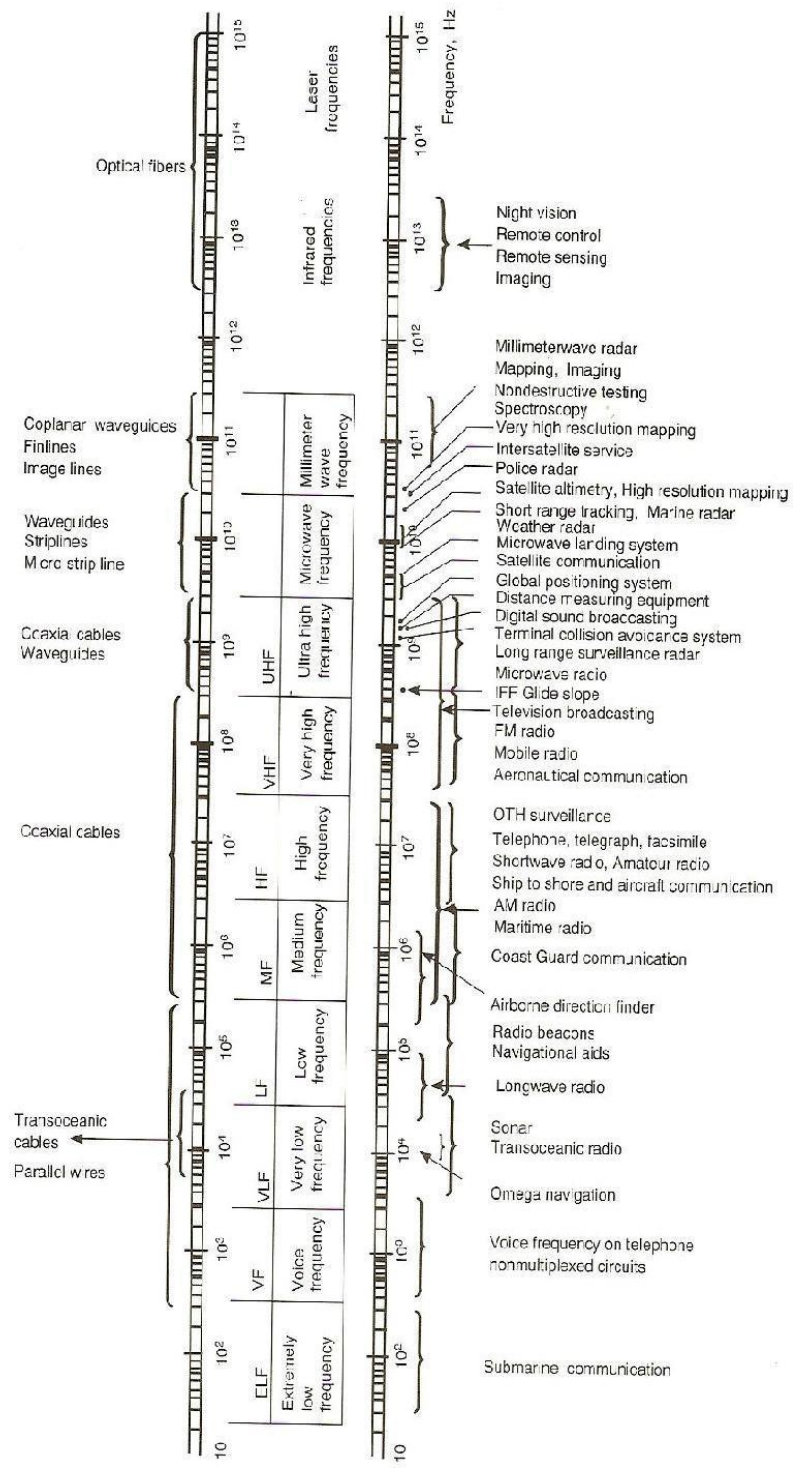


Figure 6.1 Electromagnetic spectrum [40]

## 6.2 DEFINITIONS

### 6.2.1 ELECTROMAGNETIC WAVES

Radio signals, visible light, microwaves are all types of electromagnetic waves. They differ each other in wavelength. Electromagnetic waves consist of two orthogonal fields; Electric Field and Magnetic Field. (Figure 6.2)

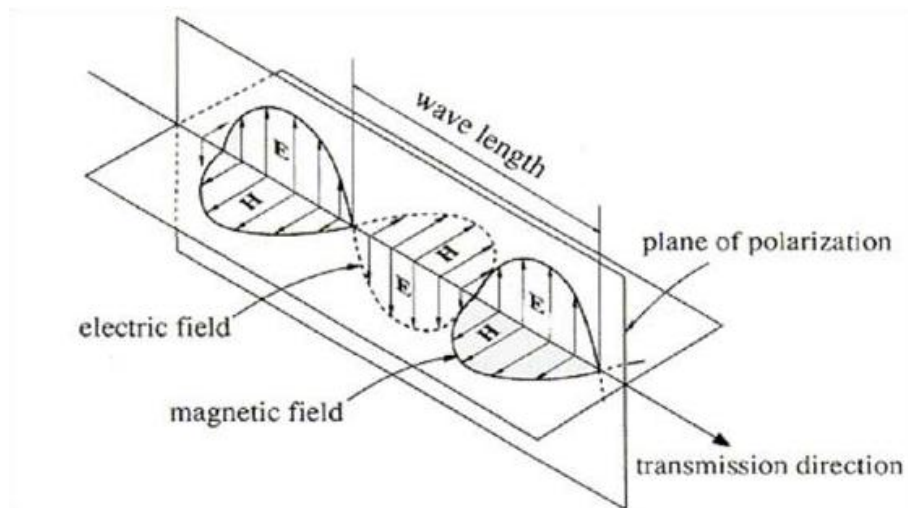


Figure 6.2 Propagation of an electromagnetic wave [58]

According to Electromagnetic (EM) Theory (Maxwell's Equations), a time-variant current within a transmission line develops a time-variant magnetic field, which gives rise to an electric field. [44]

An electric field is generated between two conductors having different potentials. It is denoted as E-Field. The field is measured in volts per meter (V/m) and is proportional

to the applied voltage divided by the distance between the conductors. It is represented by a dipole antenna.

A magnetic field is generated around a conductor carrying a current. It is denoted as H-Field and measured in amps per meter (A/m) that is proportional to the current divided by the distance from the conductor. It is represented by a loop antenna since it follows closed-loop configurations. (Figure 6.3)

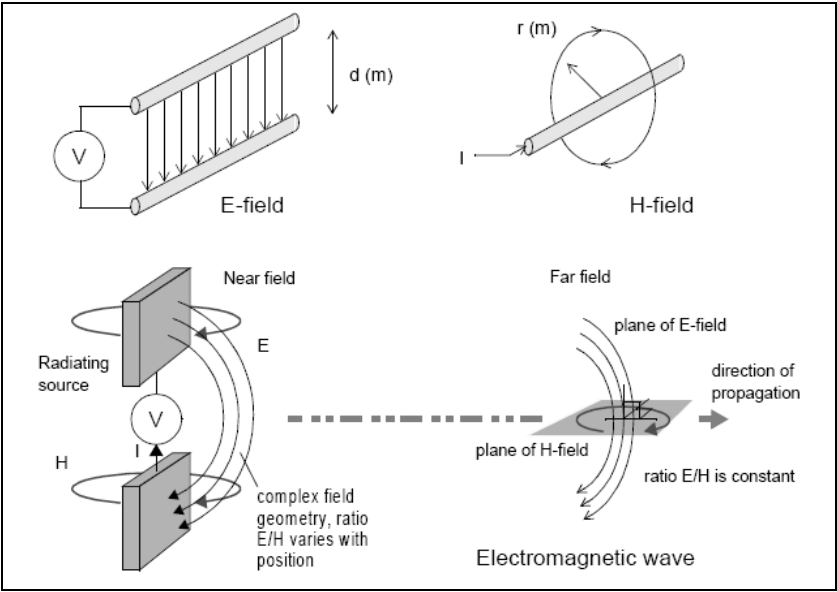


Figure 6.3 Electric field vs. magnetic field [41]

The speed of EM wave propagation is determined by the medium; in free space it is equal to the speed of light,  $3 \times 10^8$  m/s.

The ratio of the electric field to the magnetic field is called the wave impedance (Figure 6.4):

$$\eta_w = \frac{E}{H} \quad (6.1)$$

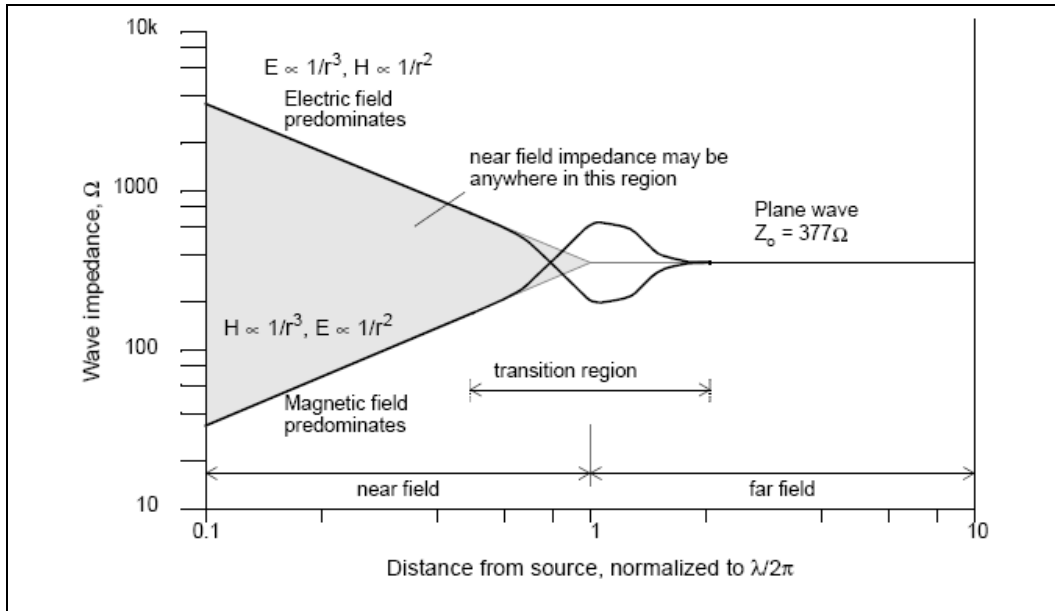


Figure 6.4 Electromagnetic wave behavior [41]

The wave impedance is a key parameter of any given wave as it determines the efficiency of coupling with another conducting structure, and also the effectiveness of any conducting screen which is used to block it [41]. In the far field, that is

$$d > \frac{\lambda}{2\pi} \quad (\text{Far field for a point source}) \quad (6.2)$$

The complex three dimensional field structure decays with the distance at the same rate and only the components which are orthogonal to each other and to the direction

of propagation remain. The wave is known as a plane wave and its impedance is constant, which is equal to the impedance of free space given by equation (6.3):

$$Z_w = \sqrt{\frac{\mu_0}{\epsilon_0}} = \sqrt{\frac{4\pi \times 10^{-7} \frac{H}{m}}{\frac{1}{36\pi} \times 10^{-9} \frac{F}{m}}} = 120 \pi = 377 \Omega \quad (6.3)$$

where  $\mu_0$  is the permeability of free space and  $\epsilon_0$  is the permittivity of free space

In the near field,

$$d < \lambda/2\pi \quad (6.4)$$

The wave impedance is determined by the characteristics of the source. A low current, high voltage radiator (such as a rod), in other words, circuit node carrying a significant  $dv/dt$  will generate mainly an electric field of high impedance, while a high current, low voltage radiator (such as a loop) which a conductor carrying a significant  $di/dt$  will generate mainly a magnetic field of low impedance. If (as a special case) [41] the radiating structure happens to have an impedance around 377  $\Omega$  which is the impedance of free space, then a plane wave can in fact be generated in the near field, depending on geometry. The region around  $\lambda/2\pi$ , or approximately one sixth of a wavelength, is the transition region between near and far fields. This is not a precise criterion; rather it indicates the region within which the field structure changes from complex to simple. [41]

If the working area is in the far field, plane waves are always assumed to be under consideration (Figure 6.4), in the near field, electric or magnetic fields must be examined individually.

## 6.2.2 EMISSIONS SUSCEPTIBILITY

Figure 6.5 illustrates various mechanisms in which electromagnetic interference can travel from its source to the receptor: [40]

- Direct radiation from source to receptor (path 1)
- Direct radiation from source picked up by the electrical power cables or the signal/control cables connected to the receptor, which reaches the receptor via conduction (path 2)

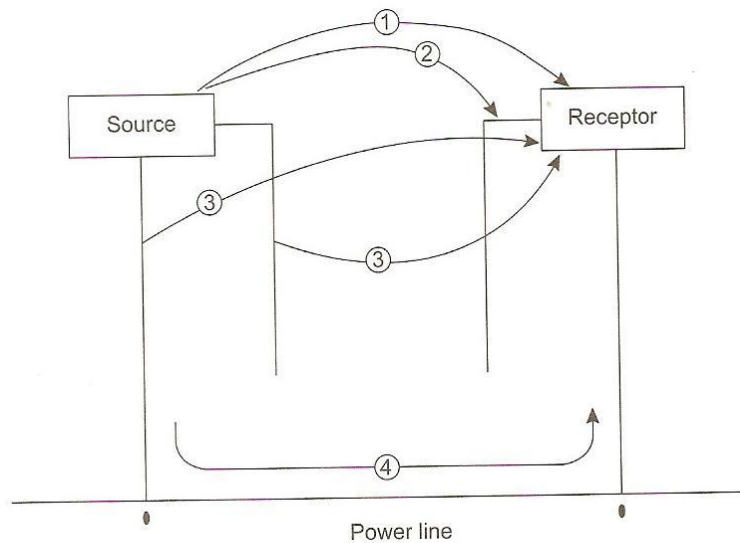


Figure 6.5 Emission susceptibility mechanism [40]

- Electromagnetic interference radiated by the electrical power, signal or control cables of the source (path 3)
- Electromagnetic interference directly conducted from its source to the receptor via common electrical power supply lines, or via common signal/control cables (path 4)

- The electromagnetic interference carried by various power/signal/control cables connected to the source, which gets coupled to the power/signal/control cables of the receptor, especially when cable harnesses are bundled (such interference reaches the receptor via conduction, even when common power/signal/control cables do not exist)

Thus the primary mechanisms by which electromagnetic interference moves from its source to the receptor are radiation and conduction. The radiated and conducted signals can be the result of emission or susceptibility.

Emissions are signals produced by the equipment or the system. As mentioned before, they can be radiated or conducted.

RE: Radiated Emission (electric field, magnetic field, or plane waves)

CE: Conducted Emission (power line conducted, signal line conducted)

Susceptibility (Immunity) [39] is the ability of the equipment to withstand various types of interference. Equipment can be susceptible to interference in the form of electric fields, magnetic fields, plane waves, power and signal line conduction and electrostatic discharge (ESD).

CS: Conducted Susceptibility

RS: Radiated Susceptibility

### **6.2.3 DIFFERENTIAL AND COMMON MODE INTERFERENCES**

The electromagnetic disturbances carried by electrical power supply lines are classified into two categories, common-mode currents/voltages and differential-mode (or normal mode) currents/voltages.

The common mode (CM) interferences are defined [40] as the unwanted electrical potential differences between (or all) current carrying conductor(s) and the reference ground.

The differential mode (DM) interferences are defined [40] as the unwanted potential differences between any two current-carrying conductors.

#### **6.2.4 ATTENUATION**

The amount of reduction or loss in signal level (voltage, current, or power) offered by a device such as an attenuator, filter, or shielded enclosure [45]. The attenuation is measured in decibels (dB) and is given by:

$$\text{Attenuation (dB)} = 20\log_{10} [\text{attenuation ratio}] \quad (6.5)$$

$$\text{Attenuation Ratio} = \frac{\text{Field Strength without Enclosure}}{\text{Field Strength with Enclosure}} \quad (6.6)$$

### **6.3 STANDARDS**

Numerous EMC standards exist. The common fundamental theme of these standards are conducted emission limits, radiated emission limits, conducted susceptibility (immunity) limits and radiated susceptibility (immunity) limits.

Some of the institutes that establish EMC standards are:

- US Military
- Radio Technical Commission for Aeronautics (RTCA)

- European Union (EU)

### 6.3.1 US MILITARY

The related standard is MIL-STD-461E. “This standard establishes interface and associated verification requirements for the control of the electromagnetic interference (emission and susceptibility) characteristics of electronic, electrical and electromechanical equipment and subsystems designed or procured for use by activities and agencies of the Department of Defense” [46].

MIL-STD-461E, briefly explains the requirements for the control of EMI Characteristics of subsystems and equipments. Some examples of this standard is listed at Table 6.1.

Table 6.1 Test examples of MIL-STD-461 E [47]

Req.'s	Description
CE101	Conducted Emission, Power Leads, 30 Hz to 10 kHz
CE102	Conducted Emission, Power Leads, 10 kHz to 10 MHz
CE106	Conducted Emission, Antenna Terminal, 10 kHz to 40 GHz
CS101	Conducted Susceptibility, Power Leads, 30 Hz to 50 kHz
CS103	Conducted Susceptibility, Antenna Port, Inter modulation , 15kHz to 10 GHz
CS104	Conducted Susceptibility, Antenna Port, Rejection of Undesired Signals, 30 Hz to 20 GHz
CS105	Conducted Susceptibility, Antenna Port, Cross Modulation, 30 Hz to 20 GHz
CS109	Conducted Susceptibility, Structure Current, 60 Hz to 100 kHz

Table 6.1 Test examples of MIL-STD-461 E [47] (Cont'd)

CS114	Conducted Susceptibility, Bulk Cable Injection, 10 kHz to 200 MHz
CS115	Conducted Susceptibility, Bulk Cable Injection, Impulse Excitation
CS116	Conducted Susceptibility, Damped Sinusoidal Transients, Cable & Power Leads, 10 kHz to 100 MHz
RE101	Radiated Emissions, Magnetic Field, 30 Hz to 100 kHz
RE102	Radiated Emissions, Electric Field, 10 kHz to 18 GHz
RE103	Radiated Emissions, Antenna Spurious and Harmonic Outputs, 10 kHz to 40 GHz
RS101	Radiated Susceptibility, Magnetic Field, 30 Hz to 100 kHz
RS103	Radiated Susceptibility, Electric Field, 10 kHz to 40 GHz
RS105	Radiated Susceptibility ,Transient Electromagnetic Field

### 6.3.2 EUROPEAN UNION (EU)

The European Union (EU) has been formed in a process of economic integration between European countries. The EU institutes define some standards for production of households and the environment.

Table 6.2 Immunity test examples of EU [47]

Standard	Description
EN61000-4-2	Electrostatic Discharge
EN61000-4-3	Radiated Susceptibility Test
EN61000-4-4	Electrical Fast/Transient Burst Test
EN61000-4-5	Surge Test

Table 6.2 Immunity test examples of EU [47] (Cont'd)

EN61000-4-6	Conducted Immunity Test
EN61000-4-8	Power Frequency Magnetic Test
EN61000-4-11	Voltage Dips and Interruptions Test
EN61000-6-1	Immunity for residential, commercial and light-industrial environment
EN61000-6-2	Immunity for industrial environment
EN61547	Equipment for general lightning purposes-EMC Immunity Requirements
EN12016	Electromagnetic Compatibility – Product family standard for lifts, escalators and passenger conveyors- Immunity

## 6.4 SHIELDING

The common and the most effective technique to control EMI in order to achieve EMC is shielding. Shielding mainly refers to metallic enclosures which covers an electronic product or a part of it if the situation is for the protection to low frequencies. If only high frequency (> 30MHz) protection will be enough then a thin conductive coating deposited on plastic is adequate [41].

There are two purposes of a shield [48], as illustrated in Fig. 6.6 a and b: The first is to prevent the emission of the electronics of the product or a portion of those electronics from radiating outside the boundaries of the product and the second is to prevent radiated emissions external to the product from coupling to the product's electronics which may cause interference in the product. Besides, shielding also

provides a return path for the filtered currents to take. If there is no return path then conductive coupling exists which is hazardous for internal circuits and conductors.

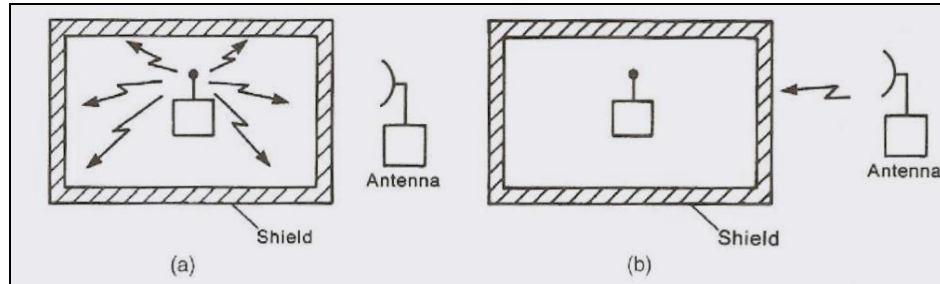


Figure 6.6 An electromagnetic shield [48]

If the desired emission limit is exceeded and the PCB layout cannot be improved, then shielding is essential. A description of shielding issues is can be split into two parts [41].

- The theory of electromagnetic attenuation through a conducting barrier of infinite extent, and
- The degradation of theoretically achievable shielding effectiveness by practical forms of shield construction.

#### 6.4.1 SHIELDING THEORY AND SHIELDING EFFECTIVENESS

The shielding theory has a close relation with electromagnetic wave theory. The shielding performance depends on a number of parameters [40] such as frequency, distance of interference source from the shielding walls, polarization of the fields,

discontinuities in a shield, and so on. These parameters cause a difference between the theoretical shielding and its practice.

A shield is a conceptually a barrier which is put in the path of electromagnetic waves between an emitter and a receptor. The effectiveness of the shield is [48] the ratio of the magnitude of the electric (magnetic) field that is incident on the barrier to the magnitude of the electric (magnetic) field that is transmitted through the barrier.

Shielding works on two basic mechanisms: reflection loss and absorption loss. Electromagnetic waves from the emitter get partially reflected from the low impedance shielding surface because of impedance mismatch between the waves and the shield [40]. After partial absorption in the shield, the remaining part gets transmitted through the shield as shown in Figure 6.7. If absorption ratio is small, there can be also re-reflections (internal reflections) between the interfaces of the shielding material.

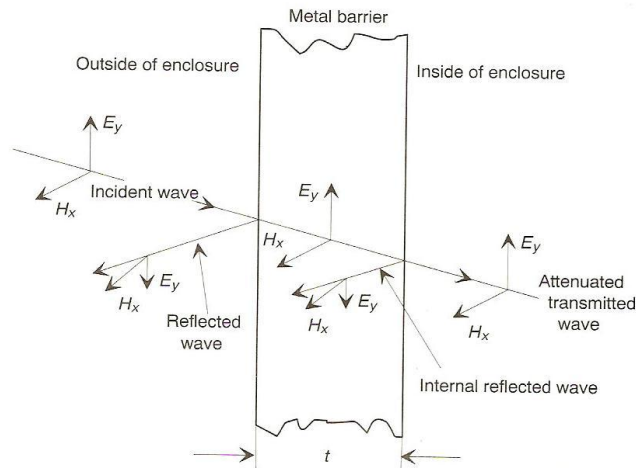


Figure 6.7 Reflection and absorption in a metal barrier [40]

So, the shielding effectiveness can be expressed as the sum of reflection, absorption, and re-reflection (internal reflection) losses, as shown in Figure 6.7 and given by Equation (6.7) [41]:

$$SE_{dB} = R_{dB} + A_{dB} + B_{dB} \quad (6.7)$$

This is known as the “transmission line model” for shielding effectiveness based on the assumption that the coupling between the screen currents and the source of the incident field is negligible [41].

As mentioned before the shielding effectiveness differs from location to location of the barrier from the source. In far field, away from the source, the incident field resembles a uniform plane wave on the other hand, in near field, regions close to the radiating sources, the field is high intensity field and it is more complex. It has transverse and longitudinal components. The characteristic of field is determined by the predominant component of electromagnetic field, which is E or H. If E-field is predominant, the wave impedance is very large; and if H-field is predominant wave impedance is very small.

The shielding effectiveness SE of these fields can be defined as the ratio of powers at the receptor without the barrier and with the barrier [40]:

$$\text{Plane-wave} \quad SE_{dB} = 10 \log_{10} \left( P_1 / P_2 \right) \quad (6.8)$$

$$\text{E-Field} \quad SE_{dB} = 20 \log_{10} \left( E_1 / E_2 \right) \quad (6.9)$$

$$\text{H-Field} \quad SE_{dB} = 20 \log_{10} \left( H_1 / H_2 \right) \quad (6.10)$$

Where suffix 1 represents quantities at the receptor without shielding barrier, and suffix 2 represents quantities at the receptor with a shielding barrier between the emitter and susceptor [40]. (For further details, see Appendix-A.)

### 6.4.2 REFLECTION AND ABSORPTION LOSSES

The losses due to a barrier in a field depend on thickness, permeability, conductivity of a barrier as much as frequency and the distance from the radiating source.

According to the theory of electromagnetic attenuation through a conducting barrier of infinite extent, an AC electric field impinging on a conductive wall will induce a current flow in that surface of the wall, which in turn will generate a reflected wave of the opposite sense in order to satisfy the boundary conditions at the wall, where the electric field must approach zero [41]. The reflected wave amplitude is different from the incoming wave amplitude, which determines the reflection loss of the wall.

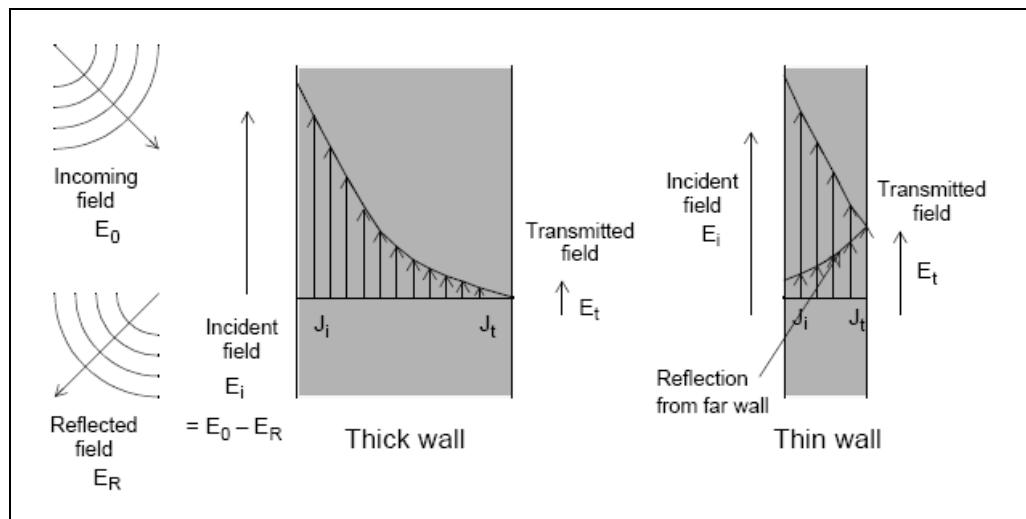


Figure 6.8 Electromagnetic attenuation through a conducting barrier of infinite extent [41]

Because shielding walls have finite conductivity, part of the incoming current passes through the wall and generates its own field on the other side of the wall. The ratio of the impinging to the transmitted fields is one measure of the shielding effectiveness of the wall [41] (Figure 6.8).

#### 6.4.2.1 REFLECTION LOSS

The reflection loss R is proportional to the electromagnetic wave impedance and it is inversely proportional to the barrier intrinsic impedance. The impedance of the barrier is a function of its conductivity and permeability and of frequency. The reflection loss is greatest for high conductivity materials like copper and aluminum. In the near field, closer than  $\lambda/2\pi$ , the distance between source and barrier also affects the reflection loss [41], but in the far field since the impinging wave becomes a plane wave which has a constant wave impedance, the distance is immaterial, reflection loss increases as frequency decreases. In the near field, the reflection of E-field [40] increases with a decrease in frequency and decrease in distance between the source and the shielding barrier, on the other hand the reflection of H-field increases with an increase in frequency and increase in distance between the source and the shielding barrier.

$$R_p = 168 - 10 \cdot \log_{10} \left( \frac{\mu_r}{\sigma_r} \cdot f \right) \text{ dB} \quad [41] \quad \text{Plane wave} \quad (6.11)$$

$$R_e = 322 - 10 \cdot \log_{10} \left( \frac{\mu_r}{\sigma_r} \cdot f^3 \cdot r^2 \right) \text{ dB} \quad [41] \quad \text{Electric field} \quad (6.12)$$

$$R_m = 14.6 - 10 \cdot \log_{10} \left( \frac{\mu_r}{\sigma_r} \cdot \mathcal{L}(f \cdot r^2) \right) \text{ dB} \quad [41] \quad \text{Magnetic field} \quad (6.13)$$

Where  $\mu_r$  is the relative permeability with respect to air,  $\sigma_r$  is the relative conductivity with respect to copper,  $F$  is the frequency in Hz, and  $r$  is the distance from the source to the shielding barrier in meters.

#### ***6.4.2.2 ABSORPTION LOSS***

Absorption loss is proportional to the barrier thickness and its skin depth. The skin depth [41] is an expression of the electromagnetic property which tends to confine AC current flow to the surface of a conductor, becoming less as frequency, conductivity or permeability increases. The skin depth depends on the barrier material's properties. Steel which has less conductivity than copper has poor reflection but it has higher absorption than copper of the same thickness.

Electromagnetic fields become attenuated by  $1/e$  (natural logarithm, 8.6 dB) for every skin depth of penetration into the barrier [43] as shown in Figure 6.9. The greater the number of skin depths that exist within a given thickness of metal, the greater the absorption loss. Since the skin depth becomes shallower as frequency increases, absorption loss becomes the dominant term at high frequencies [43]. This explains [41] why thin conductive coatings are effective at high frequencies – the current only flows on the surface, and the bulk of the material does not affect the shielding properties. For example, skin depth in aluminum at 30MHz is 0.015mm.

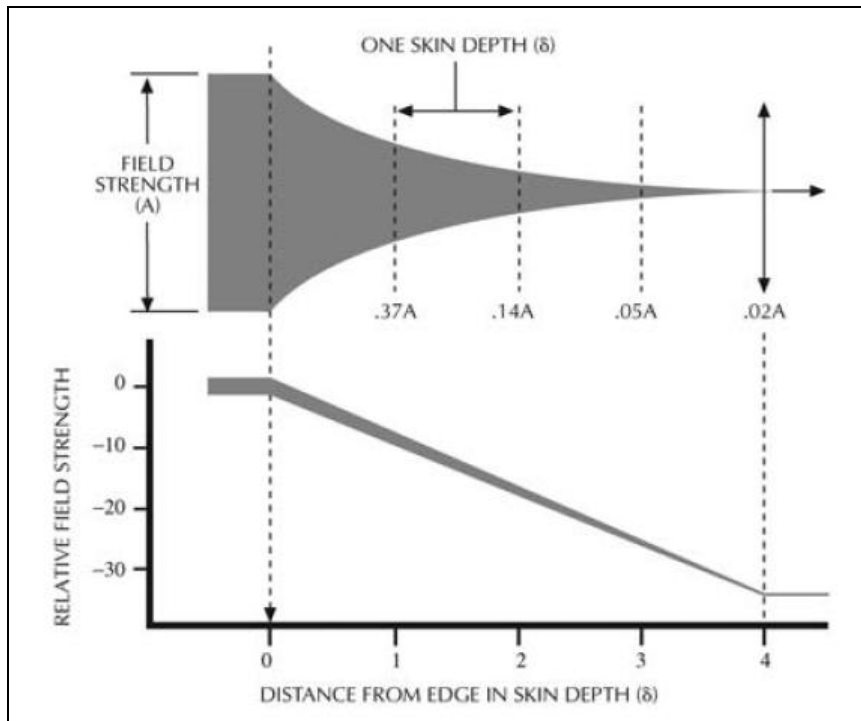


Figure 6.9 Absorption loss as a function of skin depth [43]

Skin depth is found by equation given as;

$$\delta = \frac{1}{\sqrt{\pi \cdot f \cdot \mu \cdot \sigma}} \text{ meters} \quad (6.14)$$

For a conductor with permeability  $\mu_r$  and conductivity  $\sigma_r$ , Equation (6.14) could be written as:

$$\delta = 0.0661 \cdot \sqrt{\frac{1}{f \cdot \mu_r \cdot \sigma_r}} \text{ meters} \quad (6.15)$$

or

$$\delta = 2.602 \cdot \sqrt{\frac{1}{f \cdot \mu_r \cdot \sigma_r}} \text{ inches} \quad (6.16)$$

In contrast to reflection loss, absorption loss is the same whether the field is electric, magnetic or plane wave.

When absorption loss A is greater than 10dB, the re-reflection loss B is insignificant but it is still important for thin barriers at low frequencies.

$$A = 8.69 \cdot \left( \frac{t_b}{\delta} \right)^2 \text{ dB} \quad \text{Absorption loss (A)} \quad (6.17)$$

where  $t_b$  is barrier thickness,  $\delta$  is skin depth

$$B = 20 \cdot \log_{10} \left( 1 - e^{-2\sqrt{2} \frac{t_b}{\delta}} \right) \text{ dB} \quad \text{Re-reflection loss (B)} \dots\dots(6.18)$$

B is negligible unless material thickness  $t_b$  is less than the skin depth  $\delta$  and it is always a negative value since multiple reflections degrade shielding effectiveness [41].

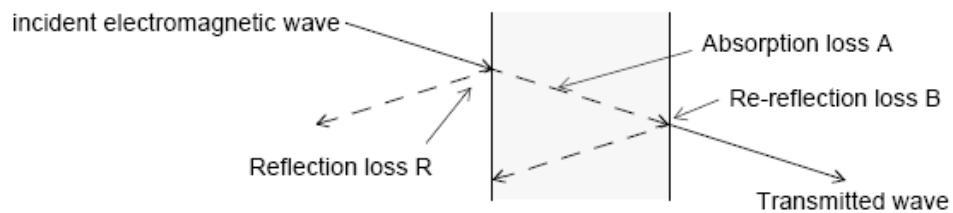


Figure 6.10 Losses due to a conductive barrier [41]

Since an incident electromagnetic wave is induced by a conductive barrier in a several mechanisms as reflection, absorption and re-reflection (Figure 6.10). Shielding Effectiveness can be also improved by using multi layer barriers. For

multilamina shielding, the total reflection loss can be calculated as the sum of the reflection losses at each interface since every shield has its own impedance. In a big shielding enclosure, a very high shielding is normally provided with double isolated conducting metal sheets separated by an inner core made up of dry ply wood [48]. Sometimes air gap is used instead of wood lamina between layers of shielding material. For magnetic shielding, the “air gap” can actually be made of a conductive but nonmagnetic material such as copper [39].

### **6.4.3 SHIELDING AT APERTURES**

For some practical reasons, the shielding surfaces have discontinuities like ventilation holes, shielding panel joints, visual access windows, control panels, input and output connections, etc. In most situations, [49] the leakage of electromagnetic (EM) energy from a metallic enclosure is dominated, not by the physical characteristics of the metal, but by the size, shape and location of these apertures.

The mechanism of degradation of shielding due to apertures can be briefly explained as follows: When a shield receives an incident field, currents are induced to flow in this shield. These currents generate “scattered” fields [48], which counteract or reduce the effects of incident fields. These scattered fields can be thought as the reflected field. The reflected field is of a polarity such that it tends to cancel the incident field in order to satisfy the boundary condition that the total electric field tangent to a perfect conductor must be zero [48]. This situation can only be achieved when the shield let induced currents flow unimpeded. If we place an aperture in the shield perpendicular to the direction of these currents, the aperture will interrupt the current flow and reduce the shielding effectiveness.

There are numerous theories for determining the recession in SE due to apertures. The simplest theory based on the assumption that [41] SE is directly proportional to the ratio of longest aperture dimension and frequency, with zero SE when  $2L = 1$  since  $SE = 20\log(1/2L)$ . Thus the SE increases linearly with decreasing frequency up to the maximum value determined by the barrier material, with a greater degradation for larger apertures [41]. This method is simple but it only gives a rough prediction even though applying a correction factor for the aspect ratio of slot-shaped apertures.

Another approach to the shielding effectiveness in the existence of apertures is again based on the size of the aperture and the frequency of the field. If the size of the aperture and the wavelength of the field are such that the linear dimension of an aperture is much smaller than  $\lambda/2\pi$ , the field in the vicinity of the hole may be represented approximately [50] by the fields existing at the side of the aperture before it is cut in the wall, plus the fields of electric and magnetic dipoles located at the center of the aperture. If the aperture is large compared to the wavelength, the shielding effectiveness becomes very poor since the incident wave can propagate considerably through the aperture ([50, 40]) as shown in Figure.6.11.

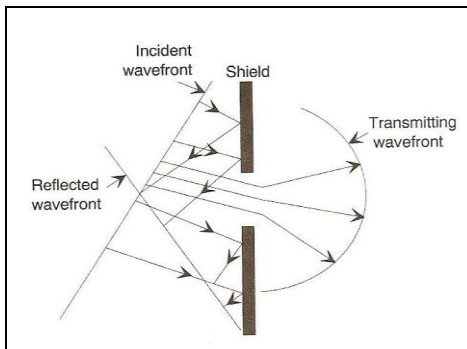


Figure 6.11 Electromagnetic wave propagation through a shield with an aperture [40]

### 6.4.3.1 SLOTS VS HOLES

The apertures on the shield are generally modeled as basic geometrical forms in order to simplify the expressions for determining the shielding effectiveness (SE). As mentioned before, the aperture in the shield wall reduces the shielding effectiveness. An aperture in the form of a long, thin slot is the worst geometry which significantly affect SE unless it is oriented parallel to the direction of induced flow. Since it is not feasible to determine the direction of the induced current and place the slot direction appropriately, a large number of small holes are used instead [48], as illustrated in Figure 6.12. Even dividing a long slot into two shorter ones improves both the magnetic and electric shielding by about 6dB [41]. The width of the slot does not have significant effect on SE.

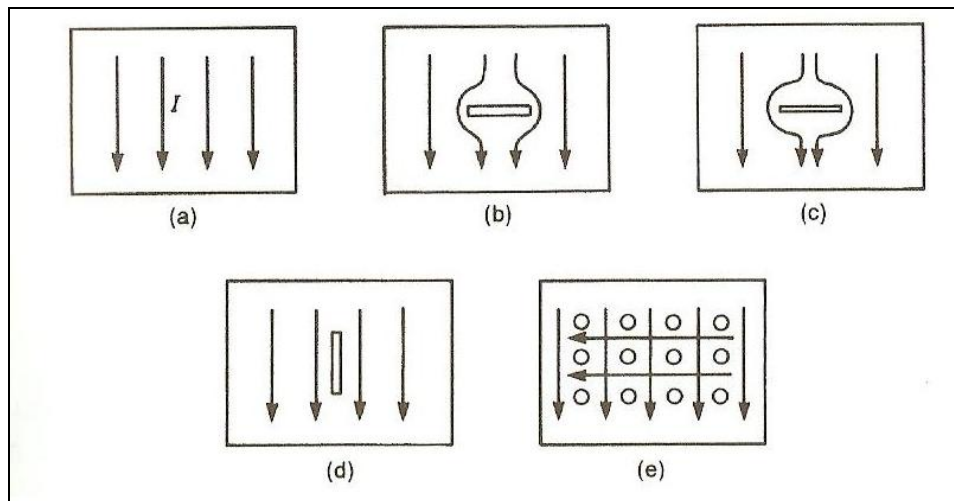


Figure 6.12 Slot vs. holes [48]

The effect of holes on SE can be examined separately for the different thicknesses of barriers. For the case of thin barrier, a good rule to follow in general design practice

is to avoid openings larger than  $\lambda/50$  to  $\lambda/20$  at the highest frequency of operation ([40]). For wavelengths greater than two times the maximum hole diameter the shielding effectiveness is primarily given by the reflection loss [43], and approximately given by

$$SE_{EB} \approx 20 \log_{10} \left( \frac{\lambda}{2D} \right) \quad \text{for } D > t_b \quad (6.19)$$

where  $D$  is the diameter of the hole and  $t_b$  is the thickness of the shielding barrier.

From equation (6.19), it can be observed that, [43] for wavelengths equal to twice the opening, the shielding is zero. The frequency at which this situation occurs is called the cutoff frequency ( $f_c$ ) [43].

$$f_c = C/2D \quad (6.20)$$

where  $C$  is the propagation velocity of electromagnetic waves

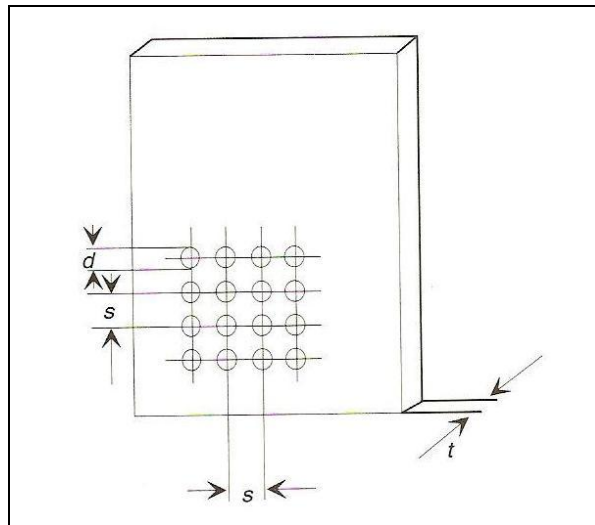


Figure 6.13 Slots on a barrier [40]

Especially for ventilation panels of thin barriers, multiple holes are used generally in rectangular patterns. These holes are either circular or square and sometimes hexagonal geometries. The important parameters in such cases are the spacing between two adjacent holes, the wavelength of the interface and the total number of holes. Since the size of these apertures is usually well below cut-off, only the dominant waveguide mode is significant in the region of these openings ([40]). For the case of normal incidence and the aperture spacing  $s < \lambda/2$ , the shielding is approximately given by [43],

$$SE_{dB} \approx 20 \log_{10} \left( \frac{\lambda}{2D} \right) + 10 \log_{10} n \quad (6.21)$$

where  $n$  is the total number of holes.

For the case of thick barrier ( $d \ll t$ ), a hole acts like a waveguide. A waveguide [52] is a structure through which electromagnetic waves can be transmitted from point to point, and within which the fields are confined to a certain extent for EMI shielding, the size of the hole should be selected such that it remains the lowest cut-off frequency at the highest interference frequency [40]. Fields transmitted through a waveguide below cut-off are attenuated approximately exponentially with the distance along the guide and the total shielding effectiveness is given by [40]

$$SE_{dB} \approx 20 \log_{10} \left( \frac{\lambda}{2d} \right) + 27.3 \frac{t}{d} \quad (6.22)$$

#### 6.4.3.2 HONEYCOMB

If improved shielding of vents is necessary, “honeycomb” panels can be used in which the honeycomb pattern functions as a waveguide below cut-off frequency [41] (Figure 6.14). Such air vent panels take the advantage of providing sufficient volume

of airflow and preventing the entry of low-frequency fields ([48]). Common honeycomb material has a depth-to-width ( $t_d/w$ ) ratio of approximately 4:1 for more than 100-dB attenuation [40]. Total shielding effectiveness for  $n$  number of rectangular cells [43] is given by

$$SE_{EB} \approx 20 \log_{10} \left( \frac{f_c}{f} \right) - 10 \log_{10} n + 27.3 \frac{t_d}{w} \quad (6.23)$$

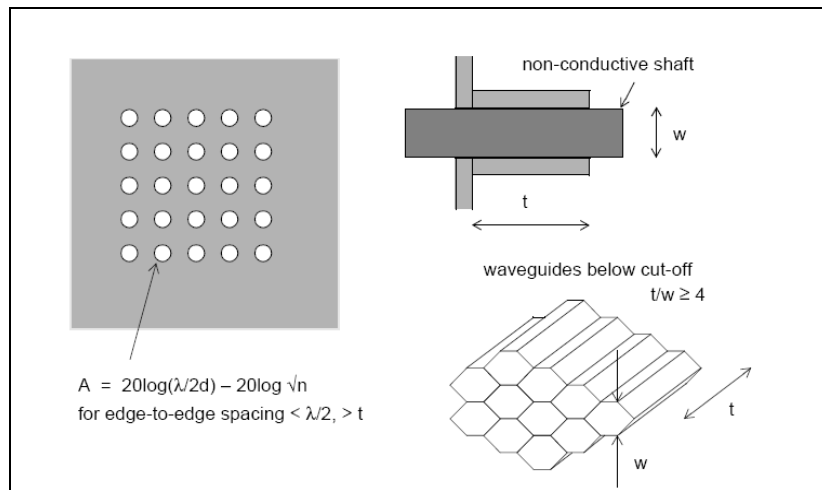


Figure 6.14 Mesh panels and waveguide below cut-off [41]

### 6.4.3.3. COVERS, DOORS, WINDOWS

When currents flow around a slot in a piece of metal, that slot acts like a dipole antenna having the same dimensions as the slot [39]. This phenomenon is called a slot radiator or a slot antenna and it illustrates that [48] the length of the gap is more important than its thickness in determining the radiated emissions of the gap.

When an enclosure and its cover are assembled, the ideal situation is one hundred percent mating, but in real life there are always gaps between them. Screws are placed between cover and the chassis but it will again not be airtight. Although they break up the slot length, the gasket usage is necessary.

The feasible distances between fixing points in order to increase shielding effectiveness are determined by experiments. For example Figure 6.15 shows the results of SE when ½-inch-wide metal-to metal joint of 0.090" aluminum is fixed with different screws with spaces from 10 inches apart to 1 inch apart [39].

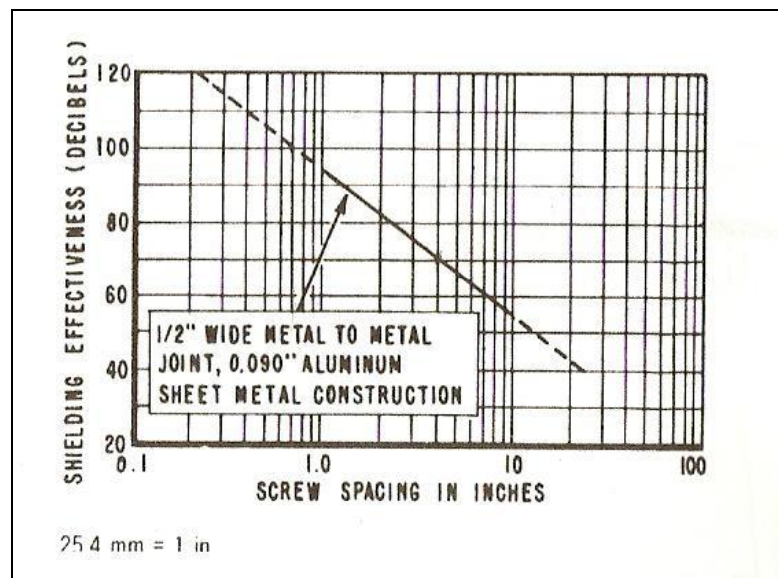


Figure 6.15 Shielding effectiveness and spacing between screws [39]

For some enclosures, there is a frequent need of access to inner components and door usage is inevitable. The building method of such parts of enclosure is summarized in Figure 6.16. The shielding effectiveness increases from “a” to “f”.

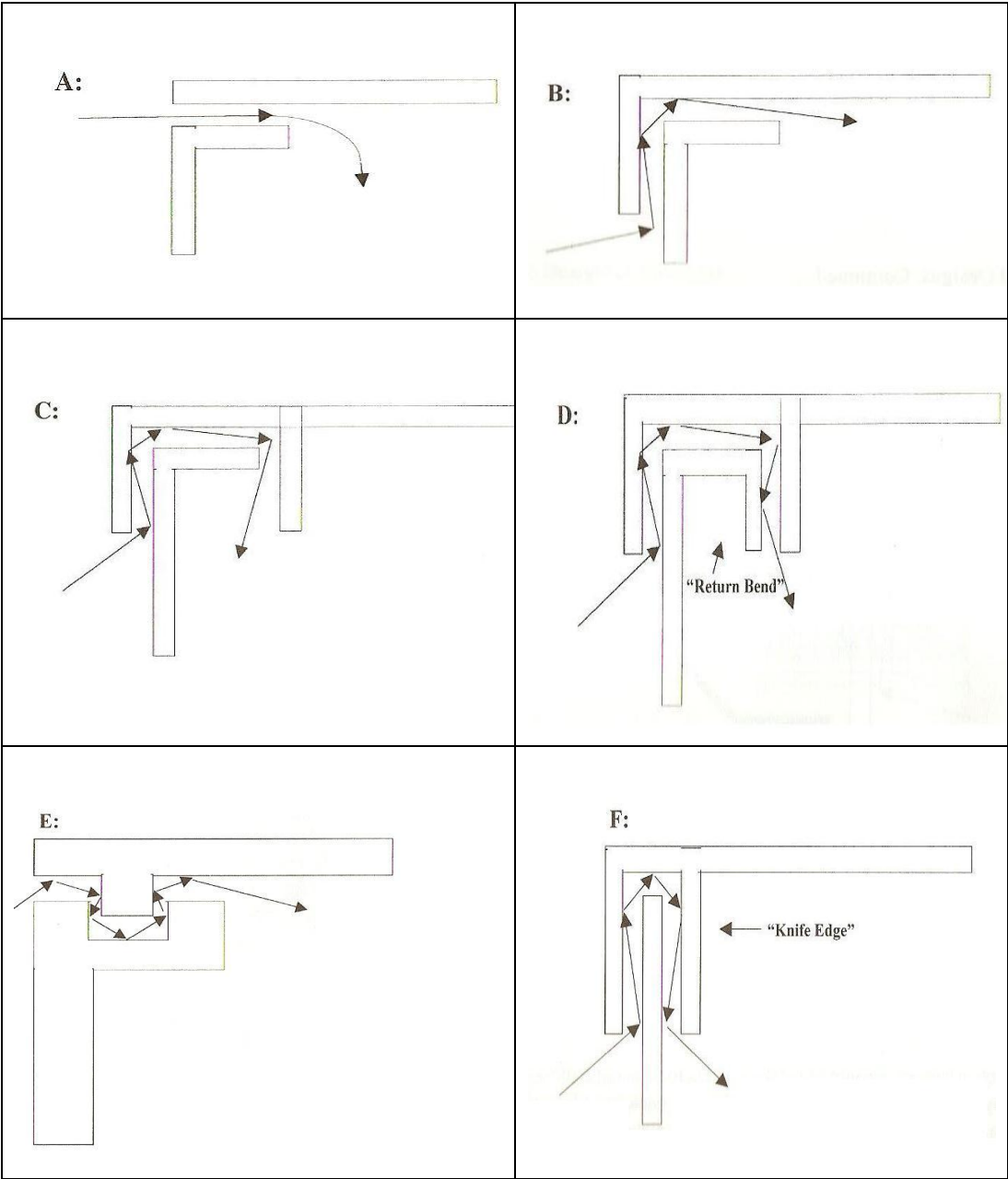


Figure 6.16 Lid designs [39]

Viewing windows normally involve a large open area in the enclosure and it significantly effects the shielding. For SE, special glasses are used in these openings. There are basically two types of shielded glass [39]: glass that is coated with a transparent, conductive coating and glass that is shielded by a fine blackened copper mesh (which is coated with a thin film of gold) sandwiched between two layers of glass or placed along one surface. Screening effectiveness of a transparent conductive coating is significantly less than a solid shield, since the coating will have a resistance of a few ohms per square meter and attenuation will be entirely due to reflection loss [41].



Figure 6.17 Shielded glasses [43]

The vision is reduced in the shielded glasses whether it is coated or meshed. By a sub-shield behind the display or a shielding at the source, a clear window can be used.

The interfering parts can be packed in a folded box or envelope of die-cut shielding foil with an insulating layer on the inside to avoid short-circuiting [45], and the electrical connections to the display must be filtered to keep the shield's integrity, and the display itself is unshielded and must therefore not be susceptible nor contain emitting sources [41].

#### 6.4.3.4 SEAMS

The enclosures for electronic devices and other shielding barriers are made from several panels joined together at seams. The electrical conductivity across the joint is imperfect. The reasons for the insulating layer can be listed as distortion of mating surfaces, painting, anodizing and corrosion. Consequently, the shielding effectiveness is reduced by seams. The problem is especially serious for hinged front panels, doors and removable hatches that form part of a screened enclosure [41].

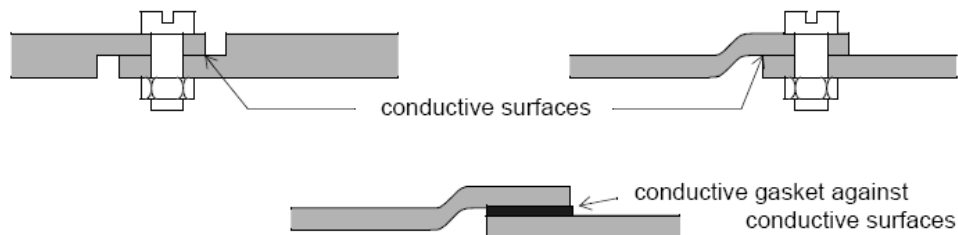


Figure 6.18 Joint cross sections [41]

In the design of seams, the important points to be considered are:

- i) **Conductive contact:** All seam mating surfaces must be electrically conductive [48].

**ii) Seam Overlap:** Since the two surfaces of the seam form a capacitor and capacitance is a function of area, seam overlap should be made as large as practical to provide sufficient capacitive coupling for the seam to function as an electrical short at high frequencies. So, the minimum seam overlap to spacing-between-surfaces ratio should be 5 to 1 [43]. as illustrated in Figure 6.19.

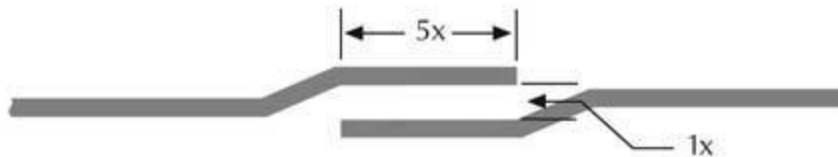


Figure 6.19 Seam overlap and spacing [43]

**iii. Seam Contact Points:** Along the entire length of every seam there should be firm electrical contact at intervals no greater than  $\lambda/20$  for most commercial devices and  $\lambda/50$  for microwave devices. This contact can be obtained by using pressure devices such as screws or fasteners, grounding pads, contact straps across the seam, or conductive gaskets [43] (Figure 6.18).

If the seam surfaces are conductive and mate tightly, an electrical short is provided. To ensure a tight seam design, conductive gasketing along the entire length of the seam may be used. Conductive gasketing should be considered in the following cases [43]:

1. Total enclosure shielding requirements exceed 40dB.
2. Enclosures with seam openings greater than  $\lambda/20$ .

3. Threat/emission frequencies exceed 100 MHz.
4. Machined mating surfaces are impractical.
5. Dissimilar materials are used on the mating surfaces of the seam and the device is designed to operate in severe environments.
6. Environmental (e.g., dust, vapor) seals are necessary.

#### **6.4.3.5 GASKETS**

Any tiny opening or gap in the enclosure has the potential of acting as a slot radiator, allowing radio signals to enter or escape; therefore all covers, doors and access panels must be gasketed or treated [39]. The purpose of these components is to be sandwiched in between the mating surfaces to ensure continuous contact across the joint, so that shield current is not diverted [41].

Shielding effectiveness of the gasketed joint decreases with the increase of frequency [48]. Typical shielding effectiveness of commercially available EMI gaskets is of the order of 80-100 dB. Gaskets should be placed on the inside of any securing screws, since if they are placed outside these screws, radiation from the screw holes will not be protected against [40].

The factors when selecting a conductive gasket or finger material can be listed as [41]:

- i) Its conductivity: it should be of the same order of magnitude as the panel material;
- ii) Ease of mounting: gaskets should normally be mounted in channels machined, cast in the housing, or by adhesive tape, welding, riveting, soldering, fasteners as seen in Figure 6.20. The right method depends on the direction of contact pressure and the type of the gasket.

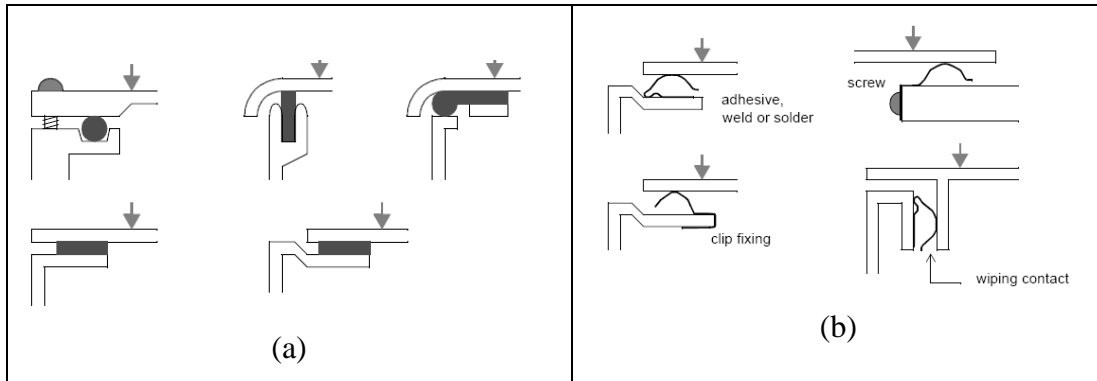


Figure 6.20 Gasket and finger stock mounting [41]

iii) Galvanic compatibility with its host

iv) Environmental performance: conductive elastomers will offer combined electrical and environmental protection, but may be affected by moisture, fungus, weathering or heat. If separate environmental and conductive gaskets are used, then the conductive gasket should be placed inside the environmental seal, and also inside screw mounting holes.

There are many commercially available EMI gasket materials. Most of these can be classified as follows [48]:

-**Knitted wire mesh**: This is thin plated, copper-clad, steel knitted, wire mesh EMI gasket of different forms and shapes, which is designed to provide EMI shielding for electronic joints, door contacts, and cables.

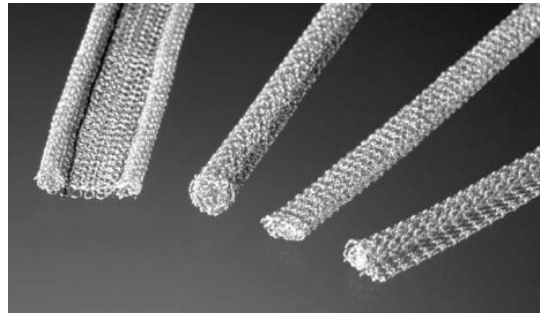


Figure 6.21 Knitted wire mesh [58]

**-Oriented wire mesh:** This is an oriented array of wires in a silicone rubber EMI gasket which is designed to be used in military, industrial, and commercial applications requiring EMI shielding and grounding in conjunction with environmental sealing, or repeated opening and closing access doors and panels.

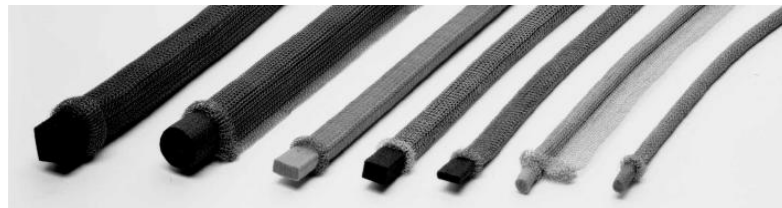


Figure 6.22 Oriented wire mesh [58]

**-Conductive elastomer:** This is a silver-aluminum filled silicone elastomer. EMI gasket that provides high shielding effectiveness and improved corrosion resistance.

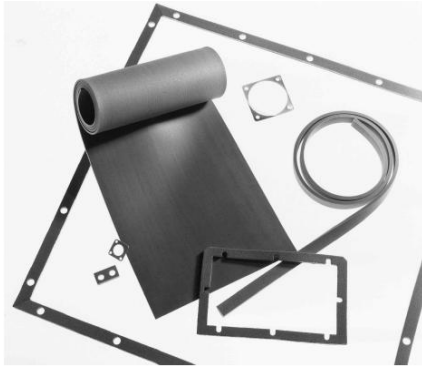


Figure 6.23 Conductive elastomers [58]

**-Spiral metal strip:** This is a tin-plated beryllium copper spiral strip EMI gasket which is designed to be placed between two flat surfaces (a case and a cover). Beryllium copper is a highly conductive, corrosion resistant spring material. Thin plating is used for its low contact resistance to other metal surfaces and it is one of the few metals which are corrosion compatible with aluminum in the presence of moisture and salt spray.

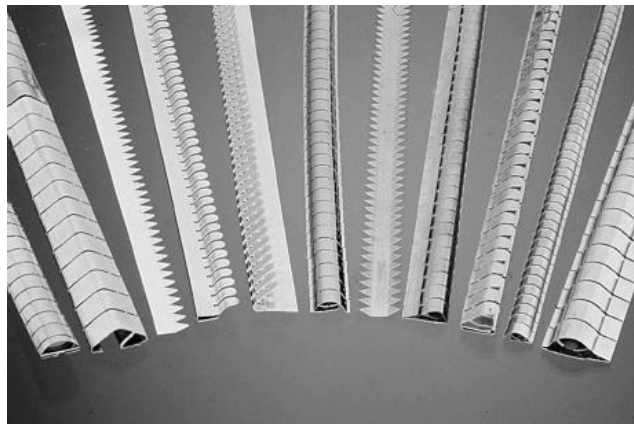


Figure 6.24 Spiral metal strips [58]

#### **6.4.4 CONDUCTIVE COATINGS**

Sometimes plastics or other nonconductive materials are used as enclosure material for their cost effective property or for aesthetic reasons. When electronic systems are packaged by such materials, they must be shielded with a conductive coating applying on one or both sides. This method provides typically 60 dB and above shielding for EMC since tiny particles of conductive materials such as carbon, silver or nickel is embedded in conductive coatings.

Thin coatings will be almost as effective against electric fields at high frequencies as solid metal cases but are ineffective against magnetic fields [41]. Except the high frequencies, the major shielding mechanism is E-field reflection loss.

An important parameter for the conductive coating is its resistivity. The coatings which have high resistivity provide less efficiency for shielding. Resistivity depends on the thickness of the coating. The shape and sharpness of the feature sometimes affects coating thickness. Sharp corners, deep and narrow crevices, close ribs are not preferred for achieving suitable coating thickness.

The same consideration for apertures and seams as for metal shields apply for conductive coatings which is any scratch or crack which breaks through the coating acts as an aperture and degrades the shielding effectiveness [41].

#### **6.4.5 GALVANIC CORROSION**

Corrosion [59] is the result of an electrochemical process involving an anodic reaction, the metal goes into solution as an ion, and a cathodic reaction takes place

where electrons released by the anodic reaction are discharged to maintain electrical neutrality by reaction with ions in solution.

There are several type of corrosion due to its mechanisms and characteristics. Galvanic corrosion (sometimes called dissimilar metal corrosion) is the process by which the materials in contact with each other oxidizes or corrodes [53] because of their potential difference. There are three conditions for galvanic corrosion to occur:

- The presence of two electrochemically dissimilar material
- Electrically conductive path between the two metals
- Conductive path for the metal ions to move from anodic metal (less corrosion resistant metal, most chemically active) to the more cathodic metal (more corrosion resistant).

For the shielding enclosure, when selecting a gasket or a fastener, galvanic corrosion must be considered. To reduce corrosion, the gasket or fastener metal and its housing should be potentially close together and the housing material should be conductively finished or plated. For this manner the metals are tabulated according to their electrical potential and this table is called “galvanic scale” or “anodic index” which can be seen in Appendix C.

## **6.5 ELECTROSTATIC DISCHARGE**

*Static electricity* is defined as an electrical charge caused by an imbalance of electrons on the surface of a material [54]. This imbalance of electrons produces an electric field that can be measured and that can influence other objects at a distance. *Electrostatic discharge* is defined as the transfer of charge as a lightning bolt when the voltage differential between the two surfaces having different electrical potentials is

sufficiently high to break down the dielectric strength of the medium separating them. ESD can occur in any one of four ways: a charged body can touch an integrated circuit (IC), a charged IC can touch a grounded surface, a charged machine can touch an IC, or an electrostatic field can induce a voltage across a dielectric sufficient to break it down [55].

Electrostatic discharge can damage or destroy metallization that results in a change of electrical characteristics of a semiconductor device. Electrostatic discharge also may upset the normal operation of an electronic system, causing equipment malfunction or failure [54].

Conductors and apertures are important since an ESD pulse can enter a piece of equipment over any of them. If an enclosure is grounded, mainly the discharge route is through the equipment back to earth. But conductors that have a probability of carrying a pulse current should not be placed near circuitry. The current should be provided a wide path in order to lower the magnetic field intensity near the path, since the changing magnetic field can couple into any loop area and damage components. This can be a conductive painted surface or a wide strip of aluminum [56].

## **6.6 GROUNDING**

Earth is having zero potential in which a rod, or wire of electrically conducting material, is driven to provide a low (ideally zero) impedance sink for unwanted currents. An electrical ground is low-impedance plane at a reference potential (often 0 V with respect to earth) to which all the voltages in systems and circuits can be related and grounding is a technique that provides a low-resistance path between electrical or electronic equipment and the earth or common reference low-impedance

plane to bypass fault current or EMI signal [48]. Thus, electrical grounding is essential for the protection of people against electrical shock, fire threat because of insulation burnout from lightning or electrical short circuit, and protection of equipment and systems against electromagnetic interference (EMI).

There are several purposes of ground system. The concept of a ground as being zero-potential surface may be appropriate at dc or low frequencies, but is never true at higher frequencies, since conductors have significant impedance and high frequency currents flow through these impedances, resulting in points on the ground having different high frequency potentials [40]. This explains the main differences between the two types of ground: safety ground and signal ground

### **6.6.1 SAFETY GROUND**

Safety ground, also known as “chassis ground” is generally used for shock-hazard protection of a system or a device. In addition to shock protection [40], it also serves an important role in draining electrostatic discharge (ESD) and diverting ESD currents away from vulnerable electronics.

### **6.6.2 SIGNAL GROUND**

Signal ground can be considered as return path for signal currents to their sources.

The signal ground network can be a single-point ground, multi-point ground, hybrid ground, or a floating ground [57]:

**-Single point ground:** In a single point ground system, the ground planes of each device are gathered at a point which is connected to the system ground point of a reference potential (Figure 6.25). Single point grounding is used for low frequencies

where [48] physical connection is small compared to wavelength at the frequency of operation and it avoids the problems of common-mode coupling.

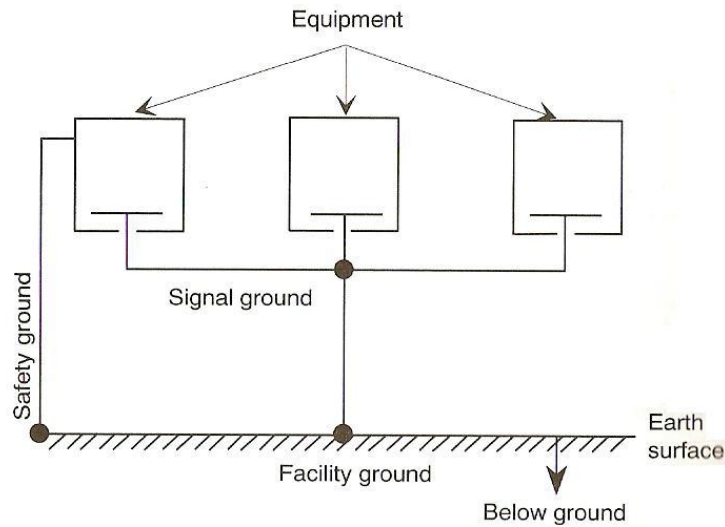


Figure 6.25 Signal point ground [48]

-**Multi-point ground:** In multi-point ground system, every device in the system is separately bonded to a ground plane which is also earthed for safety reasons.(Figure 6.26) Multi-point grounding is generally used for high frequency where there exist different potentials at different points of the interconnecting system. The dimension of the grounding is large compared to wavelength at the frequency of operation [48].

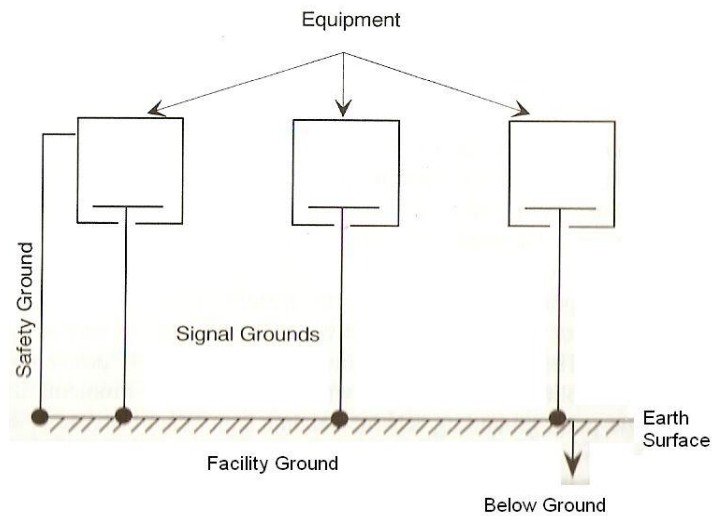


Figure 6.26 Multi-point ground [48]

**-Hybrid ground:** A hybrid ground behaves as a single-point ground at low frequencies and as a multi-point ground at high frequencies. Low-frequency ground current loop is avoided by the capacitor at one ground [57] and at high frequencies, the capacitor produces low reactance and cable shield is grounded [48]. This system is used for computer and peripheral frames for safety purposes.

**-Floating ground:** A floating signal ground system is electrically isolated from the equipment cabinets, building, ground, and other conductive objects to avoid a coupling loop for noise currents present in the ground system and their flow in signal circuits [48].

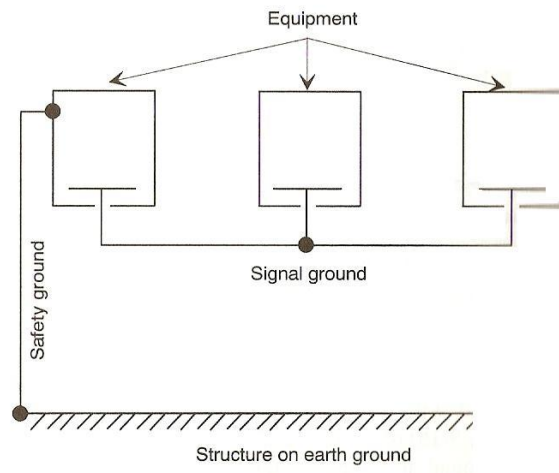


Figure 6.27 Floating ground [48]

## 6.7 DESIGN

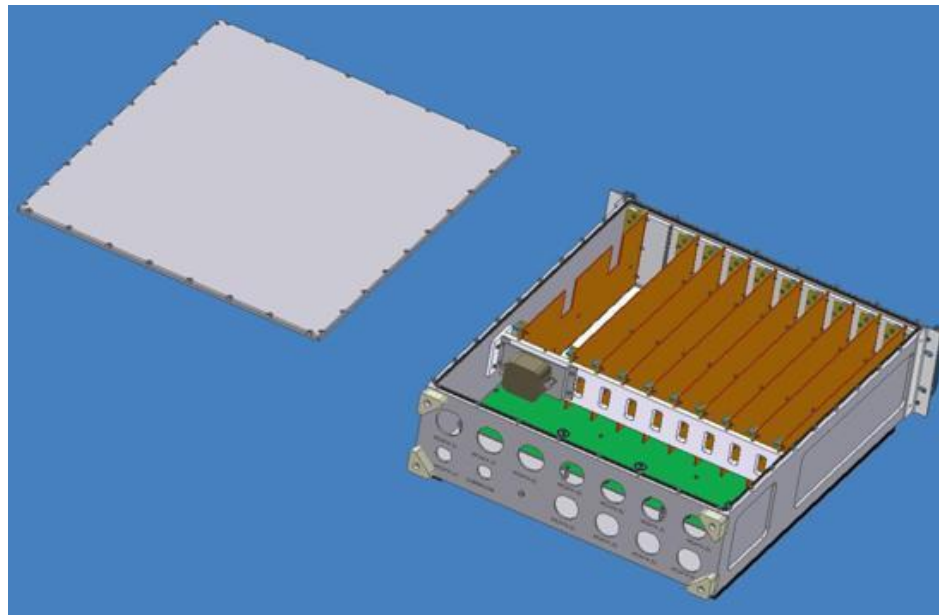


Figure 6.28 The electronic design of the device

In the electronic device which is the subject of this thesis, there are 9 audio card and one control card which are the inner electromagnetic sources as shown in Figure 6.28. The total inner source has a magnitude of 35,795 MHz. For the outer sources, the device is subjected to frequencies in a range between 30 Hz to 18GHz as test cases.

In the following parts of this section, the design steps of the chassis will be briefly explained due to the critical frequencies.

### **6.7.1 MATERIAL SELECTION**

Material is an important parameter for electromagnetic shielding. It both affects the reflection, absorption and re-reflection loss capacities of the shielding barrier. The reflection depends on the permeability and conductivity of the barrier material as well as barrier distance from the source. For absorption loss, thickness of the material is also important besides its conductivity and permeability.

Because of the corrosive effects of sea environment, aluminum is used as built-up material of the chassis and as mentioned in previous chapters for the good mechanical properties, Al 5083 H321 is preferred as a consequence of shock and vibration conditions. Aluminum has better shielding property for plane wave reflection loss, electric field and magnetic field reflection losses when it is compared with steel. On the other hand, for absorption loss, steel gives better results. The comparison of Sshielding effectiveness of aluminum, steel and copper for different frequencies is given in Appendix-B.

Roughly, nomograms can be used for determining absorption and reflection losses in order to decide which material is more suitable for the given design frequencies. An

example of plane wave reflection nomogram is given in Figure 6.29. From the nomogram, we see that Aluminum 5083 H321 (hard aluminum) has reflection loss of 64 dB for 10 GHz frequency, whereas for the same frequency, stainless steel has roughly 21 dB reflection loss. There is only slight difference between hard and soft aluminum which can be tolerable when other design parameters are considered.

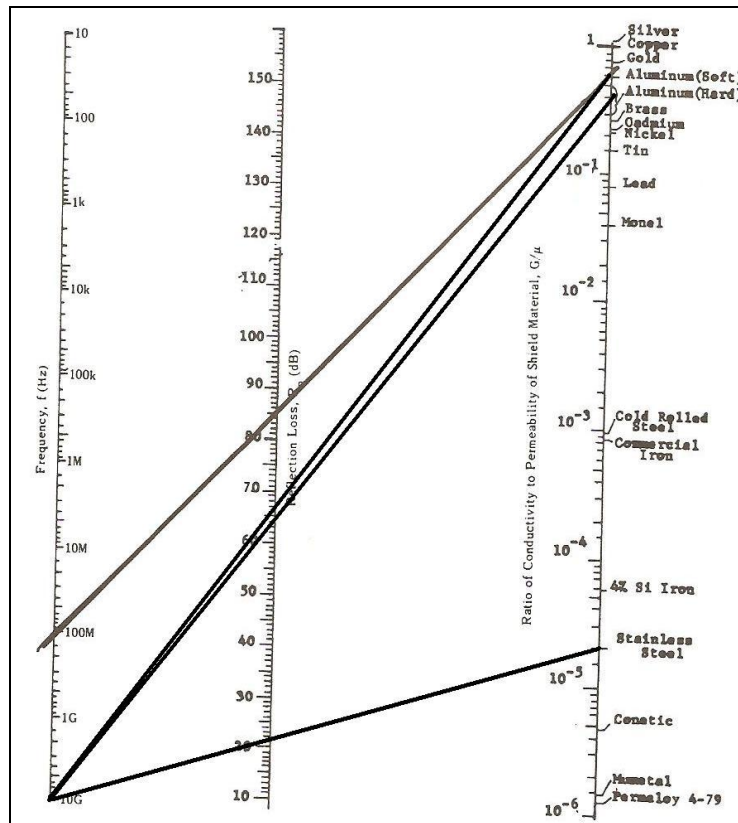


Figure 6.29 Reflection loss nomogram [39]

As explained in the previous sections shielding has two complementary aspects: the shielded device should work without interfering with other sources and it should not cause to malfunction of other systems within its operating environment. So the

shielding performance of the device will be examined for its inner source and for the outer sources.

### ***6.7.1.1 INNER SOURCE***

The distance between the source and the barrier is an important parameter for reflection loss. The region where  $d > \lambda/2\pi$  is called far field. Through far field, the complex three dimensional geometry of the electromagnetic waves decays and they propagate as plane waves. As a result, for this region there is no need to examine reflection losses of electric and magnetic fields separately.

The magnitude of the inner source of the device is 35,795 MHz. Assuming the position of the source inside the box as at the center and taking the shortest dimension for the distance between the source and barrier,  $d$  is approximately 0.212 m. (Figure 6.30)

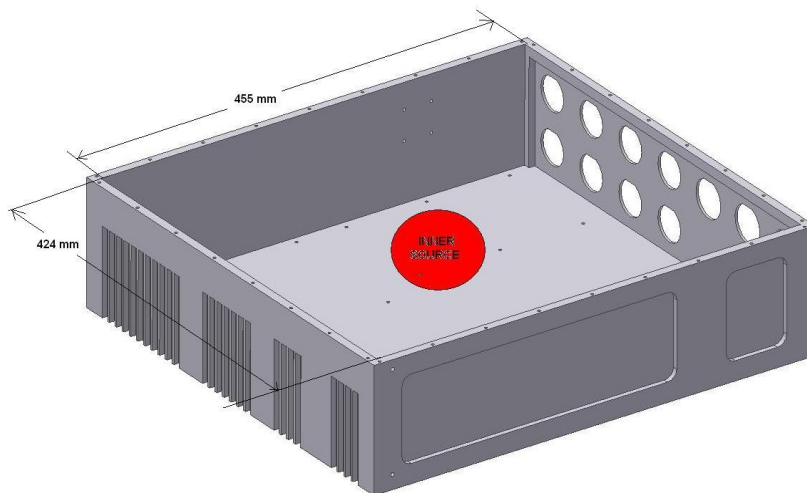


Figure 6.30 The inner source of the device

Calculating the wavelength, it can be seen that the working region for the inner source is in near field.

$$f = 35.795 \text{ MHz}, \lambda = 8.3811 \text{ m and } d = 0.212 \text{ m}$$

$$d < \lambda/2\pi \rightarrow 0.212 < 1.3339$$

And the skin depth is calculated by using Equation (6.14)

$$\delta = \frac{1}{\sqrt{\pi \cdot f \cdot \mu \cdot \sigma}} \text{ meters}$$

where

$$\mu = \mu_0 \cdot \mu_r \quad [51] \quad (6.24)$$

$$\sigma = \sigma_0 \cdot \sigma_r \quad [51] \quad \dots\dots\dots(6.25)$$

$$\mu_0 = 4 \cdot \pi \cdot 10^{-7} \text{ H/m and } \sigma_0 = 59.6 \cdot 10^6 \text{ 1/ohm.m}$$

$\mu_r$  and  $\sigma_r$  are relative permeability and conductivity, respectively.

Through the calculations the thickness of the box is taken as 9 mm and the thickness is assumed uniform. The relative permeability used for AL 5083 H321 is 1. In most cases for Aluminum, the relative conductivity is taken as 0.61 but for specific cases of Aluminum alloys, to get a more precise result, the correct value of conductivity should be used. For Al 5083, relative conductivity is 0.29 [61].

The calculated values for are given in Tables 6.3 and 6.4. Equations (6.11), (6.12), (6.13) and (6.17) were used for Plane Wave Reflection Loss, Electric Field Reflection Loss, Magnetic Field Reflection Loss and Absorption Loss, respectively.

For Total Shielding of the barrier, the related calculations were done due to Equation (6.26) [51]. This equation is for enclosures without seams or apertures.

$$SE_n = -10 \log \left( 10^{\frac{-S1_n}{10}} + 10^{\frac{-S2_n}{10}} + 10^{\frac{-S3_n}{10}} + 2 \cdot 10^{\frac{-S1_n - S2_n}{20}} + 2 \cdot 10^{\frac{-S1_n - S3_n}{20}} + 2 \cdot 10^{\frac{-S2_n - S3_n}{20}} \right) \quad (6.26)$$

where,

$$S1_n = A_n + R_{m,n} \quad \text{Absorption plus magnetic losses} \quad (6.27)$$

$$S2_n = R_{e,n} \quad \text{Electric field losses} \quad (6.28)$$

$$S3_n = R_{p,n} \quad \text{Plane wave losses} \quad (6.29)$$

And “n” is frequency counter.

Table 6.3 Frequency, wavelength and skin depth values for inner source

Frequency ,f	Wavelength, $\lambda$ (m)	$\lambda/2\pi$	Skin Depth, $\delta$ (mm)
35.795 MHz	8.38106	1.33389	0.02023

Table 6.4 Losses due to inner source

Freq., f (MHz)	Ref. Loss, E- Field (dB)	Ref. Loss, H-Field (dB)	Plane Ref. Loss (dB)	Absorp. loss (dB)	Re-Ref. Loss (dB)	SE (dB)
35.795	103.48	71.28	87.08	3865.78	0	85.86

In contrast to reflection loss, absorption loss is the same whether the field is electric, magnetic or plane wave. It is proportional to the barrier thickness and its skin depth.

Re-reflection loss is negligible unless material thickness  $t$  is less than the skin depth  $\delta$ .

For the values taken for inner source, re-reflection loss result is so small (in the order of  $10^{-13}$ ) that it is taken as zero.

$$B = 20 \cdot \log_{10} \left( e^{-2\sqrt{2}t/\delta} \right) \text{ dB} \quad \text{Re-reflection loss (B)} \quad (6.18)$$

### 6.7.1.2 OUTER SOURCES

The outer sources considered for the chassis are the sources which are used through the EMI/EMC tests performed for this device. The frequencies of the sources are in a range of 30 Hz to 18 GHz. The distance between the source and device in the test set up is 2 m. So the distance between the source and the barrier is approximately 1.8 m. Although the chassis has no ventilation holes, honey comb structure, because of the cover and its screws, it is assumed as a closed box through the calculations.

Tables 6.5 and 6.6 show the calculated values between 30 Hz and 18 MHz. Through the calculations the thickness of the box is taken as 9 mm and the thickness is assumed uniform. The relative permeability used for AL 5083 H321 is 1 the relative conductivity is taken as 0.29. “r” ,distance between barrier and the source, is 1.8 m. The same equations used for calculating the losses and shielding effectiveness of the barrier due to inner source were used for outer source calculations.

Table 6.5 Frequency, wavelength and skin depth values for inner source

Frequency ,f	Wavelength, $\lambda$ (m)	$\lambda/2\pi$	Skin Depth, $\delta$ (mm)
30 Hz	10000000	1591549.4309	22.0991
50 Hz	6000000	954929.6585	17.1178
100 Hz	3000000	477464.8292	12.1041
150 Hz	2000000	318309.8861	9.8830
200 Hz	1500000	238732.4146	8.5589
400 Hz	750000	119366.2073	6.0520
600 Hz	500000	79577.4715	4.9415
800 Hz	375000	59683.1036	4.2794
1 kHz	300000	47746.4829	3.8276
5 kHz	60000	9549.2965	1.7117
10 kHz	30000	4774.6482	1.2104

Table 6.5 Frequency, wavelength and skin depth values for inner source (Cont'd)

15 kHz	20000	3183.0988	0.9883
20 kHz	15000	2387.3241	0.8558
30 kHz	10000	1591.5494	0.6988
50 kHz	6000	954.9296	0.5413
100 kHz	3000	477.4648	0.3827
150 kHz	2000	318.3098	0.3125
200 kHz	1500	238.7324	0.2706
500 kHz	600	95.4929	0.1711
1 MHz	300	47.7464	0.1210
10 MHz	30	4.7746	0.0382
20 MHz	15	2.3873	0.0270
30 MHz	10	1.5915	0.0221
35 MHz	8.57143	1.3641	0.0204
35.795 MHz	8.38106	1.3338	0.0202
40 MHz	7.50000	1.1936	0.0191
50 MHz	6.00000	0.9549	0.0171
100 MHz	3.00000	0.4774	0.0121
500 MHz	0.60000	0.0954	0.0054
1 GHz	0.30000	0.0477	0.0038

Table 6.5 Frequency, wavelength and skin depth values for inner source (Cont'd)

5 GHz	0.06000	0.0095	0.0017
10 GHz	0.03000	0.0047	0.0012
15 GHz	0.02000	0.0031	0.0009
18 GHz	0.01667	0.0026	0.0009

Table 6.6 Losses due to outer source

Freq., f	Ref. Loss, E-Field (dB)	Ref. Loss, H-Field (dB)	Ref. Loss, Plane Wave (dB)	Absorp. loss (dB)	Re-reflection Loss (dB)	SE (dB)
30 Hz	267.20	29.10	147.85	3.53	-1.56111326	32.63
50 Hz	260.54	31.31	145.63	4.56	-1.19613236	35.88
100 Hz	251.51	34.32	142.62	6.46	-0.7932162	40.79
150 Hz	246.23	36.09	140.86	7.91	-0.605009	44.00
200 Hz	242.48	37.33	139.61	9.13	-0.4915331	46.47
400 Hz	233.45	40.35	136.60	12.92	-0.2805514	53.27
600 Hz	228.17	42.11	134.84	15.82	-0.1932196	57.93
800 Hz	224.42	43.36	133.59	18.27	-0.1449581	61.63
1 kHz	221.51	44.32	132.62	20.43	-0.1143643	64.75

Table 6.6 Losses due to outer source (Cont'd)

5 kHz	200.54	51.31	125.63	45.68	-0.0132689	96.69
10 kHz	191.51	54.32	122.62	64.61	-0.0038880	114.56
15 kHz	186.23	56.09	120.86	79.13	-0.0017075	119.33
20 kHz	182.48	57.33	119.61	91.37	-0.0009035	119.30
30 kHz	177.20	59.10	117.85	111.91	-0.0003396	117.82
50 kHz	170.54	61.31	115.63	144.48	-8.523E-05	115.61
100 kHz	161.51	64.32	112.62	204.32	-9.617E-06	112.59
150 kHz	156.23	66.09	110.86	250.24	-2.226E-06	110.81
200 kHz	152.48	67.33	109.61	288.96	-7.180E-07	109.55
500 kHz	140.54	71.31	105.63	456.89	-1.078E-08	105.47
1 MHz	131.51	74.32	102.62	646.14	-2.227E-10	102.31
10 MHz	101.51	84.329	92.62	2043.27	0	89.95
20 MHz	92.48	87.33	89.61	2889.62	0	84.91
30 MHz	87.20	89.10	87.85	3539.05	0	81.50
35 MHz	85.19	89.77	87.18	3822.61	0	80.11
40 MHz	83.45	90.30	86.60	4086.55	0	78.86
50 MHz	80.54	91.31	85.63	4568.90	0	76.70
100 MHz	71.51	94.32	82.62	6461.40	0	69.38
500 MHz	50.54	101.31	75.63	14448.14	0	50.07

Table 6.6 Losses due to outer source (Cont'd)

1 GHz	41.51	104.32	72.62	20432.75	0	41.27
5 GHz	20.54	111.31	65.63	45689.03	0	20.50
10 GHz	11.51	114.32	62.62	64614.05	0	11.49
15 GHz	6.23	116.09	60.86	79135.73	0	6.21
18 GHz	3.86	116.88	60.07	86688.85	0	3.84

For total Shielding Effectiveness, Re-reflection losses are neglected since they are getting smaller and smaller as the frequency increases.

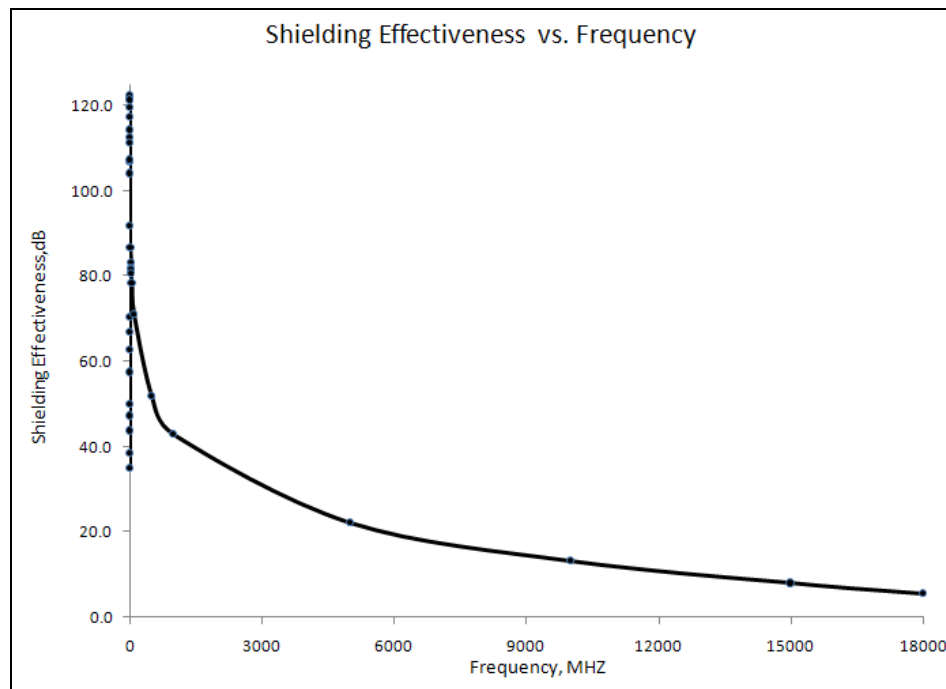


Figure 6.31 Shielding effectiveness of chassis for different frequencies

Figure 6.31 illustrates the shielding behavior of the chassis for different frequencies. The shielding effectiveness reaches 120 dB at low frequencies. The more detailed graph for lower frequencies is given in Figure 6.32.

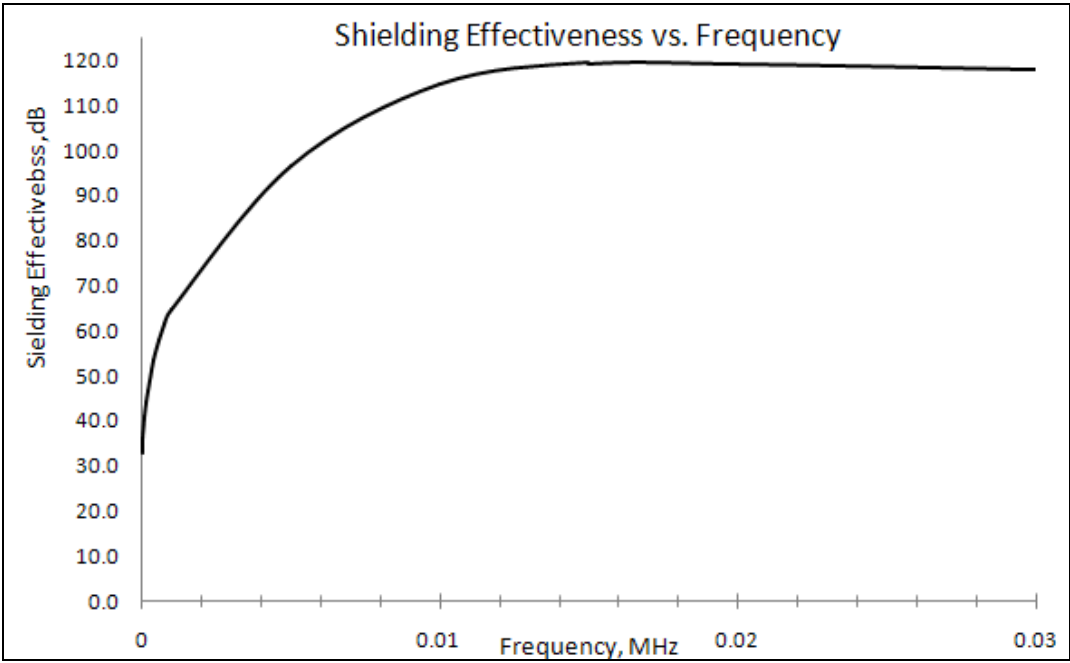


Figure 6.32 Shielding effectiveness of chassis between 10 Hz-30 MHz

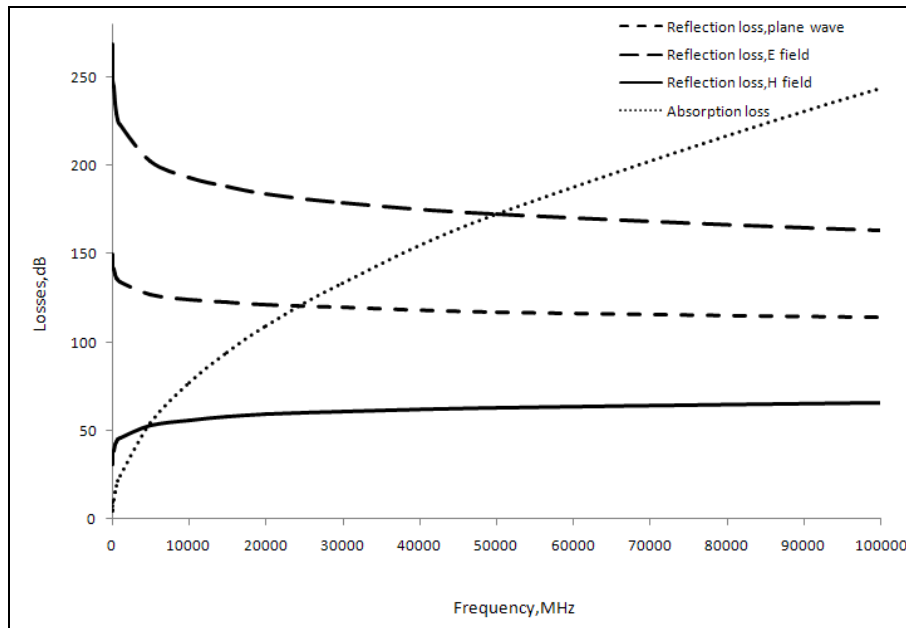


Figure 6.33 Reflection and absorption losses for different frequencies

Reflection losses for plane waves, E-field and H-Field are calculated individually. It can be observed from the tables that reflection of E-Field and plane waves increase as frequency decreases. On the other hand reflection of H-field and absorption increase with an increase in frequency. All these observations from calculations are visualized in Figure 6.33.

### 6.7.2 FIXED SEAMS AND FASTENERS

Shielding barriers are made up of some panels joined together at seams. Generally fixed seams like welding, brazing are used for such applications. The chassis of the electronic device which is a subject of this thesis is manufactured by welding. This procedure affects the shielding effectiveness of the box since the electrical conductivity at joint points is imperfect. This discontinuity forces shield current to flow around the joint and it leads [41] current diverted and creates a field coupling

path through the shield. Consequently, the shielding effectiveness of the unit box is reduced by seams. There are experimental studies on the reduction of SE by seams but still there is no realistic mathematical formulation. But at least experiment show that seam could reduce SE by 10-20 dB.

For the cover assembly, M3 screws are used as fasteners as seen in Figure 6.34. The distance between these fasteners are important for the unit's SE. As a general rule, fasteners should not be spaced more than 2.0 inches (50 mm) apart for stiff flanges, and 0.75 inch (19 mm) apart for sheet metal if high levels of shielding are required [58].



Figure 6.34 Back view of electronic equipment

EMI gasket is placed under the cover to avoid air gap between chassis and cover for an undisturbed electrical conductivity. The appropriate fastener spacing is needed to make gasket work efficiently. A one dimensional solution [58], gives a good first

order approximation of the spacing required between fasteners. In this method, the flange is approximated as a simple beam on elastic foundations.

By limiting variation in applied forces between fasteners to  $\pm 10$  percent, the formulation given below is used for determining the fastener spacing.

$$\beta \cdot d_f = 2 \quad [58] \quad (6.30)$$

where

$$\beta = \sqrt[4]{\frac{k}{4 \cdot E_f \cdot I_f}} \quad [58] \quad (6.31)$$

$k$  = foundation modulus of seal

$E_f$  = The modulus of elasticity of the flange

$I_f$  = The moment of Inertia of the flange and seal

$d_f$  = spacing between fasteners

For the device in thesis case, the spacing between fasteners is calculated as:

$$d_f = \frac{2}{\sqrt[4]{\frac{k}{4 \cdot E_f \cdot I_f}}} = 1.666 \text{ in.} = 42.320 \text{ mm}$$

where  $k = 10,000$  psi,  $E_{f,Al 5083} = 10442 \times 10^3$  psi,  $I_f = 0.00011531 \text{ in.}^4$

According to these design verifications, the actual spacing between fasteners is manufactured as 42.5 mm.

### **6.7.3 APERTURES AND AIR GAPS**

Generally electronic devices have apertures in the form of ventilation holes, display windows, covers and lids. In the design of the electronic device, there was no need for ventilation holes since it is cooled by conduction cooling, display windows or other apertures. The only holes opened through manufacturing process on the unit were the connector cut-outs. Since behind the connector bodies, conductive gaskets (silicone elastomer filled with silver-plated nickel particles) are used, the cut-outs for connectors do not affect the total shielding effectiveness of the unit.

For the cover, as mentioned in the previous part, EMI/Environmental gasket is used. The detailed explanation of this gasket will be given in the next section.

### **6.7.4 GASKETS**

The gasket, which would be used under the cover, need to have both electromagnetic shielding and environmental sealing property. For this purpose a commercial gasket of Tecknit Duosil is used.

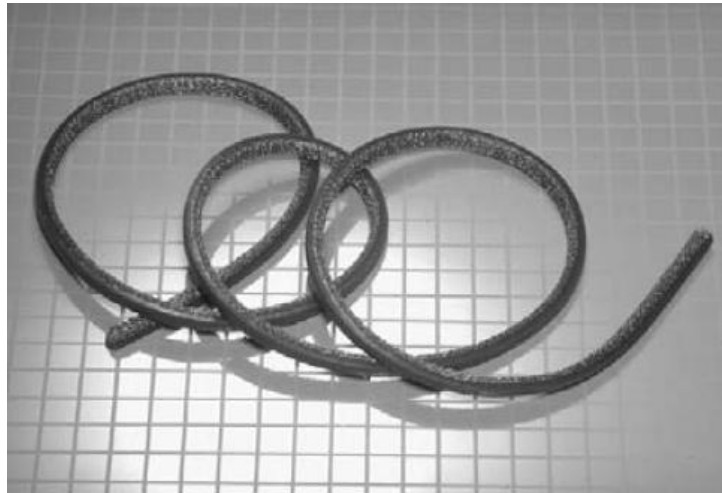


Figure 6.35 Duosil wire mesh and silicone gasket [43]

This gasket is composition of wire mesh and silicone gasket. It is developed for military applications especially for all-weather commercial electronic VHF and UHF equipment. For galvanic corrosion compatibility as a wire mesh material, “monel” was preferred. Monel is a trademark for a stainless steel alloys composed of nickel, copper and iron. For the environmental seal part of the gasket, silicone rubber was chosen. The typical shielding values of this gasket for an aperture 127 mm x 127 mm is given in Table 6.7.

Table 6.7 Shielding effectiveness of Duosil for an aperture of 127 mm x 127 mm [43]

MATERIALS	H-FIELD	E-FIELD	PLANE WAVE	
	100 kHz	10 MHz	1 GHz	10 GHz
	dB	dB	dB	Db
Monel	60	130	90	80
Sn/Ph/Bz	90	135	105	95

## 6.7.5 FINISHINGS

There are several methods of finishing for an aluminum chassis. Figure 6.35 shows the degradation effects of some coatings.

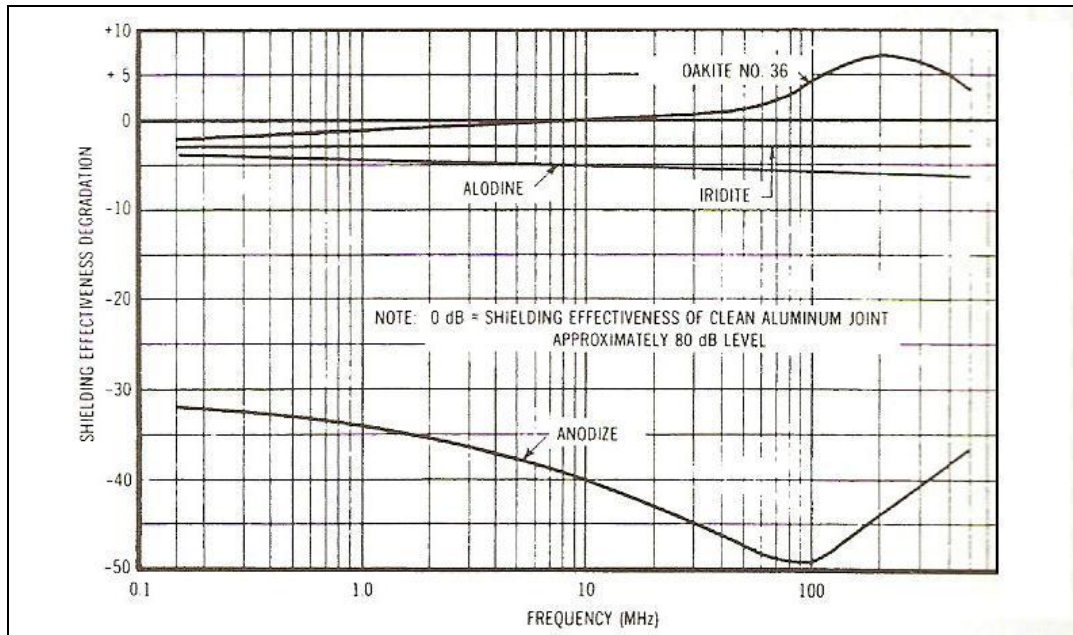


Figure 6.36 Shielding effectiveness for different finishings [39]

For the device chassis, yellow iridite is applied according to MIL-C-5541 standard. Iridite is more effective for EMI shielding compared to anodizing and alodining which are very common coatings for aluminum. (Figure 6.36)

## 6.7.6 GROUNDING AND ESD

On the back part of the chassis there are two screw-like structures for grounding: One of them is for chassis ground and the other one is for signal ground.

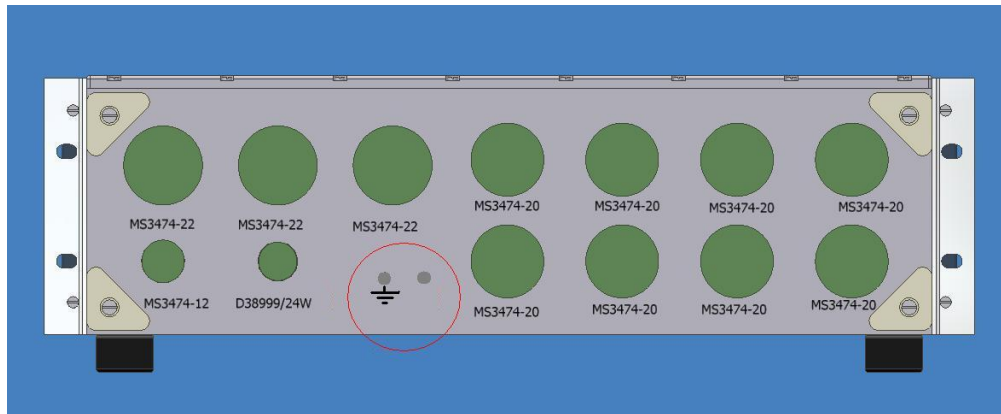


Figure 6.37 Grounds for the Device

Chassis or safety ground is for shock-hazard protection of the device. It also drains electrostatic discharge (ESD) and diverts ESD currents away from vulnerable electronics shown in Figure 6.37.

The signal ground supplies a return path for signal currents to their sources. The signal ground network used in the system, to which the device is integrated, is a single point ground. Every device has its own signal ground gathered at a point which is connected to the rack cabinet's ground point of reference potential.

## 6.8 TEST

The device which is a subject of this thesis is tested according to MIL-STD-461E and EN61000-4-2. MIL-STD-461E standard [46] establishes interface and associated verification requirements for the control of the electromagnetic interference (emission and susceptibility) characteristics of electronic, electrical, and electromechanical

equipment and subsystems designed or procured for use by activities and agencies of the Department of Defense. EN61000-4-2 standard is for immunity electrostatic discharge. The test department was responsible for the EMI/EMC Tests. All tests were performed by TUBİTAK MAM facilities at Gebze.

The device is subjected to Conducted Emission Test (CE102), Radiated Emission Test (RE101), Radiated Emission Test (RE102), Conducted Susceptibility Test (CS101), Conducted Susceptibility Test (CS114), Conducted Susceptibility Test (CS116), Radiated Susceptibility Test (RS101), Radiated Susceptibility Test (RS103) and ESD test as described by EN61000-4-2.

In an electromagnetic compatibility test, the piece of equipment being tested is called either the equipment under test (EUT) or the unit under test (UUT). According to MIL-STD-461E, the EUT working area is defined as “below deck”. Below deck [46] is an area on ships which is surrounded by a metallic structure, or an area which provides significant attenuation to electromagnetic radiation, such as the metal hull or superstructure of a surface ship, the pressure hull of a submarine and the screened rooms in non-metallic ships.

For all tests listed above, test steps and test result steps were common. The test steps which are explained in related sections of the standard are briefly,

1. Ensure that grounding is maintained properly for the safety of the test setup.
2. Place the EUT in test chamber. Prepare the functional test setup for EUT which is determined in related section
3. Perform Functional tests to the EUT and record test measurements
4. Perform and verify that visual and functional tests to the EUT are successfully completed and the measurements shall not exceed the specified limits in the standard.

The test result steps are;

1. Ensure that EUT is in its operational state.
2. Ensure that the measurements are recorded.
3. Ensure that Functional tests are successfully completed.
4. Ensure that Visual and Functional tests are successfully completed. Verify that the measurements shall not exceed the specified limits in the standard.

The general test setup described in MIL-STD-461 E is given in Figure 6.38. All the related tests are done due to this specified test set up. The impedance of power sources providing input power to the EUT shall be controlled by Line Impedance Stabilization Networks (LISNs).

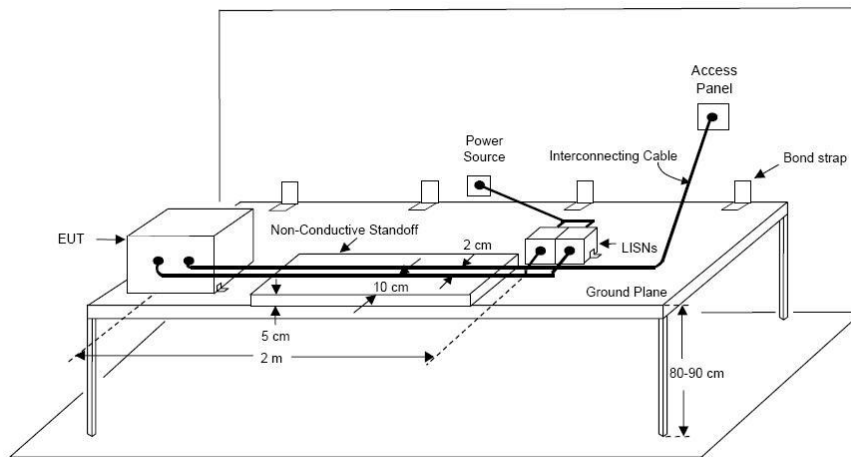


Figure 6.38 General test setup used through the tests of the device [46]

The test setup shows slight differences according to the mount method of device in its integrated system. Figure 6.39 illustrates the test set up for free standing EUT.

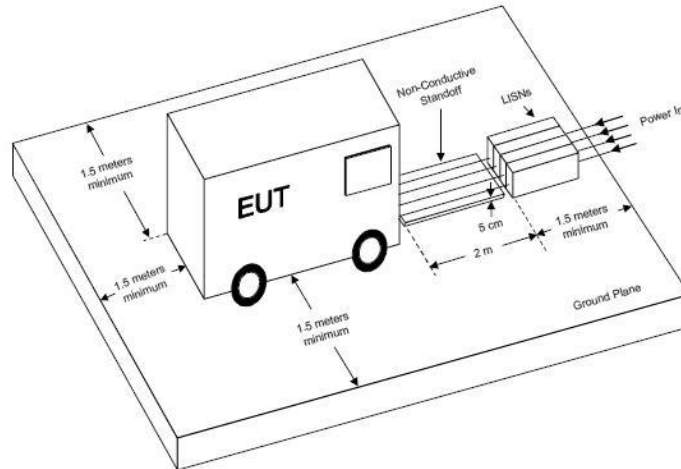


Figure 6.39 Test set up for free standing EUT [46]

### 6.8.1 CONDUCTED EMISSION TEST (CE102)

Test CE102 was performed according to MIL-STD-461E paragraph 5.5. The purpose of this test was to verify that electromagnetic emissions from the EUT do not exceed the specified requirements for AC and DC power input leads.

The EUT was tested in operational state. The conducted emission measurements was performed between 10 kHz and 10 MHz and expected not to exceed the specified limits in the standard.

EUT was placed in test chamber and prepared the functional test setup. Visual and functional tests were performed and during tests, test measurements were recorded.

## 6.8.2 RADIATED EMISSION TEST (RE101)

Test RE101, was performed according to MIL-STD-461E paragraph 6.15. This test procedure is used to verify that magnetic field emissions from the EUT and its associated cabling do not exceed the specified requirements. The magnetic field emission was measured in this test.

The EUT was tested in operational state. The radiated emission measurements were performed between 30 Hz and 100 kHz and expected not to exceed the specified limits in the standard in the operational state given in .

The limit curve for this test is given in Figure 6.40.

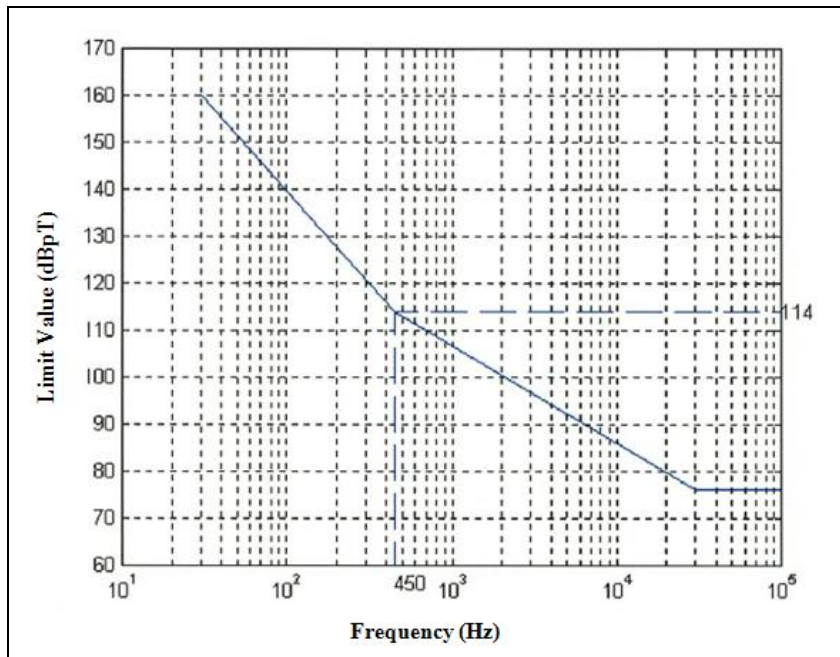


Figure 6.40 Limit curve used through RE101 test

### 6.8.3 RADIATED EMISSION TEST (RE102)

Test RE102, was performed according to MIL-STD-461E paragraph 5.16. This test procedure is used to verify that magnetic field emissions from the EUT and its associated cabling do not exceed the specified requirements. The magnetic field emission will be measured in this test.

The EUT was tested in operational state. Test was applied between 10 kHz and 18 GHz and expected not to exceed the specified limits in the standard.

For RE102 experiment of 10 KHz to 30 MHz, The rod antenna was used. The distance between the antenna and the EUT was 1 m. The height of the antenna from the floor was 0.9 m and the height of the antenna was 1.04 m. The device was passed this experiment successfully which can be observed from Figure 6.41.

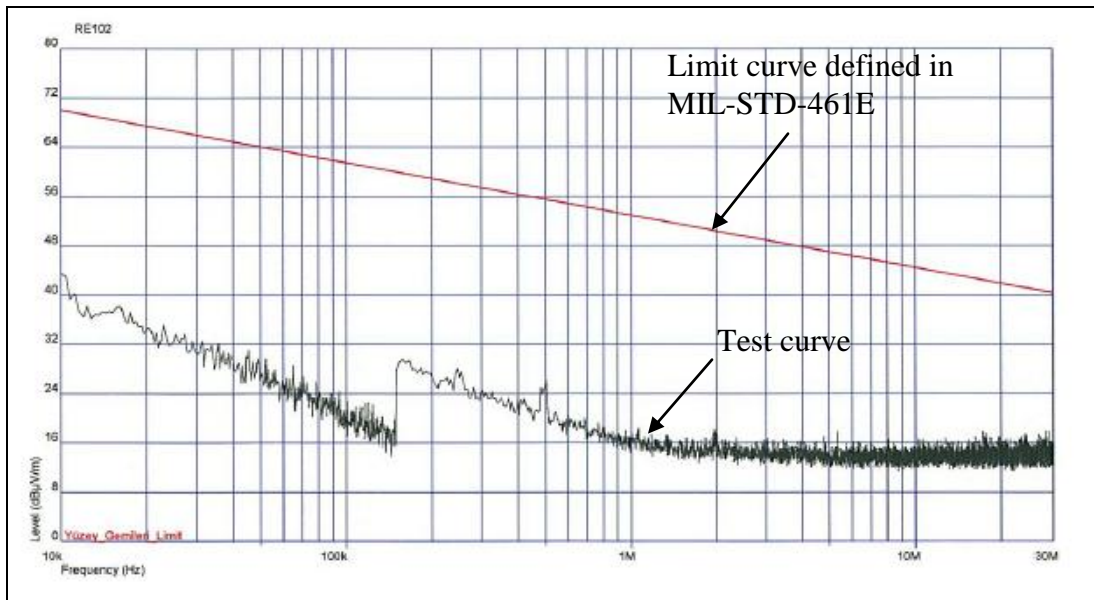


Figure 6.41. RE102 Experiment graph of back plane noise 10 kHz - 30 MHz

For RE102 experiment of 30 MHz to 200 MHz, biconical antenna was used. The distance between the antenna and the EUT was 1 m. The height of the antenna was 1.2 m. The device was passed this experiment successfully for vertical and horizontal polarizations which are illustrated by Figure 6.42 and Figure 6.43

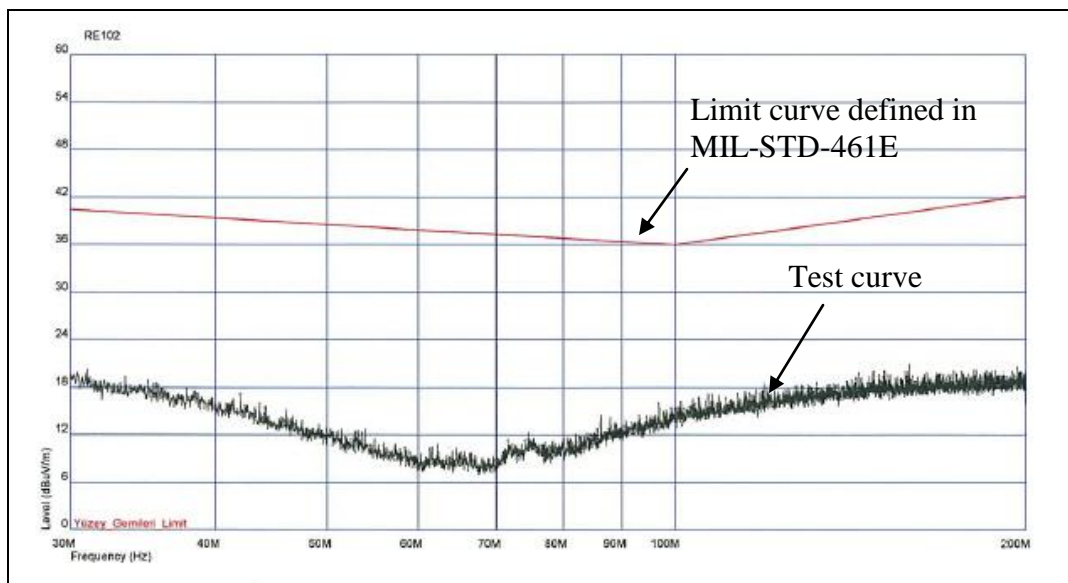


Figure 6.42 RE102 Experiment graph of back plane noise vertical polarization 30-200 MHz

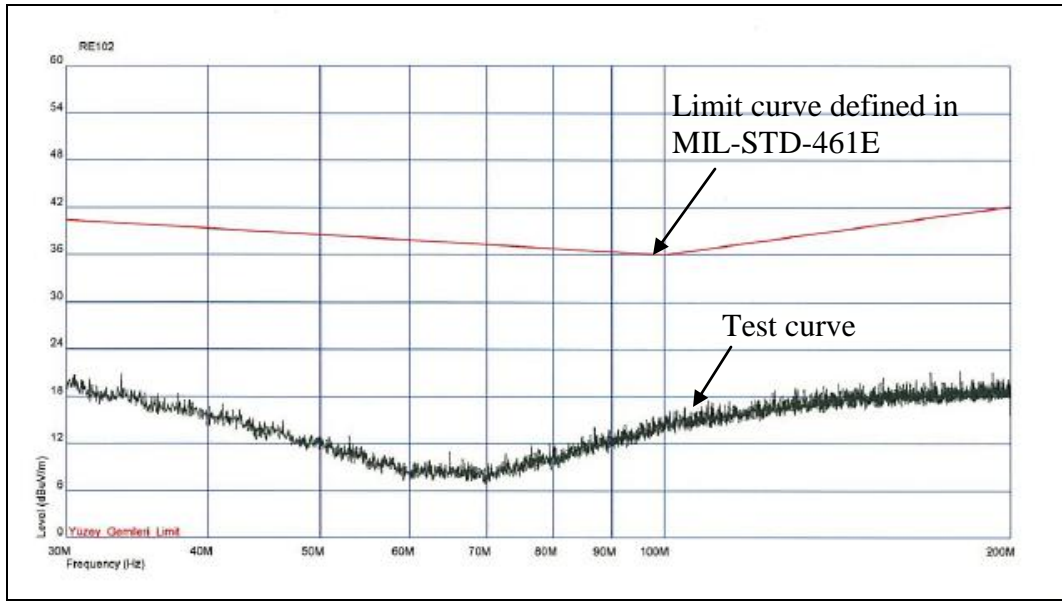


Figure 6.43 RE102 Experiment graph of back plane noise horizontal polarization 30-200 MHz

For RE102 experiment of 200 MHz to 1000 MHz, horn antenna was used. The distance between the antenna and the EUT was 1 m. The height of the antenna was 1.2 m. The device was passed this experiment successfully for vertical and horizontal polarizations which are illustrated by Figure 6.44 and Figure 6.45.

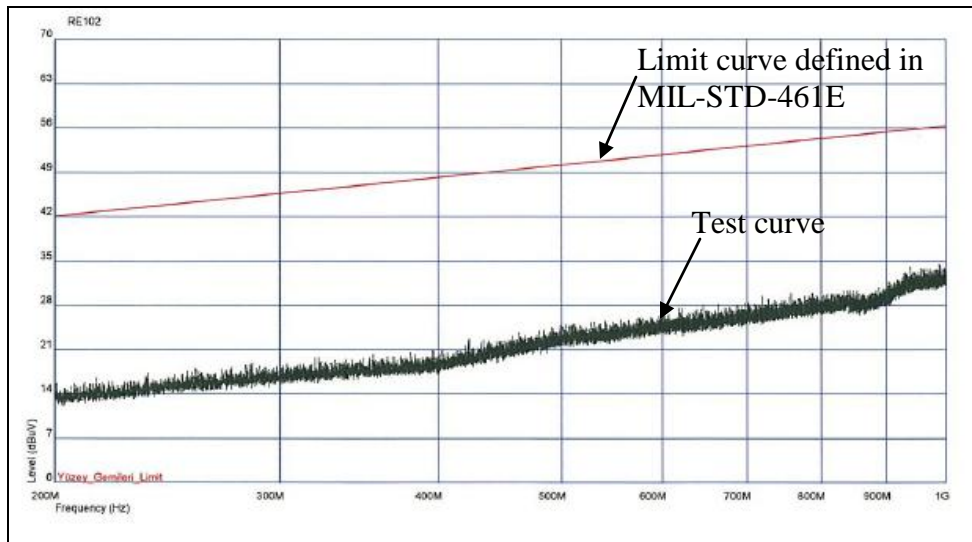


Figure 6.44 RE102 Experiment Graph of Back Plane Noise  
Horizontal Polarization 200-1000 MHz

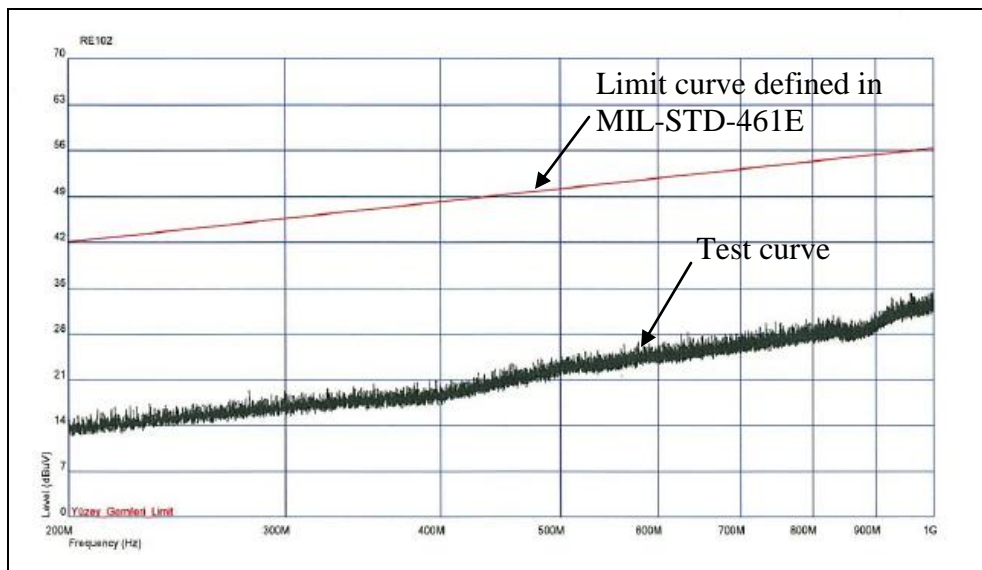


Figure 6.45 RE102 Experiment Graph of Back Plane Noise  
Vertical Polarization 200-1000 MHz

For RE102 experiment of 1 GHz to 18 GHz, horn antenna was used. The distance between the antenna and the EUT was 1 m. The height of the antenna was 1,2 m. The device was passed this experiment successfully for vertical and horizontal polarizations which are illustrated by Figure 46 and Figure 47

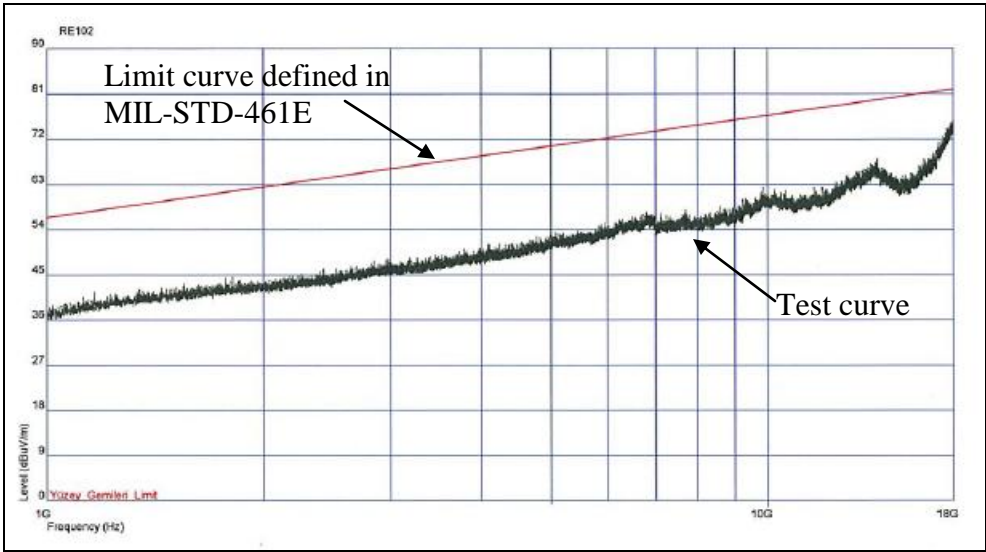


Figure 6.46 RE102 Experiment Graph of Back Plane Noise  
Vertical Polarization 1-18 GHz

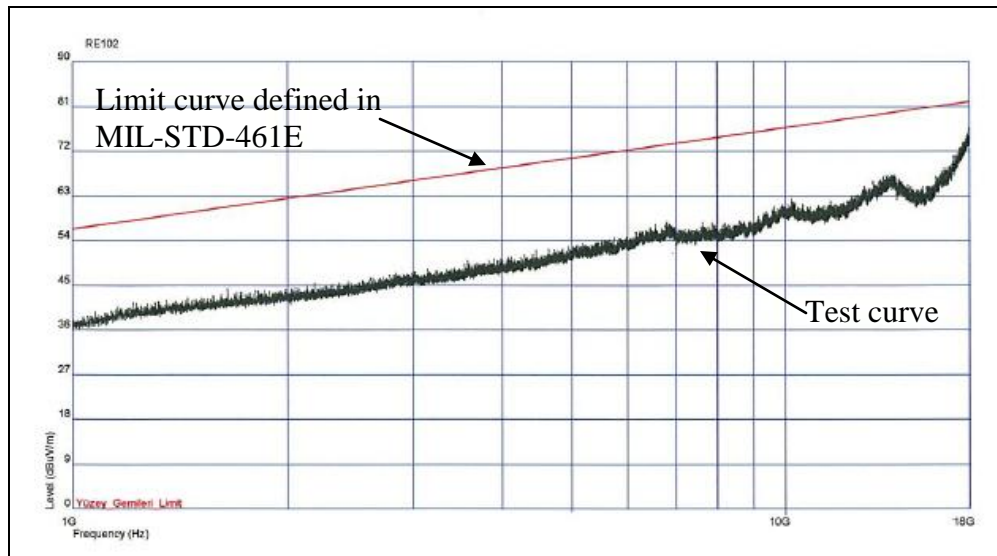


Figure 6.47 RE102 Experiment graph of back plane noise horizontal polarization 1-18 GHz

#### 6.8.4 CONDUCTED SUSCEPTIBILITY TEST (CS101)

Test CS101, was performed according to MIL-STD-461E paragraph 5.7. The purpose was to verify the ability of the EUT to sustain electromagnetic energy coupled onto input power leads.

The EUT was tested in operational state according to the MIL-STD-461E. Test was applied between 30 Hz and 150 kHz. This requirement was applicable starting from the second harmonic (It is 100Hz, if EUT is AC operated) of the EUT power frequency and extending to 150 kHz. Malfunction, degradation of performance or deviation from specifications, beyond the tolerances indicated in the specification of the EUT was not allowed during the presence of a superposed signal.

The applied profile is given in Figure 6.48. The Curve #2 was used through the experiment since ship's voltage is 28 V

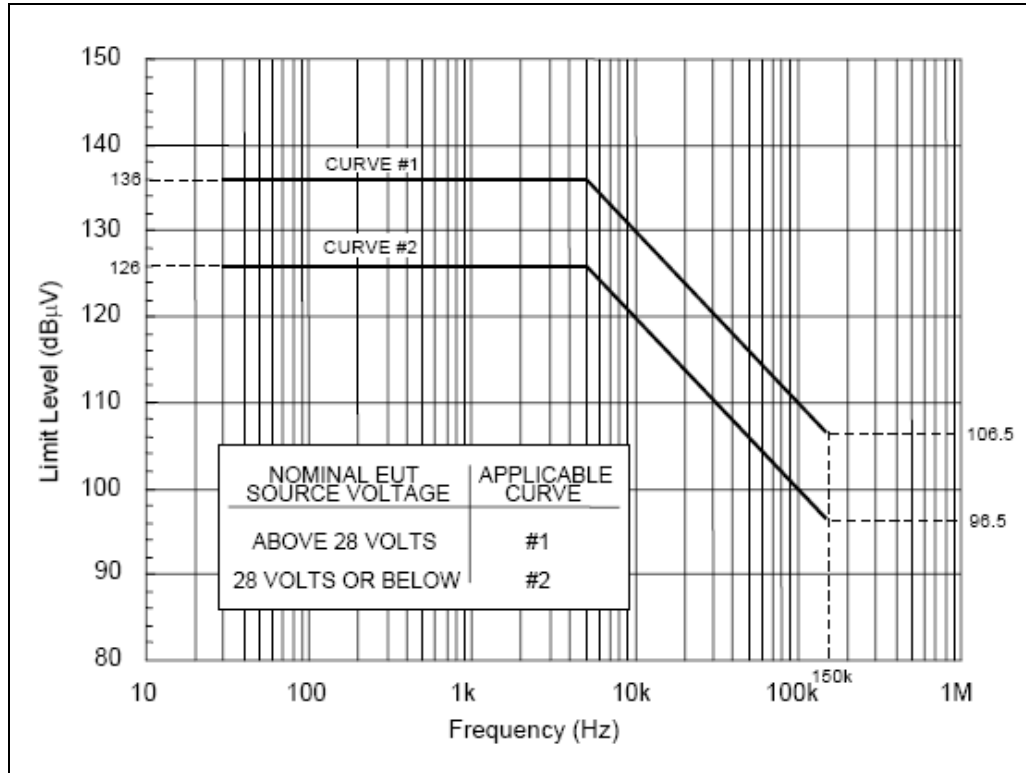


Figure 6.48 CS101 Voltage limit curve [46]

### 6.8.5 CONDUCTED SUSCEPTIBILITY TEST (CS114)

Test CS114 was performed according to MIL-STD-461E paragraph 5.12. The purpose was to verify the ability of the EUT is susceptible to bulk cable injection. This test was applicable to all cables (power cables as well as interconnecting cables) of EUT.

The EUT was tested in operational state. Test was applied between 10 kHz and 200 MHz. Malfunction, degradation of performance or deviation from specifications, beyond the tolerances indicated in the specification of the EUT was not allowed during the presence of injected currents.

The applied profile is given in Figure 6.49. For the packaging device, Curve#2 is used as experiment data

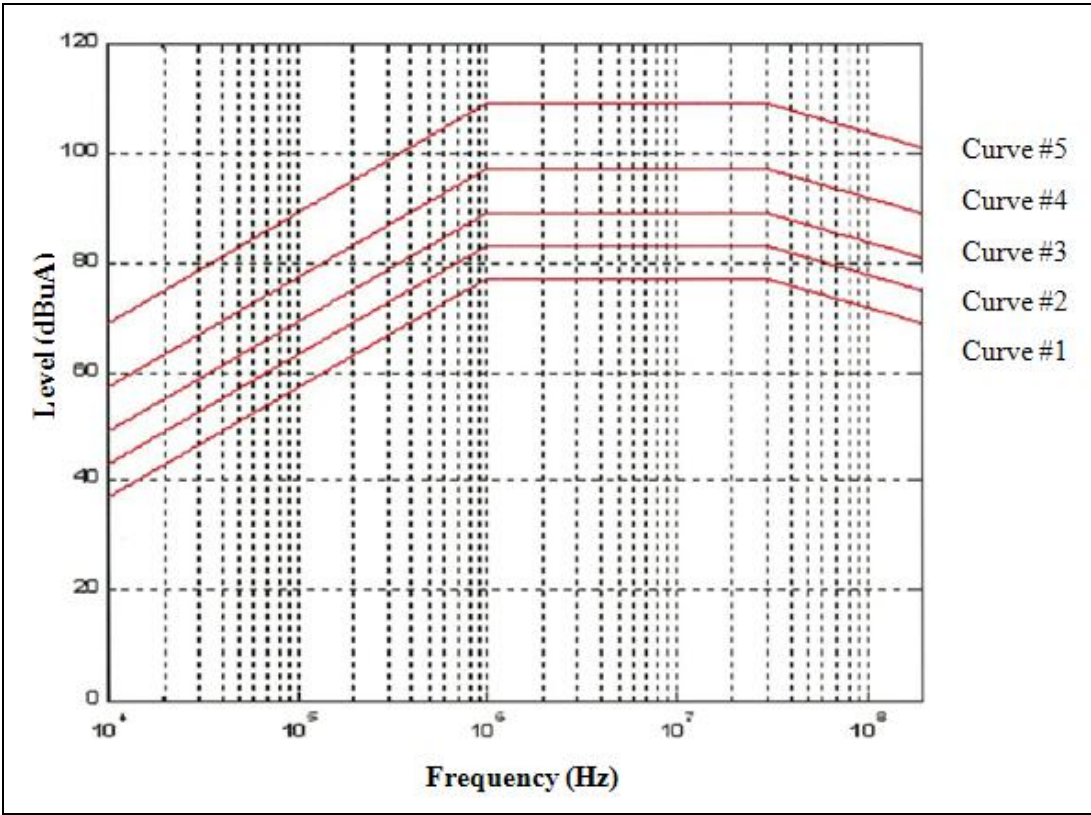


Figure 6.49 CS114 Limiting levels

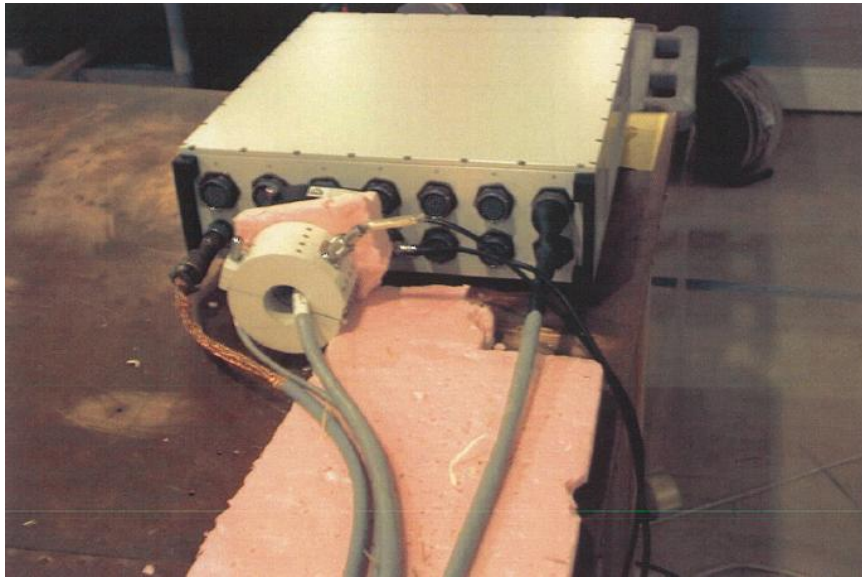


Figure 6.50 Packaging device under CS114

#### **6.8.6 CONDUCTED SUSCEPTIBILITY TEST (CS116)**

Test CS116 was performed according to MIL-STD-461E paragraph 5.14. The purpose was to verify the ability of the EUT to sustain damped sinusoidal transients in the intended frequency range. This test was applicable to all cables (power cables as well as interconnecting cables) of EUT.

The EUT was tested in operational state. Test was applied between 10 kHz and 100 MHz. Malfunction, degradation of performance or deviation from specifications, beyond the tolerances indicated in the specification of the EUT was not allowed during the presence of injected currents. The device passed the experiment successfully.

### 6.8.7 RADIATED SUSCEPTIBILITY TEST (RS101)

Test RS101 was performed according to MIL-STD-461E paragraph 5.18. The purpose was verifying the ability of the EUT to sustain magnetic field in the intended frequency range. This test was applicable to all equipment (cabinets as well as cables), however with an exception for antennas.

The EUT was tested in operational state. Test was done between 30 Hz and 100 kHz and test was applied for the 10 dB above of the limit curve given in Figure 6.x. Malfunction, degradation of performance or deviation from specifications, beyond the tolerances indicated in the specification of the EUT was not allowed during the presence of the magnetic field.

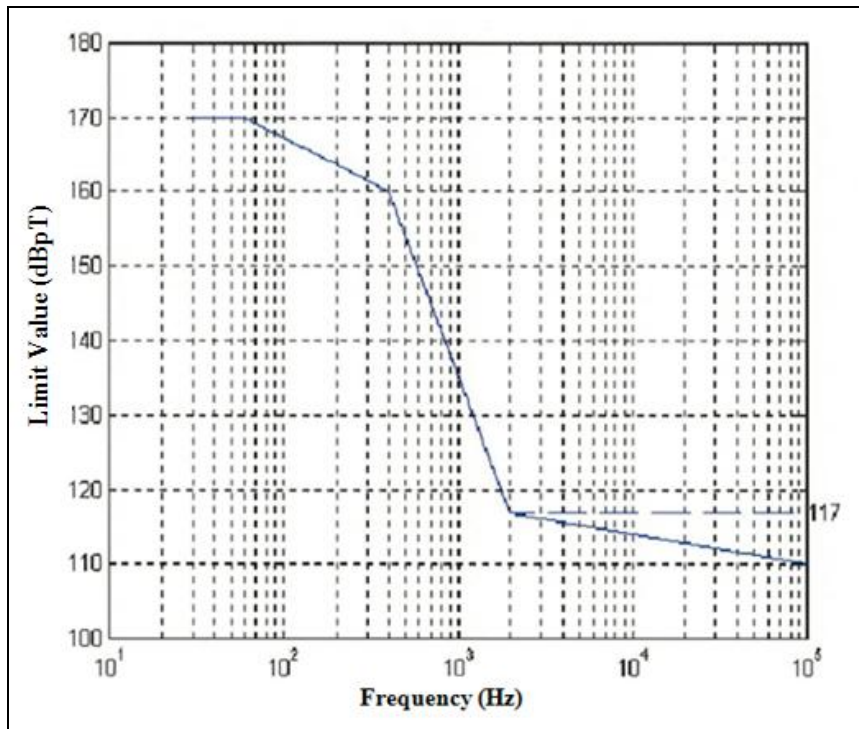


Figure 6.51 Limit curve for RS101 test

### **6.8.8 RADIATED SUSCEPTIBILITY TEST (RS103)**

Test RS103 was performed according to MIL-STD-461E paragraph 5.19. The purpose was to verify the ability of the EUT to sustain electric field. This test was applicable to all EUT.

The EUT shall be tested in operational state. Test was applied between 2 MHz and 18 GHz. Malfunction, degradation of performance or deviation from specifications, beyond the tolerances indicated in the specification of the EUT was not allowed during the presence of the magnetic field. EUT completed the test without any failures specified in the standard.

### **6.8.9 ESD TEST**

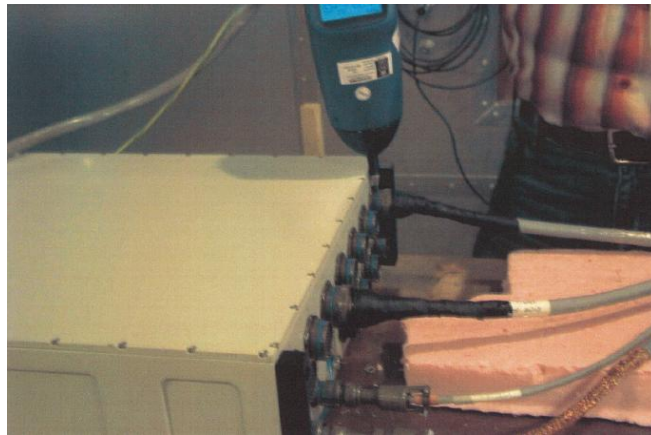


Figure 6.52 Application of ESD test

This experiment was applied to EUT through air and through direct contact. The application points were the back shells of some connectors, ground screw and all the

other screws on EUT. For every point the experiment was done 10 times with negative and positive polarization. The aim of this test was verifying the ability of EUT for protection against ESD. The device passed this experiment successfully.

## **6.9 RESULTS**

The device which is a subject of this thesis was designed to have a sufficient electromagnetic shielding for its own source of noise and the outer environmental sources simulated through the tests. The material selection, chassis thickness, effective joint spacing, appropriate gasket usage were examined through the EMI shielding theory and verified through calculations. After the manufacturing and performance tests, the device is tested according to related sections of MIL-STD-461E. There were no minor neither major failures were observed through the tests.

## **CHAPTER 7**

### **CONCLUDING REMARKS AND FUTURE WORK**

In this thesis, an electronic packaging of a device which is subjected to the environmental and electromagnetic compatibility tests is examined including its design steps and verification procedure by computer aided analyses before performing operational environmental tests.

Electronic packaging and verification of the design is mainly formed by four main parts: design, manufacturing, analysis and test. The borders of the design are defined by the function of the device, working environment, and the test standards. The environmental tests which the device will be subjected to and will be analyzed in this thesis are mechanical shock, vibration and high temperature test. For verification of the electromagnetic compatibility, the device is also subjected to both conducted/radiated susceptibility and emission tests.

The device would be used in a military frigate and function as a part of the naval network system. Therefore, the very first design criteria were corrosion and humidity. The main build-up material used in the electronic packaging is chosen as Al 5083 H321 which is aluminum alloy having good corrosion resistance property. Chassis of the device was manufactured by welding of aluminum panels having 9 mm thickness. These panels were milled in some locations in order to reduce the excess weight. There is a cover used in the structure for accessing the cards inside the device. The cover is assembled to the chassis by M3 screws. The spacing between the screws was calculated by the shielding effectiveness of the device. The precautions for

electromagnetic waves were very strict for the packaging. The device was designed as if there were no air gaps left. Special gaskets were used when closing every aperture in the chassis like cover and connectors.

Considering the vibratory environment, plain and elastic washers were used under screws. There are some aluminum interfaces assembled to the main chassis in order to fix 9 audio cards and a control card inside the equipment. On the back side of the chassis, connectors and ground screws are placed. Ground screws were important for electromagnetic discharge.

For pre-design of the packaging, it was predicted that the inner temperature of the equipment would not reach critical values. Therefore, no cooling apparatus was used inside device like fan, air or water cooled systems. As the heat dissipation method, only conduction and natural convection mechanisms were used.

Since the equipment is mounted on a 19" Rack Cabinet in the frigate's cabin, the package was designed according to 19" rack standards. The height of the device is 3U and it is assembled to the cabinet from front handles. These handles were manufactured from 2 mm R St 37-2 structural steel by bending from inner edge with 2 mm radius. In case of failure, in order to have quick access to the equipment and work on equipment without totally uninstalling it from the cabinet, a tray with telescopic slides is designed and used under the device.

The shock test for the equipment was performed for simulating the effects of mine explosion or harsh sea environment. This test was performed according to the standards set forth in MIL-STD-810F, method 516.5, Procedure I (Functional shock). According to this specification, the equipment should be subjected to a shock loading of 20 g for 11 ms in every axes and both in negative and positive directions. Before the shock test, the design of the equipment is verified by "Flexible Dynamic" module

of ANSYS Work Bench 11.0. This analysis was done by defining shock load as half sine wave in every direction of every axes. The analyzed model was a shell model in order to save time and prevent unnecessary memory usage. The calculated maximum Von-Mises stresses were generally found under the critical values. This result gave idea about the behavior of the equipment under test conditions and under harsh working environment. After the shock analysis step, operational test was performed. During the operational test, device continued its functions and after the test device also worked properly. There was no structural failure observed during visual inspections after the test procedure.

There are two main sources of vibration for a ship environment: the interactions between ship's body and the fluid and the engine. The vibration test performed for monitoring the vibratory environment was based on the vibration profile which is given in MIL-STD-810F, Method 514.5, Procedure I, Category 10, Figure 514.5-C-15. This profile defines a random vibration spectrum. Test is done by giving random excitations within the related profile to the device by a vibration shaker. But before the application of the test, random vibration analysis is performed by "Random Vibration" module of ANSYS Workbench 11.0. Similar to the shock analysis, shell model was used for the analyzed model. As a pre-analysis, modal analysis was done and the mode shapes, mode numbers used for random vibration analysis and mode frequencies of the device were calculated. The statistical method used during the random vibration analysis was  $3\sigma$ . This means that the real stress and the deformation would have a probability of %99.737 to be in the range of resultant stress and deformation values found from the analysis. The calculated maximum Von-Mises stresses were small compared with the critical values. Since, most of the mode shapes occurred around the cover, the analysis also verified the locations of PCBs inside the device. The device was also tested for functional state after the analysis. It passed the operational test without any functional or structural failures.

Another source of failure for electronic equipment is temperature. This device was tested both for high temperature and low temperature according to MIL-STD-810F Method 501.4 Procedure II and Method 502.4 Procedure II, respectively. The heating modules and the working environment of some modules made the high temperature test critical. Therefore, before test step, high temperature condition was analyzed by "Steady-State" module of ANSYS Workbench 11.0. Heat dissipation method was assumed for inner chassis as heat conduction between PCBs and chassis and for outer chassis as natural convection. No radiation was included during the analysis. In order to achieve the analysis conditions, the normal and planar conduction coefficients of PCBs which were composite materials, were defined in ANSYS. The ambient temperature was taken as 35 Celsius degrees as specified in the test standard. The average convection coefficients of the chassis were found by making iterations for maximum surface temperatures. The results of the analysis gave a temperature range between 50-55 Celsius degrees for chassis surface and between 54-55 Celsius degrees for audio and control card surfaces. These ranges were safe for critical components. The equipment was tested for low and high temperatures and both tests were accomplished successfully for an operational condition.

Finally, MIL-STD-461 tests were applied to the device for verifying its electromagnetic compatibility. Before tests, the total shielding of the chassis was calculated and it was found good enough to protect the device from outer hazardous source and to protect the outer devices from harmful emission of the device. The device passed all the related EMI/EMC tests without any minor or major failures.

Although the device which is a subject of this thesis was designed for naval applications, it could be used for land and air platforms.

As for the future work the following studies are proposed:  
-Weight optimization especially for aerospace applications.

- Monitoring and analysis of the fatigue life of the cards.
- Thermal design and analysis for the no outer air conditioner cases.
- Investigating and testing the effects of chassis thickness on electromagnetic compatibility.

## REFERENCES

- [1] McKeown S., *Mechanical Analysis Of Electronic Packaging Systems*, Marcel Dekker Inc.,1999
- [2] Fackler W., *Mechanical Engineer's Handbook*, edited by Kutz M., John Wiley @ Sons Inc., 1998
- [3] Blackwell,E.,*The Electronic Packaging Handbook*, CRC Press LLC,2000
- [4] The Johns Hopkins University Applied Physics Laboratory Website,  
<http://www.jhuapl.edu/techdigest/td2001/Bevan.pdf>,  
Last accessed date: April 2008
- [5] Astronautics Website,  
<http://www.astronautics.com/new/Products/ProdPik.asp?cat=Air&sub=NavSys>,  
Last accessed date: April 2008
- [6] Steinberg,D., *Vibration Analysis of Electronic Equipment*, 3<sup>rd</sup> edition,Wiley,2000
- [7] MIL-STD-810-F, *Department of Defense Test Method Standard for Environmental Engineering Considerations and Laboratory Tests*, 1 January 2000
- [8] MIL-STD-167-1A, *Department of Defense Test Method Standard Mechanical Vibrations od Shipboard Equipment*, 2 November 2005
- [9] MIL-S-901D (NAVY), *Military Specification Shock Tests, H. I. (High-Impact) Shipboard Machinery Equipment, and Systems, Requirements for*, 17 March 1989

- [10] MIL-T-18303 (WEBS), *Military Specification for Test Procedures, Preproduction and Inspection for Aircraft Electronic Equipment, Format for*, 1991
- [11] NATO STANAG 4370, *Environmental Testing*, 19 April 2005
- [12] <http://asm.matweb.com/search/SpecificMaterial.asp?bassnum=MA5083H116>  
Last accessed date: April 2008
- [13] “The A to Z Materials” Website,  
<http://www.azom.com/details.asp?ArticleID=2804>  
Last accessed date: April 2008
- [14] SAĞAYLAR Demir San. ve Tic. A.Ş Website,  
<http://sagaylar.com.tr/sac.htm>  
Last accessed date: April 2008
- [15] Fullmetric Website,  
[http://www.fullermetric.com/products/stainless/din7985phillips\\_pan\\_head.html](http://www.fullermetric.com/products/stainless/din7985phillips_pan_head.html)  
Last accessed date: April 2008
- [16] Jamnia, A., *Practical Guide to the Packaging of Electronics Thermal and Mechanical Design and Analysis*, Marcel Dekker Inc., 2003
- [17] Gatti, P. L., Ferrari, V., *Applied Structural and Mechanical Vibrations*, Taylor & Francis Group LLC, 2003
- [18] Harris, C. M., *Shock and Vibration Handbook*, 3<sup>rd</sup> Edition, McGraw-Hill, 1988

- [19] Belcan ANSYS Website,  
[http://ansys.belcan.com/d/Struct\\_Element\\_Types.pdf](http://ansys.belcan.com/d/Struct_Element_Types.pdf)  
Last accessed date: April 2008
- [20] Cook, R. D., *Finite Element Modeling for Stress Analysis*, John Wiley @ Sons Inc., 1995
- [21] BOEING Commercial Airplanes, *Finite Element Modeling Guide for Aircraft Structural Analysis*, Document No.D6-25400-0006, 1989
- [22] ANSYS Structural Analysis Guide Release 9.0, ANSYS, Inc.,2004
- [23]..ANSYS Inc., ANSYS Release 11.0 Documentation for ANSYS Workbench, 2007
- [24] Labworks Inc. Website,  
[http://www.labworks-inc.com/enginfo/random\\_vib\\_test.htm](http://www.labworks-inc.com/enginfo/random_vib_test.htm)  
Last accessed date: April 2008
- [25] Mobley R. K.,*Vibration Fundamentals*, Butterworth-Heinemann,1999
- [26] Kreith ,F. , Goswami, D. Y., *The CRC Handbook of Mechanical Engineering*, 2<sup>nd</sup> edition , CRC Press LLC, 2005
- [27] Taylor, I. J., *The Vibration Analysis Handbook*, VCI, 2003
- [28] Irvine, T., Tutorial,*Damping Properties of Materials Rev.C*, November 2004  
<http://www.cs.wright.edu/~jslater/SDTCOutreachWebsite/damping%20properties%20of%20materials.pdf>  
Last accessed date: April 2008

- [29] Lutes, L. D., Sarkani, S., *Random Vibrations Analysis of Structural and Mechanical Systems*, Elsevier Butterworth-Heinemann, 2004
- [30] Kelly, G. S., *Fundamentals of Vibrations*, McGraw-Hill, 1993
- [31] Malhammar, A., Component or PCB Oriented Design, December 2005  
<http://www.coolingzone.com/library.php?read=530>  
Last accessed date: April 2008
- [32] Amkor Technology Website,  
[http://www.amkor.com/services/thermal/Articles/calc\\_corner\\_Sep98\\_RevB.PDF](http://www.amkor.com/services/thermal/Articles/calc_corner_Sep98_RevB.PDF)  
Last accessed date: April 2008
- [33] Amkor Technology Website,  
<http://www.rushpcb.co.uk/article/fr-4-pcb-laminate.html>  
Last accessed date: April 2008
- [34] Amkor Technology Website,  
[http://www.amkor.com/services/thermal/Articles/Calc\\_Cor\\_May98\\_RevC.PDF](http://www.amkor.com/services/thermal/Articles/Calc_Cor_May98_RevC.PDF)  
Last accessed date: April 2008
- [35] Electronics Cooling Website  
[http://electronics-cooling.com/articles/1995/oct/oct95\\_tb.php](http://electronics-cooling.com/articles/1995/oct/oct95_tb.php)  
Last accessed date: April 2008
- [36] Shabany Y., *Component Size and Effective Thermal Conductivity of Printed Circuit Boards*, Applied Thermal Technologies, LLC

[37] Steinberg, D. S., *Cooling Techniques for Electronic Equipment*, 2<sup>nd</sup> Edition, John Wiley @ Sons Inc.,1999

[38] Angelantoni Inc. Website,  
[http://www.angelantoni.it/acs/manuali/PP\\_ACS06\\_gb.pdf](http://www.angelantoni.it/acs/manuali/PP_ACS06_gb.pdf)  
Last accessed date: April 2008

[39] Gnecco,T. L. *The Design of Shielded Enclosures: Cost Effective Methods to Prevent EMI*, Butterworth-Heinemann, 2000

[40] Kodali,V.P. *Engineering Electromagnetic Compatibility* ,IEEE, 1996

[41] Williams,T. *EMC for Product Designers*, Butterworth-Heinemann,2001

[42] IEC50 (161): (BS4727 : Pt 1 : Group 09) Glossary of electrotechnical, power, telecommunication, electronics, lighting and colour terms: Electromagnetic compatibility

[43] Tecknit Website, EMI Shielding Design Guide.  
[www.tecknit.com](http://www.tecknit.com)  
Last accessed date: April 2008

[44] Montrose,M.I.,Nakauchi E.M. *Testing for electromagnetic compliance: Approaches and Techniques* , John Wiley, 2004

[45] Hollandshielding Website, Mechanical Design Tips for EMI Shielding,  
<http://www.hollandshielding.com/>  
Last accessed date: April 2008

[46] MIL-STD 461 E , Department of Defense Interface Standard, 20 August 1999

[47] Calotte, J., EMC DESIGN FUNDAMENTALS

[http://www.ieee.li/pdf/viewgraphs\\_emc\\_fundamentals.pdf](http://www.ieee.li/pdf/viewgraphs_emc_fundamentals.pdf),

Last accessed date: April 2008

[48] Paul,C.R. *Introduction to Electromagnetic Compatibility*, Wiley-Interscience, 2006

[49] Kodali,V.P.,Kanda,M. *EMC/EMI Selected Readings* ,IEEE, 1996

[50] Vance E.F, *Electromagnetic Interference Control*, IEEE Trans EMC, Vol. EMC-5,No 1,Feb.1993

[51] Mann, J.M., *Application of Shielding Effectiveness Methodology to Unit Design*, Loral Federal Systems, Owego

[http://interferencetechnology.com/ArchivedArticles/shielding\\_aids/I95art11.htm?regid=](http://interferencetechnology.com/ArchivedArticles/shielding_aids/I95art11.htm?regid=)

Last accessed date: April 2008

[52] Hayt,W.H. ,Buck, A.J. *Engineering Elecromagnetics* McGraw-Hill, 2001

[53] Engineersedge Website,

[http://www.engineersedge.com/galvanic\\_capatability.htm](http://www.engineersedge.com/galvanic_capatability.htm)

Last accessed date: April 2008

[54] Electrostatic Discharge Association Website, [www.esda.org](http://www.esda.org)

Last accessed date: April 2008

[55] Electrostatic Discharge (ESD), Texas Instruments, Application Report, SSYA010-January 2001, <http://focus.ti.com/lit/an/ssya010/ssya010.pdf>.

[56] Morrison, R. *Grounding and Shielding Techniques*, John Wiley & Sons, 1998

[57] Mardigian, M., *Grounding and Bonding*, Vol.2, Interference Control Technologies Inc., Gainesville, Virginia, 1988.

[58] Comerics Website,

[www.chomerics.com](http://www.chomerics.com)

Last accessed date: April 2008

[59] Gooch J.W., Daher J.K., *Electromagnetic Shielding and Corrosion Protection for Aerospace Vehicles*, Georgia Institute of Technology, Springer Science and Business Media, 2007

[60] Exetel, *Shielding Calculations*,

[home.exetel.com.au/comapps/tonyt/Applets/Refraction/ShieldingCalc.doc](http://home.exetel.com.au/comapps/tonyt/Applets/Refraction/ShieldingCalc.doc)

Last accessed date April 2008

[61] Nondestructive Testing-Education Organization Website,

[http://www.ndt-ed.org/GeneralResources/MaterialProperties/ET/Conductivity\\_A1.pdf](http://www.ndt-ed.org/GeneralResources/MaterialProperties/ET/Conductivity_A1.pdf)

Last accessed date April 2008

## APPENDIX A

### ELECTROMAGNETIC SHIELDING: SOME USEFUL DATA AND BASIC EQUATIONS

*This part is taken from reference [60].*

Electronic equipment can be effectively shielded by the use of a conductive barrier placed between the source of electromagnetic waves and the equipment to be shielded.

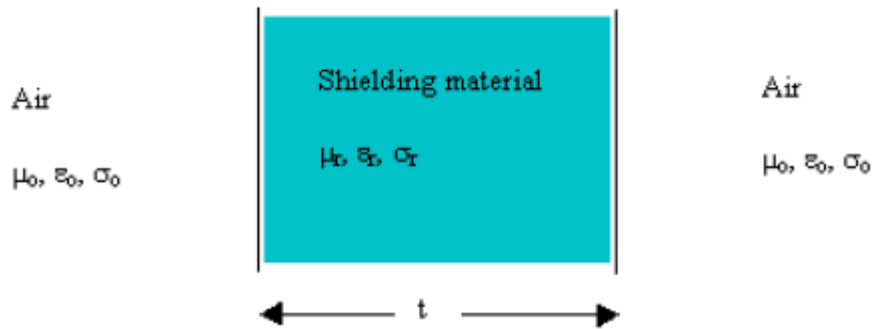


Figure A-1 Conductive Barrier

The shielding effectiveness (SE) factor may be expressed as the ratio of the transmitted field magnitude to the incident field magnitude.

$$SE_{dB} = 20 \log \left| \frac{\hat{E}_t}{\hat{E}_i} \right| = 20 \log \left( \frac{1}{SE_{factor}} \right) \quad (\text{A.1})$$

The relevant equations that are used by the applet in calculating the shielding effectiveness are given in the following part. All units are in SI units. The equations are developed using oblique incidence of uniform plane waves and are made general, so that air does not have to be the surrounding media to the shield, although, the media surrounding the shield must be the same. Two sets of calculations are performed. The first is where the incident wave has parallel polarization and the other, where the incident wave has perpendicular polarization.

The permittivity of free space,  $\mu_0 = 4\pi \cdot 10^{-7}$  F/m (A.2)

The permeability of free space,  $\epsilon_0 = 8.845187818 \cdot 10^{-12}$  H/m (A.3)

The propagation constant,  $\gamma = \sqrt{j\omega\mu \left( \sigma + j\omega\epsilon \right)} = \alpha + j\beta$  (A.4)

where  $\sigma$  is the conductivity of the material (S/m) and  $\omega$  is the radian frequency,

$$\omega = 2\pi f \text{ rad/s} \tag{A.5}$$

and  $f$  is the carrier frequency (Hz).

The attenuation constant,

$$\alpha = \frac{\omega \sqrt{\mu\epsilon}}{\sqrt{2}} \left( \sqrt{1 + \left( \frac{\sigma}{\omega\epsilon} \right)^2} - 1 \right)^{1/2} \text{ Np/m} \tag{A.6}$$

The phase-delay constant,

$$\beta = \frac{\omega \sqrt{\mu\epsilon}}{\sqrt{2}} \left( \sqrt{1 + \left( \frac{\sigma}{\omega\epsilon} \right)^2} + 1 \right)^{1/2} = \frac{2\pi}{\lambda} \text{ rad/m} \tag{A.7}$$

Where  $\lambda$  is the carrier wavelength (m).

The phase velocity,

$$u_p = \frac{\omega}{\beta} \text{ m/s} \quad (\text{A.8})$$

The intrinsic impedance of the medium,

$$\eta = \frac{j\omega\mu}{\gamma} = \frac{1}{\omega\epsilon \sqrt{1 + \left(\frac{\sigma}{\omega\epsilon}\right)^2}} \left[ \beta + j\alpha \right] \Omega \quad (\text{A.9})$$

A good conductor is where  $\sigma \gg \omega\epsilon$  (conduction current > displacement current)

A good dielectric is where  $\omega\epsilon \gg \sigma$  (displacement current > conduction current)

A perfect conductor is where  $\sigma \rightarrow \infty$  but  $\epsilon$  and  $\mu$  are finite and all time-varying fields are zero.

A lossless medium is where  $\sigma = 0$  (perfect dielectric) but  $\epsilon$  and  $\mu$  are finite

In free space  $\mu = \mu_0$ ,  $\epsilon = \epsilon_0$ ,  $\rho = 0$  and  $J = 0$  (the free current density)

Consider the Figure A-2 below showing a shield (Media 2) inserted in some media (Media 1). If media 1 is the air, the permeability, permittivity and conductivity can be considered to be approximately the same as that of free space.

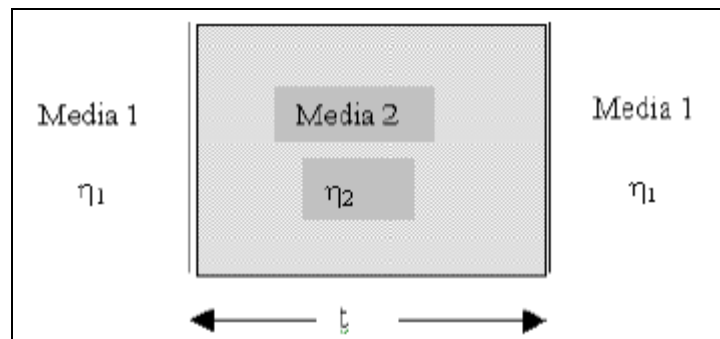


Figure A-2 A shield in a Media

## APPENDIX-B

### SHIELDING EFFECTIVENESS OF ALUMINUM, STEEL AND COPPER

*This part is taken from reference [41].*

A theoretical example for shielding effectiveness is given in Table A-1 where  $r=12''$ ,  
 $\mu_{r,aluminum}=1$ ,  $\mu_{r,cr\ steel}=180$ ,  $\mu_{r,copper}=1$ ,  $\sigma_{r,aluminum}=0.6$ ,  $\sigma_{r,cr\ steel}=0.17$ ,  $\sigma_{r,copper}=1$

Table A-1 Shielding effectiveness of Al, St and Cu for different frequencies.

Freq (Hz)	Aluminum (60 mils)			Cold Rolled Steel (60 mils)			Copper (3mils)		
	Magnetic (dB)	Electric (dB)	Plane (dB)	Magnetic (dB)	Electric (dB)	Plane (dB)	Magnetic (dB)	Electric (dB)	Plane (dB)
10 k	58	>200	141	125	>200	>200	45	>200	129
100 k	101	>200	165	>200	>200	>200	57	186	121
1 M	>200	>200	>200	>200	>200	>200	74	162	118
10 M	>200	>200	>200	>200	>200	>200	106	154	130
100 M	>200	>200	>200	>200	>200	>200	184	193	188
1 G	>200	>200	>200	>200	>200	>200	>200	>200	>200

## APPENDIX-C

### GALVANIC CORROSION

*This part is taken from reference [53].*

For *harsh environments*, such as outdoors, high humidity, and salt environments, there should be not more than 0.15 V difference in the “Anodic Index”

For *normal environments*, such as storage in warehouses or non-temperature and humidity controlled environments, there should be not more than 0.25 V difference.

For *controlled environments*, such that are temperature and humidity controlled, 0.50 V can be tolerated.

Table A-2 Anodic index

METALLURGICAL CATEGORY	ANODIC INDEX
Gold; solid and plated, Gold-platinum alloy	0.00
Rhodium plated on silver-plated copper	0.05
Silver, solid or plated; monel metal. High nickel-copper alloys.	0.15
Nickel, solid or plated, titanium and alloys, Monel	0.30
Copper, solid or plated; low brasses or bronzes; silver solder; German silver high copper-nickel alloys; nickel-chromium alloys	0.35
Brass and bronzes	0.40
High brasses and bronzes	0.45
18% chromium type corrosion-resistant steels	0.50
Chromium plated; tin plated; 12% chromium type corrosion-	0.60

resistant steels	
Tin-plate; tin-lead solder	0.65
Lead, solid or plated; high lead alloys	0.70
Aluminum, wrought alloys of the 2000 series	0.75

Table A-2 Anodic index (Cont'd)

Iron, wrought, gray or malleable, plain carbon and low alloy steels	0.85
Aluminum, wrought alloys other than 2000 Series Aluminum, cast alloys of the silicon type	0.90
Aluminum, cast alloys other than silicon type, cadmium, plated and chromate	0.95
Hot-dip-zinc plate; galvanized steel	1.20
Zinc, wrought; zinc-base die casting alloys; zinc plated	1.25
Magnesium % magnesium-base alloys, cast or wrought	1.75
Beryllium	1.85